2007

Pile capacity utilization for bridge bents designed using simplified procedures

Md Rubiat Ferdous
Louisiana State University and Agricultural and Mechanical College, rubyatf@yahoo.com

PILE CAPACITY UTILIZATION FOR BRIDGE BENTS DESIGNED USING SIMPLIFIED PROCEDURES

A Thesis

Submitted to the Graduate Faculty of the
Louisiana State University and
Agricultural and Mechanical College
in partial fulfillment of the
requirements for the degree of
Master of Science in Civil Engineering

in

The Department of Civil and Environmental Engineering

By
Md Rubiat Ferdous
B.S., Bangladesh University of Engineering and Technology, Bangladesh, 2003
August, 2007

ACKNOWLEDGMENTS

I am grateful to, Dr. Ayman M. Okeil, my major professor and chairman of my advisory committee, for accepting me as his research assistant and providing me financial support throughout my Master's study. I would also like to thank him for his active mentorship and constant encouragement. With his knowledge, experience, and research capabilities he continuously guided me towards my goal of completing this work. It has been the biggest honor of my life to work with such a brilliant, considerate, and friendly scholar. My thanks to him can not be enough in mere words. I shall always remember my learning from him.

I express my deepest and sincere thanks to Dr. Khalid A. Alshibli and Dr. Steve Cai for accepting to serve on my advisory committee and guiding me throughout my research. I also express my gratitude for their patience, time, help and support.

I am greatly indebted to my parents, Mr. Khorshed Alam and Mrs. Ferdous Ara Begum, for their loving care and support throughout my life and especially through my academic pursuit. I am blessed to have parents like them; this wouldn't have been possible without their support.

Last but not least, I would like to thank everyone at LSU who played their roles in making this work successful.

TABLE OF CONTENTS

page

LIST OF TABLES

LIST OF FIGURES

ABSTRACT

Bent substructure systems are being used increasingly in bridge construction. Among the various bent systems, pile bents are considered a popular choice due to their effectiveness in reducing time and cost. They are constructed by first driving piles to a specified elevation above the ground surface. Then, a cast-in-place reinforced concrete bent cap ties the piles together at their top end. The current Louisiana Department of Transportation and Development Bridge Design Manual provides guidelines for the structural analysis and construction details for general use in the preparation of plans for pile bents. The manual allows the use of a simplified method in which ranges of allowable axial compressive loads for different pile sizes can be used in selecting a recommended pile size once the pile axial load is known. The procedure requires axial load demands to be determined due to dead and live load effects only. However, at high wind velocity or as bridge spans become larger, lateral loads and moments acting on the pile increase and cannot be neglected. Therefore, identifying limitations on the use of the simplified procedure is the main motivation behind this research.

This study makes an endeavor to analyze many bridges that cover a wide design space including different span lengths, unsupported pile lengths, skew angles, and pile-cap continuity. The bridges are supported on pile bents to investigate the applicability of the simplified design procedure under different limit states. The pile sizes and layouts for the bridges of different configurations were selected considering the existing guidelines. The scope of this study is to determine the load and moment demand on the piles using refined analyses. The capacity of the piles was then determined taking into account the interaction between axial loads and flexure. Based on the results, the capacity utilization for each pile was determined and used to investigate the limitations on the use of simplified method.

The results show that the simplified procedure should not be universally used for pile design. At high wind velocity (Strength III limit state) the procedure results in unsafe designs. A summary of the limitations was mapped for the 128 bridge cases considered in this study for pile caps with two pile-to-cap continuity assumptions. Recommendations for future research have been identified to further refine the simplified design procedure.

CHAPTER 1. INTRODUCTION

1.1 General Background

Nowadays, bent substructure systems are being used increasingly in bridge construction due to their effectiveness in reducing time and cost. Pile bents are the most commonly used bent type for the bridge substructures in over waterways where multiple, simple span structures cross relatively shallow channels. In a pile bent, the piles are driven to a specified elevation above the ground surface. At this elevation, the piles are tied together with a cast-in-place (CIP) reinforced concrete (RC) bent cap. The precast-prestressed concrete pile is the most commonly used driven pile type. Steel pipe piles or H piles may also be used in site specific locations. These types of piers are very economical because they reduce construction stages and minimize the need for formworks. The can be used for stream crossing, highway crossing and railroad crossings when aesthetics are not a consideration. A typical elevation and end view of a typical pile bent is shown in Fig1.1.

Pile bent type piers are limited in height by the slenderness and buckling capacity of the piles. These partially embedded piles experience even larger moments when subjected to lateral loads. Pile bents may be designed to resist the lateral loads via the use of battered piles or by being rigidly cross braced or via cantilever action with moment-resistant deck connections (Gaythwaite 2004); with the former being the most commonly practiced solution for precast-prestressed concrete piles. The depth of fixity is a primary factor in determining the slenderness and therefore buckling capacity of the piles. The effective length of the partially embedded pile is equal to the laterally unsupported length of the pile above the ground plus its depth of fixity which depends on the soil characteristics. Davison and Robinson (1965) proposed a procedure to calculate the depth of fixity for a partially embedded pile which is currently adopted in AASHTO LRFD bridge design specifications(AASHTO 2004).

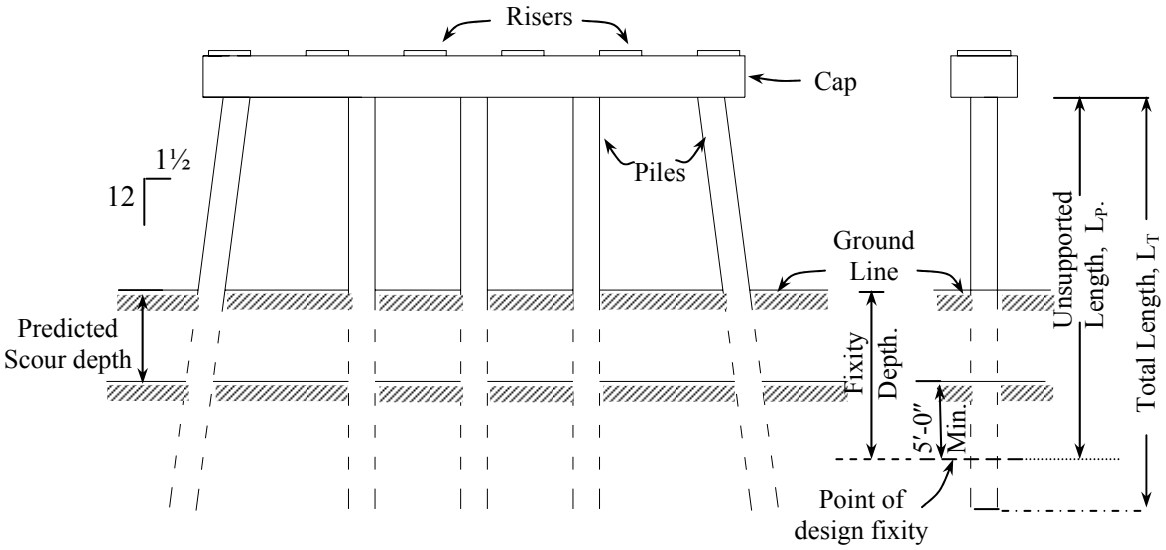

Figure 1.1 Typical pile bent pier

The current Louisiana Department of Transportation and Development (LA-DOTD) Bridge Design Manual (BDM) (2004) provides guidelines for the structural analysis and construction details for general use in the preparation of plans for pile bents. The manual allows the use of a simplified method in which the piles are designed based on the LRFD factored pile axial compression loads due to dead and live loads only. Ranges of allowable axial compressive loads for different pile sizes are given in the manual that can be used in selecting pile size once the pile axial load is known. However, these partially embedded piles are subjected to significant bending moments corresponding to the applied axial loads under different service load conditions. The guideline for the selection of pile size is based only on the applied compressive loads. As bridge spans become larger, lateral loads and moments increase and become a dominant design force. Therefore, a thorough investigation of the table provided in the manual is deemed necessary.

This study makes an endeavor to analyze wide variety of parameters for a popular bridge system to investigate the design of the piles under different limit states. The pile sizes and layouts for the bridges of different span lengths, skew angles, and pile slenderness ratios are selected considering the existing guidelines. Analytical models are developed for three span bridges using general purpose Finite Element software package "SAP2000". The bridge models are analyzed for the load combinations (dead load, live load and wind load) that produce the maximum pile axial load and moment. Pile/Column interaction diagram for prestressed concrete is used to assess the applicability of the selected pile size.

1.2 Objective

The main objectives of this study can be summarized in the following: (a) study the feasibility of the simplified design approach as recommended by LA-DOTD under different limit states, and (b) investigate the appropriate limits on the applicability of the approximate method if needed.

1.3 Scope of Study

The study focuses on the design of pile bents of various skewed and non-skewed, straight, prestressed concrete slab-girder bridges under different limit states specified by AASHTO LRFD bridge design specifications (AASHTO 2004). It investigates the capacity utilization of piles under the most critical load combination. The pile capacity referred to in this study is the structural capacity of the pile cross section. The soil capacity is assumed to be adequate for resisting the applied loads.

1.4 Organization

This thesis is organized in seven chapters.

Chapter 1 gives a general introduction to the concepts of pile bent, its vulnerability to high slenderness ratio, and depth of fixity. The objectives, scopes and organization of the thesis are also presented.

Chapter 2 presents a literature review of pile bents, types and details of piles, pile depth of fixity and the use of interaction diagrams for the design of prestressed-concrete piles. An overview of past studies on finite element model generation for bridge structures, load distribution factors used for the analysis in simplified methods, and evaluation of both finite element and simplified approaches are also presented in Chapter 2. Finally the guidelines for the design of piles for bridge bents provided as given in the LA-DOTD BDM (2004) are discussed.

Chapter 3 presents the procedures used to analyze the bridge bents using two-dimensional frame models. The commercially-available software package STAAD Pro 2004 was used in this study to analyze the non-skew bridges and select the pile sizes using existing Louisiana's guidelines. Procedures used for the calculation of different loadings and girder reactions based on AASHTO LRFD (2004) are presented in this chapter.

Details of the finite element model generation for three-span bridges with pile bents are presented in Chapter 4. Models with different skew angles, span lengths, unsupported pile lengths and pile-cap continuities are presented. The material properties, attributes assigned, types of elements used, and mesh generation are also described. The methods applied to model the pile and cap connections, links between two adjacent girders, and bearing pads are also discussed. Procedures used to apply the loads specified in AASHTO (2004) are also presented. Finally, the analytical verification of the models using the results obtained from conventional analysis is presented.

Chapter 5 contains the process used to calculate the moment capacity of individual piles. The interaction diagram developed by the Precast/Prestressed Concrete Institute for PPC piles is also presented. The spreadsheet program was used to determine the maximum moment capacity (with slenderness consideration) of the piles for the axial loads obtained from structural analysis.

Chapter 6 presents the results obtained from different FE models. The percent utilization of the moments by the piles for bridges with different span lengths, skew angles and unsupported pile lengths are also presented. The chapter also contains a detailed discussion on the results obtained.

In Chapter 7, conclusions are drawn from the study and directions for future research are recommended.

CHAPTER 2. LITERATURE REVIEW

2.1 Introduction

The finite element (FE) method has been used by many researchers to understand the behavior of piles in a pile bent system. Several FE models of bridge structures have been proposed in the literature. Experimental tests as well as simplified analysis approaches were used to validate these models. Several papers on live load distribution factors used for the simplified approaches have been published. Among them the procedures proposed by Zokaie et al. (1991) have been adopted by AASHTO LRFD Bridge Design Specifications (2004).

The interaction diagram is the most widely used design tool for prestressed concrete piles. The construction of interaction diagram for prestressed concrete piles is explained in many publications.

In this chapter, a review of research efforts in the above mentioned field is presented. First, an overview of different forms of piers used in bridge substructure, and pile types used in bent type systems is given. Second, a brief review of previous studies on structural capacity of bent piles, live load distribution factors applied in simplified analysis, and finite element model generation and their evaluation for super and substructure of the bridges is presented. Finally, the guidelines for pile bent design as provided in Louisiana Department of Transportation and Development Bridge Design Manual are presented.

2.2 Pier Types

2.2.1 Introduction

The main function of a bridge pier is to support the superstructure which consists of deck floor and girders. It transfers the loads coming from the superstructure to the foundation. The bridge seats are provided on pier caps to support the bridge girders. Pier cap can be supported by a single column, multiple columns, a solid wall, or a group of piles. These supporting elements

are in turn connected to the pier foundation which is composed of footings, piles or a combination of both. Following are some pier types that are commonly used in bridge substructures (Tonias 1994):

2.2.2 Hammerhead

A hammerhead pier (Figure 2.1a) consists of one or more RC columns with a hammer shape pier cap. These types of piers are predominantly found in urban settings as they are aesthetically appealing and require minimum space, thus providing room for underpass traffic, utilities, or other land usage. They also provide feasible solutions to structures that are located on a skew by allowing tight alignments constraints for the underpass traffic.

2.2.3 Column Bent

A typical column beam pier can be seen in Figure 2.1b. It is typically constructed using a reinforced concrete frame consisting of a cap beam and supporting columns which are attached to a separate foundation of pile footings, spread footings or drilled shafts. The supporting columns can be either circular or rectangular in cross section, the former being used more frequently. For moderate clearance structure with plenty of room for underpass traffic, the column bent pier provides an attractive solution. In dense urban interchange, however, extensive use of column bent piers can lead to a cluttered image producing a concrete jungle effect, which is not aesthetically appealing.

2.2.4 Pile Bent

The pile bent pier (Figure 2.1c) is a variation of the column bent pier with the supporting column and footing replaced by individual supporting piles. The end piles are generally battered in the transverse direction. Pile bents are limited in height due to the slenderness and buckling capacity. These type of piers are extremely popular in marine environment where multiple, simple span structures cross relatively shallow channels. Deterioration of exposed piles, impact

with marine traffic and accumulation of debris at the bottom of the piles are some of the maintenance problems that are generally associated with these types of piers. When provided with adequate protection against these adverse conditions, pile bent piers represents an economic solution for many bridges because they reduce construction stages and minimize the need for formworks.

2.2.5 Solid Wall

A solid wall (Figure 2.1d) pier, also called gravity pier, consists of a solid wall extended up from a foundation consisting of a footing or piles. The top of the wall is equipped with individual pedestals upon which the superstructure rests. Solid wall piers are not suitable for very wide superstructures as they can cause a "tunnel effect" for motorists passing under the structure and may require the placement of a special lighting system under the structure. These are, however, well suited for placement in stream crossings as their slender and streamlined proportions provide a minimal resistance to flood flow.

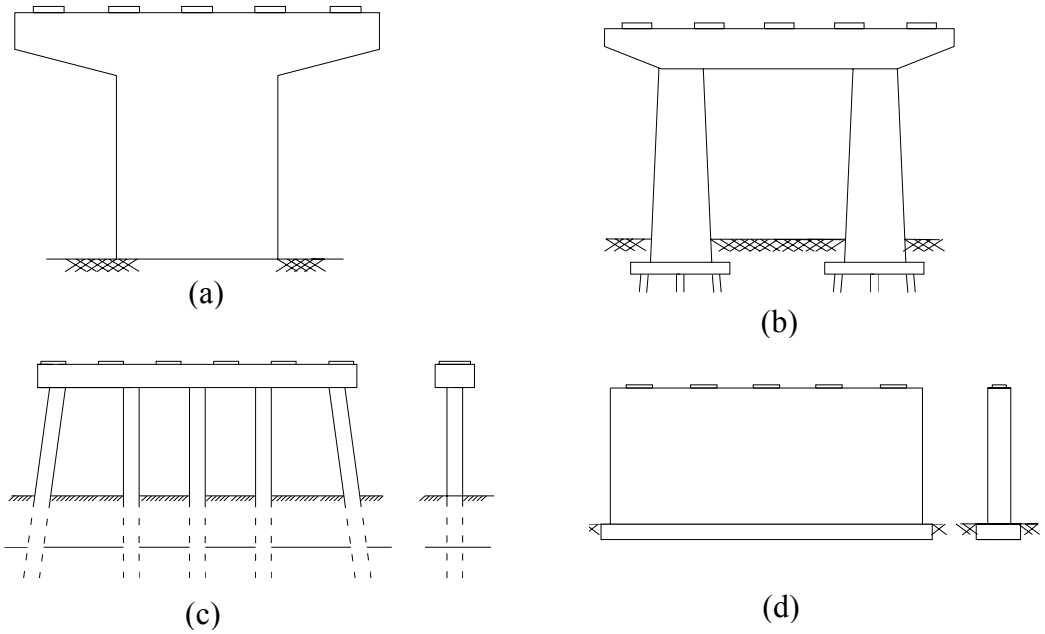

Figure 2.1 Different types of piers. (a) Hammerhead (b) Column Bent (c) Pile Bent (d) Solid Wall

2.2.6 Integral

An integral pier has a pier cap to which the superstructure's primary members are rigidly connected. These types of piers constitute a small percentage pf constructed piers. In most cases they are limited to special structures, particularly when tight vertical clearance constraints pose a problem.

2.2.7 Single Column

An obvious advantage of single column piers is that they occupy a minimum amount of space. This type of pier is extremely attractive when combined with prestressed concrete box type superstructure by providing an open and free flowing appearance to traffic passing underneath the structure.

2.3 Types of Piles Used in Pile Bent System

Pile bent piers consist of partially embedded piles connected to a cast-in-place (CIP) reinforced concrete cap. Several pile types are used in pile bent systems such as: precast-prestressed concrete piles, cast-in-place concrete piles, steel pipe piles, steel "H" piles and timber piles. Table 2.1 lists pile types used for the pile bent system (LA-DOTD 2004). For economic reasons, the precast-prestressed concrete piles are being used more widely. Prestressed piles are used because the pre-compression in the concrete controls cracking that develops due to the reflected tension waves generated during the pile driving. These types of piles have relatively high and reliable cracking moment capacities and therefore can be handled easily in long sections.

Figure 2.2 shows the typical cross section of a precast prestressed concrete square pile. Table 2.2 presents the details of square piles with square spiral layouts provided in Louisiana DOTD's Bridge Design Manual (BDM). Two possible sections for each pile size are presented in the table. Each section has 0.5″ diameter, seven wire, uncoated low relaxation, Grade 270

strands. Table 2.3 presents details of the precast prestressed concrete square piles provided by the Florida DOTD. Most of the pile sizes have the same section for Louisiana and Florida DOTD standards. Florida DOTD standard however include more alternatives as it allows for using strand diameters other than 0.5″.

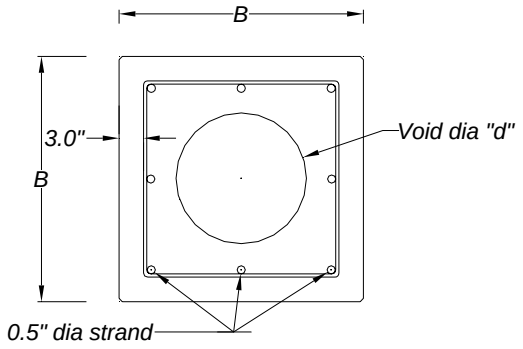

Figure 2.2 Typical square pile (with square spiral layout) section.

Table 2.1 Types of piles used for pile bent system (LA-DOTD BDM 2004)

	Pile Types						
	Precast prestressed Concrete pile (Square)	Precast prestressed Concrete pile (Cyl.)	Cast-in-place Concrete: Steel Pipe piles	Cast-in-place Concrete: Tapered	Timber	Steel "H"	Steel Pipe
Pile Size	14″	54″	14″	14″	Butt Dia. (20″-12″) Tip Dia. (9″-5″)	HP10×62	PP18×3/8″
	16″					HP10×85	
	18″					HP14×108	PP18×3/8″
	24″		16″	16″		HP10×132	
	30″					HP10×152	PP18×3/8″
	36″					HP10×174	

Table 2.2 Precast prestressed concrete pile information (LA-DOTD standards)

Pile Size (in.)	Void "d" (in.)	Strand Dia (in.)	Strand Type	No. of Strands	
				Sec. I	Sec. II
14 solid square	0	0.5	Low relaxation, Grade 270	-	8
18 solid square	0	0.5		-	12
24 solid square	0	0.5		20	24
24″ voided square	10.5	0.5		16	20
30″ voided square	18.5	0.5		24	28
36″ voided square	22.5	0.5		28	36

Table 2.3 Precast prestressed concrete pile information (Florida-DOTD 2004)

Pile Size (in.)	Void "d" in.	Strand Dia. (in.)	Strand Type	No. Of strands	
				Sec. I	Sec. II
14″ solid square	0	0.5	Low relaxation, Grade 270	-	8
		7/16		-	12
		3/8		-	16
18″ solid square	0	0.5		12	16
		7/16		-	20
		3/8		-	24
24″ solid square	0	0.5		20	24
		9/16		-	20
		0.6		-	16
30″ voided square	18	0.5		24	28
		9/16		-	24
		0.6		-	20
High Capacity 30″ voided square	18	0.6		-	28

2.4 Depth of Fixity

A structural frame supported by partially embedded piles subjected to bending moments, shear forces and axial forces can be analyzed considering the piles as free standing columns with fixed base located at some distance below the ground surface. Several studies have been conducted to find out the location of the point of fixity.

Davisson and Robinson (1965) studied the bending and buckling problems associated with partially embedded piles. They developed Equations 2.1 and 2.2 for calculating the depth of fixity of partially embedded piles in different types of soils. AASHTO-LRFD (2004) uses these equations (Article 10.7.3.13.4) for preliminary design purpose.

For clays:

$$L_{df} = 1.4\left[\frac{E_p I_p}{E_s}\right]^{0.25} ft \qquad (2.1)$$

For Sands:

$$L_{df} = 1.8\left[\frac{E_p I_p}{n_h}\right]^{0.2} ft \qquad (2.2)$$

where, L_{df} (ft) is the depth of fixity below ground level, E_p (tsf) is the modulus of elasticity of pile, I_p(ft^4) is the weak axes moment of inertia of pile, n_h (tsf/ft) is the rate of increase of elastic soil modulus with depth for sand, and E_s(tsf) is elastic soil modulus for clay. E_s is equal to $67\ S_u$, where, S_u (tsf) *is* the undrained shear strength of clays.

More sophisticated models represent the soil-pile interaction by accounting for the soil resistance to lateral pile deformation.

2.5 Pile-to-Cap Connections

Partially embedded piles in pile bent type pier systems are often subjected to large lateral deflections and thus high curvatures and bending moments. The behavior of pile-to-pile cap interface plays a significant role in moment demands for both pile and cap. Pile-to-pile cap fixity results in high moment demands at the pile head. However, when rotations are permitted the demands on the connection are reduced.

Harries and Petrou (2001) investigated the capacity of square pile-to-pile cap connections where precast-prestressed pile is embedded in the cast-in-place pile cap. They concluded that (1) the simple plain embedment can be designed to develop the required capacity of the pile, and (2) conservatively, the required embedment length to develop the flexural capacity of the pile may be taken as the width of the pile with a minimum embedment length of 12 in.

The Louisiana DOTD BDM (LA-DOTD 2004) specifies the detailing for the pile-to-pile cap connection. It specifies a simple plain embedment with a minimum embedment length of 9 inch for both single row and double row pile bents. For voided piles the void of the pile embedded into the cap should be poured monolithically with the pile cap. Figure 2.3 shows

typical section of a single row pile bent specified in the manual. It should be noted that the BDM requirement for minimum embedment length is less than what is recommended by Harries and Petrou (2001). This obstruction will have an impact on the research conducted in this study.

Single Row Requirements			
A	*B*	*W*	*H*
14″ϕ	*6″*	*2'-2″*	*2'-0″*
16″ϕ	*6″*	*2'-4″*	*2'-0″*
18″ϕ	*6″*	*2'-6″*	*2'-0″*
20″ϕ	*6″*	*3'-2″*	*2'-0″*
24″ϕ	*6″*	*3'-6″*	*2'-3″*
30″ϕ	*6″*	*4'-0″*	*2'-3″*
36″ϕ	*6″*	*4'-6″*	*2'-3″*

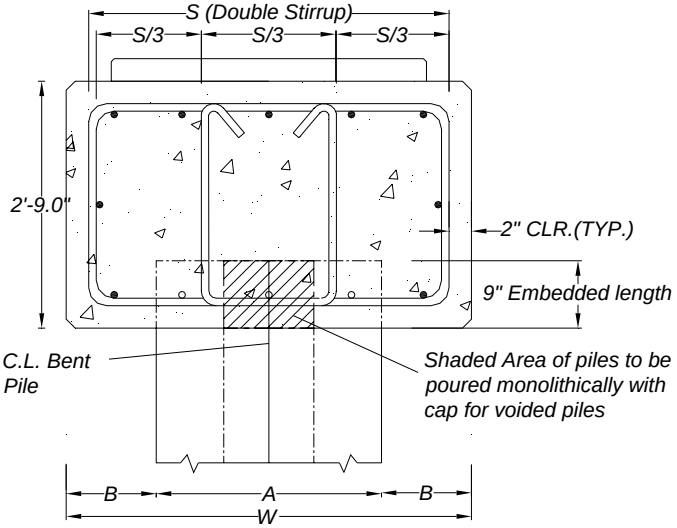

Figure 2.3 Typical Section of Single Row Pile Bents (LA-DOTD 2004)

2.6 Structural Capacity of Prestressed Concrete Piles

2.6.1 Introduction

Due to the load eccentricity and buckling behavior of slender columns, compression members are often subjected to combined axial and bending moments. The axial load-bending moment interaction diagram is the most widely used design tool for compression members. It can be defined as an envelope of all combinations of axial loads and bending moments that would cause failure for a given compression member. Ultimate applied axial load, ultimate applied bending moment and, slenderness ratio (L_P/r) are three essential parameters for these diagrams. Partial fixity connection between the pile and the pile cap will produce some bending in most of the piles (NCHRP 2001). Even when the loadings were applied with zero eccentricity the piles themselves may not be perfectly concentric and the center of resistance may not coincide with the geometric centroid of the section. Furthermore, the pile bent systems in bridge

substructures are subjected to lateral loads that can induce lateral deflection and hence bending moment. When a pile is cut off at grade in stiff soil the slenderness ratio is equal to zero and its lateral deflection is reduced by the surrounding soils. When the pile extends above grade or is driven into very soft soil, it acts as a laterally unsupported column with a slenderness ratio greater than zero. Therefore to design a partially embedded pile one has to consider its failure capacity for the combined effect of axial load and bending moment. Interaction diagrams enable designers to rapidly identify an economic section for this type of pile.

2.6.2 Slenderness Effect

A slender pile can be defined as a pile that has a significant reduction in its axial load capacity due to moments induced by lateral deflection of the pile. An eccentrically loaded pin ended slender column is shown in Figure 2.4**.** The moments at the ends of the pile are M_e. If the pile deflects laterally by an amount "δ", for equilibrium the internal moment at mid height must be $M_m = M + P\delta$. The dashed radial line O-A in the interaction diagram shown in Figure 2.5 represents the load-moment curve for the end moment "M_e" and the curved solid line O-B represents the load-moment curve for maximum column moment "M_m" at an eccentricity "e" where, $e = M_e/P$. The failure of the pile occurs at point B where the load-moment curve O-B intersects the interaction diagram. Thus the axial load capacity is reduced from A to B because of the increase in maximum moment due to lateral deflection. This reduction in axial capacity is termed as the slenderness effect. A generalized interaction diagram is based on a mathematical concept in which the elastic stability of the pile as a slender column is recognized.

2.6.3 Resistance Factor

The capacity reduction factors for flexure and compression are required in order to create interaction diagrams for the piles for resistance factor design. These factors vary depending on

the specifications used. In AASHTO LRFD specifications (2004), for flexure and tension of prestressed concrete members the resistance factor is taken as 1.0. The LRFD specifications use a factor of 0.7 for compression members regardless of whether the transverse reinforcement is tied or spiral (Article 5.5.4.2.1).

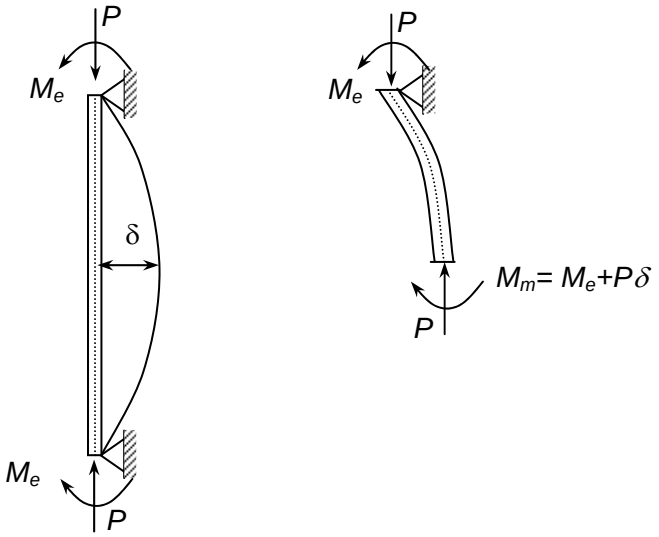

Figure 2.4 Forces in deflected slender pile.

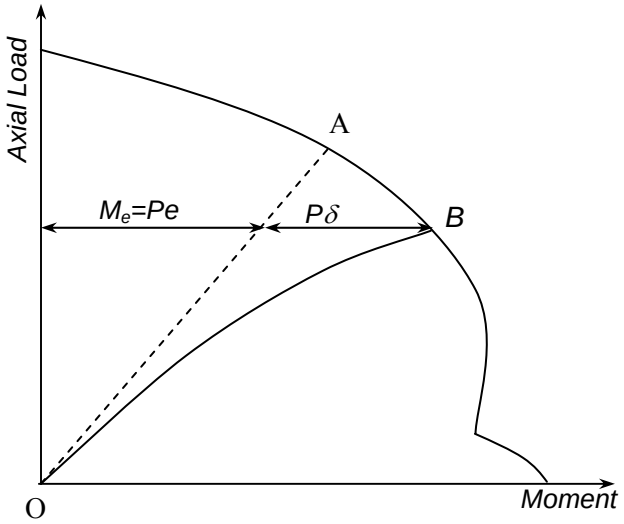

Figure 2.5 Interaction diagram for prestressed concrete pile and slenderness effect

2.6.4 Past Studies on Prestressed Concrete Pile Capacity

Hromadik (1962) presented a method to analyze the ultimate strength of slender prestressed concrete piles. He load tested three prestressed piles and developed a method of

analysis for elastic buckling of slender piles under concentric axial load. The lateral deflection of the pile was ignored until the load reached Euler's critical load. The method considered the nonlinear stress –strain relationship of concrete provided by Hognested (1951).

Zia and Moreadith (1966) presented numerical examples of ultimate strength of 10 in square prestressed column with an eccentricity equal to 30% of the column size, slenderness ratio of 43 and concrete strength of 6500 psi.

Anderson and Moustafa (1970) presented interaction diagrams for the ultimate capacity of a series of standard prestressed concrete piles. Equation 2.3 and 2.4 were used to calculate ultimate load P_u and ultimate moment M_{ur} resisted by the piles respectively.

$$P_u = \int f_c dA_c + \sum_{i=1}^{n} A_{si} f_{si} \qquad (2.3)$$

$$M_{ur} = \int f_c y dA_c + \sum_{i=1}^{n} A_{si} y_i f_{si} \qquad (2.4)$$

Where, P_u is the ultimate axial Load, A_{si} is the area of tendon I, f_{si} is the stress in tendon I, y is the distance from centroid to element dA_c, and y_i is the distance from centroid to tendon i.

In case of piles cut off at grade in stiff soil (with zero slenderness ratio) the ultimate resisting moment is equal to the ultimate applied moment as the surrounding soil prevents lateral deflection or moment magnification. Conversely, partially embedded piles will be subjected to applied moments that are smaller than the ultimate resisting moment due to lateral deflection amplification. Equation 2.5, which is referred to as the secant formula for long column, is the relation between ultimate applied and resisting moment considering the slenderness effect.

$$M_u = M_{ur} / \sec\left(\sqrt{P_u h'^2 / 4EI}\right) \qquad (2.5)$$

Where, M_u and M_{ur} are ultimate applied and resisting moments and h' is the effective height. In this equation the flexural stiffness EI of the member is assumed to have a constant value along

the full height of the member. Using these equations, Anderson and Moustafa (1970) developed a computer program to construct the interaction diagram for prestressed concrete piles stressed to various prestress levels and with various concrete strengths.

Gamble (1979) presented a method for assessing the strength of prestressed concrete piles that are subjected to combined axial and bending moment. He presented some examples of load-moment interaction diagrams for several pile sections. Nominal strength was plotted in his examples excluding the design reduction factors. The strength reduction factor should be higher for piles that can be inspected than those that cannot be inspected after completion. Hence, the author recommended distinguishing between the piles that have been precast or are cast in metal forms from piles cast in uncased holes or holes from which casings have been withdrawn. Former types are the examples of members that can be inspected after completion while the later type is the example of member that can not be inspected.

Nathan (1983) reviewed the behavior of reinforced and prestressed concrete slender columns to point out the differences in response between these two types of members. The author also presented several methods to design slender column and their applicability to prestressed concrete columns.

Rodriguez-Gutierrez and Aristizabal-Ochoa (2001) developed an analytical model and numerical algorithm to determine the M-P-ϕ diagrams including the inelastic structural response, ultimate strength, and failure mode of reinforced concrete, partially prestressed concrete and fully prestressed concrete sections of any cross shape under combined axial and bending load. M-P-ϕ diagram can be defined as the moment-curvature relation for the cross sections under biaxial bending and axial loads. Authors suggested that the biaxial bending behavior and M-P-ϕ diagram of any concrete section depend on cross-sectional characteristics, reinforcement layout,

constitutive stress-strain characteristics of concrete and reinforcement, and type and intensity of applied loads.

2.6.5 PCI Prestressed Concrete Pile Interaction Diagram Spreadsheet

The Precast/Prestressed Concrete Institute (2004) prepared an excel spreadsheet to construct the interaction diagram for prestressed concrete piles as a state-of-the-art design aid for professional engineers. The national specifications, guidelines, and standards which were in effect and applicable as of the date of publication have been incorporated. Slenderness effects are also considered in constructing the interaction diagrams. Two methods, the ACI approach and the Secant Method, are available in the spreadsheet. The methods are based on the aforementioned work by Anderson and Moustafa (1970). The stress-strain relationship for the prestressing strand is modeled using Equation 2.6 from PCI Bridge Design Manual (Eq 8.2.2.5-1), which has been calibrated for typical 270ksi low-relaxation strands. In the equation, f_{si} is the stress in a given layer of reinforcement whose strain is ε_{si}.

$$f_{si} = \varepsilon_{si}\left[887 + \frac{27613}{\left\{1+\left(112.4\varepsilon_{si}\right)^{7.36}\right\}^{\frac{1}{7.36}}}\right] \le 270ksi \qquad (2.6)$$

The following specifications and Codes were used to develop the spreadsheet:

- AASHTO Standard Specification for Highway bridges (17th edition, 2002).
- AASHTO LRFD Bridge Dsign Specifications (3rd edition, 2004).
- ACI 318-99.

2.7 Finite Element Techniques

Several papers that used the finite element approach for bridge analysis have been reviewed to select an efficient model that can accurately capture the response of the pile bents under different loading cases. AASHTO load distribution factors have been used to compare the

girder moments obtained from the line girder analyses to those obtained from FE analyses. In these studies AASHTO distribution factors were found to be larger than the factors obtained in FE analysis.

Imbsen and Nutt (1978) used the finite element method to study load distribution factors on highway bridges. They idealized bridge deck using ICES-STRUDL quadrilateral shell elements with six degree of freedoms at each node. Girders were modeled using eccentrically connected space frame elements. The finite element model set up is similar to that shown in Figure 2.6 except that the rigid links were imposed to accommodate the eccentricity of the girders.

Hayes et al. (1986) studied the lateral load distribution factors using FE models. The bridge superstructure was modeled using plate elements for the concrete slab and space frame elements for the steel girders. The centroid of each girder was coinciding with the centroid of concrete slab as shown in Figure 2.6.

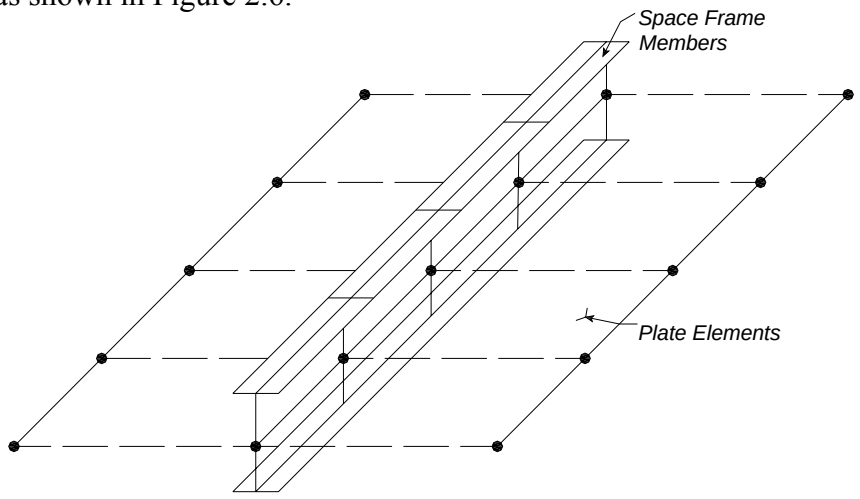

Figure 2.6 Typical Concrete Deck and Girder Element (Case 1).(Hays et al. 1986)

Brockenbrough (1986) used FE models to study the distribution factors for curved I girder bridges. The bridge superstructure was idealized using MSC/NASTRAN quadrilateral shell

elements for the concrete deck, space frame members for girder flanges, shell elements for the girder web. Flange to deck eccentricity was model using rigid links as shown in Figure 2.7.

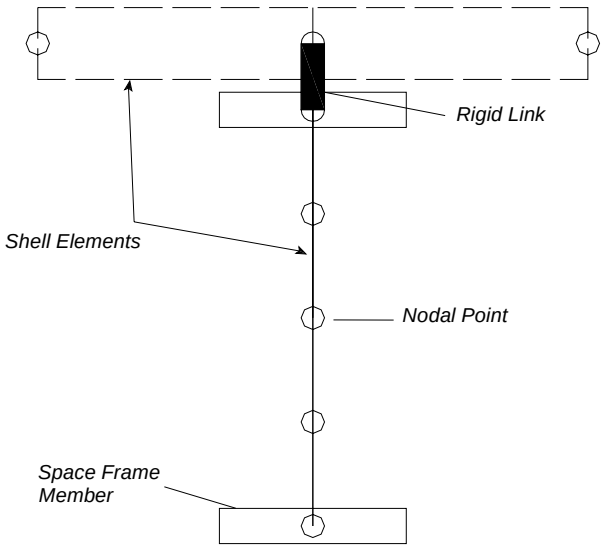

Figure 2.7 Typical Cross section of a part of finite element model (Case 3).
(Brockenbrough 1986)

Tahrini and Fredrick (1992) used ICES-STRUDL II finite element package to idealize the bridge superstructure using. The concrete slab was modeled as an isotropic eight node brick element with three degrees of freedom at each node. The steel girder flanges and webs were modeled using quadrilateral shell elements with six degrees of freedom at each node.

Tarhini et al. (1995) compared various finite element techniques reported in the literature that could be adopted in evaluating bridge superstructures. The finite element program SAP90 was used to reproduce three types of models proposed in past studies and perform the analysis for a typical one span composite I-girder highway bridge. The first model (see Figure 2.6) reproduced the model proposed by Hayes et al. (1986). The second model idealized the deck as quadrilateral shell elements with 5 DOFs at each node and the girders as space frames with 6 DOFs at each node. The separately generated nodes for deck and girders had the same

coordinates and were linked using the CONSTRAINTS option in SAP90. The Third model (see Figure 2.7) reproduced the model proposed by Brockenbrough (1986) and idealized the concrete deck as quadrilateral shell elements, girder flanges as space frame elements and girder webs as quadrilateral frame elements. The CONSTRAINTS option was used to link the common nodes at the interface between deck and girder flanges. Finally, the fourth model idealized the concrete deck as brick elements and the girder flanges and webs as quadrilateral shell elements. The study concluded that (1) the bridge superstructures can be modeled using shell elements for the concrete deck and space frame elements for the girders, (2) rigid links can be used to account for eccentricity, and (3) Cases 3 and 4 can be used for special bride cross sections to represent actual geometry but they are more time consuming in terms of both model generation time as well as computation time.

Zokaie (2000) presented the background on the development of the latest AASHTO-LRFD live load distribution formulas and compared their accuracy with the more simplified S/D method adopted in AASHTO Standard Specifications (AASHTO 1994). A discussion on the extension of the single girder design to the skewed bridges is also presented in his paper. A computer program GENDEK5A (Powell and Buckle 1970) was used to model the bridges. The program uses plate element to model the deck slab and it can model the eccentricity of the beams. The distribution factors were calculated by loading the deck model with truck loads positioned at the longitudinal location that produces the maximum moment. The trucks were then moved transversely across the width of the bridge. The largest girder moment for all locations was selected as the maximum moment. The procedure was repeated for any number of trucks that fit on the bridge transversely, and the maximum moment was adjusted by the multiple presence reduction factors. The ratio of the controlling moment to the moment obtained from a

simple beam loaded by one truck wheel line represents the wheel load distribution factor. The study concluded that the formulas developed for the moment/shear distribution for both non-skewed and skewed bridges generally produce results that are within 5% of the results of a finite element analysis.

Barr et al. (2001) conducted a study to evaluate the accuracy of finite element model strategy on load distribution. The study focused on strategies for: (1) evaluating code expressions for live load distribution factors for prestressed concrete girder bridges and, (2) evaluating the influence of the haunch (the layer of concrete between the top of the girder and the bottom of the deck), intermediate and end diaphragms, continuity, skew and load type (truck or lane) on load distribution. The finite element program SAP2000 was used to model the superstructure. Figure 2.8 shows the arrangement of the nodes and elements in the model. The vertical location of the deck, haunch, and girder elements reflected accurately the location of those members in the bridge. The finite-element model included columns and a pier cap beam at the intermediate piers. Both were modeled with 2 node 1 foot long frame elements that have 6 degrees of freedom (DOFs) at each node. At each abutment, the elastromeric bearings were represented by releasing the horizontal displacement. The study led to the following conclusions: (1) a detailed modeling strategy of the bridge using shell elements, frame elements and rigid constraints can accurately reproduce the moments calculated from strains measured during live load tests, (2) AASHTO LRFD live load distribution factors gave conservative results for all bridge configurations, however, the degree of conservatism varied greatly among the configurations. The distribution factors calculated with the AASHTO LRFD procedures were up to 28% larger than the factors calculated with the finite element model that has been verified against the live load test. However, for the configuration most similar to that considered in developing the LRFD

specifications (Simply supported, no haunch, no diaphragms) the code distribution factors were on average only 6% higher than those computed with finite element analysis., (3) if the distribution factors from the finite element model of the bridge had been used to design the girders instead of the conservative factors from the LRFD specifications, the bridge could have been designed for a 39% higher live load.

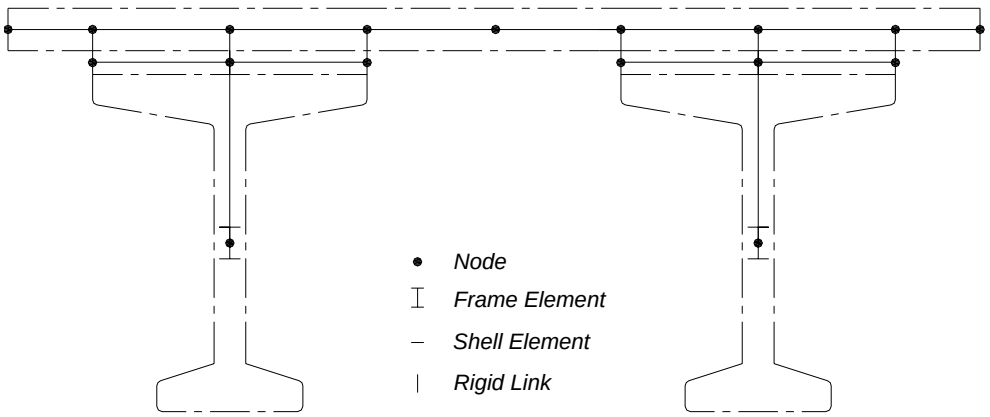

Figure 2.8 Cross section of finite element model for two girders (Barr et al. 2001).

2.8 Louisiana DOTD Guidelines for Design of Pile Bents

2.8.1 Introduction

The LA-DOTD BDM (2004) provides a simplified design procedure for pile bents. The simplified method is only applicable to situations where certain conditions are met. These are allowable slenderness ratio, pile spacing, and allowable axial loads. Some of the guidelines are cited below:

2.8.2 Allowable Slenderness Ratio

According to the BDM (2004), the pile size should be proportioned so that the maximum slenderness ratio, L_P/d is no larger than 20, where d is the least dimension or diameter of the pile section (ft) and L_P is the unsupported length (ft.). The unsupported length is measured down below the ground level accounting for the scour depth (5 ft. minimum), if appropriate, plus a

distance to the assumed point of pile fixity. In general, the depth of pile fixity can be assumed 5 ft below scour line or ground line. If the slenderness ratio, L_P/d, exceeds 12, the exterior piles should be battered and the maximum batter is usually 1.5 on 12 for pile bents.

2.8.3 Pile Spacing

Center to center spacing for the piles should not be less than three times the pile diameter or least dimension. The centerline at the top of the exterior pile shall not be more than 18 inch beyond the centerline of the exterior girder.

2.8.4 Allowable Axial Load

The manual provides Table 2.4 for the selection of pile size. Allowable factored axial loads for different pile types and sizes are presented in the table. The bridge should be analyzed to determine the factored axial compression load in piles according to AASHTO LRFD (2004) considering dead and live loads only. The maximum factored compression load on the pile must fall within the range shown in the table for each pile size.

Table 2.4 Maximum factored axial compressive load allowed for the pile bents.

Pile Type	Pile Size	Maximum Factored Axial Compressive Load Allowed	Standard Detail Name
Precast Prestressed Concrete Piles (square)	14″	55-85 tons	CS-216
	16″	70-100 tons	
	18″	75-115 tons	
	24″	120-180 tons	
	30″	200-300 tons	
	36″	260- 400 tons	
Precast Prestressed Concrete Piles (Cylindrical)	54″	340 -420 tons	54″ Prestressed Cylinder pile

The simplified design approach in LA-BDM is intended to save time without jeopardizing safety. It was initially developed before the introduction of AASHTO-LRFD. Consequently, load demands have changed since it was introduced. Furthermore, superstructure span lengths have

been increasing as better materials and construction methods become available. Hence, it is prudent to investigate the limitation of this method considering current design practices. This is the main motivation behind this study.

CHAPTER 3. CONVENTIONAL ANALYSIS

3.1 Introduction

This chapter describes the details of the conventional structural analysis procedure used for the design of bridge bents. AASHTO-LRFD (2004) loads and limit states were considered in this analysis. Girder reactions due to dead load, live load, and wind load on super structure were determined and applied on a two dimensional (2-D) frame model consisting of piles and pile cap. Substructure loads were also calculated and applied on the frame model. The model was then analyzed using the commercially available structural analysis software package STAAD Pro. to investigate the straining action demand on the piles. A full design example is provided in Appendix B. The example is intended to provide guidance on the application of the AASHTO LRFD bridge design specifications when applied to bridges supported on pile bents.

3.2 Bridge Geometry

An existing bridge model (Buyou Ramos Bridge 1990) was considered for selecting the common bridge parameters including bridge width, barrier type, girder spacing, cap width, and cap height. Bridges with 30ft, 50ft, 76ft, and 100ft span lengths were selected for this study. Type of girder for each span was selected using the "Chart of Span Range Limit for Precast-Prestressed Girder" (Appendix C) provided in BDM (LA-DOTD 2004). Trial analyses were conducted considering assumed pile sizes to obtain factored axial loads on bent piles for dead load and live load only. These factored loads were then used to determine the final pile size for each case in accordance with Table 2.4. In determining the number of piles, the limits on pile spacing in the BDM were complied with. Different unsupported pile lengths for each pile size within the allowable slenderness ratio were considered. Table 3.1 presents the various bridge parameters considered in this study. The cross-sectional properties for AASHTO Type II, III and IV prestressed girders are given in Table 3.2. Table 3.3 presents the material properties used for

the bridge model. Figure 3.1 shows a typical bridge cross section of the analyzed bridges. The main superstructure dimensions were similar for all four spans. Figure 3.2 shows the elevation of a typical four span segment. In the bent arrangement it was assumed that Bent #4 is the only longitudinal force resisting component. Hence, it is a 'double-pile' bent and the connection between it and the superstructure is indicated with 'F'. The other bents were assumed to resist lateral loads in the transverse direction but not in the longitudinal direction. This arrangement is typical in bridge construction. This study focuses on a typical 'single-pile' bent that is more susceptible to lateral loads than 'double-pile' bent. Therefore, all results reported in the research are extracted for Bent #5.

Table 3.1 Bridge parameters for different span lengths used for the study.

Span (ft)	Girder type	No. of Girders	Girder Spacing (ft)	Pile Size (in.)	No. of Piles	Pile Spacing (ft)	Unsupported Pile Length L_P(ft)	Slenderness Ratio	Exterior pile orientation
30	II	6	7.33	18″ Solid	6	6.73	18	12	Straight
							24	16	Battered
							30	20	Battered
50	II	6	7.33	24″ Solid	5	8.41	18	9	Straight
							24	12	Straight
							30	15	Battered
							40	20	Battered
76	III	6	7.33	30″ Voided	3	15	18	7.2	Straight
							24	9.6	Straight
							30	12	Straight
							40	16	Battered
							50	20	Battered
100	IV	6	7.33	36″ Voided	3	15	30	10	Straight
							40	13.3	Battered
							50	16.6	Battered
							60	20	Battered

Table 3.2 Section properties of the prestressed girders used for the study.

Girder Type	Area ($in.^2$)	Girder Ht. (in.)	y (in.)	Moment of Inertia (in^4)	Bottom Sec. Mod. (in^3)	Top Sec. Mod. (in^3)
II	369	36	15.83	50,980	3,220	2,527
III	559	45	20.27	125,390	6,186	5,070
IV	789	54	24.73	260,730	10,543	8,908

Table 3.3 Material Properties used for bridge model

Material Type		Ultimate Strength (ksi)	Modulus of Elasticity (ksi)	Poisson's ratio
Concrete	Deck	4.0	3,834	0.18
	Type II Girder	6.0	4,696	0.18
	Type III Girder	6.0	4,696	0.18
	Type IV Girder	6.0	4,696	0.18
	Pile	6.0	4,696	0.18
Steel	Prestessing Strand (0.5″ L.R.)	270	28,500	0.29

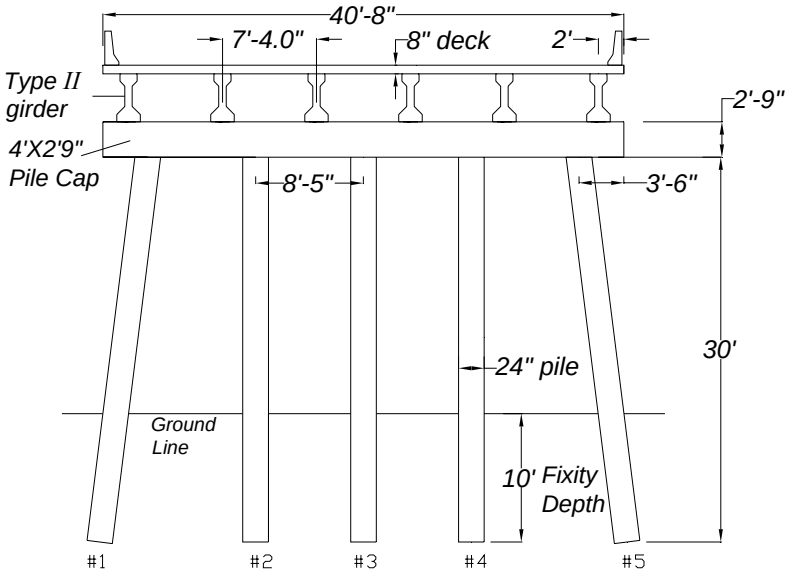

Figure 3.1 Typical cross section of a 50ft span Pile Bent Type Bridge.

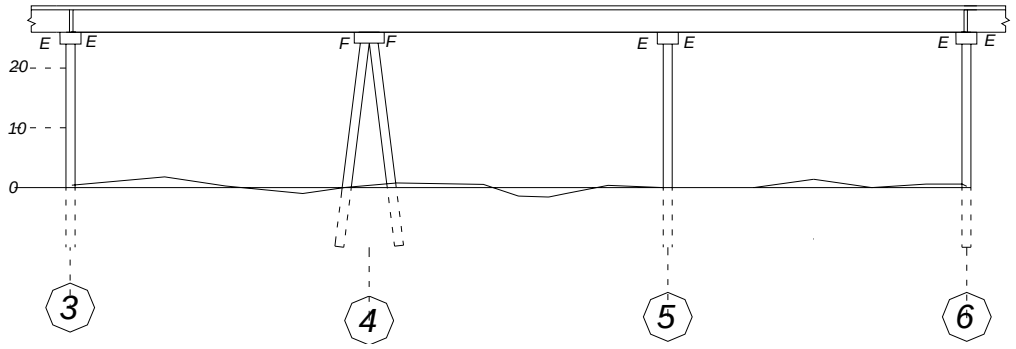

Figure 3.2 Bridge elevation showing typical three-span segment considered in this study.

3.3 Load Cases, Factors and Combinations

Different static load cases based on AASHTO-LRFD bridge design specifications (AASHTO 2004) were considered. Two load combinations were considered to determine the critical axial loads and moments on the pile bents, namely Strength III and Strength V. Table 3.4 lists the load factors for each limit state. Strength III is the limit state for bridges exposed to wind velocities exceeding 55 mph. High wind prevents the presence of significant live load on the bridge as vehicle become unstable at excessive wind velocity and hence is not included in Strength III. Strength V is another limit state that considers wind effects on bridges. Because of the limitation on wind velocity (55 mph) vehicular loads are not ignored.

Table 3.4 Load factors (γ) for different load combinations.

Static Load Case	Load Designation	Load Combination	
		Strength III	Strength V
Dead Load of Structural Components and Nonstructural Attachment	DC	1.25	1.25
Dead Load of Wearing Surface and Utilities	DW	1.5	1.5
Vehicular Live Load (HL-93)	LL	-	1.35
Wind on Live Load	WL	-	1.00
Wind Load on Structure	WS	1.4	0.4
Breaking Force	BR	-	1.35

3.4 Load Calculation for Different Load Cases

3.4.1 Introduction

Frame models consisting of piles and pile cap were generated in STAAD Pro 2004 for different non-skew bridges considering the parameters shown in Table 3.1. Girder reactions due to loads on superstructures for each load cases were calculated to apply on the pile cap. Loads on

substructure were also calculated and applied on the model. A computer program was written to calculate individual girder reactions which are then applied on as the loads on the substructure. The source codes for the program are provided in Appendix A.

3.4.2 Girder Reactions Due to Loads on Super Structure

3.4.2.1 Dead Load (DC and DW)

The self weight of the super structure consisting girder, slab, haunch, barrier, and diaphragms were calculated for interior and exterior girders according to their geometric dimensions and unit weights. The superstructure self weight per girder line was assumed to be applied on each girder and exterior and interior girder reactions on the pile cap, P_{DC}, were calculated considering the loadings as shown in Figure 3.3.

A 30 psf surface load for future wearing surface (FWS) was also considered. It was assumed that it will be applied on the deck surface excluding the surface occupied by the barrier.

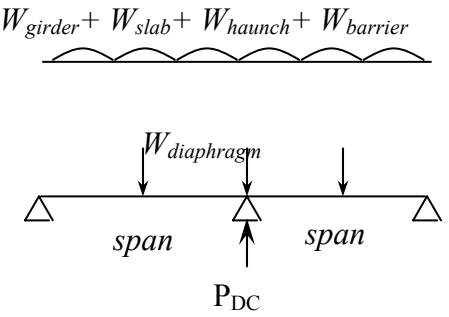

Figure 3.3 Superstructure self weight on girder line

3.4.2.2 Live Load (LL)

AASHTO's HL-93 vehicular live load (AASHTO-LRFD 2004) was used in this study. Figure 3.4 shows the transverse positioning of the design truck considered in the study. As can be seen, two and three lane loads positioned near the barrier were considered to capture the

maximum pile reaction. Wind effects on the design trucks (Wind on Live) were considered from two opposite directions to append the wind action. Figure 3.5 shows another two positions of the design truck that were considered during the initial stage of the study. However, results obtained for these two cases were not critical and hence were discarded later. From several analyses of a single bridge model with different vehicle positions as shown in figure 3.4 and 3.5 it was found that the vehicular loads positioned near the barrier produced maximum capacity utilizations by the critical piles. To obtain the maximum response on the piles along intermediate pier line #5 (Figure 3.2), longitudinal loading position as shown in Figure 3.6 was considered. Maximum live load reaction per span per wheel, P, as shown in Figure 3.7 can be calculated using equation 3.1.

$$P = \frac{1}{2} \times m.f. \times \left[\left\{ 32 + 32 \times \frac{(L_1 - 14)}{L_1} + 8 \times \frac{(L_2 - 14)}{L_2} \right\} \times \frac{1}{2} + 0.64 \times \frac{\frac{1}{2}(L_1 + L_2)}{2} \right] \tag{3.1}$$

where, m.f. is the multiple presence factor with the values, 1.0 for two lane loading and 0.85 for three lane loading cases, L_1 and L_2 are the span lengths on two sides of the bent. It should be noted that Equation 3.1 is only valid for girders designed with live load continuity measures. Girder reactions R1 through R6 on the pile cap due to live load were calculated using the lever rule. Figure 3.8 shows the simply-supported deck segments used for the reaction calculations according to the lever rule. These reactions were applied on the pile cap as shown in Figure 3.9.

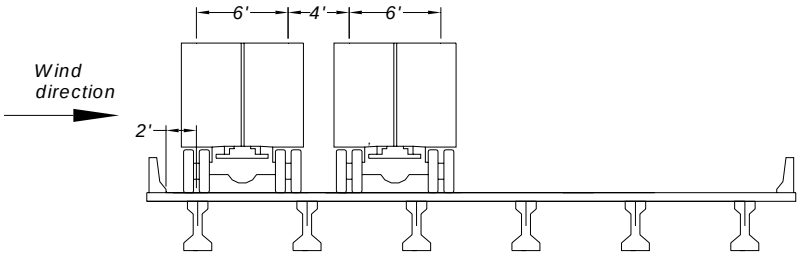

(a)

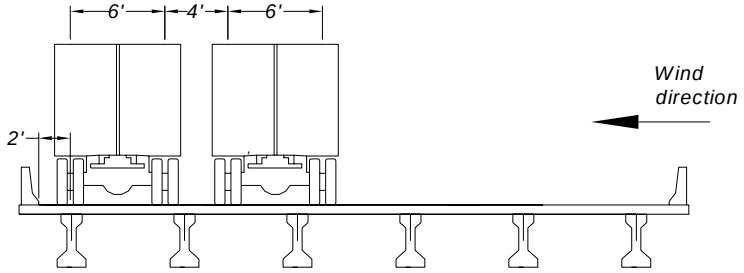

(b)

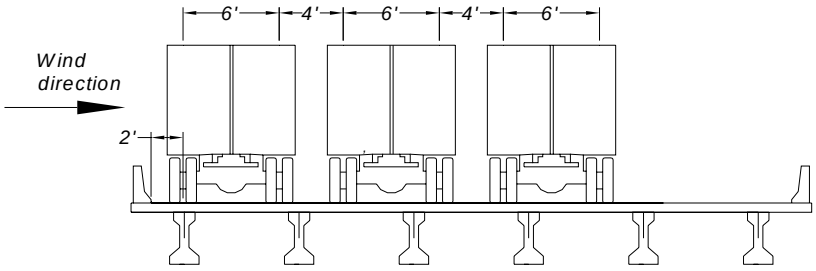

(c)

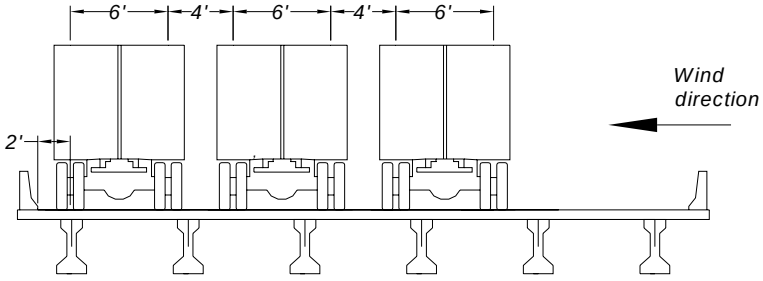

(d)

Figure 3.4 Live Load and Wind Load Cases: (a) Two lane live load, rightward wind load (b) Two lane live load leftward wind load(c) Three lane live load, rightward wind load and (d) Three lane live load, leftward wind load.

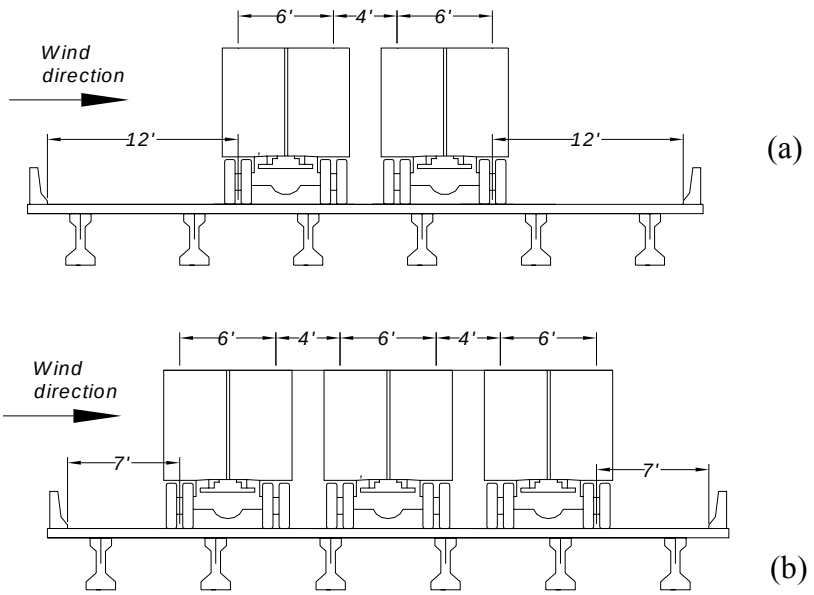

Figure 3.5 Live and Wind Load Cases: (a) Two lane live load, (b) Three lane live load centered at the mid section of the bridge in transverse direction.

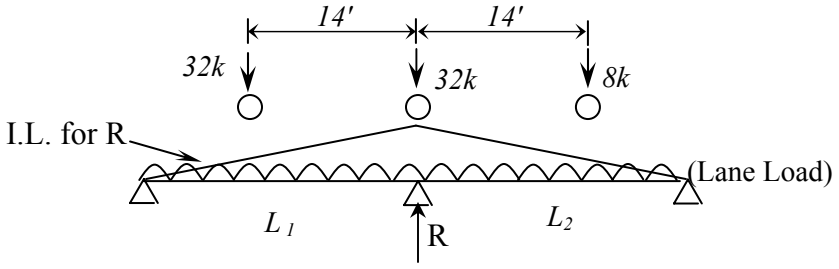

Figure 3.6 Longitudinal LL axle position for maximum pier reaction.

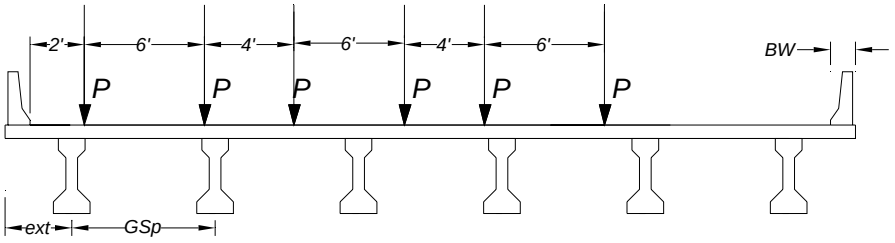

Figure 3.7 Transverse LL wheel positions for Cases C and D

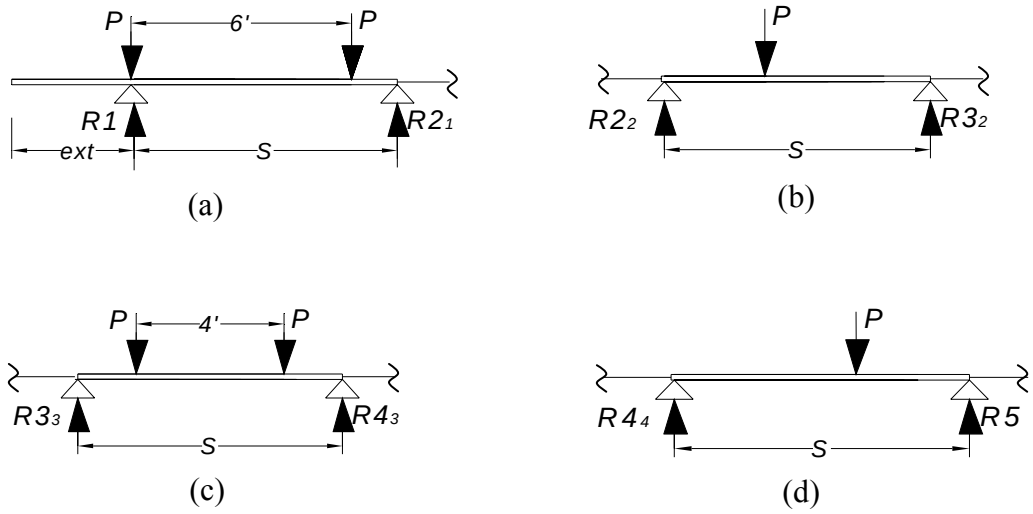

Figure 3.8 Assumed Simply-supported deck segments for LL reaction calculations using lever rule

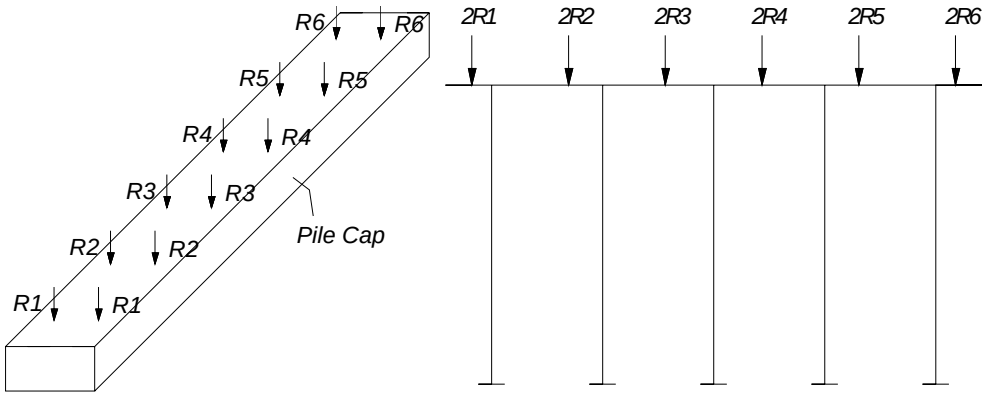

Figure 3.9 Girder reactions on pile cap due to live load.

3.4.2.3 Breaking Force (BR)

Breaking forces are applied on the pile caps where connections between the girders and the pile cap are considered to be fixed. Therefore, the breaking force effect can be neglected for calculating maximum pile response along the intermediate pier line #5 (Figure 3.2) where

longitudinal girder movement is permitted. However to generalize the load calculation procedure, a method to calculate the girder reactions due to breaking force is described next.

According to AASHTO (2004) article 3.6.4, breaking force,

$$\text{BR} = \text{greater of} \begin{cases} = 0.25 \times (DesignTruck) \times N_L \times m.f. \\ = 0.05 \times (DesignTruck + LaneLoad) \times N_L \times m.f \\ = 0.05 \times (DesignTendem + LaneLoad) \times N_L \times m.f \end{cases}$$

i.e., For HL-93 loading

$$\text{BR} = \text{greater of} \begin{cases} = 0.25 \times (32 + 32 + 8) \times N_L \times m.f. \\ = 0.05 \times (72 + 70 \times 2 \times 0.64) \times N_L \times m.f. \\ = 0.05 \times (25 \times 2 + 70 \times 2 \times 0.64) \times N_L \times m.f. \end{cases}$$

Breaking force per vehicle, $P_B = \dfrac{BR}{N_L}$

where, *m.f.* is multiple presence factor, and N_L is the number of lanes. According to the AASHTO-LRFD (2004), the breaking force per vehicle, P_B, should be placed on all design lanes which are considered to be loaded and should be assumed to act horizontally at a distance 6 ft above the deck surface in either longitudinal direction to cause extreme force effects. The effect of 6ft eccentricity above the deck surface, however, can be neglected for the longitudinal vehicle position considered in this study. This is because the moment generated due to the eccentricity causes an equal amount of increase and decrease in load on the front and rear wheel respectively (Figure 3.10).

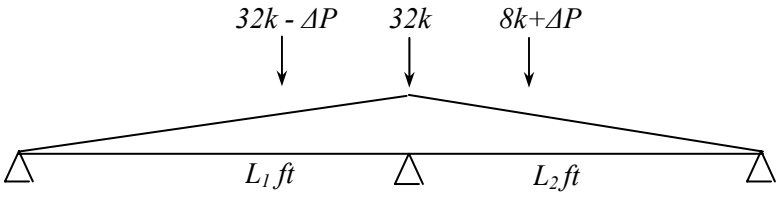

Figure 3.10 Overturning effect on the vehicle due to the eccentricity of Breaking Force

In response to the horizontal action of the breaking force, the bridge superstructure may be assumed to act as rigid body causing a moment about vertical axis. Using Figure 3.11 the horizontal reactions on the girders due to the breaking forces can be written as:

$$B_i = \frac{\sum_j P_{Bj}}{N} + \frac{\sum_j P_{Bj} \times e_j}{\sum_i y_i^2} \times y_i \qquad (3.2)$$

where, B_i is the horizontal reaction on girder i, P_{Bj} is the breaking force per vehicle for vehicle j, e_j and y_i are the eccentricity of vehicle j and girder i respectively with respect to centerline of the bridge cross-section.

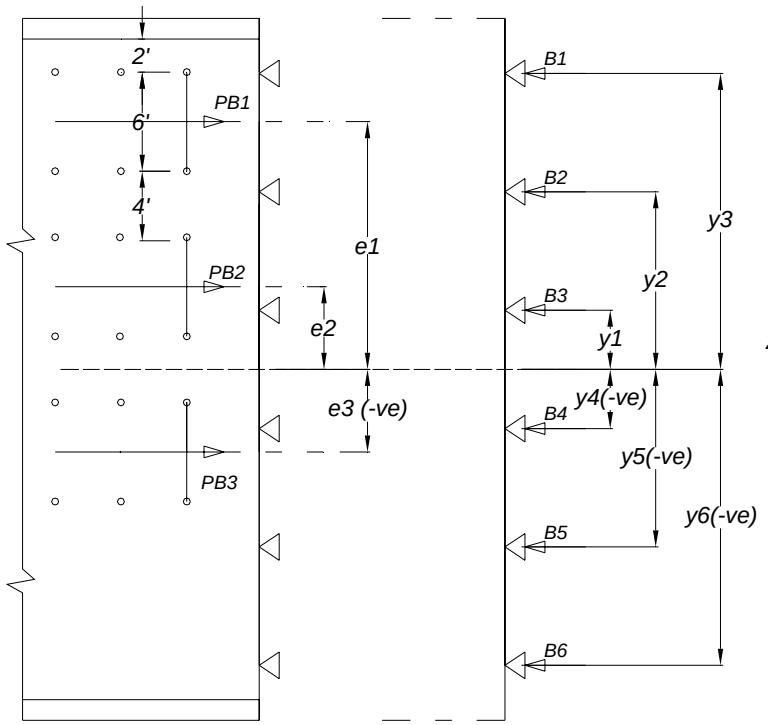

Figure 3.11 Girder reactions due to breaking force acting on a bridge deck for three lanes loading.

3.4.2.4 Wind on Live Load (WL)

Figure 3.4 shows the vehicle position in transverse direction for two live load cases. For each case, wind from two opposite direction was considered in this study while calculating the

wind load. According to AASHTO-LRFD (2004), wind load on vehicle should be represented by a moving force of 0.1 klf acting normal to and 6.0ft above the roadway. When wind on vehicle is taken at an angle with the normal from the structure, the component of normal and parallel force applied on the live load may be taken as specified in Table 3.5. The horizontal line load and its eccentricity can be treated as concentrated vertical forces acting on the deck surface as shown in Figure 3.12. The transverse wind force, which numerically is the same as the vertical forces in Figure 3.12, was calculated using the following equation:

$$F_{TLL} = F_w \times \frac{\left(Span_{back} + Span_{ahead}\right)}{2}. \qquad (3.3)$$

where, F_w is the wind component on Live Load whose values are presented in Table 3.5**.** Girders reactions due to the wind pressure on live load can be calculated using the lever rule (Figure 3.12b).

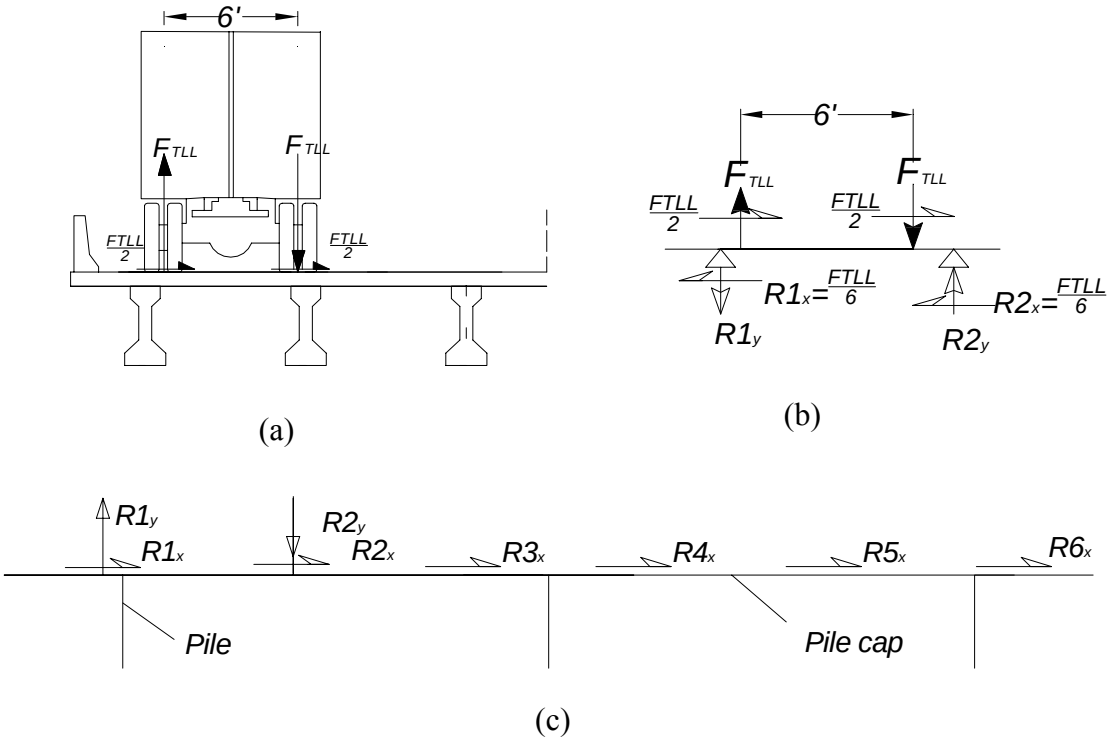

Figure 3.12 (a) Simplified Loading on the deck surface due to the wind pressure on live load (b) Beam segment simplified according to the lever rule, and (c) Girder reactions on the pile cap.

Table 3.5 Wind Component on live load (AASHTO 2004, Table 3.8.1.3-1)

Skew Angle (degrees)	Normal Component (klf)	Parallel Component (klf)
0	0.100	0.000
15	0.088	0.012
30	0.082	0.024
45	0.066	0.032
60	0.034	0.038

3.4.2.4 Wind on Super Structure (WS)

In the absence of more precise data, according to Article 3.8.1.2 of AASHTO-LRFD (2004), design wind pressure, P_w, may be determined as

$$P_w = P_B \times \left(\frac{V_{DZ}}{V_B}\right)^2 = P_B \times \left(\frac{V_{DZ}}{100}\right)^2 \quad (3.4)$$

$$V_{DZ} = 2.5 V_o \left(\frac{V_{30}}{V_B}\right) \ln\left(\frac{Z}{Z_0}\right) \quad (3.5)$$

where P_B (ksf) is the base wind pressure specified in Table 3.6, V_{DZ} (mph) is the design wind velocity and can be calculated using Equation 3.5. V_B (mph) is the base wind velocity of 100mph at 30 ft height, Z(ft) is the height of structure at which wind loads are being calculated as measured from low ground or water level (>30ft). V_0 (mph) is the friction velocity, a meteorological wind characteristic taken as specified in Table 3.7, and Z_0(ft) is the friction length of upstream fetch taken as specified in Table 3.7. V_{30} is the wind velocity at 30ft above low ground or design water level and can be obtained from the fastest mile-of-wind charts as given in ASCE 7-95 for various recurrence intervals. The chart is provided in Appendix C. The maximum wind velocity at 30 ft height is 150mph in Louisiana. Table 3.8 presents design wind velocities obtained using Equation 3.5 for various V_{30}'s of Louisiana under different upstream surface conditions. For V_{DZ} greater than 55mph Strength III limit state should be used in which higher load factors are considered for wind while live loads are ignored. As can be seen, for Louisiana

state city areas Strength V limit state can be used to obtain critical pile capacity as the design wind velocities, V_{DZ}, for city areas are below 55 mph for most of the cases.

Table 3.6 Base wind pressure, P_B for various angles of attack for Vb=100mph (Table 3.8.1.2.2-1 in AASHTO 2004).

Skew Angle of wind (degree)	Trusses, Columns and Arches		Girders	
	Lateral Load (ksf)	Longitudinal load (ksf)	Lateral Load (ksf)	Longitudinal load (ksf)
0	0.075	0.000	0.050	0.000
15	0.070	0.012	0.044	0.006
30	0.065	0.028	0.041	0.012
45	0.047	0.041	0.033	0.016
60	0.034	0.050	0.071	0.019

Table 3.7 Values of V_0 and Z_0 for various upstream conditions (Table 3.8.1.1-1 in AASHTO 2004)

Condition	Open Country	Suburban	City
V_0(mph)	8.20	10.90	12.00
Z_0 (ft)	0.23	3.28	8.20

Table 3.8 Design wind velocity for various V_{30}'s (wind velocity at 30ft above ground level) of Louisiana under different upstream surface conditions.

V_{30} (mph)	150	140	130	100
Upstream surface condition	Design wind velocity V_{DZ} (mph)			
City	58	54	51	39
Suburban	90	84	78	60
Open Country	150	140	130	100

The wind load on super structure was calculated by multiplying the contributing area (Figure 3.12) by the design wind pressure. Equation 3.6 and 3.7 were used to calculate the wind load on superstructure in the direction perpendicular to the bridge span (F_{Tsuper}) and parallel to the bridge span (F_{Lsuper}) respectively. The resultant wind load perpendicular to the pier axis (F_{Lp}) was calculated using equation 3.8. Similarly, the resultant wind load parallel to the pier axis (F_{Tp}) acting on the center of the contributing area as shown in Figure 3.13 was calculated using Equation 3.9.

$$F_{T\,super} = P_w \times H_{wind} \times \frac{\left(Span_{back} + Span_{ahead}\right)}{2} \tag{3.6}$$

$$F_{L\,super} = P_w \times H_{wind} \times \frac{\left(Span_{back} + Span_{ahead}\right)}{N_{fixedpier}} \tag{3.7}$$

$$F_{Lp} = F_{L\,super} \times \cos(\theta_{skew}) + F_{T\,super} \times \sin(\theta_{skew}) \tag{3.8}$$

$$F_{Tp} = F_{L\,super} \times \sin(\theta_{skew}) + F_{T\,super} \times \cos(\theta_{skew}) \tag{3.9}$$

where P_w, is the design wind pressure, H_{wind} is the height of the contributing area (Figure 3.13) and hence is the summation of the heights of barrier, deck, haunch and girder, $N_{fixedpier}$ is the number of pier lines with pile cap-to-girder connections capable of resisting horizontal movement due to the wind load parallel to the bridge span, θ_{skew} is the skew angle (angle with respect to an imaginary line normal to the longitudinal axis) of the critical wind direction.

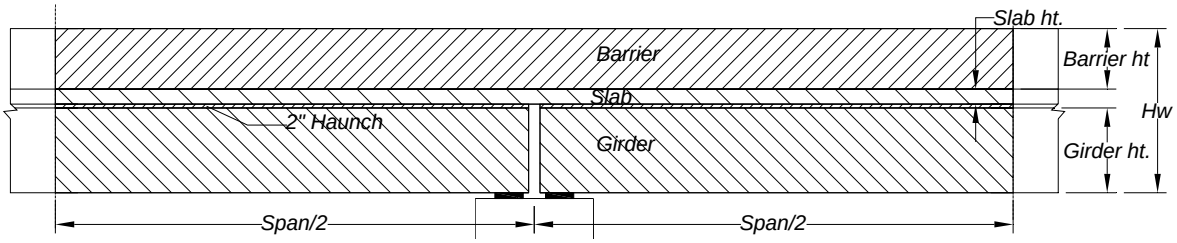

Figure 3.13 Contributing area for transverse wind load for each pier line.

In response to the transverse wind load as shown in Figure 3.14, the superstructure may be assumed to act as a rigid body which causes an overturning effect. The vertical reaction on the girders due to this effect can be written as:

$$R_i = \frac{F_{tp} \times e}{\sum y_i^2} \times y_i \tag{3.10}$$

where R_i is the vertical reaction on girder i due to the transverse wind load on superstructure; F_{Tp} is the wind load acting parallel to the pier axis; e is the eccentricity of F_{Tp} with respect to the

girder centroid; y_i is the eccentricity of girder i with respect to the center of the bridge cross section.

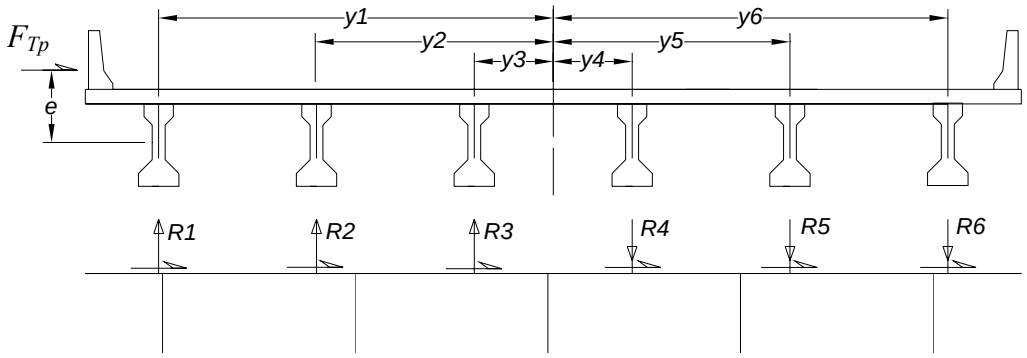

Figure 3.14 Girder reactions on pile cap due to wind load on super structure

3.4.3 Loads on Sub Structure

3.4.3.1 Dead Load for Sub Structure (DC)

Dead load or self weight of the substructure for a pile cap-pile model can be assigned directly on the frames in structural analysis software like STAAD Pro. The model will generate the self weight itself from the section and material properties assigned for each member.

3.4.3.2 Wind on Sub Structure (WS)

According to the article 3.8.1.2.3 in AASHTO-LRFD (2004), the transverse and longitudinal forces to be applied directly on the substructure should be calculated from an assumed base wind pressure, P_B of 0.040 ksf. The design wind pressure was calculated using Equation 3.4. Transverse wind load on pile cap, F_{Tcp} was applied as a concentrated load on the centroid of the cap face and was calculated by multiplying the area of the cap face in transverse direction with the design wind pressure. Longitudinal wind load on pile cap, W_{Lcp} can be applied as a line load on the cap frame. The line load can be obtained by multiplying the cap length with the design wind pressure. Transverse wind load on pile, W_{Tpile} was also applied as a line load on the pile frame. The value was obtained by multiplying the pile width with the design wind

pressure. Figure 3.15 shows the pile cap-pile model with the transverse wind load on substructure. The depth of fixity was assumed to be minimum (10 ft) in this study. This choice leads to the most critical wind loading condition without affecting other load effects.

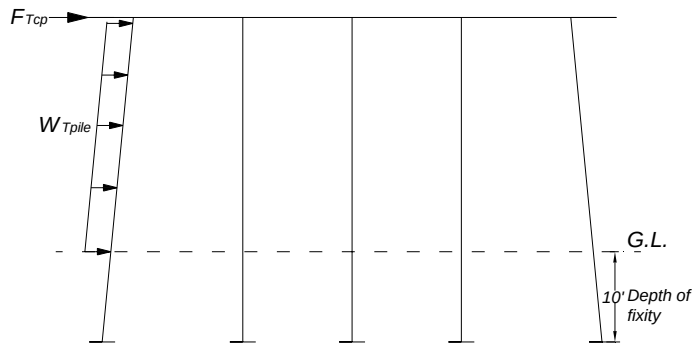

Figure 3.15 Pile Cap- Pile model generated in STAAD Pro 2004 with the transverse wind load on substructure.

3.4.4 Computer Program for the Load Calculation

Using the procedures described above, a computer program was developed in FORTRAN to calculate the bridge loads that can be applied on a simple cap-piles model. The input file for the program requires bridge dimensions, 1st wheel position from the barrier interior face, breaking force per vehicle and base wind pressure. The program source code, sample input file, and output file generated by the program are provided in Appendix A.

3.5 Conclusion

The conventional analysis approach was used in this study to (i) select the pile sizes for different bridge spans using Louisiana's BDM guidelines, and (ii) validate the results obtained from the finite element bridge models generated for the parametric study. This chapter provides a guideline on the application of the AASHTO-LRFD bridge design specifications, and the conventional analysis method for bridge bents.

CHAPTER 4. REFINED ANALYTICAL PROCEDURE AND PARAMETRIC STUDY

4.1 Introduction

Detailed finite element analyses of bridges with different configurations were conducted in this study to investigate the capacity utilization of bent piles. This chapter presents the procedures used to develop the 3-D finite element models using the commercially available finite element package SAP 2000. The decision to use a refined analysis method was deemed more appropriate to account for any three-dimensional (3-D) structural system interactions that can not be captured using two-dimensional (2-D) models. The model was first verified by comparing the girder load distributions to AASHTO load distribution factors. The model was then used in parametric study where various characteristics were changed to investigate their effects on the pile response. The parametric study included 128 models to study the response.

4.2 Bridge Characteristics

Four major parameters were considered in the present study. These are: (1) Span length, (2) Unsupported pile length, (3) Skew angle, and (4) pile-to-cap connectivity. A typical roadway width and bridge cross section (girder spacing, deck thickness, barrier) were assumed for the study. The actual pile-to-cap connection is not completely rigid. To address this partial fixity, two cases of pile-to-cap connections were considered: (i) Rigid pile-cap connections (RPC) and (ii) Hinged pile-cap connections (HPC). For hinged cases, moments about major and minor axes of the piles at the connections with cap were released. For rigid cases, all the six degrees of freedom (DOF) for the piles were fully compatible with the corresponding DOF's in the pile cap. Table 4.1 lists the main bridge characteristics considered in this study.

Table 4.1 Characteristics of bridges considered in the parametric study.

Model Case	Span Length (ft)	Pile Size	Unsupported Pile Lengths (ft)	Skew angle	Pile-to-cap Connection
Nonskew_ (RPC)	30′	18″Solid	18′,24′,30′	0 deg.	Rigid
	50′	24″Solid	18′, 24′, 30′, 40′		
	76′	30″voided	18′,24′,30′,40′, 50′		
	100′	36″voided	30′,40′, 50′,60′		
Nonskew_ (HPC)	30′	18″Solid	18′,24′,30′	0 deg.	Hinged
	50′	24″Solid	18′, 24′, 30′, 40′		
	76′	30″voided	18′,24′,30′,40′, 50′		
	100′	36″voided	30′,40′, 50′,60′		
30deg.skew_ (RPC)	30′	18″Solid	18′,24′,30′	30 deg.	Rigid
	50′	24″Solid	18′, 24′, 30′, 40′		
	76′	30″voided	18′,24′,30′,40′, 50′		
	100′	36″voided	30′,40′, 50′,60′		
30deg.skew_ (HPC)	30′	18″Solid	18′,24′,30′	30 deg.	Hinged
	50′	24″Solid	18′, 24′, 30′, 40′		
	76′	30″voided	18′,24′,30′,40′, 50′		
	100′	36″voided	30′,40′, 50′,60′		
45deg.skew_ (RPC)	30′	18″Solid	18′,24′,30′	45 deg.	Rigid
	50′	24″Solid	18′, 24′, 30′, 40′		
	76′	30″voided	18′,24′,30′,40′, 50′		
	100′	36″voided	30′,40′, 50′,60′		
45deg.skew_ (HPC)	30′	18″Solid	18′,24′,30′	45 deg.	Hinged
	50′	24″Solid	18′, 24′, 30′, 40′		
	76′	30″voided	18′,24′,30′,40′, 50′		
	100′	36″voided	30′,40′, 50′,60′		
60deg.skew_ (RPC)	30′	18″Solid	18′,24′,30′	60 deg.	Rigid
	50′	24″Solid	18′, 24′, 30′, 40′		
	76′	30″voided	18′,24′,30′,40′, 50′		
	100′	36″voided	30′,40′, 50′,60′		
60deg.skew_ (HPC)	30′	18″Solid	18′,24′,30′	60 deg.	Hinged
	50′	24″Solid	18′, 24′, 30′, 40′		
	76′	30″voided	18′,24′,30′,40′, 50′		
	100′	36″voided	30′,40′, 50′,60′		

4.3 Development of Finite Element (FE) Model

All bridge models were developed in the commercially available finite element package SAP2000. Each model idealized deck and pile caps as quadrilateral shell elements. Frame elements were used to model the girders and piles. Composite cross sectional properties were assumed for girders even though the centroids of deck shell elements were assumed to be at the same level as girder frame elements. This modeling choice is deemed appropriate since the focus of the study is mainly influenced by lateral loads on the substructure. Hence, local straining actions in the superstructure are not of interest and will not be extracted. Figure 4.1 shows typical concrete deck and girder elements used in the model. The girder, deck, pile, and pile cap properties were assigned to their respective elements in the mesh. Table 3.2 presents the material properties used for each element. Deck continuity, which is often used in new bridge constructions, was modeled using truss elements as links between two adjacent girders. Barrier weights were modeled using frame elements with negligible stiffness. Different constraint options are available in SAP2000 to consider the translation and rotation constraints at the connections between two nodes. In the model, truss elements were used to idealize the bearing pads that connect the girders and the pile cap. Equal constraints for global Z and Y axis translation at both ends of truss elements were applied to address the roller type bearing connections that is often referred to as 'E' for expansion. Equal constraints for global X, Y and Z axis translations at both ends of truss elements were applied to address the hinged type bearing connections (often referred to as 'F' for fixed). Frame elements were used at pile and pile cap connections to address the eccentricity between the cap centroid and the pile top. The properties for these elements were same as that of the solid piles. Body constraints were used to ensure the equal rotation and translation of both ends of the connecting elements. All the six DOF's for the piles at RPC connections were fully compatible with the corresponding DOF's in the pile cap.

For HPC connections, however, moments about major and minor axes of the piles at the connections with cap were released. Fixed joint restraints were applied at the bottom end of each pile considering 10 ft depth of fixity. The choice of 10 ft is conservative since it exposes more of the pile surface to wind loads. Figure 4.2 shows the longitudinal profile of girder, pile cap, pile, and connecting elements used in the model. Figure 4.3 presents a typical finite element model for bent type bridge generated in SAP2000.

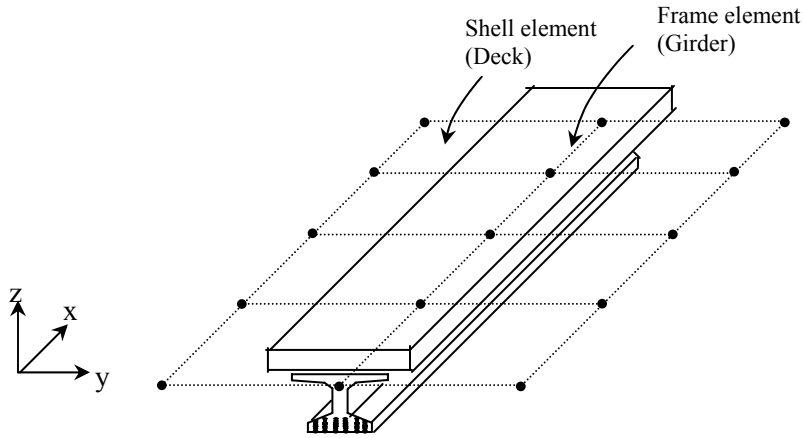

Figure 4.1 Typical Concrete Deck and Girder elements

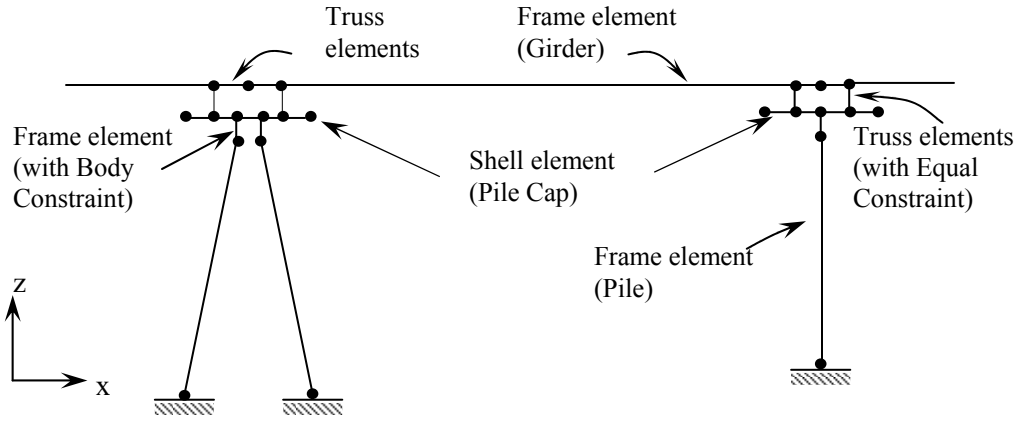

Figure 4.2 Longitudinal profile of girder, pile cap, pile and connecting elements.

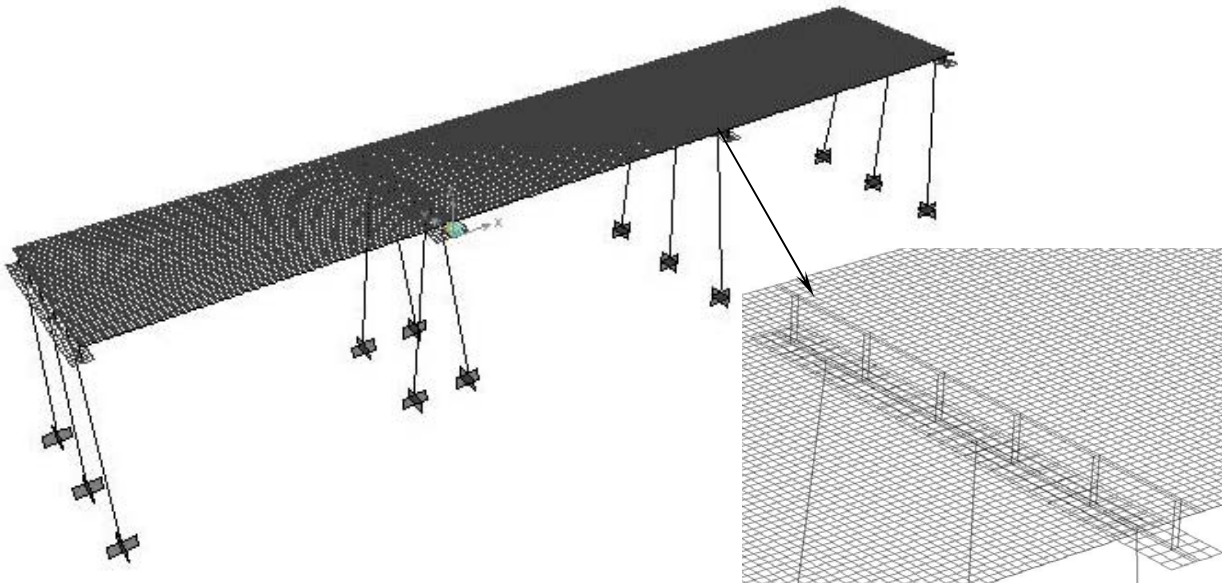

Figure 4.3 Typical finite element model for a 76 ft span non-skew bridge.

4.3.1 Elements Used in the Study

Two types of elements were used in the development of the bridge models from SAP2000 element library. These are: (i) shell elements, and (ii) frame element. The bridge deck and pile caps were modeled using quadrilateral shell elements. Girders, piles, and barriers were modeled using frame elements.

4.3.1.1 Shell Elements

In SAP2000, the quadrilateral shell element, which may be reduced to a three-node (triangular) shell element, combines membrane and plate bending behavior. Membrane behavior uses an isoperimetric formulation that includes translational in-plane stiffness components and a rotational component in the direction perpendicular to the plane of element. The plate bending behavior includes two-way, out-of-plane, rotational stiffness components and a translational stiffness component in the direction normal to the plane of element (SAP2000 2002). For each shell element in the structure one can choose to model pure membrane (in-plane forces), pure plate (bending moment), or full shell (combination of membrane and plate behavior) behavior.

Among the triangular and quadrilateral shell elements the quadrilateral formulation is the more accurate one. Figure 4.4 presents the face definition and joint connectivity of a four-node quadrilateral element.

Each shell element has its own element local coordinate system for defining material properties, loads and outputs. The axes of this local system are denoted 1, 2 and 3. The first two axes lie in the plane of the element with a user defined orientation and the third axis is normal to the plane defined by the first two axes. The relationship between the local 3 axis and global Z axis determines the default orientation of the local 1 and 2 axes.

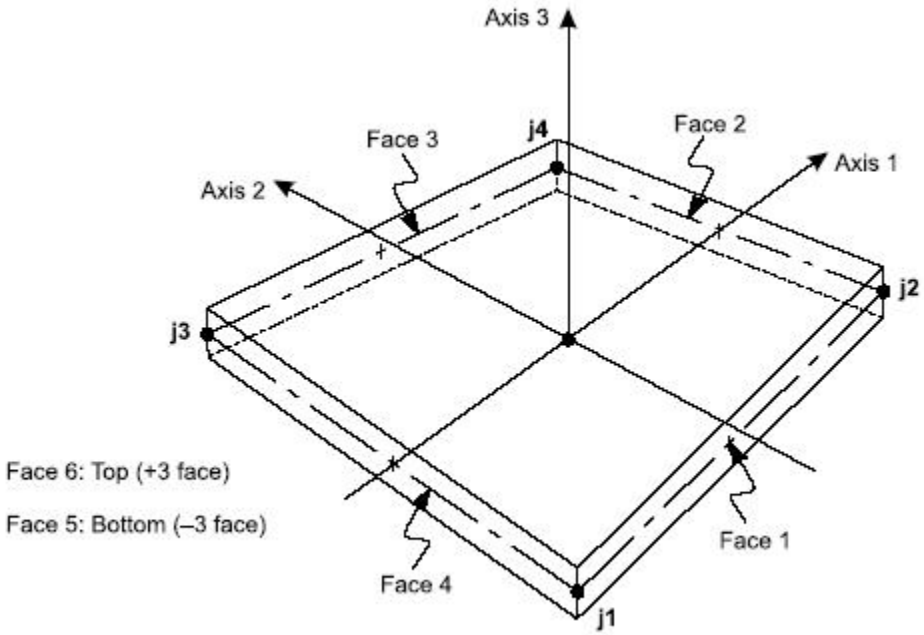

Figure 4.4 Face definition and joint connectivity of a four-node quadrilateral shell element.

Two thickness formulations are available in SAP2000. The difference between both formulations is whether or not transverse shearing deformations are included in the plate-bending behavior of a shell element. The thick plate (Mindlin/Reissner) formulation includes the effect of transverse shearing deformation and the thin plate (Kirchhoff) formulation neglects transverse shearing deformation. Shearing deformation tends to be important when shell thickness is greater than about one-tenth to one-fifth of the span. However, it only affects plate bending behavior but

has no effect on membrane behavior. The thick plate formulation tends to be more accurate for thin-plate bending problems. However, the accuracy of the thick-plate formulation is more sensitive to large aspect ratios and mesh distortion. Each shell element section has a constant membrane thickness and a constant bending thickness. The membrane thickness is used to calculate (i) the membrane stiffness for full shell and pure-membrane sections and (ii) the element volume for the element self weight and mass calculation. The bending thickness, on the other hand, is used to calculate the plate-bending and transverse-shearing stiffness for full-shell and pure-plate sections.

In this study, quadrilateral shell elements, that can support both the membrane and plate behavior, were used to model the bridge deck and pile cap. Thin shell elements for the bridge deck had a thickness smaller than one-tenth of its span length. However, to model the pile caps, thick shell elements were used since cap thickness was greater than the allowable range of thickness-to-span ratio for thin plate. Modeling the pile cap using shell elements allowed for placing the girders eccentrically which simulates actual conditions. Both the membrane and plate thicknesses were kept the same for deck and pile cap elements.

4.3.1.2 Frame Elements

Frame element uses a three dimensional, beam-column formulation which includes the effects of biaxial bending, torsion, normal, and biaxial shear deformation. In SAP 2000, each frame element may be loaded by gravity in any direction, multiple concentrated and distributed loads, prestressing loads, and loads due to temperature change. End releases are available to model different fixity conditions at the ends of the elements. Normally, 3 translational and 3 rotational degrees of freedom at each end of the Frame element are continuous with those of the joint and hence with those of all other elements connected to the joint. However, it is possible to release one or more of the elements DOF's from the joint when it is known that the

corresponding element force or moment is zero. Truss or cable elements that contribute only axial deformation to the system are modeled by releasing the bending (R2 and R3) and the torsional (R1) rotations at both ends. Same objective can be obtained by setting section properties J, I22 and I33 all to zero for the frame elements.

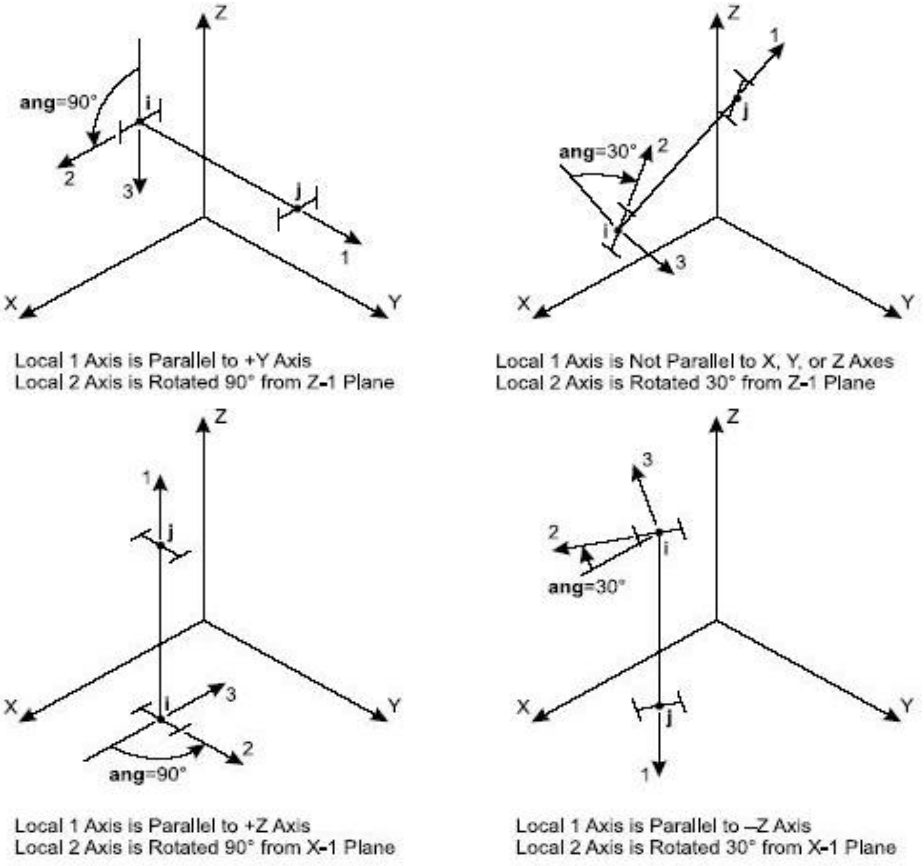

Figure 4.5 Frame element local coordinate angles with respect to the default orientation

Each frame element has its own local coordinate system used to define section properties, loads, and output. Figure 4.5 shows the frame element local coordinate angle with respect to the default orientation. The axes of this local system are denoted as 1, 2 and 3. The first axis is directed along the length of the element from the first node (*i*) to the second one (*j*). The remaining two axes lie in the plane perpendicular to the element with a user specified orientation. The default orientation of the local 2 and 3 axes is determined by the relationship between local 1 axis and global Z axis.

Material properties and six geometric section properties define the stiffness of the section for a frame element. These properties are: the cross sectional area, A, for axial stiffness, the moment of inertia about 3 axis and 2 axis for bending in 1-2 plane and 1-3 plane respectively, the torsional constant J for torsional stiffness, and shear areas AS2 and AS3 for transverse shear in the 1-2 and 1-3 planes respectively. Torsional constant, J can be obtained using the formulae provided in Table C-1 (Young and Budynas 2002). Formulae for calculating the shear areas of typical sections are given in Table 4.2.

Table 4.2 Shear area formulae for different sections

Section	Description	Effective Shear Area
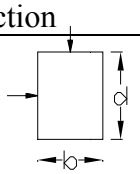	Rectangular section shear force parallel to the b or d direction	$\frac{5}{6}bd$
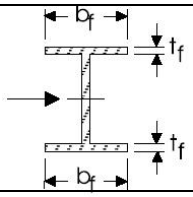	Wide flange section Shear force parallel to flange	$\frac{5}{3}t_f b_f$
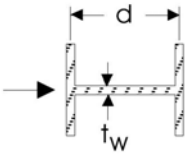	Wide flange section Shear force parallel to web	$t_w d$
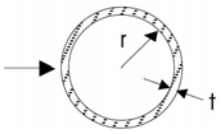	Thin walled circular tube section Shear force from any direction	πrt
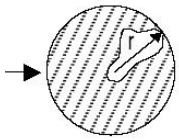	Solid circular section Shear force from any direction	$0.9\pi r^2$
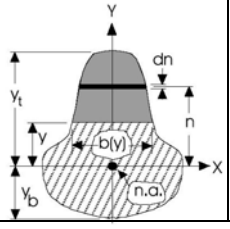	General section Shear force parallel to y-direction $Q(y)=\int_{y}^{y_t} nb(n)dn$	$\frac{I_x^2}{\int_{y_b}^{y_t}\frac{Q^2(y)}{b(y)}dy}$

Automatic section property calculation is available for some standard shapes such as pipe sections, or solid square sections. Six geometric properties must be specified in the "general section" option for other types. Table 4.3 presents the section properties used in this study for different frame elements. As can be seen, truss elements were used to model the connections between two adjacent girders and the bearings between girders and pile cap. Section properties like area and inertia for the bearing type truss elements did not affect the results because of the equal constraints applied at their ends. The Composite moment of inertia about local axis 3 was used for the girders to address the effect of the eccentricity between girder and deck centerline. Table 4.2 was used to determine the shear area.

Table 4.3 Geometric section properties used in the model for the frame and truss elements.

Description	Element Type	Section Type (SAP2000)	Area (in^2)	Comp.Mom.of Inertia(I_{33})(in^4)	Torsional Constant *J*, (in^4)	Shear Area (in^2)	Joint constraint
Type II girder	Frame	General	369	I_{int}=736824 I_{ext}=692583	6817	216	---
Type III girder	Frame	General	559	I_{int}=423681 I_{ext}=388873	15032	315	---
Type IV girder	Frame	General	789	I_{int}=727292 I_{ext}=664181	26413	432	---
Bearings between pile cap and girders	Truss	General	100	1.0	1.0	--	Equal Constraint
Links between two adjacent girders	Truss	General	100	1.0	1.0	216	---
Solid Pile (18″and 24″)	Frame	Solid Square	--	--	--	--	---
Hollow pile (30″)	Frame	General	631	61750	103605	508	---
Hollow pile (36″)	Frame	General	1027	134218	225895	838	---

4.3.2 Joint Constraints

A constraint consists of a set of two or more constrained joints whose displacements are related by mathematical expression. The types of the behavior that can be enforced by joint constraints are: (i) Rigid body behavior, in which constrained joints translate and rotate together as if connected by rigid links, (ii) Equal-displacement behavior, in which the translations and rotations are equal at the constrained joints, and (iii) Symmetry and Anti-Symmetry conditions. There are several types of constraints available in SAP2000 to model different types of rigid behavior and to impose certain types of symmetry conditions. Among them the following two types of constraints were used in this study. Figure 4.2 shows the positions of the constraints in the model.

4.3.2.1 Body Constraints

A Body Constraint causes all of its constrained joints to move together as a 3D rigid body. By default all degrees of freedoms at each connected joint participate. However a subset of the DOF's can also be selected to be constrained. The constraint can be used to: (i) model rigid connections, (ii) connect different parts of the structural model that were defined using separate mesh, and (iii) connect frame elements acting as eccentric stiffeners to shell elements. The constraint equations that relate the displacement at any two constrained joints (i and j) in a Body Constraint are,

$$u1_j = u1_i + r2_i(x3_j - x3_i) - r3_i(x2_j - x2_i)$$

$$u2_j = u2_i + r3_i(x1_j - x1_i) - r1_i(x3_j - x3_i)$$

$$u3_j = u3_i + r1_i(x2_j - x2_i) - r2_i(x1_j - x1_i)$$

$$r1_i = r1_j; \qquad r2_i = r2_j; \qquad r3_i = r3_j$$

where, u1, u2, and u3 are translations; r1, r2, and r3 are rotations, and x1, x2, and x3 are the coordinates taken in the constraint local coordinate system. In this study Body Constraints were used to ensure the equal rotation and translation of both ends of the frame elements connecting pile top and cap centerline. All the six DOF's for the piles at RPC connections were fully compatible with the corresponding DOF's in the pile cap. For HPC connections, however, moments about major and minor axes of the piles at the connections with cap were released.

4.3.2.2 Equal Constraints

All of the constrained joints in an equal constraint move together with the same or opposite displacement for each selected degree of freedom taken in the local coordinate system. The other degrees of freedom remain unaffected. Unlike Body Constraint there is no coupling between the rotations and the translations in an Equal Constraint. This constraint can be used to: (i) model symmetry and anti-symmetry conditions with respect to plane, and (ii) partially connect different parts of the structural model such as at expansion joints and hinges. In this study, Equal Constraints were applied to model the connections between the pile cap and girders. Truss elements, with equal constraints at their both ends, were used to model the bearings. For bearings with hinged connections, translations in all three directions were kept the same for both ends of each truss element. For bearings with roller connections, horizontal displacement along the bridge width (global Y) and vertical displacement (global Z) of both ends of the truss elements were kept the same.

4.4 Application of Loads

Different static load cases based on AASHTO-LRFD bridge design specifications (AASHTO 2004) were considered for the analysis of bridge model. Factored load combinations were considered to determine the critical axial loads and moments on the pile bents. Table 3.4 presents the static load cases, load factors and combinations used in this study.

4.4.1 Dead Load (DC and DW)

The self weight load option in SAP2000 was used to activate the component self weight (DC) of all elements in the model. Future wearing surface (FWS) loading (DW) was applied using surface pressure load on shell elements in negative Z direction. The contributing surface area for the FWS load is the deck surface area excluding the barrier.

4.4.2 Live Load (LL)

Figure 3.4 shows the live load cases considered in this study. The truck load portion of HL-93 loading was applied using joint loads. The 0.064 klf lane load was applied as a surface pressure on shell elements based on an application width equal to loading lane (10ft) multiplied by number of design lanes. Figure 4.6 shows two cases of longitudinal live load positions considered in this study to obtain maximum pile capacity utilization. However case 2 (Figure 4.6b) produced lower pile capacity utilizations for the models considered and was discarded later. Figure 4.7 and 4.8 show typical truck loading and lane loading applied on one of the bridge models. Loads were adjusted by multiple presence factor for two and three lane loaded cases.

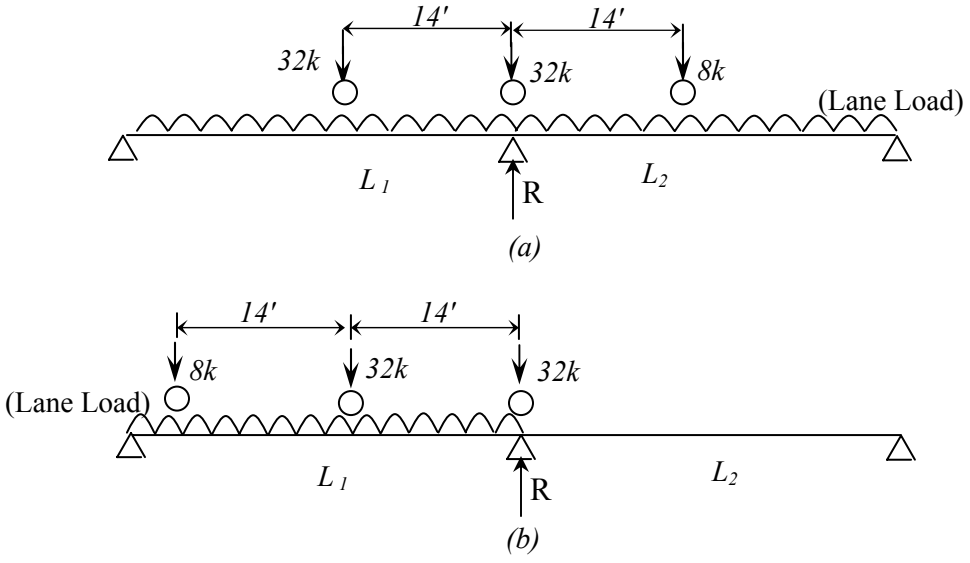

Figure 4.6 Longitudinal LL axle position for maximum pile capacity utilization:
(a) Case 1, and (b) Case 2.

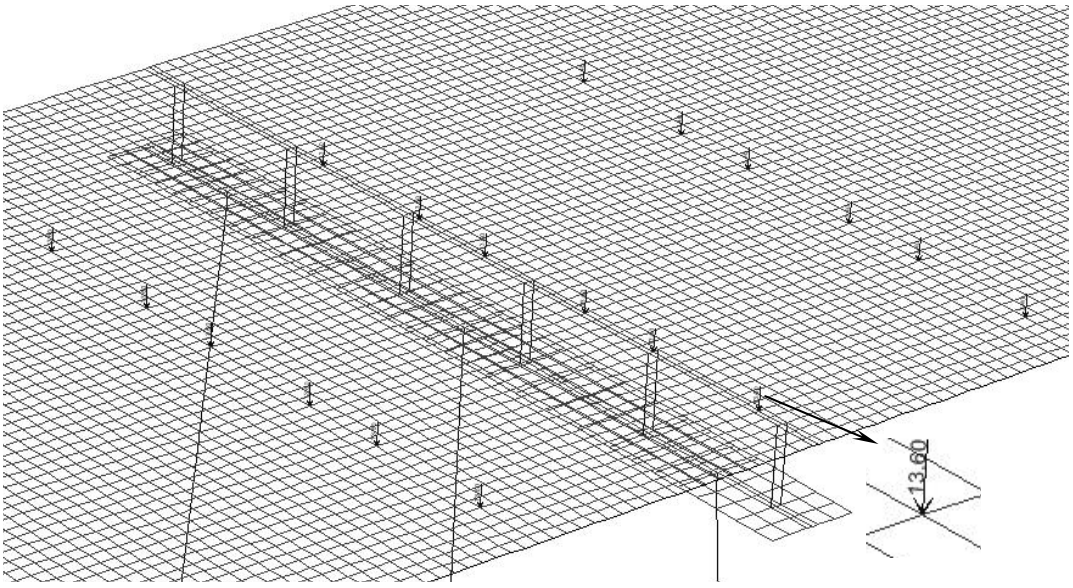

Figure 4.7 Three lane truck loading (m.f. included) on a 76 ft span bridge model.

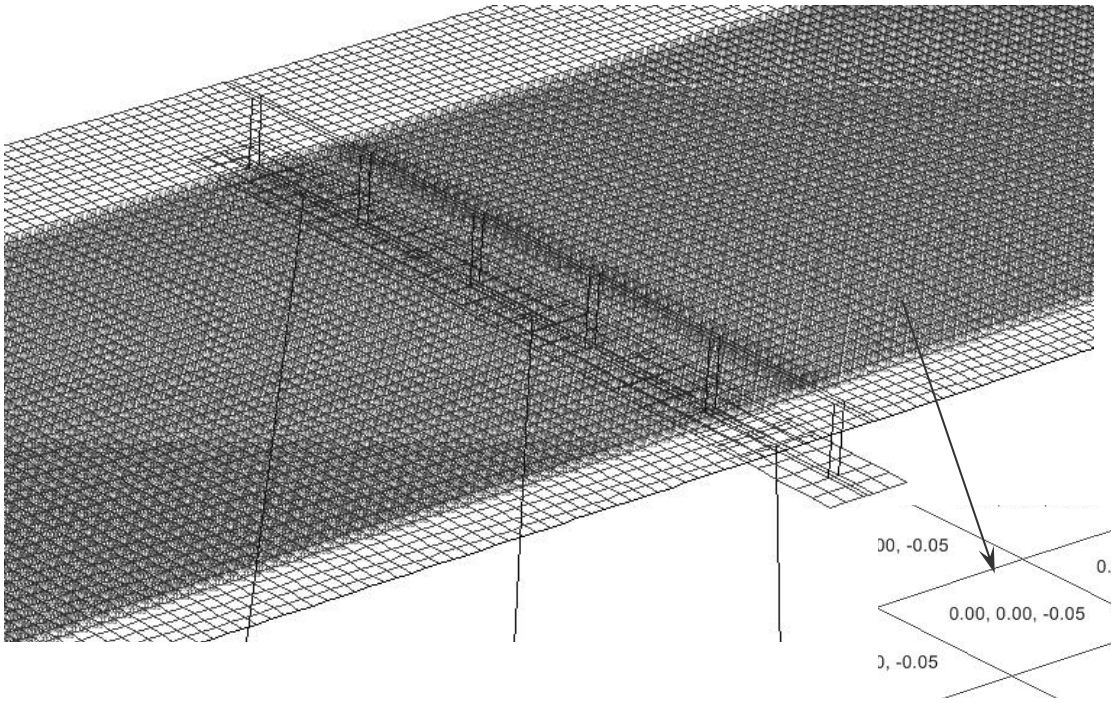

Figure 4.8 Lane loading (m.f. included) on a 76 ft span bridge model.

4.4.3 Wind Load

Figure 3.4 shows different wind load cases considered in this study. The intensity, direction, and elevation of the applied wind loads conformed to AASHTO-LRFD (2004)

specifications. Two types of wind loads were considered namely wind on live load (WL) and wind on structure (WS). They are described next.

4.4.3.1 Wind on Live Load (WL)

According to AASHTO-LRFD (2004), an interruptible wind load on the traffic vehicle should be applied as a moving force, F_w, acting normal to and 6.0ft above the roadway. F_w is the wind component on live load and can be obtained using Table 3.5. For each wind load case (Figure 3.4), the vehicles facing the wind are responsible for WL loading. Figure 4.9a shows the equivalent frame loads due to an eccentric moving force acting normal to the roadway. The vertical loads, F_{TLL}, on the wheel positions of the vehicle facing the wind were applied to account for the overturning effect of the wind. F_{TLL} is numerically same as F_w and was applied as line load. Figure 4.9 b shows a 3-D perspective of the loading on the deck surface of a typical bridge model.

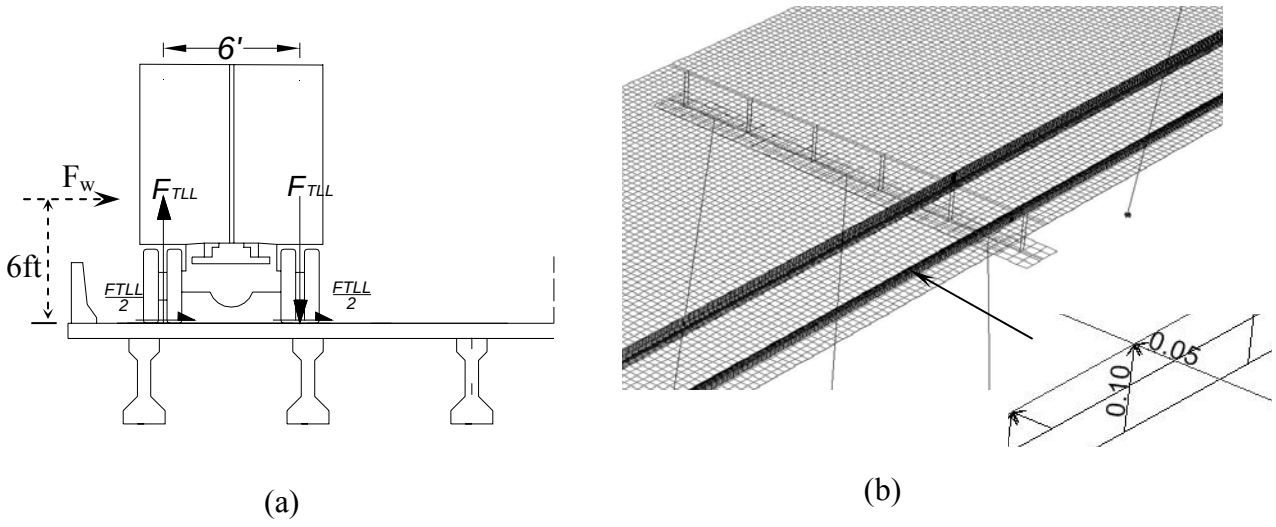

Figure 4.9 (a) Equivalent wind on live load (b) Wind load on live load applied on the Deck surface.

4.4.3.2 Wind on Super Structure (WS)

Wind loads on the superstructure were applied as a uniformly distributed transverse line load acting on the side of the deck elements. An additional distributed moment was applied on the barrier frame elements located at the edge of the deck. In the model, girder and barrier centroid were considered at same height. Hence, equation 4.1 and 4.2 were used to calculate the frame loads due to wind on superstructure.

$$P_{w\text{sup}} = TH \times P_w \tag{4.1}$$

$$M_{w\text{sup}} = P_{w\text{sup}} \times \left(\frac{TH}{2} - \frac{GH}{2} \right) \tag{4.2}$$

where, P_{wsup} is the uniformly distributed horizontal load and M_{wsup} is the uniformly distributed moment acting on the longitudinal barrier frame elements. *TH* is the total height of girder, haunch, deck and barrier, and *GH* is the girder height. The design wind pressure, P_w, was calculated as described earlier using Equations 3.4 and 3.5. Table 3.8 shows the design wind velocity for different upstream condition under highest V_{30} values in Louisiana obtained from fastest miles wind velocity chart. Table 4.4 shows different design wind velocity and corresponding limit states used in this study. Figure 4.10 shows the applied wind load on the superstructure for typical bridge model. Table 4.5 shows the values of P_{wsup} and M_{wsup} used for different span lengths at 150 mph wind velocity (V_{DZ}).

Table 4.4 Design wind velocity and corresponding limit state used in this study

Design wind velocity, V_{DZ} (mph)	Limit State
55	Strength V
100	Strength III
150	Strength III

Table 4.5 P_{wsup} and M_{wsup} values for different span lengths (V_{DZ}=150 mph).

Span length (ft)	Girder height *(ft)*	Total Height *(ft)*	P_{wsup} *(k/ft)*	M_{wsup} *(k-ft/ft)*
30	3.0	6.58	0.74	1.32
50	3.0	6.58	0.74	1.32
76	3.75	7.33	0.82	1.52
100	4.5	8.07	0.89	1.58

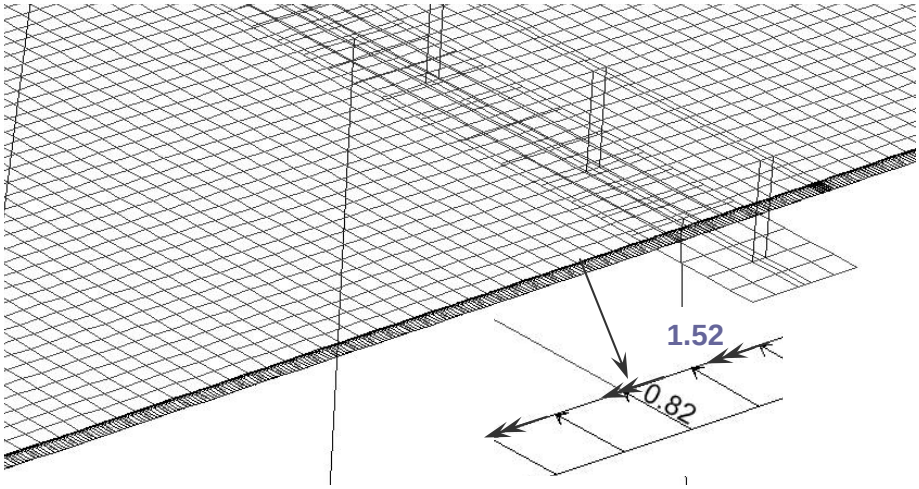

Figure 4.10 Transverse wind load on superstructure applied on the girder centerline.

4.4.3.3 Wind on Sub Structure (WS)

Transverse wind loads on the substructure were applied as concentrated load on the center joint of the cap face and a uniformly distributed line load on the frame element that represents pile facing the wind direction. Minimum (10ft) depth of fixity was assumed to consider the highest effect of the wind load on pile element. The designed wind pressure, P_w, was calculated using equation 3.4 and 3.5. According to AASHTO-LRFD (2004), the transverse wind load on substructure should be calculated from a base wind pressure P_B of 0.04 ksf. The transverse concentrated load acting on the centroid of the cap face, C_{wsub}, and line load above the ground level on the pile element, P_{wsub}, are as follows:

$$C_{wsub} = P_w \times (CA) \tag{4.3}$$

$$P_{wsub} = P_w \times (PS) \tag{4.4}$$

where, *CA* is the cap area facing the wind, and *PS* is the pile size. Figure 4.11 shows the wind load on substructure applied on a typical bridge model.

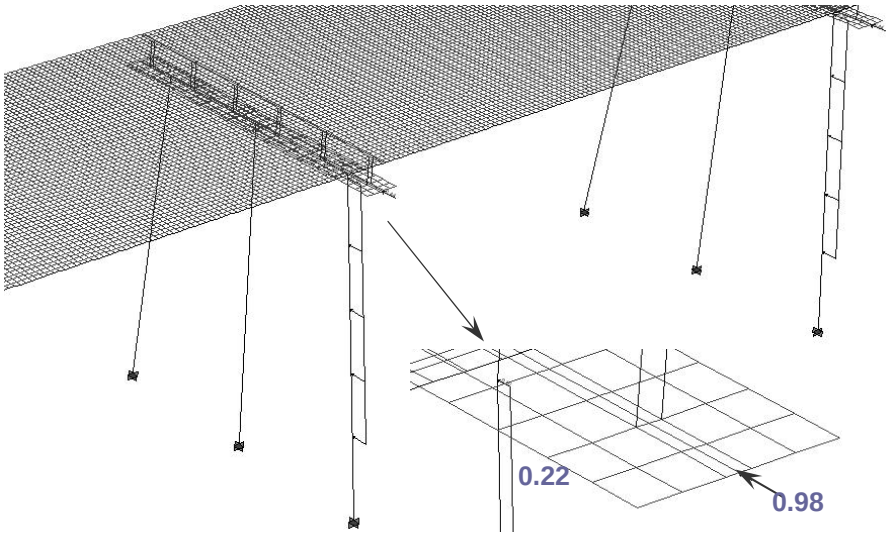

Figure 4.11 Transverse wind load on Substructure applied on the Model.

4.5 Model Validation

No experimental data for pile response due to bridge loading were available to evaluate the results obtained from the finite element models. Hence, the results obtained from the FE analyses were compared with those obtained using widely accepted conventional methods.

Results obtained from the conventional analysis discussed in Chapter 3 were compared to the results obtained from the finite element analysis of a non-skew bridge. Table 4.6 shows the comparison of axial loads and moments in a single pile (with HPC connection) for different load cases obtained using finite element analysis and conventional analysis. It can be seen that the axial loads obtained using two analyses were roughly identical. However for wind load on structure (WS) pile moments obtained using finite element analysis were slightly higher than

those obtained using conventional analysis. Conversely, pile moments due to live load (LL) and wind on live load (WL) were smaller for finite element analysis. For the finite element analysis, the lateral restraints of adjacent piers (#3, #4, and #6) contributed significantly to resist moments due to live load positioned near the intermediate pier line #5 (Figure 3.2). For Strength V limit state the load factor (1.35) for live load case further increased the difference between the two analyses. However at wind velocity higher than 55 mph, strength III limit state should be used which excludes the presence of live load. At this limit state difference between the results obtained from conventional frame and refined FE analyses were minimal.

The finite element models were further evaluated by comparing the live load distribution factors obtained using finite element analysis with those obtained using AASHTO code. Table 4.7 was used to calculate load distribution factors for interior and exterior girders of a 76ft span bridge. Table 4.8 presents maximum live load girder moments for a 76ft span bridge obtained for two lane live load case using line girder analysis and finite element analysis. It can be seen that the live load distribution factors obtained using finite element analysis were 10-15% higher than those obtained using AASHTO codes. Barr et al (2001) showed that the load distribution factors obtained using finite element analysis were on average 6% lower than those obtained using codes for the configuration most similar to that considered in developing the LRFD specifications (Simply supported, no haunch, no diaphragms). Three span-continuous bridge models (including haunch) were used in this study for FE analysis. However, more accurate distribution factors could be obtained through a time consuming procedure of modeling the deck and girder elements at different heights and attaching them with rigid links. Since the models were used for the analysis of pile capacity, further enhancement of the model was not necessary.

Table 4.6 Comparison of axial loads and moments in a single pile with HPC connection for different load cases obtained using finite element analysis and conventional analysis.

Bridge Type; Pile type; Wind velocity.	Load Case		Axial Load (k)		Moment (k-ft)	
	Load Designation	Description	FE	STAAD	FE	STAAD
100 ft Span Non-skew Bridge 50ft long; 36in. Hollow/Square Pile; HPC Connection; (Pile # 1)	DC	Super Structure	-333.4	-336	-3.6	-2
		Sub Structure	-75.0	-76	-42.4	-44.0
	DW	Future Wearing Surface	-33.9	-34	-0.3	-0.2
	LL	Three lane load	-115.6	-126	-47.6	-188.0
	WL	Wind from left	4.8	5	-87.2	-162.0
		Wind from right	-1.6	-6.7	87.1	145.0
Wind Velocity 55 mph	WS	Wind from left	3.0	2.2	-241.0	-209.6
		Wind from right	-1.4	-2.0	226.0	213.0
	Strength V	Wind from left	-711.6	-730.2	-305.8	-557.4
		Wind from right	-719.8	-743.6	55.3	-81.4
Wind Velocity 150 mph	WS	Wind from left	22.5	16.2	-1792.1	-1559.0
		Wind from right	-10.7	-15.2	1680.2	1584.0
	Strength III	Wind from left	-529.9	-543.3	-2567.6	-2240.4
		Wind from right	-576.4	-587.3	2295.1	2159.8

Table 4.7 Distribution of live load per lane for moment in interior and exterior girder (Table 4.6.2.2b-1, AASHTO 2004)

Type of beam	Load Distribution Factor	
	Interior Girder	Exterior Girder
Concrete Deck on Girder	One design lane load $g_{\text{int}(1Ln)} = 0.06 + \left(\frac{S}{14}\right)^{0.4}\left(\frac{S}{L}\right)^{0.3}\left(\frac{K_g}{12.0Lt_s^3}\right)^{0.1}$ Two design lane load $g_{\text{int}(2Ln)} = 0.075 + \left(\frac{S}{9.5}\right)^{0.6}\left(\frac{S}{L}\right)^{0.2}\left(\frac{K_g}{12.0Lt_s^3}\right)^{0.1}$ Where, $K_g = n\left(I + Ae_g^2\right)(in^4)$; A=Girder area($in^2$) e_g=distance between the c.g. of the girder and deck S=girder spacing(ft) L=Span length(ft) Ts=slab thickness(in)	One design lane load $g_{ext(1Ln)}$=using lever rule Two design lane load $g_{ext(2Ln)} = e \times g_{\text{int}(2Ln)}$ Where, $e = 0.77 + \frac{d_e}{9.1}$ d_e=distance from exterior web of exterior beam to the interior edge of traffic barrier

Table 4.8 Comparison of Live Load Distribution Factors obtained using FEA and AASHTO code.

Live Load Case		Maximum Girder Moment (k-ft)			Load Distribution factor		
	Girder Type	Line Girder analysis	AASHTO Code	FE analysis (2Lane)	AASHTO Code, g_{AS}	FE analysis, g_{FE}	$\frac{g_{AS}}{g_{FE}}$
Truck	Interior	707	453	535			
	Exterior		375	479			
Lane	Interior	278	178	168			
	Exterior		147	142			
LL+IM (Tr Load × 1.33+Ln load)	Interior	1218	780	879	0.64	0.72	0.89
	Exterior		645	779	0.53	0.64	0.83

4.6 Conclusion

In this chapter the procedures for modeling the bridges for different cases, types and geometric properties of the elements, types of constraints, and application of loads on the models for different loading cases are presented. The method used for model generation and validation are also discussed.

CHAPTER 5. CAPACITY OF PRESTRESSED CONCRETE PILES

5.1 Introduction

Bent piles are eccentrically loaded beam-column members. They are subjected to axial forces and corresponding flexural moments. The capacity of each member is conveniently determined using interaction diagrams. Moment capacities of the piles corresponding to the axial loads obtained from finite element analyses of different bridges discussed in the previous chapter were calculated using a commercially available prestressed concrete pile interaction diagram spreadsheet (PCI_PSCPile.xls). The Precast/Prestressed Concrete Institute (2004) prepared the excel spreadsheet to construct interaction diagram for prestressed concrete piles as a state-of-the-art design aid for professional engineers. This chapter discusses the methodology used for the construction of the spreadsheet.

5.2 Analysis Method and Assumptions

5.2.1 Strain Compatibility Method

The strain compatibility approach was used in the PCI spreadsheet to develop the points for the interaction diagram (I.D.). The approach is based on three fundamental assumptions: (a) plane section remains plane after bending, (b) compatibility of strain, i.e., full bond between reinforcing strands and concrete at the section being considered, and (c) equilibrium of forces within the section. In addition, the equivalent rectangular stress block with the intensity of $0.85f_c'$and depth, $a=\beta_1 c$ (where c is neutral axis and β_1 is a coefficient defined in section 8.2.2.2.1.1 of PCI BDM, 2002) is used for the concrete stress-strain relationship. The tool utilizes the following stress-strain relationship for 270 ksi, low-relaxation strands

$$f_{si} = \varepsilon_{si}\left[887 + \frac{27613}{\left\{1+\left(112.4\varepsilon_{si}\right)^{7.36}\right\}^{\frac{1}{7.36}}}\right] \le 270ksi \qquad (5.1)$$

which is adopted by PCI Design Manual (2002). In Equation 5.1, f_{si} is the stress in a given layer of reinforcement whose strain is ε_s.

In the spreadsheet (PCI 2004), the contribution of concrete is calculated using a "strip" method in which the cross-section is divided into small strips with a height Δh=(Pile Size)/100 and a width b_{avg}, where b_{avg} is the average width of the top and bottom widths of the strip including any reductions required due to an inner void or chamfer. This allows the circular, octagonal and square sections to be analyzed using one spreadsheet routine. The strain, stress and force for each pretensioned strand are analyzed individually and the summation of the net effects is used to compute the pretensioned strand contribution.

The points for the I.D. are computed for a series of assumed strain distribution similar to that shown in Figure 5.1. The figure illustrates the combination of strain and stress distribution across the pile section at ultimate load resulting from three causes: (1) prestress, (2) applied axial load, and (3) flexure due to eccentricity of axial force or applied bending moment. For laterally unsupported pile, an incremental increase in bending is produced by the magnification of strain across the pile section. Figure 5.1(a) illustrates the strain and stress conditions in the concrete, while Figure 5.1(b) deals with the strain and stresses in prestressing strands. The ultimate compressive strain, ε_{cu}, corresponding to compression failure of concrete is set at 0.003. An equivalent rectangular stress block with the intensity of $0.85f_c'$ and depth, $a=\beta_1 c$ is used for the concrete stress-strain relationship. The maximum axial tension with flexure point is computed by allowing the pretensioned strand farthest from the compression zone to reach a strain corresponding to strand rupture of 0.035 in./in. The points for pure tension are computed using the LRFD Equations 5.6.3.4.1-1 and 5.7.6.1-1 (AASHTO 2004):

$$P_n = f_y A_{st} + A_{ps}(f_{pe} + f_y) \tag{5.2}$$

$$P_r = \phi P_n \tag{5.3}$$

where, P_r and P_n are the factored and nominal tension resistance, A_{st} and f_y are the total area and yield strength of longitudinal mild steel reinforcement, A_{ps} and f_{pe} are the area of prestressed steel and stress in prestressing steel due to prestress after loss, and ϕ is the resistance factor specified in article 5.5.4.2 (AASHTO 2004). For flexure and tension of prestressed concrete, ϕ is 1.0.

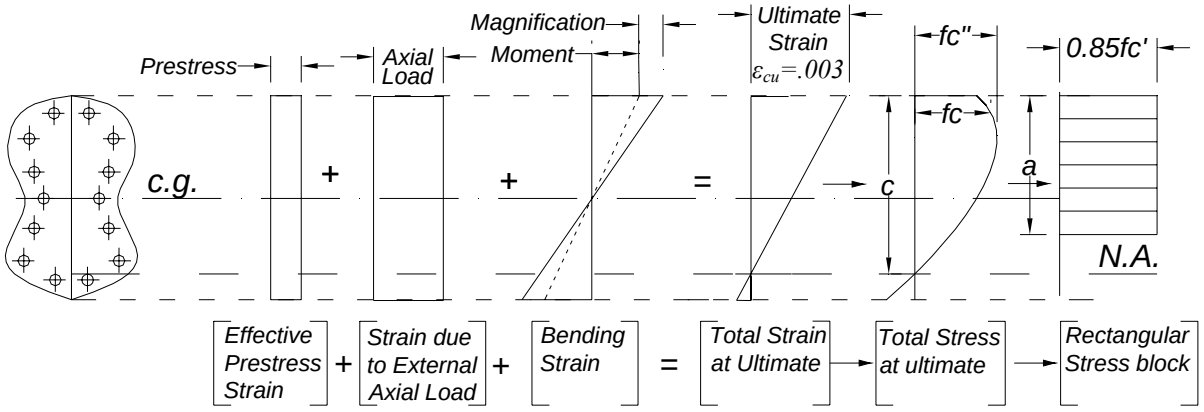

(a)

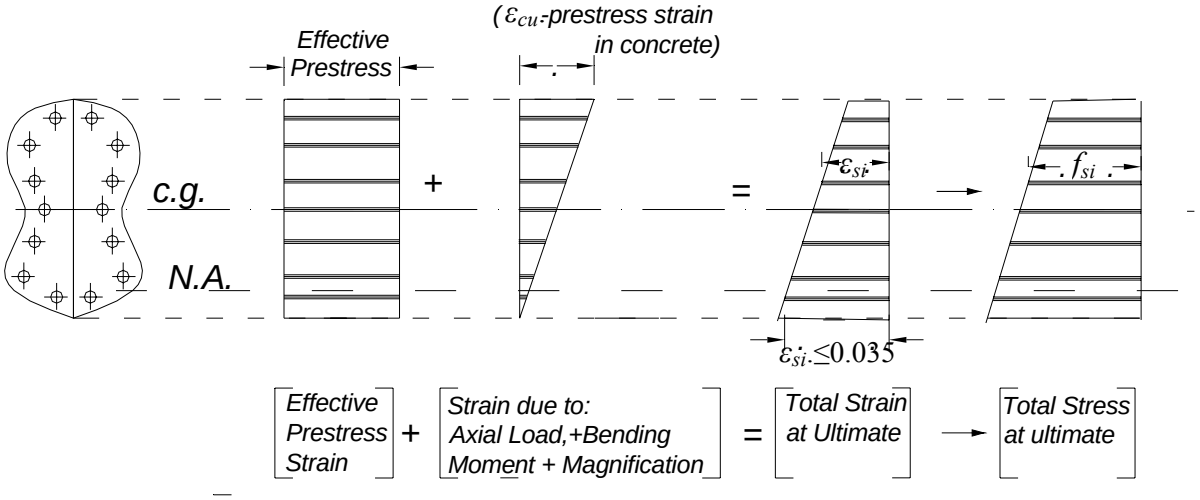

(b)

Figure 5.1 (a) Concrete strain and stresses in pile section and (b) Steel strains and stresses in pile strands.

5.2.2 Slenderness Effect

A slender pile can be defined as a pile that has a significant reduction in its axial load capacity due to moments induced by lateral deflection of the pile. A slender pile subjected to axial load starts to deflect laterally as soon as the axial load exceeds a critical value. This lateral deflection increases the maximum moment in the pile by an amount $P\delta$, which in turn reduces the axial capacity of the pile. This reduction in axial capacity of a slender pile is called the slenderness effect. This effect is considered in the interaction diagram spreadsheet using two methods: (a) ACI method and (b) Secant method. Equations 5.4 and 5.5 (Anderson and Moustafa, 1970) were used in developing the spreadsheet program to calculate the ultimate load, P_u, and ultimate moment, M_{ur}, resisted by the piles.

$$P_u = \int f_c dA_c + \sum_{i=1}^{n} A_{si} f_{si} \tag{5.4}$$

$$M_{ur} = \int f_c y dA_c + \sum_{i=1}^{n} A_{si} y_i f_{si} \tag{5.5}$$

where, P_u is the ultimate axial load, A_{si} is the area of tendon i, f_{si} is the stress in tendon i, y is the distance from centroid to element dA_c, and y_i is the distance from centroid to tendon i.

In case of piles cut off at grade in stiff soil (with zero slenderness ratio) the ultimate resisting moment is equal to the ultimate applied moment as the surrounding soil prevents lateral deflection or moment magnification. Conversely, partially embedded piles will be subjected to applied moments that are smaller than the ultimate resisting moment due to lateral deflection amplification. The slenderness effect was incorporated in the program using Equation 5.6, which is also known as secant formula for long column. The equation is the relation between ultimate applied and resisting moment considering the slenderness effect.

$$M_u = M_{ur} / \sec\left(\sqrt{P_u h'^2 / 4EI}\right) \tag{5.6}$$

where, M_u and M_{ur} are ultimate applied and resisting moments and h' is the effective height. In this equation the flexural stiffness EI of the member is assumed to have a constant value along the full height of the member.

5.3 Input Parameters

5.3.1 Pile Information

Figure 5.2 presents the pile information input unit for the PCI spreadsheet. As can be seen, there are two methods available for establishing a pile cross section: [1] selecting the pile size from the pile library using dropdown box, and [2] entering each of the pile cross-sectional parameters manually.

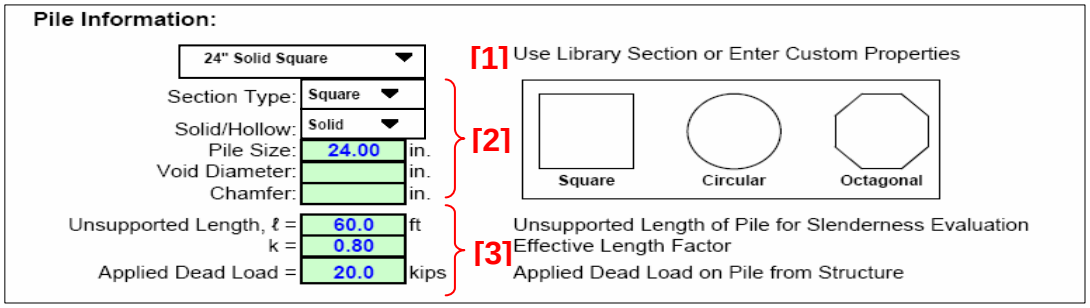

Figure 5.2 Pile information input section for the PCI Prestressed Concrete Interaction Diagram Spreadsheet (2004)

The unsupported length of the pile is used for the slenderness calculations. An effective length factor k is used to consider the pile end condition. The effective length factor, k, for sway or non-sway frame can be obtained using Figure 5.3. In the figure, Ψ's are the ratios of the summation of the stiffness (EI/L) for all compression members intersecting at the joints, $\sum(EI/L)_c$, to the similar quantity, $\sum(EI/L)_b$, for flexure members. Two Ψ values are determined for the compression member; one at each end. For fixed ends, Ψ can be considered as 1.0, while a value of 10 is normally used for hinged ends. Two charts are provided in the

figure for different conditions; namely, sway and non-sway frame. ACI (2005) allows using a Stability Index, Q, to determine whether a frame is sway-inhabited of not.

$$Q = \frac{\sum P_u \Delta_0}{V_{us} l_P} \tag{5.7}$$

In Equation 5.7, $\sum P_u$ is the total factored vertical load, V_{us} is the horizontal shear in the story due to lateral load, l_P is the height of the story measured from center to center of the joints above and below the story, and Δ_0 is the first order relative deflection between the top and bottom of the story due to V_{us}. If , Q is less than or equal to 0.05 the story within the structure is non-sway. Applying this equation to the bridge models revealed that the Q's for all the cases considered in this study are less than 0.05 for both strength V and strength III limit states. Therefore these models should be considered as non-sway to calculate the effective length factors for the piles. Table 5.1 presents the computed Q-values. Table 5.2 presents the k values obtained for different piles using Figure 5.3. For HPC connection, are 1.0 and 10.0 respectively, hence the effective length factor k is 0.85.

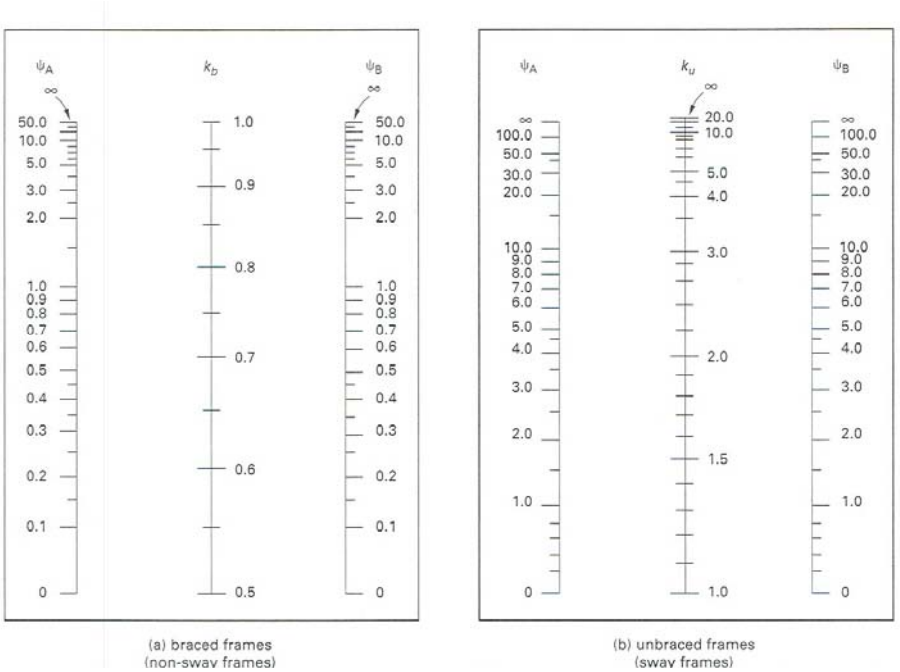

Figure 5.3 Effective length factor k for (a) Non-sway Frames (b) Sway Frames (ACI 2005)

Table 5.1 Stability index, Q For the bridges with different spans and unsupported pile lengths.

Limit State	Bridge Span (ft)	l_P(ft)	$\sum P_u$ (k)	V_{us}(k)	Δ_0(in)	Q	Frame Type
Strength V	30	18	545.12	0.0155	4.20	0.0093	Nonsway
		30	545.12	0.0435	4.30	0.0154	Nonsway
	50	18	817.23	0.0141	6.95	0.0077	Nonsway
		40	817.23	0.0941	7.15	0.0224	Nonsway
	76	18	1360.1	0.0167	10.83	0.0097	Nonsway
		50	1360.1	0.1755	11.18	0.0356	Nonsway
	100	30	1900.7	0.0462	14.65	0.0166	Nonsway
		60	1900.7	0.2016	14.78	0.0360	Nonsway
Strength III	30	18	349.1	0.0552	14.83	0.0060	Nonsway
		30	349.1	0.1674	15.79	0.0103	Nonsway
	50	18	566.8	0.0502	24.19	0.0055	Nonsway
		40	566.8	0.3491	26.63	0.0155	Nonsway
	76	18	970.2	0.0577	40.01	0.0065	Nonsway
		50	970.2	0.6758	44.38	0.0246	Nonsway
	100	30	1452.3	0.1755	57.64	0.0123	Nonsway
		60	1452.3	0.7638	59.27	0.0260	Nonsway

Table 5.2 Effective length coefficient k for different piles used in the study.

Pile-to-cap Connection	Span Length	L_P (ft)	L_{b1} (ft)	L_{b2} (ft)	I_c $\times 10^3$ (in^4)	I_b $\times 10^5$ (in^4)	$\sum(EI/L)_c$ (in)	$\sum(EI/L)_b$ $\times 10^7$(in)	Ψ_B	Ψ_A	k
RPC	30ft	18	3.5	6.73	8.75	1.44	180384	1.89	0.0	1.0	0.63
		24	3.5	6.73			135288		0.0	1.0	0.63
		30	3.5	6.73			108231		0.0	1.0	0.63
	50ft	18	3.5	8.41	27.6		570103	1.76	0.03	1.0	0.63
		24	3.5	8.41			427577		0.02	1.0	0.63
		30	3.5	8.41			342062		0.019	1.0	0.63
		40	3.5	8.41			256546		0.014	1.0	0.63
	76ft	18	3.5	15	61.8		1273288	1.54	0.08	1.0	0.65
		24	3.5	15			954966		0.06	1.0	0.64
		30	3.5	15			763973		0.05	1.0	0.63
		40	3.5	15			572980		0.03	1.0	0.63
		50	3.5	15			458384		0.03	1.0	0.63
	100ft	30	3.5	15	134.2		1660549	1.54	0.11	1.0	0.66
		40	3.5	15			1245412		0.08	1.0	0.65
		50	3.5	15			996329		0.07	1.0	0.64
		60	3.5	15			830275		0.05	1.0	0.63
HPC	All Models								10.0	1.0	0.85

5.3.2 Reinforcement

Figure 5.4 presents the input sections for the pile reinforcement. Input required for the pretensioned strands include size, number, modulus of elasticity, ultimate strength, and the fraction of the strand's strength used for initial stress. Table 2.2 presents the diameters, types and number of strands used for different square/hollow pile sizes with square strand layouts specified in Louisiana DOTD's Bridge Design Manual (LA-BDM, 2004). Table 5.3 presents the input parameters for the reinforcement section used in this study.

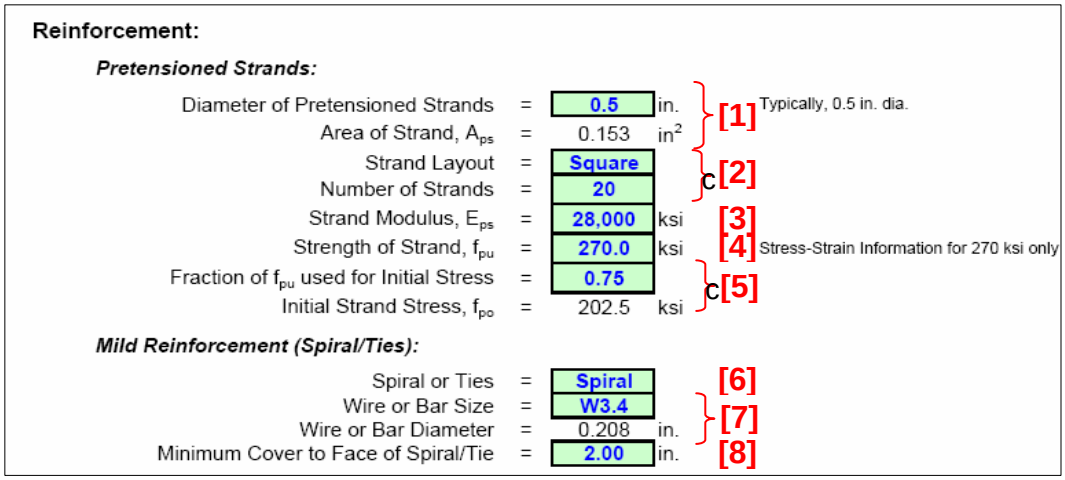

Figure 5.4 Input units for reinforcement in PCI Prestressed Concrete Interaction Diagram Spreadsheet (2004)

Table 5.3 Input parameter used in the PCI prestressed Concrete Interaction diagram Spreadsheet

Pile Type	Pretenstioned strand					Concrete strength	
	Dia. (in.)	No.	Modulus of Elasticity (ksi)	Strength (f_{pu}, ksi)	Fraction of f_{pu} used for initial stress f_{po}	at transfer f'_{ci} (ksi)	28 days f'_c (ksi)
18″ square pile	0.5″	12	28000	270	0.75	4.0	6.0
24″ square pile		20					
30″ hollow square pile		24					
36″ hollow square pile		28					

5.3.3 Concrete Properties

Five basic inputs are required for the concrete properties. These include: 28 days concrete strength, f'_c and strength at transfer f'_{ci}, unit weight (150pcf), ambient relative humidity (used for shrinkage loss), and ultimate strain (usually 0.003 in/in). Table 5.3 shows the concrete strengths used for the piles in this study.

Concrete Properties:

Concrete Strength at Transfer, f'_{ci}	=	4.00	ksi	
Specified Concrete Strength f'_c	=	6.00	ksi	
Concrete Unit Weight, w_c	=	0.150	kcf	
Ambient Relative Humidity, H	=	75	%	(Used for Shrinkage Loss)
Concrete Ultimate Strain, ε_{cu}	=	0.003	in./in.	

Figure 5.5 Input sections for concrete properties in PCI Prestressed Concrete Interaction Diagram Spreadsheet (2004)

5.3.4 Resistance Factor, Slenderness and Design Points

The capacity reduction factors for flexure and compression are required in order to create interaction diagrams for the piles for resistance factor design. Figure 5.6 presents the input sections for the resistance factor and design points in the PCI spreadsheet. These factors vary depending on the specifications used. In AASHTO-LRFD specifications (2004), for flexure and tension of prestressed concrete members the resistance factor is taken as 1.0. The LRFD specifications use a factor of 0.7 for compression members regardless of whether the transverse reinforcement is tied or spiral (Article 5.5.4.2.1). Factored pile axial loads obtained from the finite element analysis of the bridges were used as design points to determine the factored moment capacity of the piles under consideration.

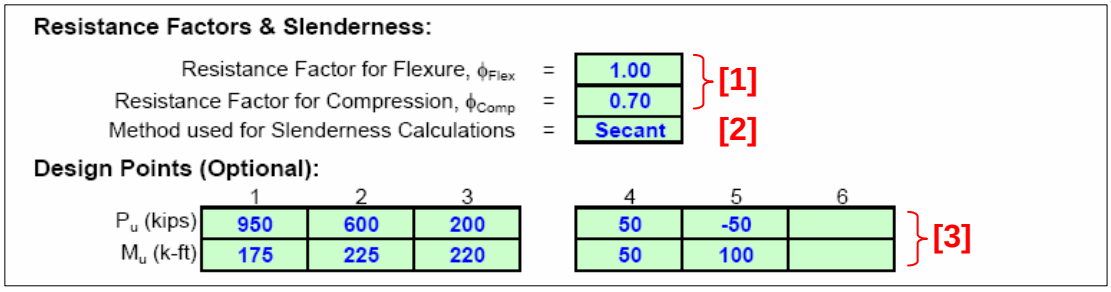

Figure 5.6 Input sections for resistance factor, slenderness and design points in PCI Prestressed Concrete Interaction Diagram Spreadsheet (2004)

5.4 Output from the PCI Spreadsheet

In the PCI spreadsheet the output is reported in two separate worksheets. The first worksheet, seen in Figure 5.7, includes a tabulation of the design points along with the maximum moment, including slenderness effects, for the specified axial loads. The second worksheet contains the key points on the basic interaction diagram (I.D.) after applying the resistance factors (Figure 5.8) and the interaction diagram (Figure 5.9) produced by the spreadsheet. The output as shown in Figure 5.9 contains: [1] the I.D. without slenderness consideration, [2] the slenderness ratio along with other pile information, reported within the caption of the diagram, [3] the I.D. with slenderness consideration, [4] the maximum axial load cutoff, as required by AASHTO specifications, and [5] the design points entered in the input section.

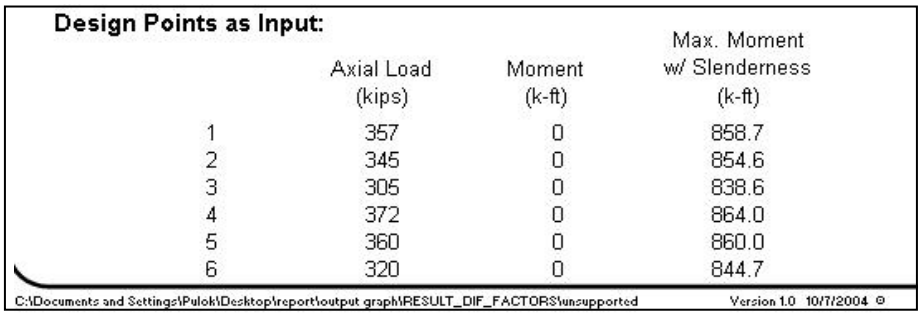

Design Points as Input:

	Axial Load (kips)	Moment (k-ft)	Max. Moment w/ Slenderness (k-ft)
1	357	0	858.7
2	345	0	854.6
3	305	0	838.6
4	372	0	864.0
5	360	0	860.0
6	320	0	844.7

C:\Documents and Settings\Pulok\Desktop\report\output graph\RESULT_DIF_FACTORS\unsupported Version 1.0 10/7/2004

Figure 5.7 Output worksheet with maximum moment (including slenderness effects) for the specified axial loads.

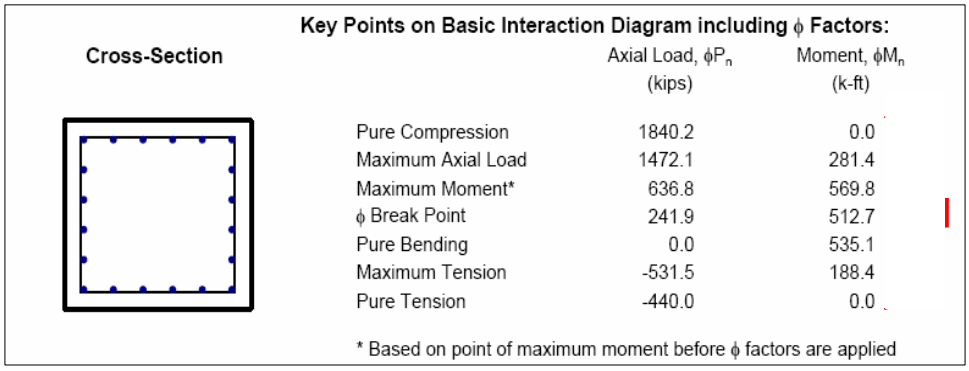

Figure 5.8 Output worksheet with key points on Interaction diagram including ϕ factor

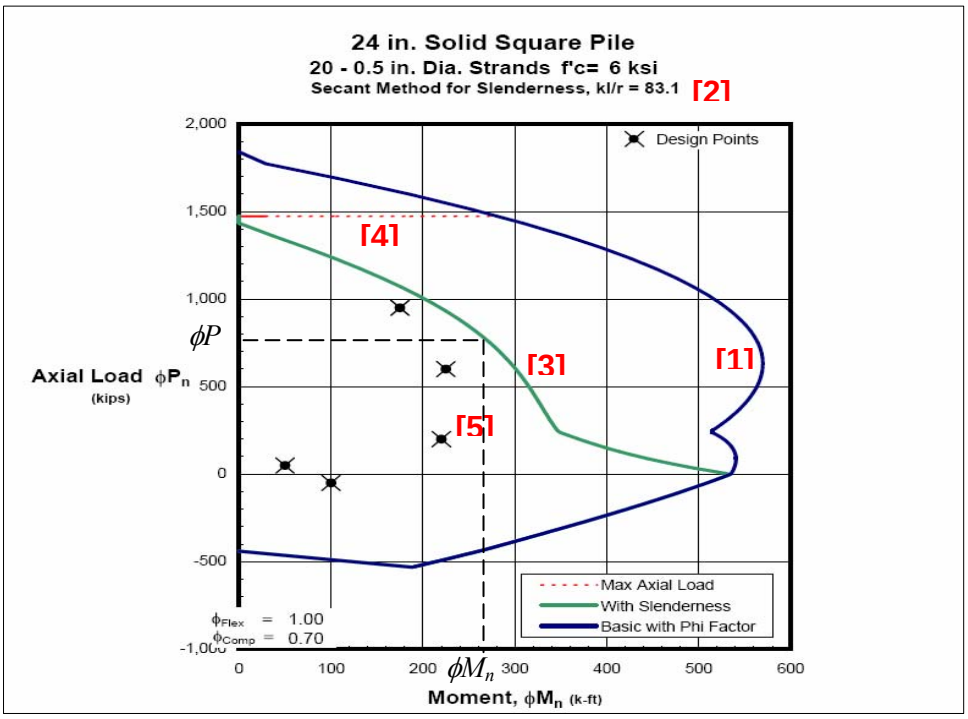

Figure 5.9 Interaction diagram produced by the PCI prestressed concrete spreadsheet

5.5 Capacity Utilization

In this study finite element analyses were performed for the bridge bents to obtain applied axial loads and bending moments for the piles under different limit states. Prestressed concrete pile interaction diagram was used to determine the capacity of each pile. The PCI spreadsheet generated the factored moment capacity, ϕM_n, (Figure 5.9) of each pile for factored applied axial

load, P_u, obtained from FE analysis. Capacity utilizations for the piles were then computed by dividing the applied bending moments by the moment capacities.

5.6 Conclusion

Prestressed concrete interaction diagrams were used in this study to determine the capacity of the piles selected using LA-DOTD design tools for the bridges analyzed in Chapter 4. An excel spreadsheet prepared by Precast/Prestressed Concrete Institute (PCI 2004) was used to construct the interaction diagrams. This chapter discusses the process and input parameters used to obtain the pile capacity.

CHAPTER 6. ANALYTICAL RESULTS AND DISCUSSION

6.1 Introduction

This chapter presents the straining action results obtained from finite element analyses described in Chapter 4. It also presents pile capacity results obtained using the procedures discussed in Chapter 5. Capacity utilization of the piles for bridge bents with different bridge spans, skew angles, and unsupported pile lengths were calculated. These piles were selected considering LA-DOTD guidelines. Based on the percentages of capacity utilizations, limitations on the use of LA-DOTD pile design table for different skew angles, spans, unsupported pile lengths, and wind velocities have been identified.

6.2 Pile Straining Actions

The SAP2000 FE software package was used to analyze bridges with different configurations. The pile size for each bridge was selected considering allowable factored axial load for pile bents (Table 2.4) provided in LA-DOTD BDM (2004). Table 6.1 presents the factored axial loads and selected pile sizes for different span lengths. It should be noted that these factored loads are only due to the effects of dead and live loads according to the BDM.

To assess the feasibility of this method, straining action from the refined method (FE) were determined. The straining actions were obtained for different dead, live and wind load cases as specified in AASHTO-LRFD (2004). Vehicular loads were placed on the deck immediately above the pile cap to obtain the maximum pile axial load. Four design wind velocities (55mph, 60 mph, 100mph, and 150mph) applicable for Louisiana were applied to obtain the maximum axial loads and bending moments acting on the most critical piles. Strength III and Strength V limit states, based on design wind velocities, were considered to obtain factored demands on all piles.

Table 6.1 Selection of pile size for different bridge span considering LA-DOTD guide line

Span (ft)	Maximum factored axial Load, (k) for dead load and live load only	Selected Pile Size (in)	Allowable load range, (k)
30	176	18"	150-230
50	301	24"	240-360
76	587	30"	400-600
100	790	36"	520-800

6.3 Pile Capacities and Capacity Utilization

The factored moment capacities of all piles were calculated for the applied axial loads using prestressed concrete pile interaction diagram as described in Chapter 5. Pile capacity utilizations were obtained by dividing the applied moments by the moment capacities as illustrated in Figure 6.1. In the figure, M_u is the applied factored moment for the pile and ϕM_n is the factored capacity of the pile when it is subjected to the applied axial load. In other words the capacity utilization is computed as

$$\text{Capacity Utilization (\%)} = \frac{M_u}{\phi M_n}$$

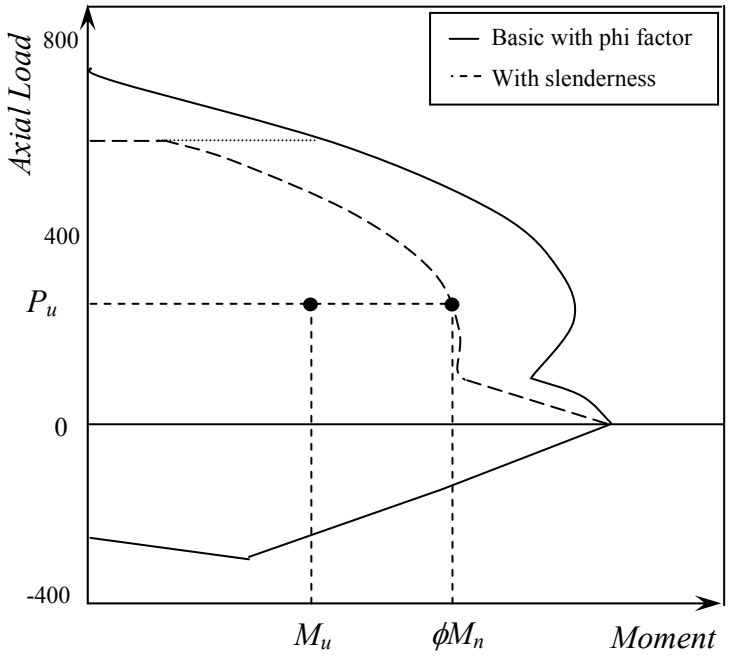

Figure 6.1 Interaction Diagram for prestress concrete piles.

The Pile with maximum percentage of moment capacity utilization for each model case was selected as the critical pile. Two types of pile cap connection (RPC and HPC) were considered since the exact type of pile-cap continuity for a pile bent system is unknown. Tables 6.2 to 6.5 presents the percentages of capacity utilization of critical piles with RPC and HPC connections for different bridge spans, skew angles, unsupported pile lengths (L_P) and wind velocities. Failure of a pile should be considered at or above 100% capacity utilization. However, 75% limit on capacity utilization is recommended because of the approximate nature of the simplified procedure.

Table 6.2 Percentages of capacity utilizations of critical piles at 55 mph wind velocity (Str. V)

span length (ft)	L_P (ft)	Rigid Pile-Cap (RPC) Connection				L_P (ft)	Hinged Pile-Cap (HPC) Connection			
		Skew angle(degree)					Skew angle(degree)			
		0	30	45	60		0	30	45	60
30	18	11.9	13.4	20.0	34.6	18	4.8	5.0	4.6	5.5
	24	15.1	17.5	22.4	35.4	24	11.7	13.1	13.1	13.8
	30	14.3	16.6	21.6	32.5	30	14.4	16.9	16.9	17.8
50	18	3.0	11.1	14.7	21.3	18	3.7	4.2	5.0	5.2
	24	3.1	11.6	13.8	22.0	24	4.9	5.1	5.2	10.0
	30	7.5	13.7	16.1	23.6	30	11.5	13.9	14.9	15.1
	40	10.3	15.3	18.8	22.3	40	14.9	19.5	22.4	21.1
76	18	8.0	8.5	9.0	17.4	18	5.5	7.0	6.7	8.8
	24	8.6	8.8	9.7	16.6	24	7.2	8.0	7.9	10.7
	30	11.2	9.5	9.8	15.8	30	9.7	10.0	10.5	13.0
	40	13.2	12.0	15.5	17.9	40	21.7	22.7	21.7	21.7
	50	16.7	14.8	20.8	20.0	50	27.4	31.0	32.7	29.6
100	30	7.9	9.6	7.9	11.4	30	7.7	12.0	7.7	12.7
	40	9.6	10.6	9.7	13.8	40	16.6	16.3	16.6	18.1
	50	12.1	12.8	10.5	17.1	50	22.5	23.5	22.5	24.4
	60	15.1	15.9	13.6	20.5	60	30.2	32.2	30.2	26.7

Table 6.3 Capacity Utilizations for critical piles at 60 mph wind velocity (Str. III)

span length (ft)	L_P (ft)	Rigid Pile-Cap (RPC) Connection				L_P (ft)	Hinged Pile-Cap (HPC) Connection			
		Skew angle(degree)					Skew angle(degree)			
		0	30	45	60		0	30	45	60
30	18	10.5	11.3	15.9	26.6	18	7.5	8.2	8.9	11.1
	24	11.7	12.1	15.2	24.9	24	10.9	11.5	13.3	16.2
	30	12.4	12.6	17.1	22.5	30	14.0	17.4	18.9	20.6
50	18	4.3	11.3	13.6	18.9	18	5.7	6.4	7.3	8.8
	24	4.8	11.1	13.0	24.6	24	7.9	8.6	8.6	26.5
	30	7.0	12.4	13.8	22.0	30	9.7	12.5	13.0	15.2
	40	9.6	14.7	16.2	21.3	40	12.6	18.5	19.3	22.0
76	18	6.4	13.4	11.5	14.6	18	9.8	13.5	12.1	14.3
	24	7.9	13.4	12.4	18.0	24	13.2	15.0	15.2	18.3
	30	13.3	15.4	15.1	21.0	30	17.8	18.8	19.8	22.9
	40	18.8	20.7	20.4	26.6	40	27.7	28.4	28.9	32.2
	50	22.6	25.2	23.6	32.1	50	37.8	39.3	40.7	43.5
100	30	9.6	16.3	16.0	21.6	30	15.3	19.7	15.6	21.2
	40	14.1	22.3	19.7	29.0	40	24.1	27.2	24.5	28.4
	50	17.6	26.2	23.1	35.9	50	33.1	31.7	33.7	38.7
	60	21.9	31.2	27.1	41.1	60	44.9	46.9	45.6	48.1

Table 6.4 Capacity Utilizations for critical piles at 100 mph wind velocity (Str. III)

span length (ft)	L_P (ft)	Rigid Pile-Cap (RPC) Connection				L_P (ft)	Hinged Pile-Cap (HPC) Connection			
		Skew angle(degree)					Skew angle(degree)			
		0	30	45	60		0	30	45	60
30	18	14.7	15.6	19.8	26.6	18	20.6	23.0	24.7	33.4
	24	19.0	20.2	24.9	33.6	24	26.8	29.9	35.0	46.1
	30	23.5	24.7	36.0	40.1	30	33.8	45.8	49.8	58.6
50	18	9.2	14.1	16.3	20.8	18	15.9	17.4	18.9	23.0
	24	12.0	17.2	20.8	24.6	24	22.0	24.1	25.9	26.5
	30	15.0	21.6	24.6	33.4	30	23.2	31.7	34.6	40.9
	40	20.5	28.5	36.1	43.7	40	28.6	46.0	51.3	59.5
76	18	17.0	31.1	26.1	32.3	18	27.3	35.9	32.2	35.4
	24	21.4	32.0	32.8	41.2	24	36.9	40.7	42.8	47.8
	30	35.2	37.9	40.6	49.8	30	49.5	52.0	55.5	61.4
	40	40.6	46.6	53.4	63.3	40	71.7	75.0	79.4	86.8
	50	51.5	58.3	64.9	78.9	50	98.8	103.4	110.3	118.1
100	30	26.1	38.9	38.7	50.3	30	42.9	49.2	43.9	53.3
	40	32.1	47.5	47.6	63.9	40	62.1	67.4	63.3	71.2
	50	40.3	58.2	58.3	83.4	50	84.6	82.0	86.2	100.3
	60	49.8	70.3	70.4	103.1	60	113.1	119.3	115.2	132.8

Table 6.5 Capacity Utilizations for critical piles at 150 mph wind velocity (Str. III)

span length (ft)	L_P (ft)	Rigid Pile-Cap (RPC) Connection				L_P (ft)	Hinged Pile-Cap (RPC) Connection			
		Skew angle(degree)					Skew angle(degree)			
		0	30	45	60		0	30	45	60
30	18	26.2	30.1	36.0	53.9	18	45.4	51.5	53.3	75.5
	24	34.2	38.2	45.3	68.2	24	56.3	63.8	72.1	102.3
	30	43.7	47.6	67.9	83.0	30	73.4	98.9	100.1	128.3
50	18	19.4	26.2	33.1	42.2	18	35.7	38.5	43.1	50.3
	24	25.7	33.6	43.7	47.9	24	49.2	53.9	58.6	58.0
	30	30.1	40.9	48.1	67.8	30	50.4	68.1	75.4	90.4
	40	40.9	55.1	75.2	90.6	40	58.5	96.4	110.6	130.6
76	18	38.3	66.2	56.5	67.7	18	61.8	79.6	71.2	77.0
	24	48.0	71.9	74.3	87.6	24	83.6	91.4	96.3	106.1
	30	79.4	85.2	91.1	107.4	30	111.9	117.1	124.8	137.4
	40	89.3	101.2	119.6	137.8	40	158.2	166.9	177.9	194.9
	50	112.4	125.4	146.1	173.3	50	218.9	229.7	245.7	265.3
100	30	58.8	86.5	83.3	107.8	30	97.5	107.5	98.8	116.9
	40	69.7	102.2	102.7	136.0	40	137.4	147.4	139.3	156.9
	50	86.8	125.2	127.1	180.7	50	186.5	183.0	189.0	223.0
	60	108.3	152.0	154.4	228.3	60	248.3	262.6	251.5	300.2

6.4 Effect of Studied Parameters on Capacity Utilization

6.4.1 Unsupported Pile Lengths

The effects of different parameters on percentage capacity utilizations of the critical piles are discussed below. According to AASHTO-LRFD (2004) specification, Strength V limit state should be considered for normal vehicular use of the bridge with 55 mph wind velocity. The live load case causing the maximum capacity utilization differed according to span length. The two loaded lanes configuration (Figures 3.4a and 3.4b) was found to be critical for 30 ft and 50 ft span bridges, while the three loaded lane (Figures 3.4c and 3.4d) produced the critical condition for 76 ft and 100 ft span lengths. For wind velocity higher than 55 mph Strength III limit state should be considered where higher load factor is applied to the wind load and live loads are not considered since vehicles become unstable at excessive wind velocity. The effect of unsupported pile length on capacity utilization under both limit states is discussed below.

6.4.1.1 Strength V

Figures 6.2 to 6.5 present the effect of unsupported pile length on capacity utilization of piles considering Strength V limit state; i.e. at 55 mph wind velocity. It can be seen that the capacity utilization of the piles for all the span lengths and skew angles are below 40% at 55 mph wind velocity. Therefore LA-DOTD guideline for pile design is applicable for normal vehicular use of all the spans and skew angles considered in this study provided that the unsupported pile lengths are no larger than 20 times the least dimension of the piles. For all the cases, capacity utilization increases with the increase in unsupported length. Percentages of pile capacity utilization for 30 ft span bridge seem to be higher than that for higher span lengths. This is because smaller pile size with lower pile capacity was considered for smaller span length due to lower axial load. For piles shorter than 30 ft, moments on pile-cap joints of the critical piles with RPC connection were higher than moments at the bottom of the piles with HPC connection. Hence, for these cases capacity utilizations of the piles with RPC connection were higher than those of the piles with HPC connection

Critical pile and controlling wind direction for each case are also presented in Figures 6.1 to 6.4. It can be seen that for 30 ft and 50 ft span bridges, piles facing the wind and closest to the live load are the critical piles. However, for 76 ft and 100 ft span bridges piles with wind acting in the opposite direction and far away from the live load are critical for 0 degree skew angles. This difference in location of critical pile for different span lengths is due to the fact that all the bridges have the same width and for 76 ft and 100 ft span bridges three-lane live load produces the maximum utilization where for 30 ft and 50 ft span bridges two-lane live load is critical. For higher span lengths skew angle seem to have more effect on the location of the critical pile.

6.4.1.2 Strength III

Piles facing the wind were critical at high wind velocity since live load effects are not considered in Strength III limit state. Figures 6.6 and 6.7 present the effects of unsupported pile lengths (L_p) on capacity utilization at 100 mph wind velocity for different skew angles and bridge spans. It can be seen that the capacity utilizations are than those obtained for Strength V although it appears that 30 ft and 50 ft span bridge capacity utilizations are still well below 75% limit. Larger span lengths seem to exceed the conservative 75% limit and even the 100% failure limit. For example, the 76ft span bridge capacity utilization seem to start exceeding 75% and 100% threshold line at 36 ft and 44 ft unsupported lengths, respectively. The similar unsupported pile length limits for 100 ft span are 42 and 50 ft. Figures 6.8 and 6.9 present the effects of unsupported pile lengths (L_p) on capacity utilization at 150 mph wind velocity. As may be expected, higher demands lead to exceeding the threshold limits for many of the analyzed bridges. These findings will result in recommendations to limit the applicability of the simplified approach based on wind velocity.

6.4.2 Skew Angle

6.4.2.1 Strength V

Figures 6.10 and 6.11 present the effect of skew angle on pile capacity utilization for different span lengths at 55 mph wind velocity. As can be seen, the capacity utilizations of all the piles regardless of skew angles are below 40%. A sharp increase is observed in capacity utilization of piles (with RPC connection) in bridges with skew angles exceeding 45 degree. This observation is true for 30 ft and 50 ft span bridges. This behavior is not observed for longer span bridges.

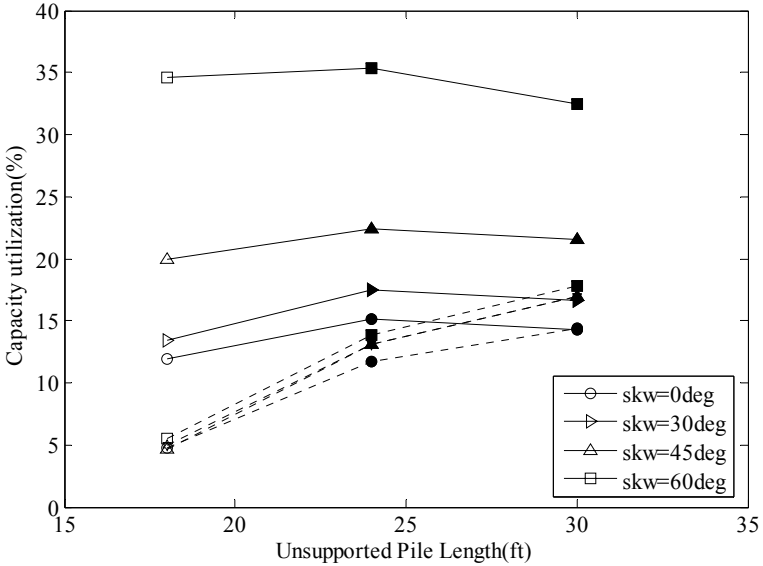

RPC
HPC
Void Straight ext. pile
Filled Battered ext. pile

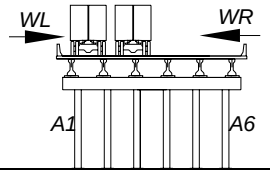

Critical Pile and Wind direction						
Skw (deg.)	Pile Length (ft)					
	18		24		30	
	RPC	HPC	RPC	HPC	RPC	HPC
0	A1 WL	A1 WL	A1 WL	A1 WL	A1 WL	A1 WL
30	A1 WL	A1 WL	A1 WL	A1 WL	A1 WL	A1 WL
45	A1 WL	A1 WL	A1 WL	A1 WL	A1 WL	A1 WL
60	A1 WR	A1 WL	A1 WR	A1 WL	A1 WR	A1 WL

Figure 6.2 Effect of unsupported pile length (L_p) on capacity utilization for 30 ft span bridge at 55 mph wind velocity (Strength V).

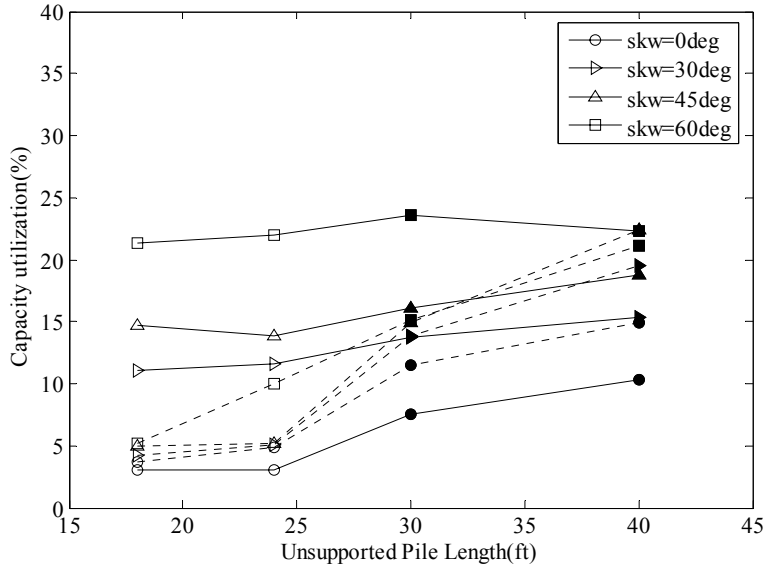

RPC
HPC
Void Straight ext. pile
Filled Battered ext. pile

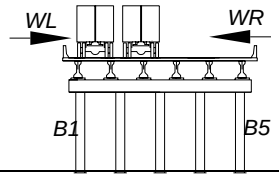

Critical Pile and Wind direction								
Skw (deg.)	Pile Length (ft)							
	18		24		**30**		**40**	
	RPC	HPC	RPC	HPC	RPC	HPC	RPC	HPC
0	B5 WR	B1 WL	B5 WR	B1 WL	B1 WL	B1 WL	B1 WL	B1 WL
30	B5 WR	B1 WL	B5 WR	B1 WL	B1 WL	B1 WL	B1 WL	B1 WL
45	B5 WR	B1 WL	B5 WR	B1 WL	B1 WL	B1 WL	B1 WL	B1 WL
60	B5 WR	B1 WL	B5 WR	B1 WL	B1 WR	B1 WL	B1 WR	B1 WL

Figure 6.3 Effect of unsupported pile length (L_p) on capacity utilization for 50 ft span bridge at 55 mph wind velocity (Strength V)

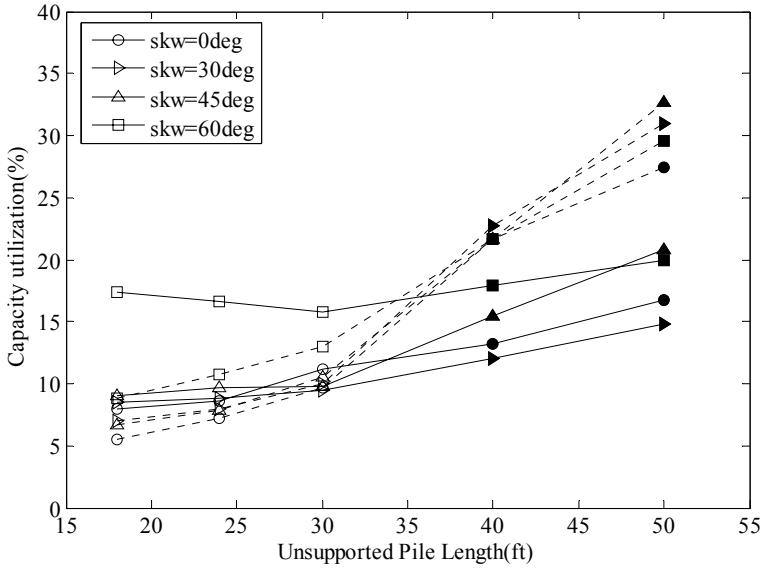

Skw (deg.)	Critical Pile and Wind direction									
	Pile Length (ft)									
	18		24		30		40		50	
	RPC	HPC	RPC	HPC	RPC	HPC	RPC	HPC	RPC	HPC
0	C3 WL	C3 WL	C3 WL	C3 WL	C3 WL	C3 WL	C3 WL	C1 WL	C3 WL	C1 WL
30	C3 WL	C1 WR	C1 WR	C1 WR	C1 WR	C3 WR	C2W L	C1 WL	C2 WL	C1 WL
45	C1 WL	C3 WR	C1 WR	C3 WR	C1 WR	C3 WR	C2 WL	C1 WL	C2 WL	C1 WL
60	C1 WL	C3 WR	C1 WL	C3 WR	C1 WR	C3 WR	C2 WL	C1 WL	C2 WL	C1 WL

Figure 6.4 Effect of unsupported pile length (L_p) on capacity utilization for 76 ft span bridge at 55 mph wind velocity (Strength V)

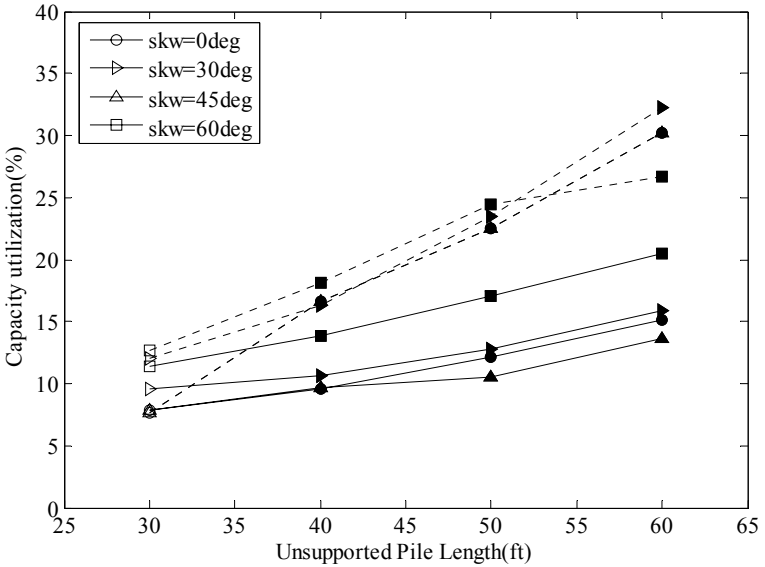

Skw (deg.)	Critical Pile and Wind direction							
	Pile Length (ft)							
	30		40		50		60	
	RPC	HPC	RPC	HPC	RPC	HPC	RPC	HPC
0	D3 WL	D3 WL	D3 WL	D1 WL	D3 WL	D1 WL	D3 WL	D1 WL
30	D1 WR	D3 WR	D1 WL	D1 WL	D1 WL	D3 WL	D1 WL	D1 WL
45	D1 WR	D3 WL	D2 WL	D1 WL	D1 WL	D1 WL	D2 WL	D1 WL
60	D3 WR	D3 WR	D3 WR	D1 WL	D3 WR	D1 WL	D3 WR	D1 WL

Figure 6.5 Effect of unsupported pile length (L_p) on capacity utilization for 100 ft span bridge at 55 mph wind velocity (Strength V)

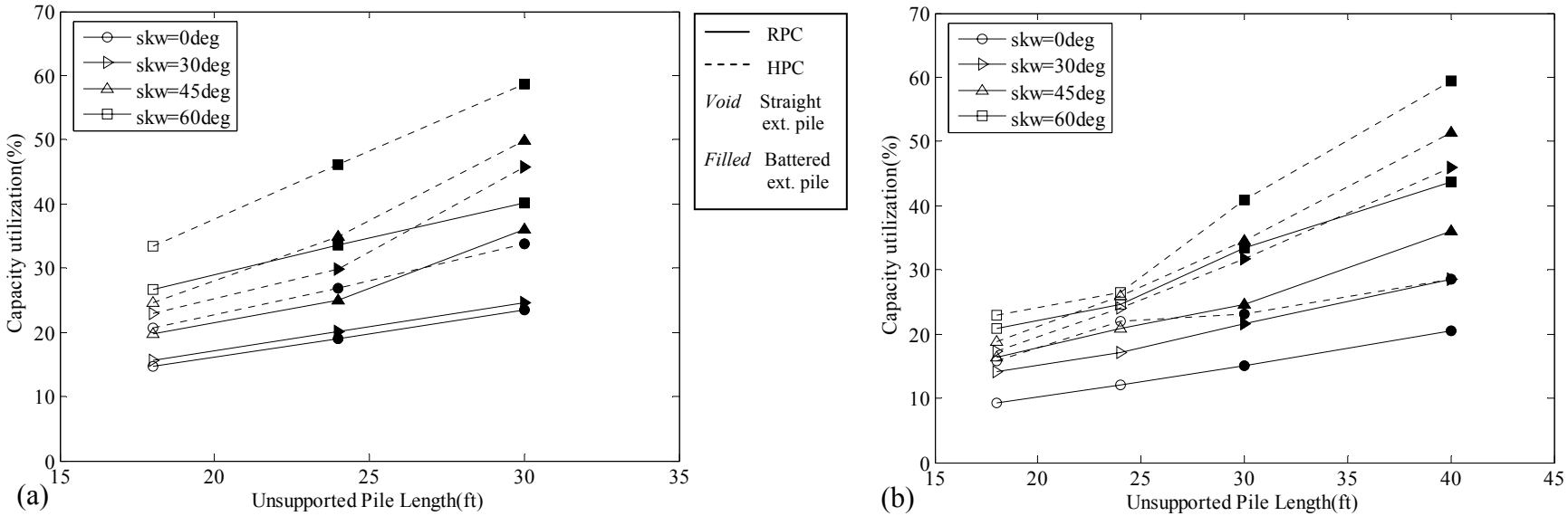

Figure 6.6 Effect of L_p on capacity utilization at 100 mph wind velocity for (a) 30 ft and (b) 50 ft span Bridges (Str. III).

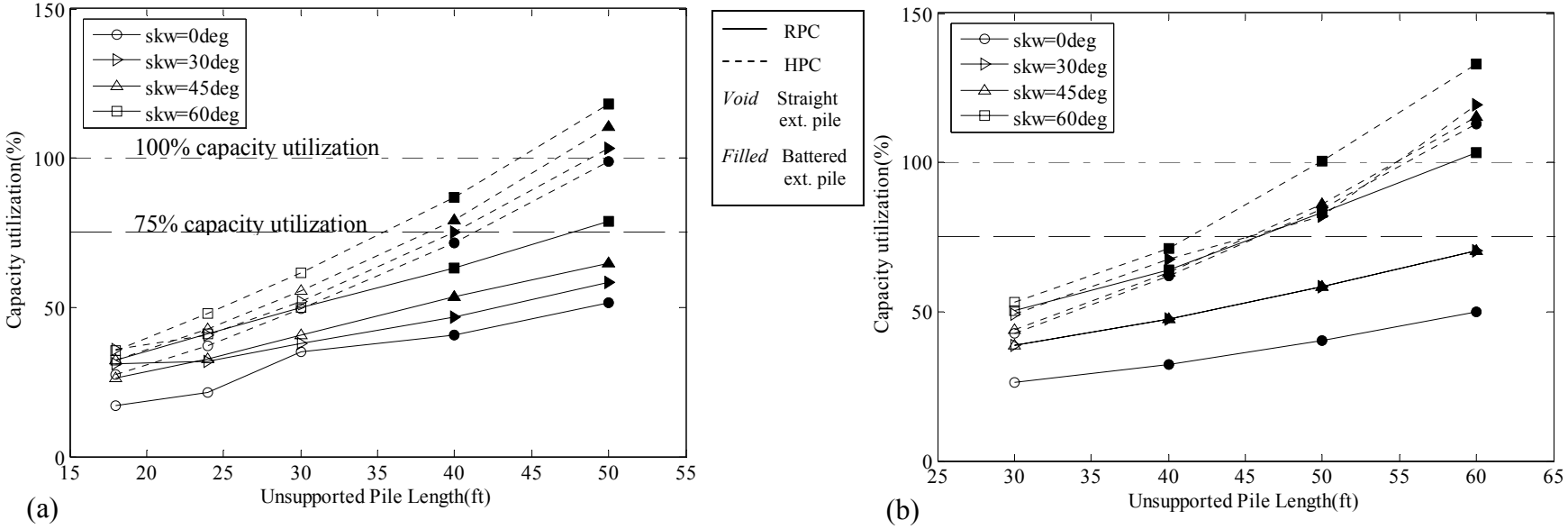

Figure 6.7 Effect of L_p on capacity utilization at 100 mph wind velocity for (a) 76 ft and (b) 100 ft span Bridges (Str. III).

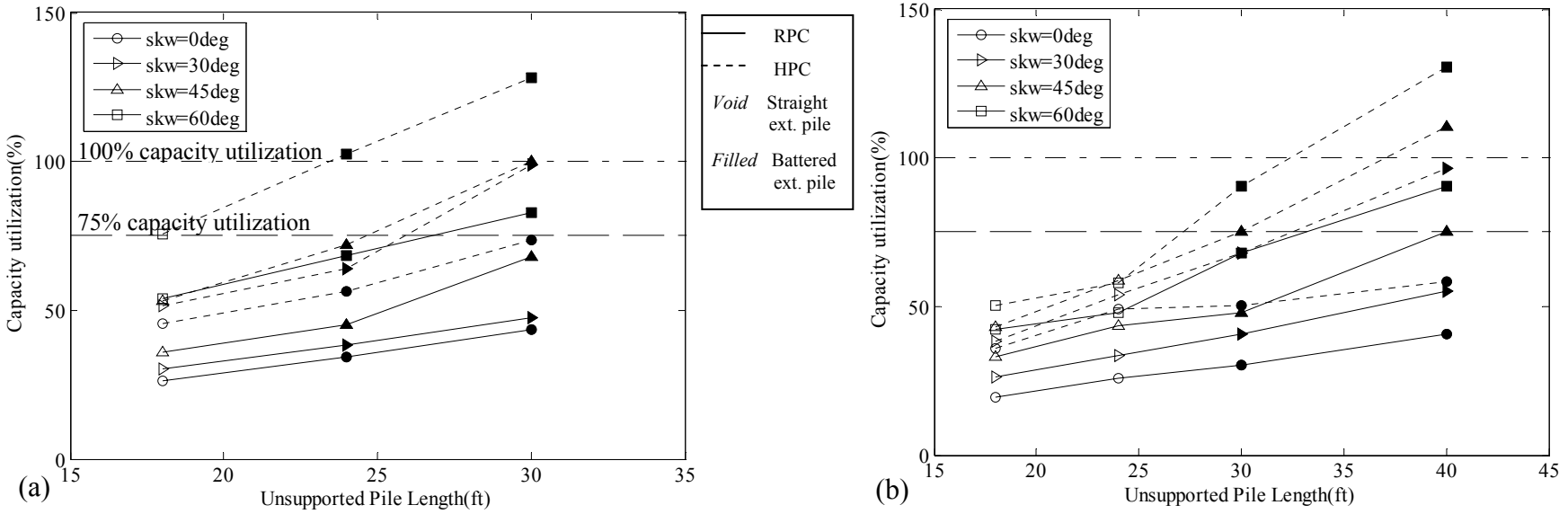

Figure 6.8 Effect of L_p on capacity utilization at 150 mph wind velocity for (a) 30 ft and (b) 50 ft span Bridges (Str. III).

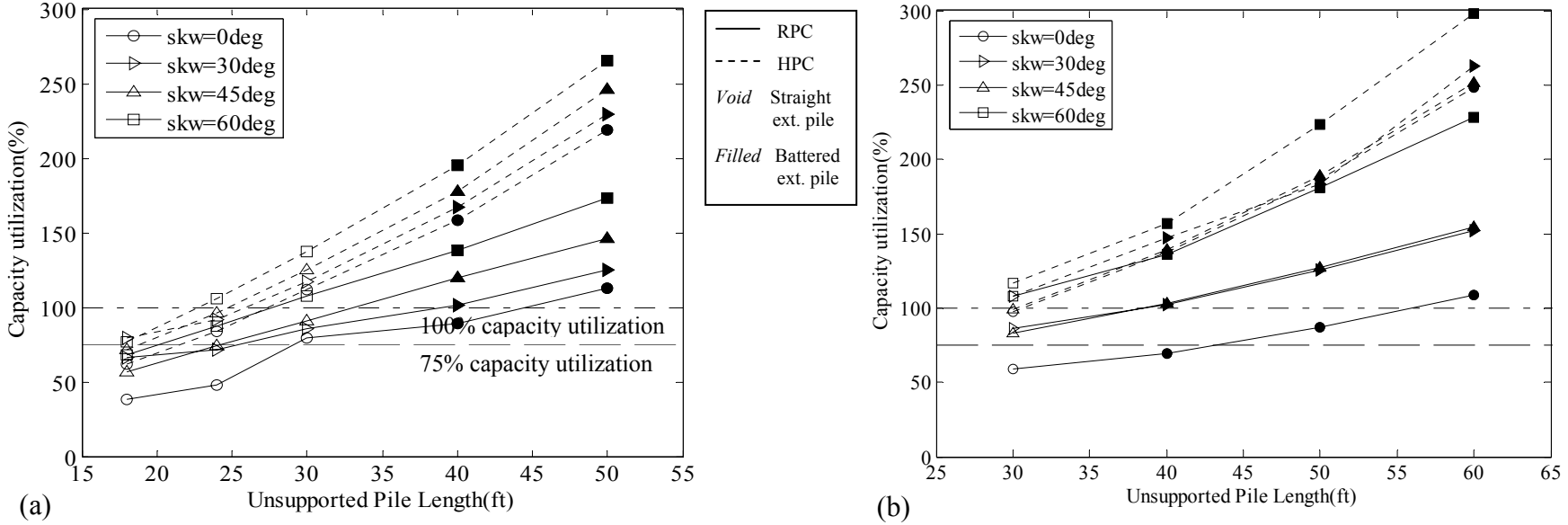

Figure 6.9 Effect of L_p on capacity utilization at 150 mph wind velocity for (a) 76 ft and (b) 100 ft span Bridges (Str. III).

6.4.2.2 Strength III

Figures 6.12 to 6.15 present the effect of skew angle on pile capacity utilization for 100 mph and 150 mph wind velocities. Gradual increase in capacity utilization is observed with the increase in skew angle for all the cases. At 100 mph wind velocity capacity utilizations of the piles for 30 ft and 50 ft span bridges are below 75% for all skew angles. However, at 150 mph wind velocity longer piles start to exceed the threshold limit as the skew angle increases. Fifty-ft long piles for 76 ft span bridges show unacceptable capacity utilization for all skew angles at 100 mph wind. At 150 mph wind velocity, most of the unsupported lengths join the group. For 100 ft span bridge shorter piles with skew angle not exceeding 45 degree do not exceed the 75%limit at 100 mph wind, and as expected most of the piles show unacceptable capacity utilization at 150 mph wind velocity.

6.4.3 Wind Velocity

Figures 6.16 to 6.23 show the effect of wind velocity on the capacity utilization of piles for bridges with different span lengths and skew angles. A sharp and almost linear increase in pile capacity utilization is observed with the increase in wind velocity for most cases. In the case of 60-degree skew angle and 30 ft span bridge, the longest pile even exceeds the 100% capacity utilization (indicates failure) at wind velocity higher than 130 mph. The wind velocity limits that can be allowed for 50 ft span bridge are 140 mph and 130 mph for the longest pile at 45 degree and 60 degree skew angles respectively. For 76 ft and 100 ft span bridges the longest pile seems to fail at or above 90 mph wind velocity. However higher wind velocities can be allowed for shorter piles.

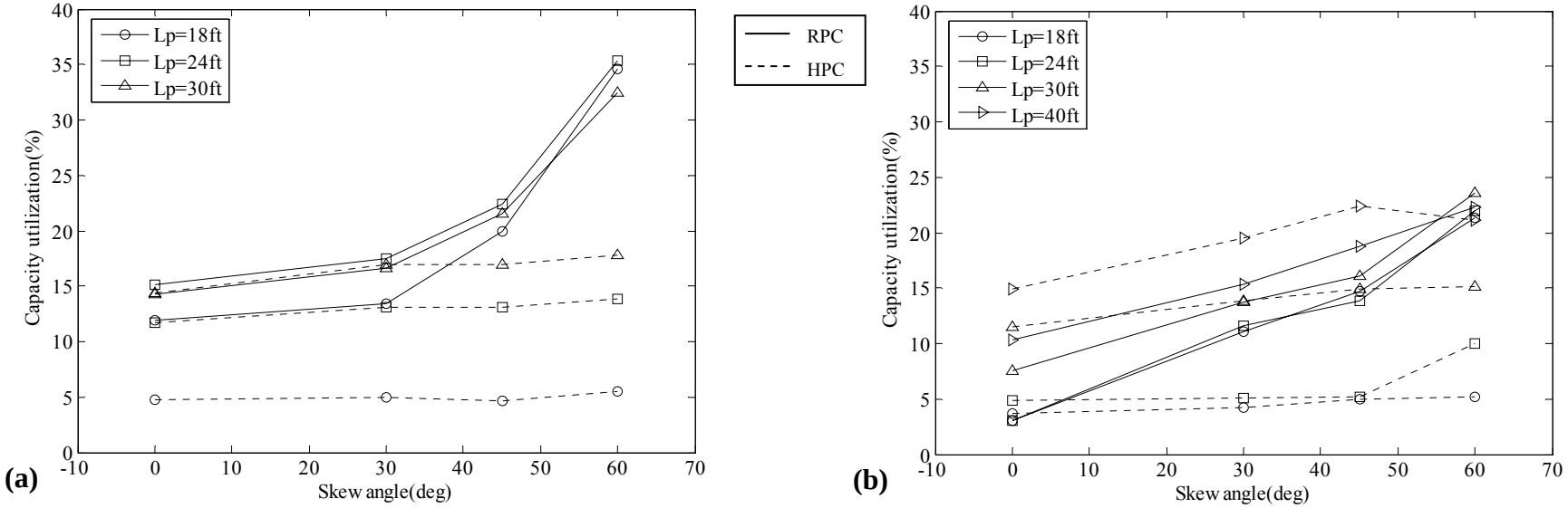

Figure 6.10 Effect of skew angle on capacity utilization at 55 mph wind velocity for (a) 30 ft span and (b) 50 ft span bridge (Str. V)

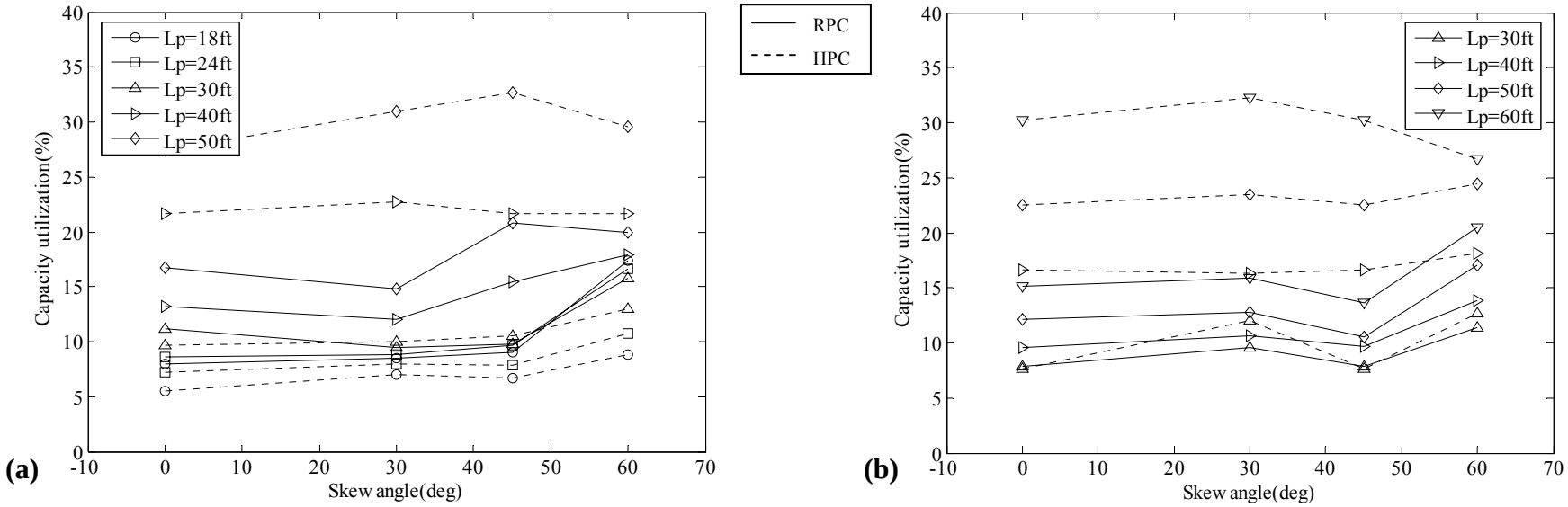

Figure 6.11 Effect of skew angle on capacity utilization at 55 mph wind velocity for (a) 76ft span and (b)100ft span bridge (Str.V)

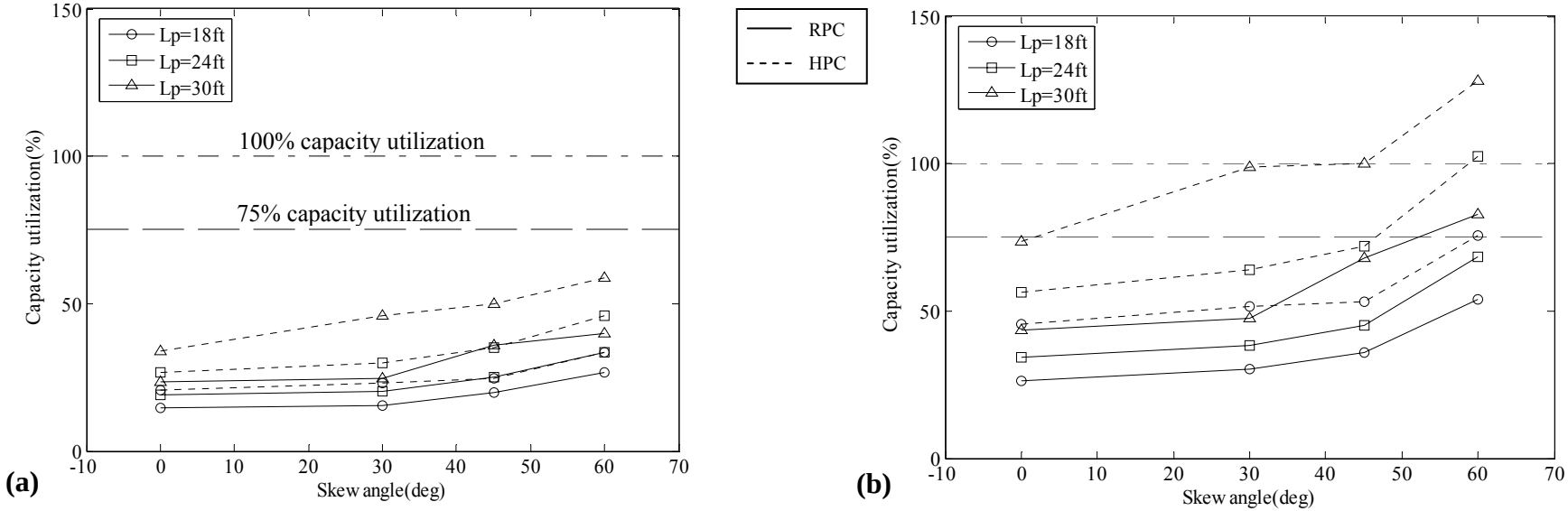

Figure 6.12 Effect of skew angle on capacity utilization for 30 ft span bridge at (a) 100mph and (b)150 mph wind velocity (Str.III)

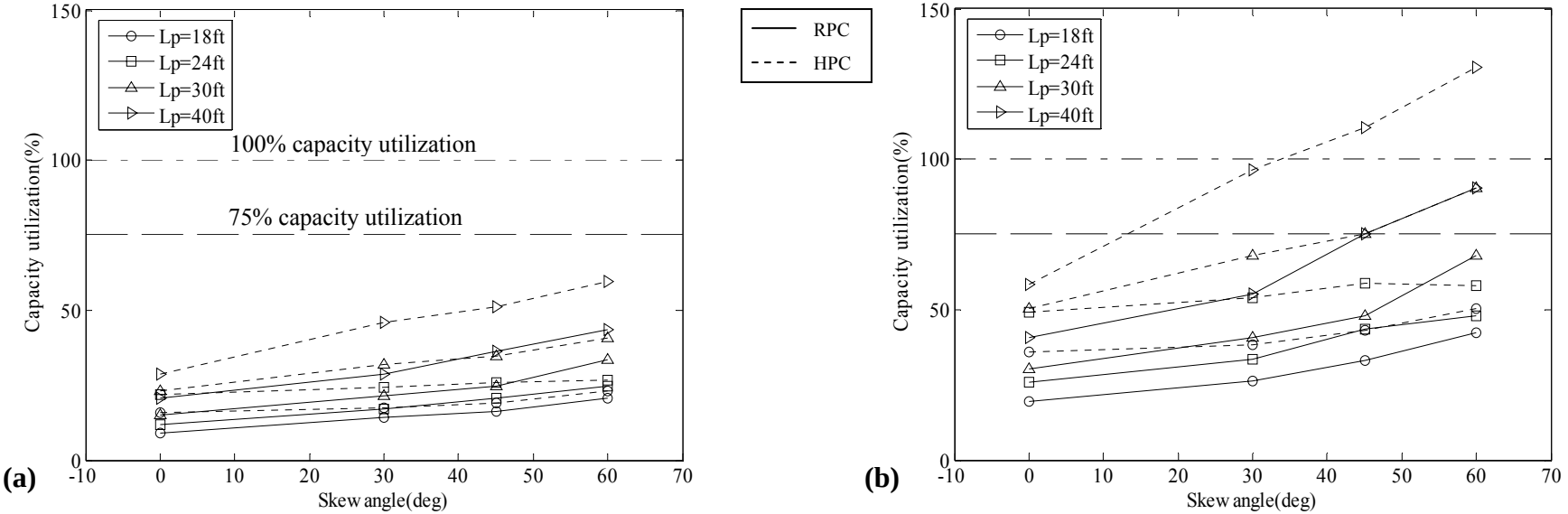

Figure 6.13 Effect of skew angle on capacity utilization for 50 ft span bridge at (a) 100mph and (b)150 mph wind velocity (Str.III)

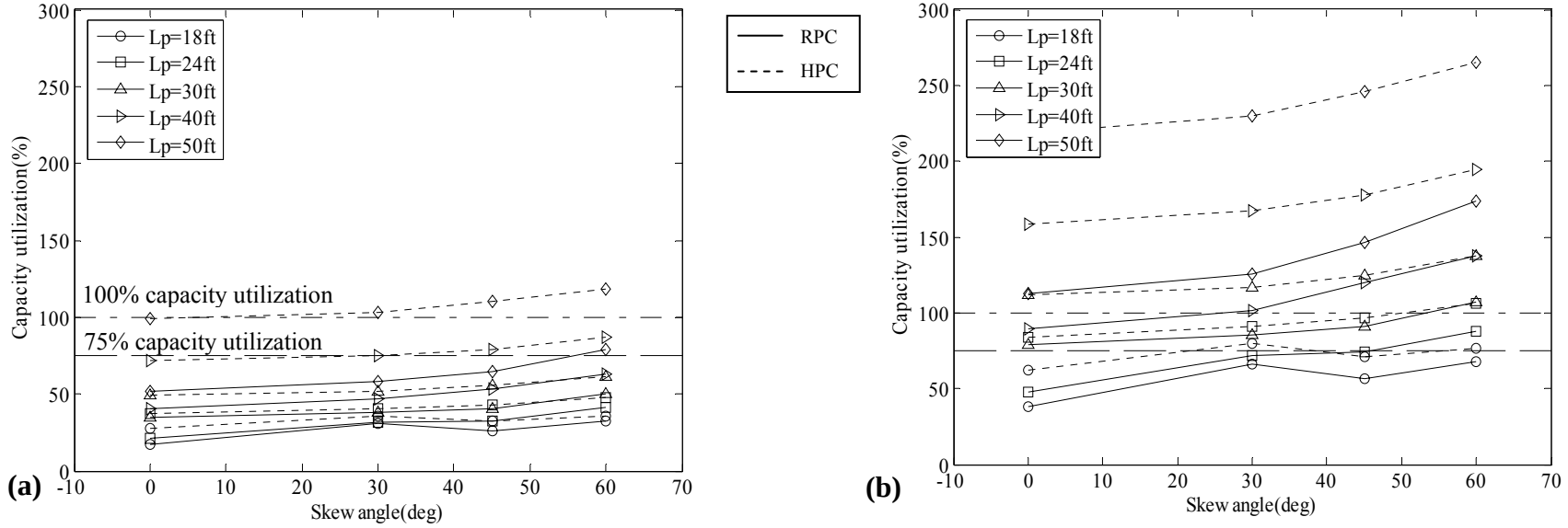

Figure 6.14 Effect of skew angle on capacity utilization for 76 ft span bridge at (a) 100mph and (b)150 mph wind velocity (Str.III)

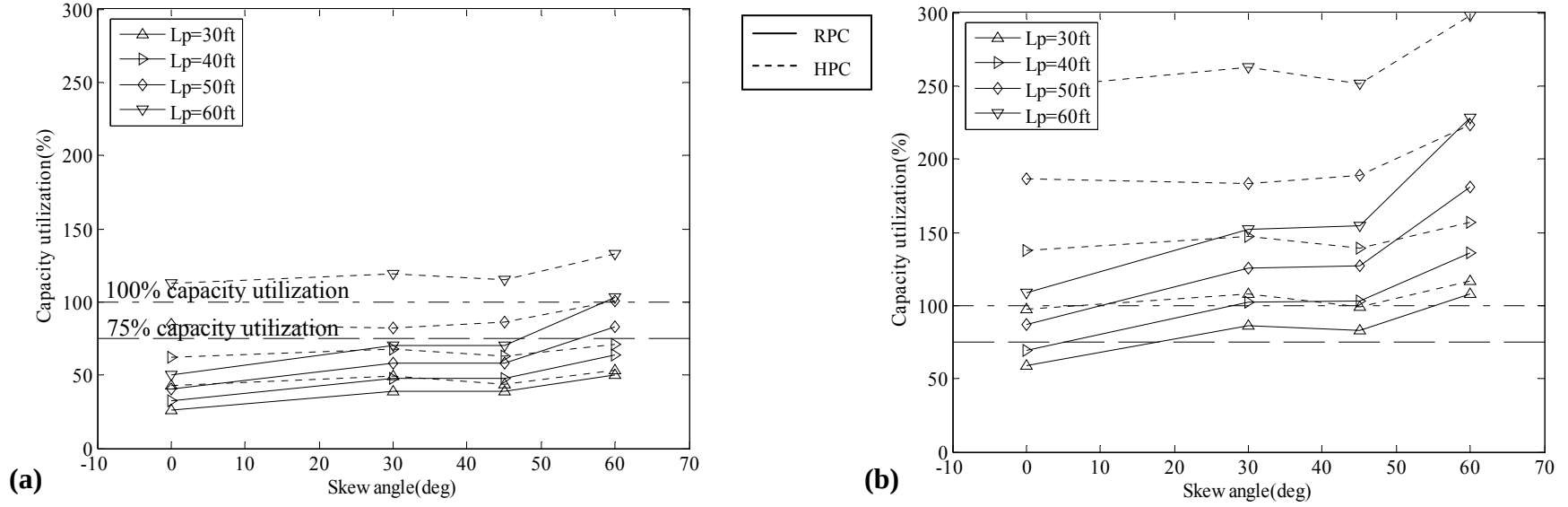

Figure 6.15 Effect of skew angle on capacity utilization for 100ft span bridge at (a) 100mph and (b)150mph wind velocity (Str.III)

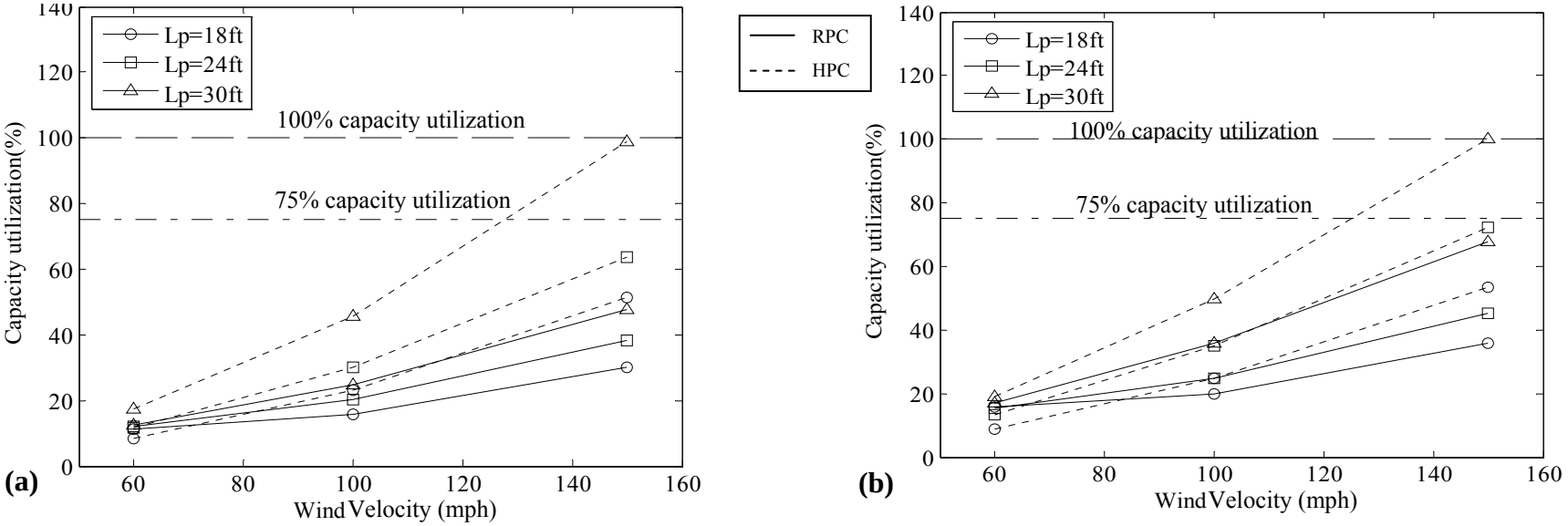

Figure 6.16 Effect of wind velocity on capacity utilization for 30 ft span bridge at (a) 0 deg. and (b) 30 deg. Skew angle (Str.III)

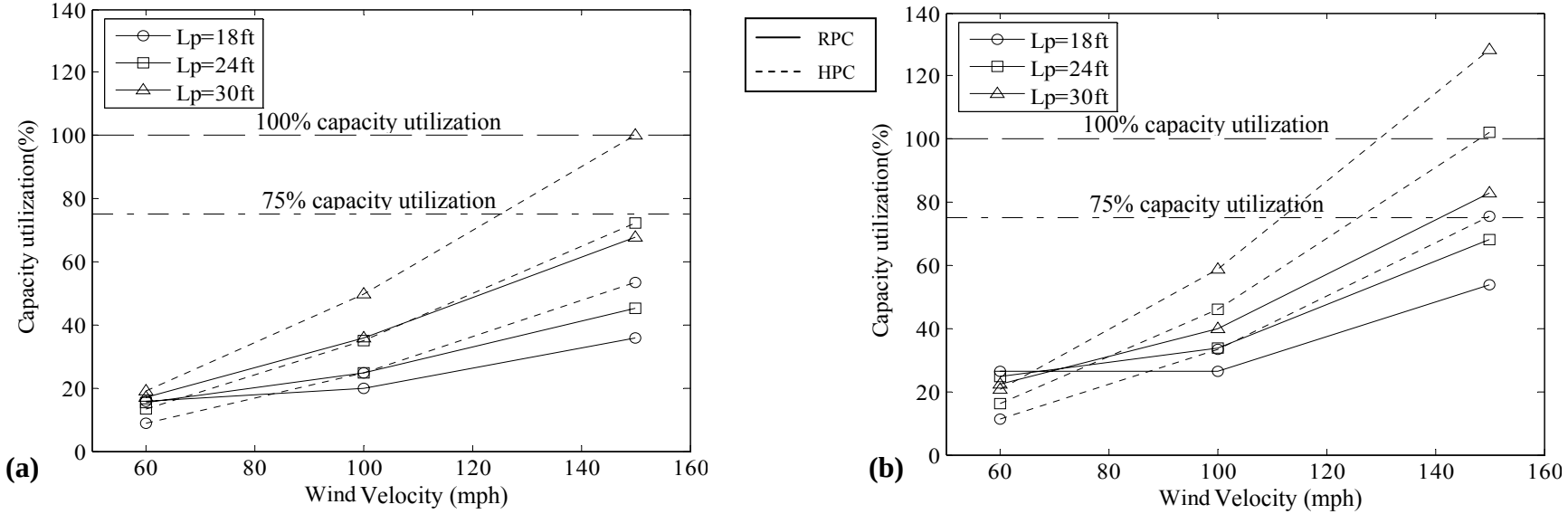

Figure 6.17 Effect of wind velocity on capacity utilization for 30 ft span bridge at (a) 45 deg. and (b) 60 deg. Skew angle (Str.III)

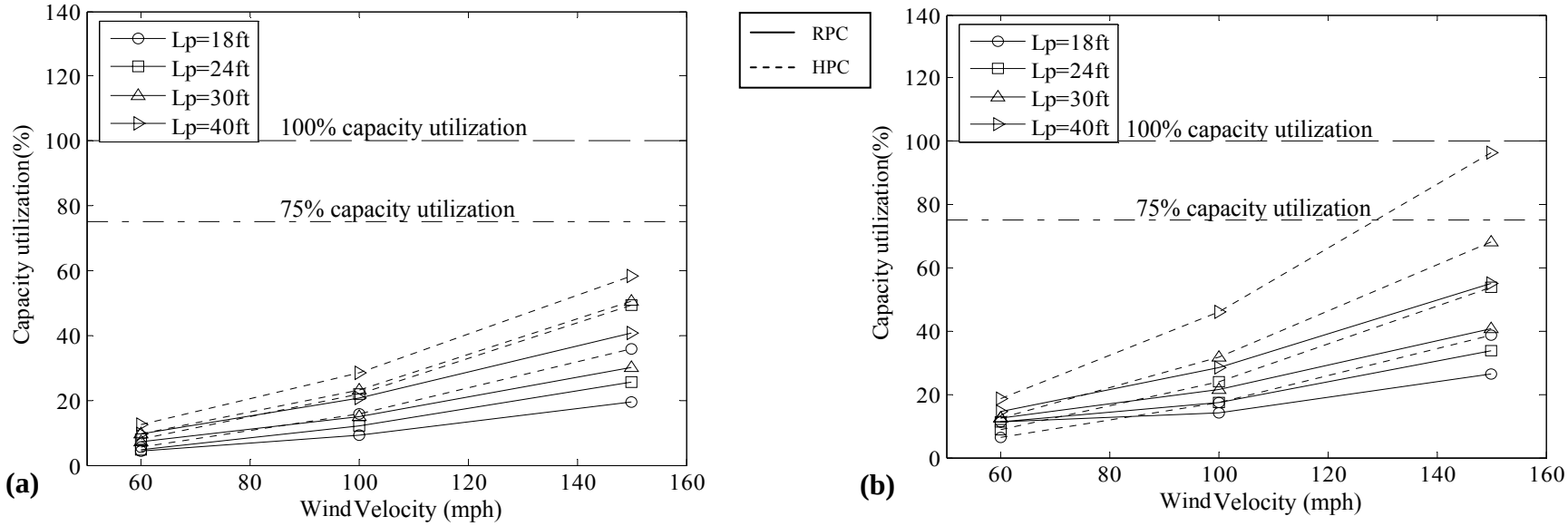

Figure 6.18 Effect of wind velocity on capacity utilization for 50 ft span bridge at (a) 0 deg. and (b) 30 deg. Skew angle (Str.III)

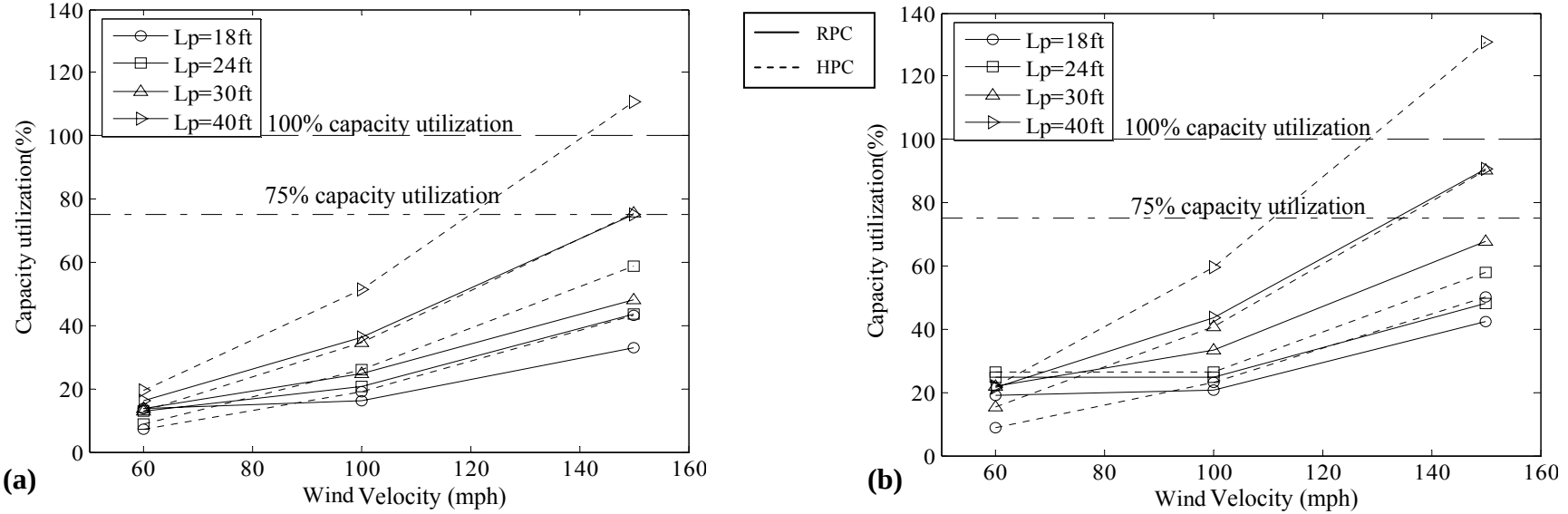

Figure 6.19 Effect of wind velocity on capacity utilization for 50 ft span bridge at (a) 45 deg. and (b) 60 deg. Skew angle (Str.III)

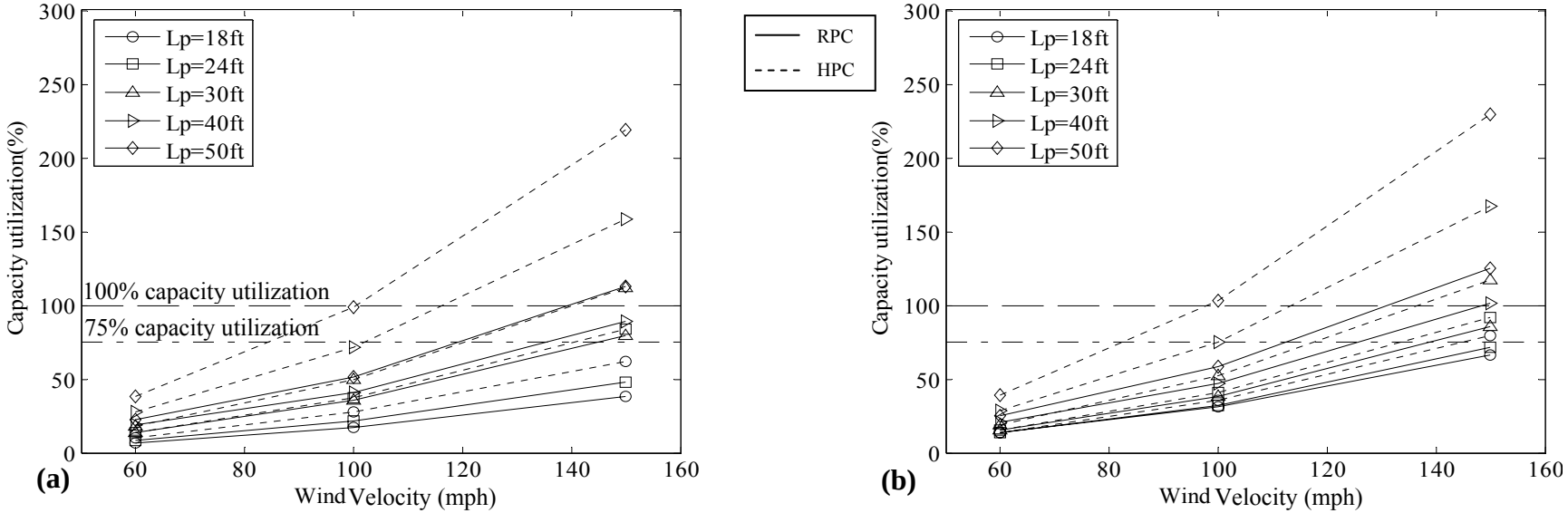

Figure 6.20 Effect of wind velocity on capacity utilization for 76 ft span bridge at (a) 0 deg. and (b) 30 deg. Skew angle (Str.III)

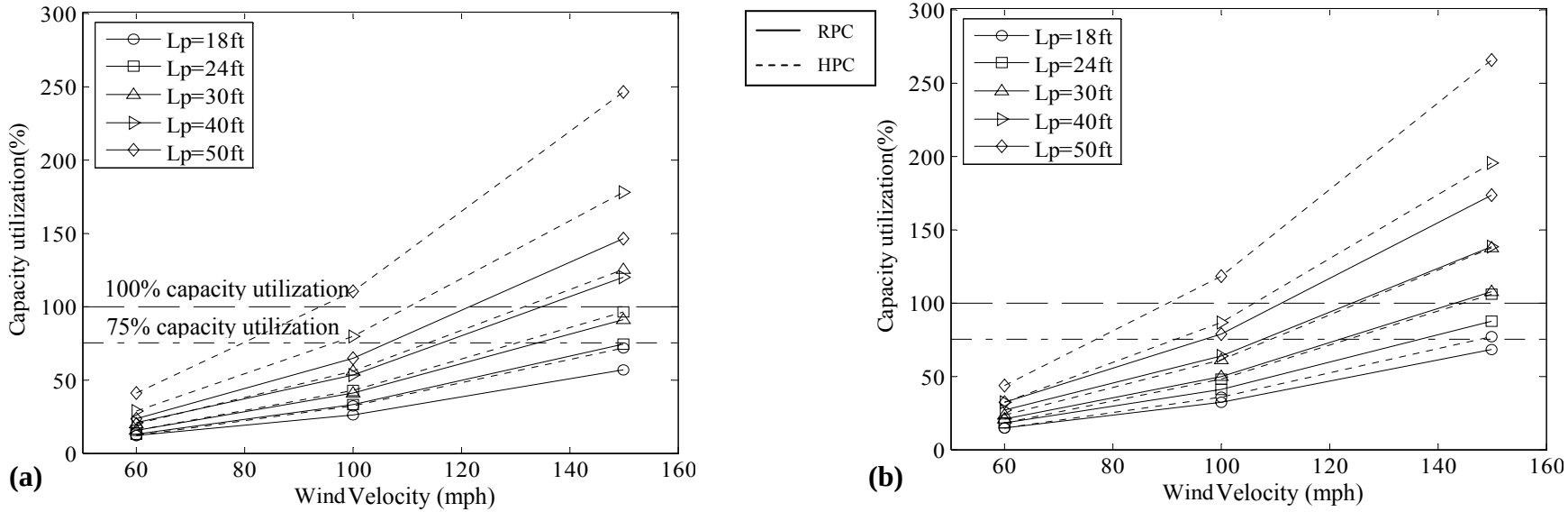

Figure 6.21 Effect of wind velocity on capacity utilization for 76 ft span bridge at (a) 45 deg. and (b) 60 deg. Skew angle (Str.III)

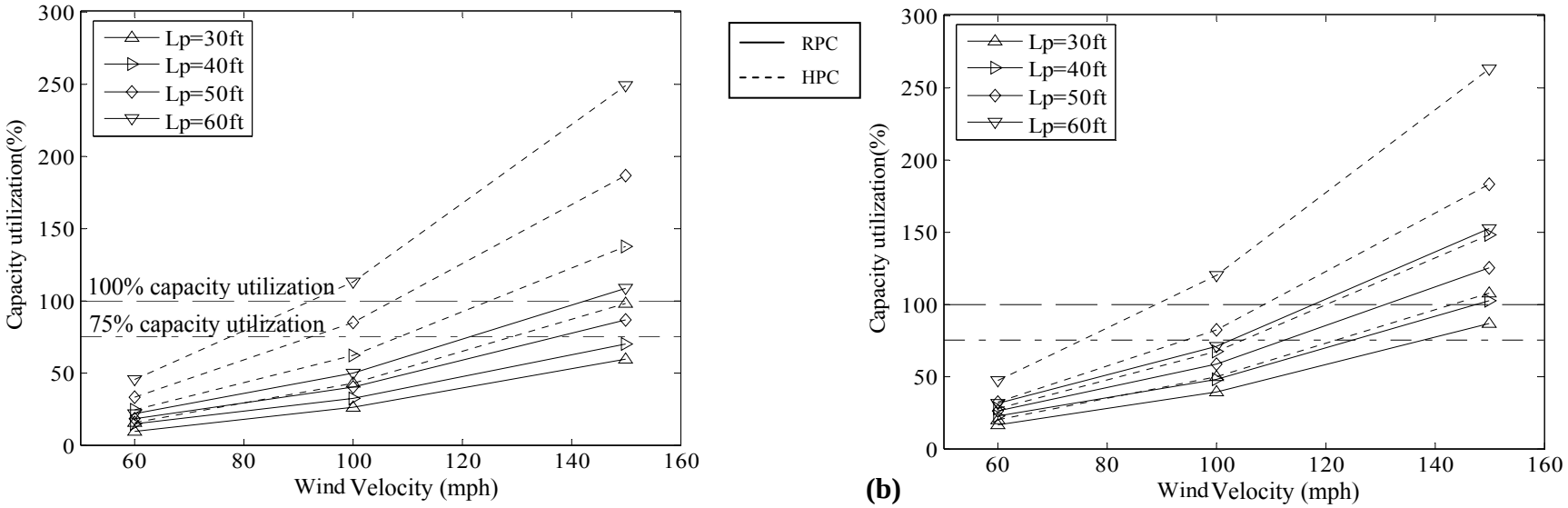

Figure 6.22 Effect of wind velocity on capacity utilization for 100 ft span bridge at (a) 0 deg. and (b) 30 deg. Skew angle (Str.III)

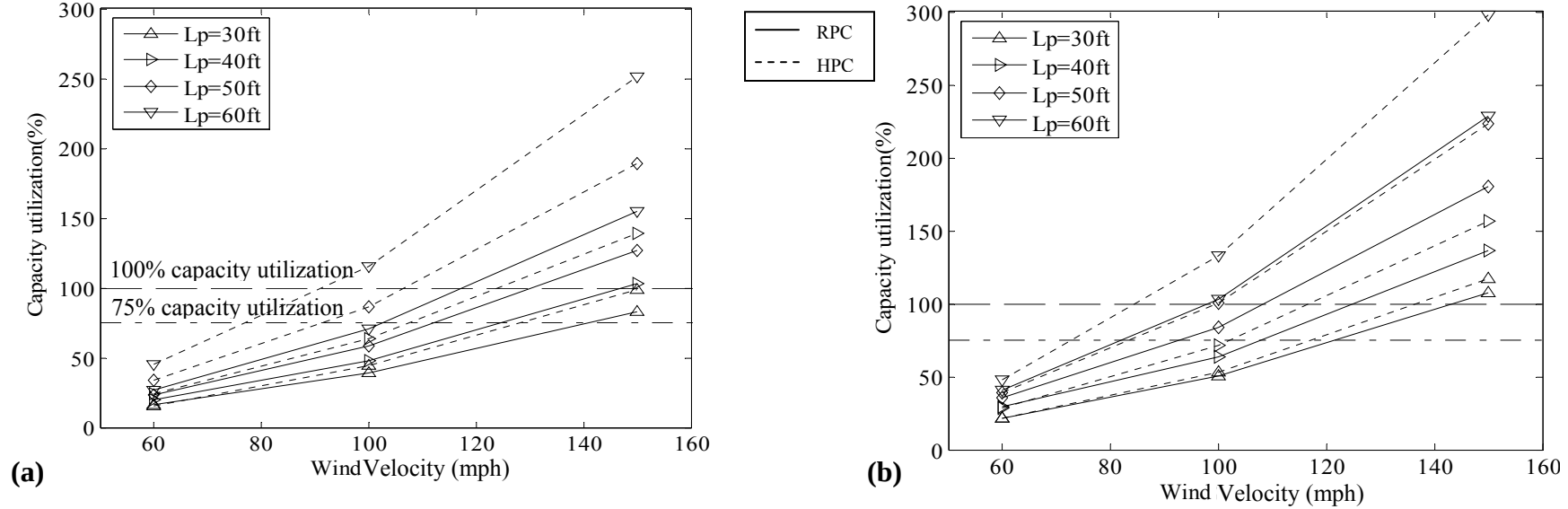

Figure 6.23 Effect of wind velocity on capacity utilization for 100ft span bridge at (a) 45 deg. and (b) 60 deg. Skew angle (Str.III)

6.5 Limitations of Using LA-DOTD Design Tool

Even though the substructures covered in this study were designed according to LA-DOTD BDM, it is clear that some cases exceed the intended capacity of the piles. It is therefore prudent to identify some limitations on the use of this approximate method

A theoretically acceptable capacity utilization of 100% indicates that the pile will exceed its capacity for the slightest load increase. Therefore a more conservative capacity utilization of 75% is recommended for pile design. Based on the computed capacity utilizations it was found that most of the piles are within acceptable limit for low wind velocity (55mph). However at high wind velocities (100 mph and 150 mph) some of the piles seem to exceed the 75% threshold limit at higher span lengths, unsupported pile lengths, or skew angles. Figures 6.24 to 6.31 show the combined effect of skew angles and unsupported pile lengths on pile capacity utilization for bridges with different spans at 100 mph and 150 mph wind velocities.

Table 6.6 presents the maximum slenderness (L_P/d) ratio that can be allowed for all the bridges covered in this study. The table provides the values for piles with RPC and HPC connections at 75% and 100% capacity utilizations. In most cases, piles with HPC connections are subjected to higher loads. Since the exact pile-cap continuity for pile bents is unknown, limitations on using LA-DOTD guideline for piles with both HPC and RPC connections were investigated. Based on Table 6.6, it is possible to identify the bridges where the simplified method is not applicable: All L_P/d ratios that do not meet the allowable limit as specified in BDM (12 for straight pile, 20 for battered pile). Tables 6.7 and 6.8 summarize the range of applicability of the simplified method among the bridges considered in this study. These results are discussed next.

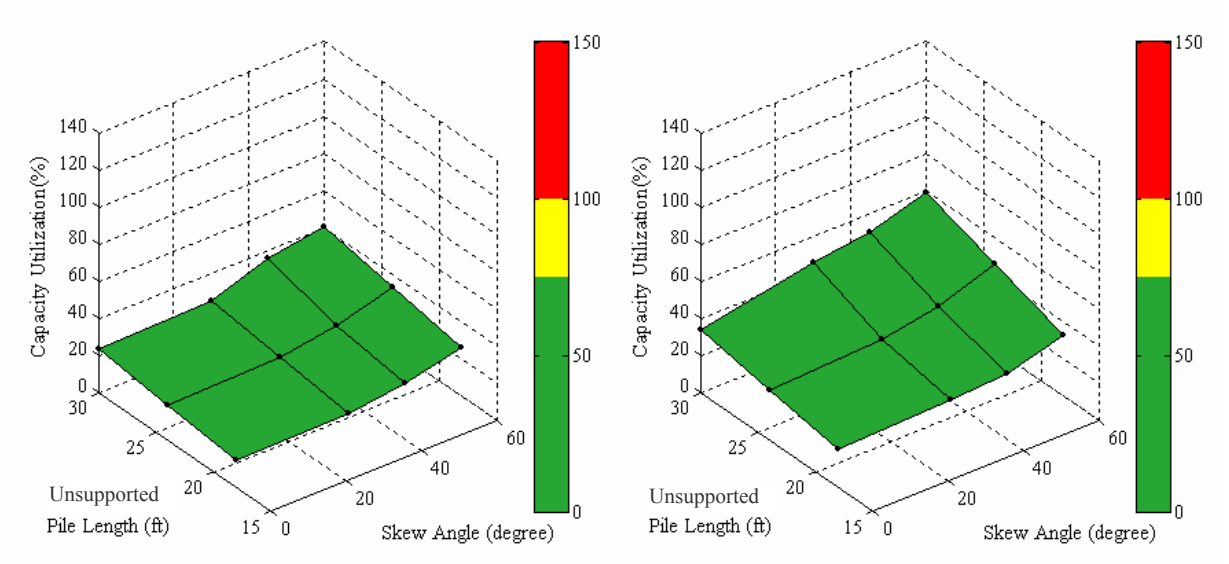

Figure 6.24 Combined effect of unsupported pile length and skew angle on capacity utilization of pile with (a) RPC and (b) HPC connection for 30 ft span bridge at 100 mph wind velocity.

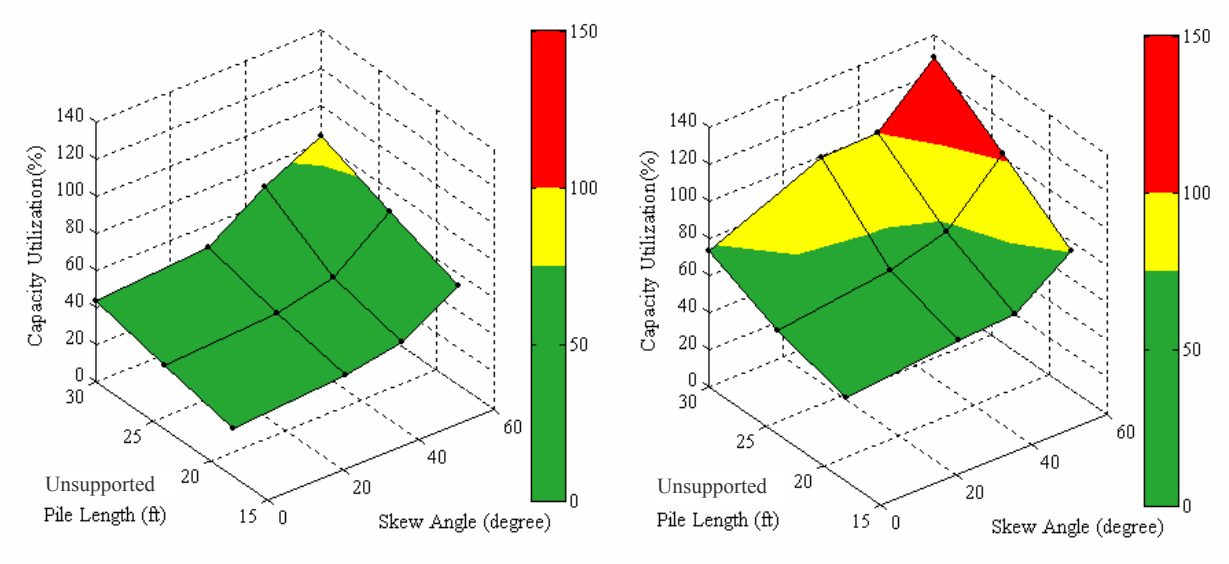

(a) (b)

Figure 6.25 Combined effect of unsupported pile length and skew angle on capacity utilization of pile with (a) RPC and (b) HPC connection for 30 ft span bridge at 150 mph wind velocity.

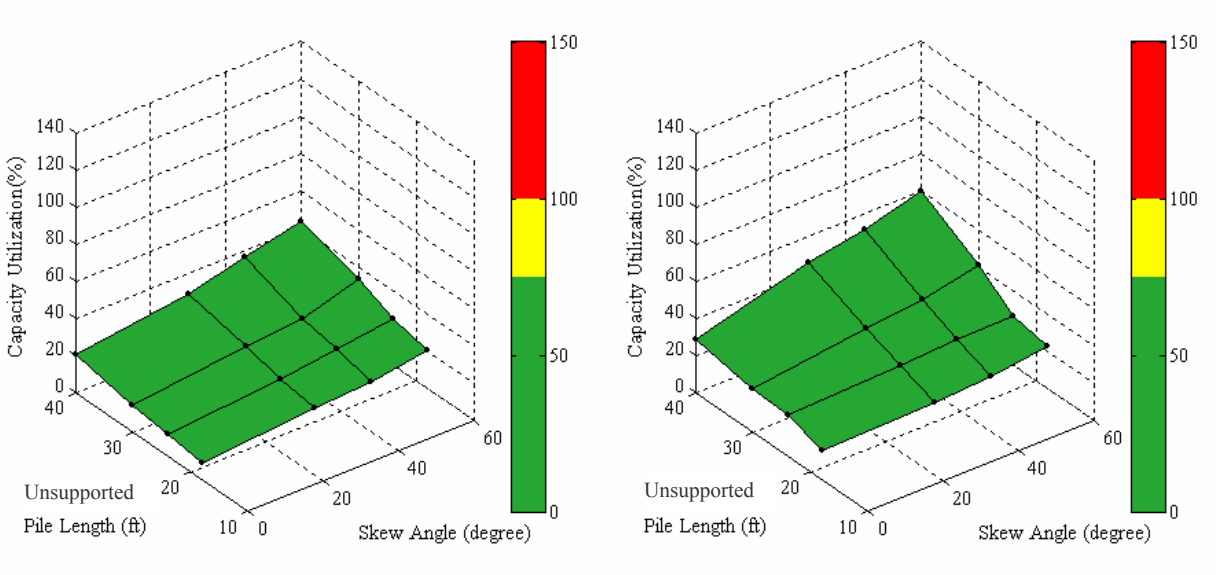

(a) (b)

Figure 6.26 Combined effect of unsupported pile length and skew angle on capacity utilization of pile with (a) RPC and (b) HPC connection for 50 ft span bridge at 100 mph wind velocity.

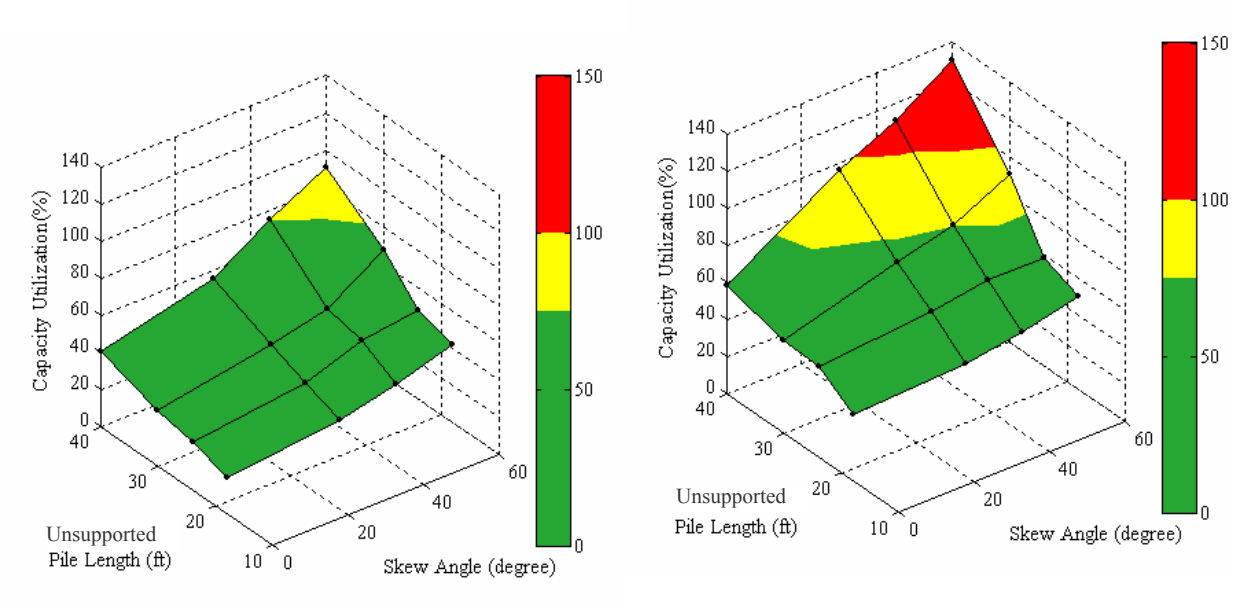

(a) (b)

Figure 6.27 Combined effect of unsupported pile length and skew angle on capacity utilization of pile with (a) RPC and (b) HPC connection for 50 ft span bridge at 150 mph wind velocity.

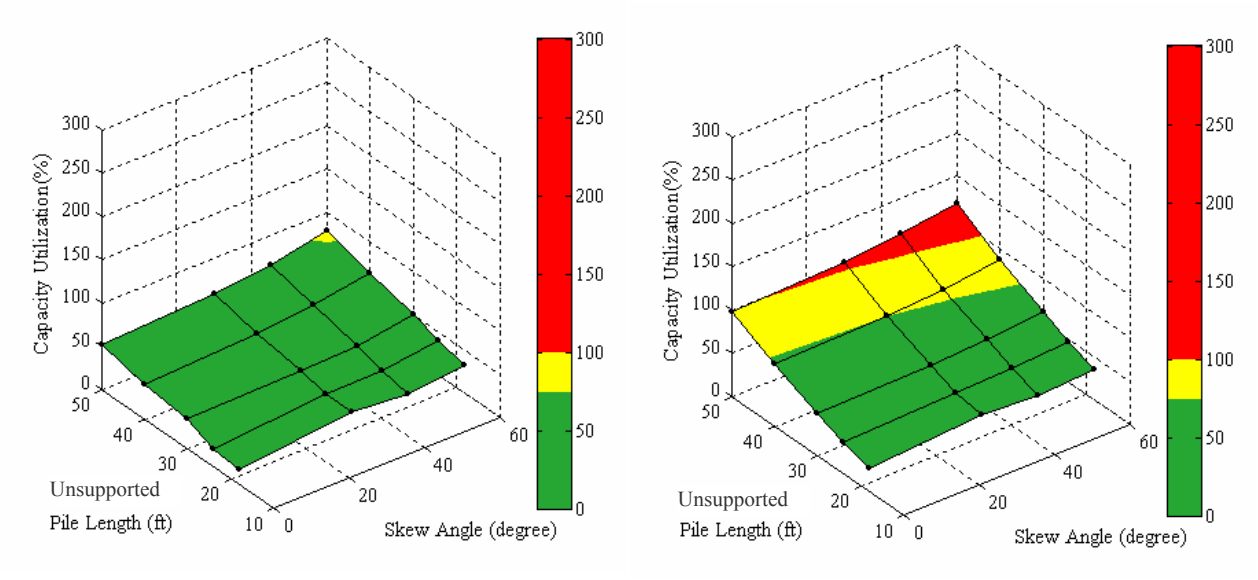

(a) (b)

Figure 6.28 Combined effect of unsupported pile length and skew angle on capacity utilization of pile with (a) RPC and (b) HPC connection for 76 ft span bridge at 100 mph wind velocity.

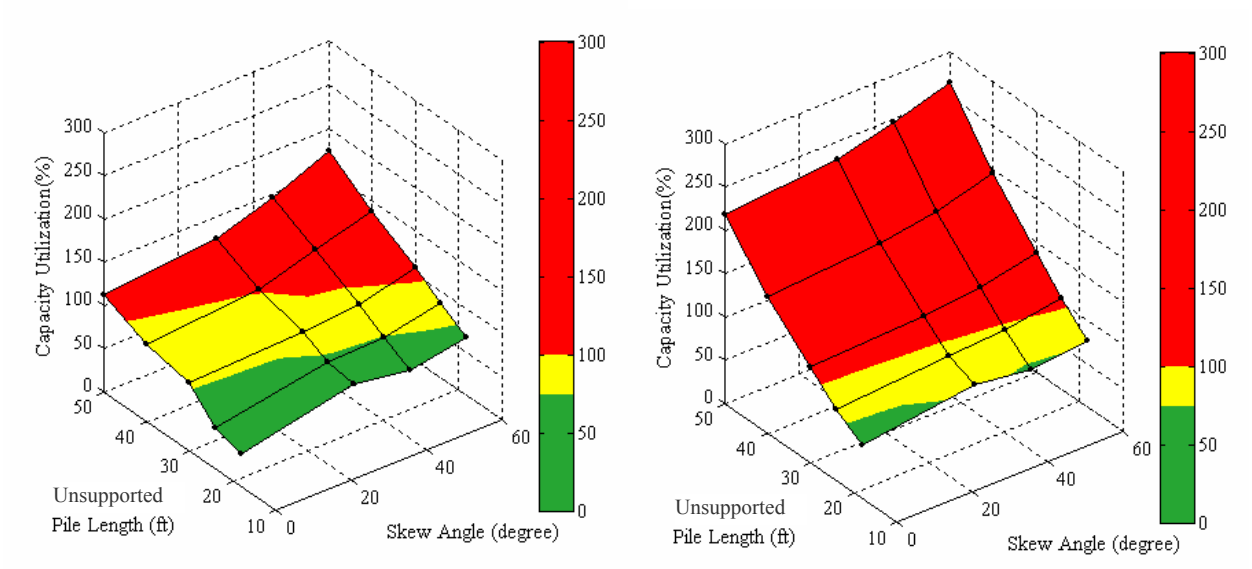

(a) (b)

Figure 6.29 Combined effect of unsupported pile length and skew angle on capacity utilization of pile with (a) RPC and (b) HPC connection for 76 ft span bridge at 150 mph wind velocity.

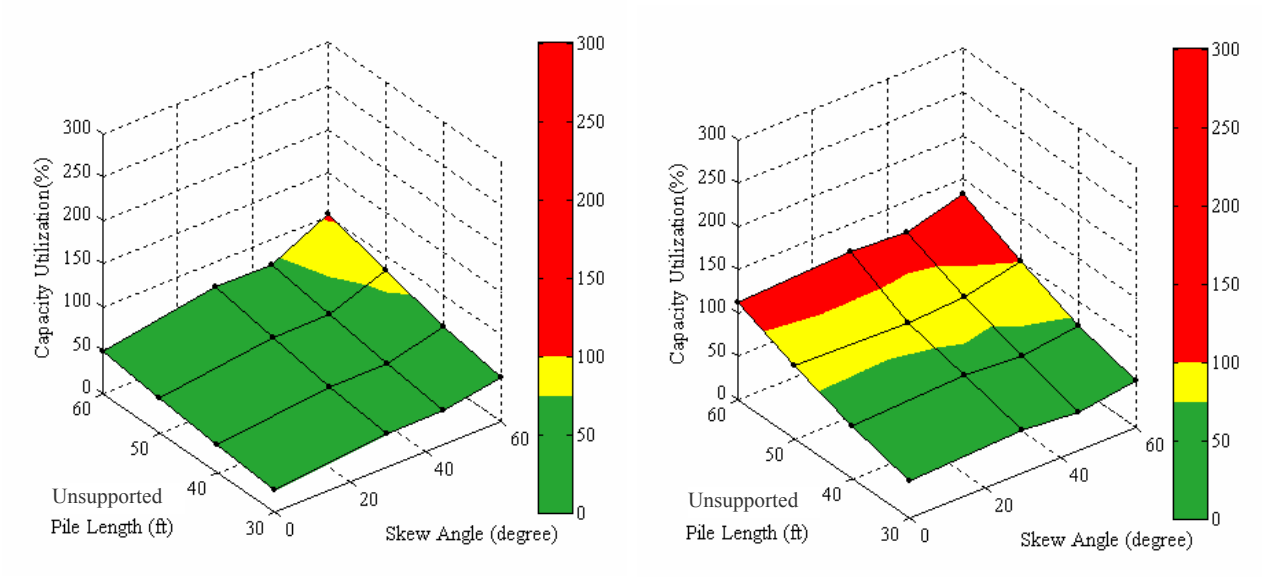

(a) (b)

Figure 6.30 Combined effect of unsupported pile length and skew angle on capacity utilization of pile with (a) RPC and (b) HPC connection for 100 ft span bridge at 100 mph wind velocity.

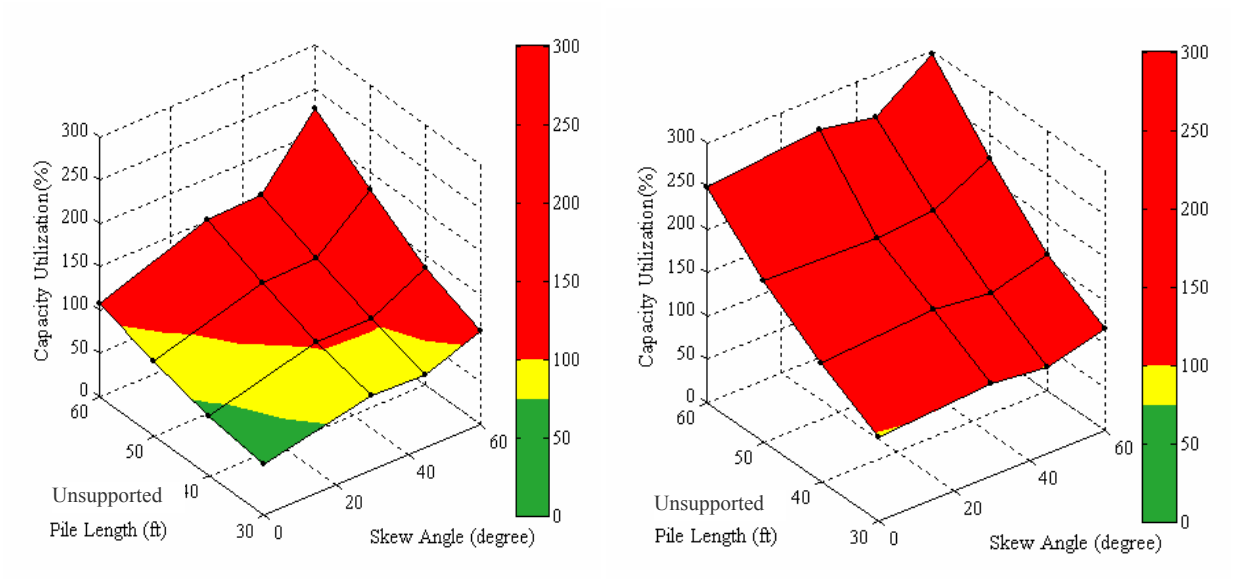

(a) (b)

Figure 6.31 Combined effect of unsupported pile length and skew angle on capacity utilization of pile with (a) RPC and (b) HPC connection for 100 ft span bridge at 150 mph wind velocity.

Table 6.6 Allowable slenderness (L_P/d) ratio for piles based on 75% and 100% capacity utilizations that for different span lengths, skew angles, and wind velocities.

Wind velocity	Span (ft)	Least Pile Dimension (d)	Pile-cap Connectio	Based on 75% capacity utilization				Based on100% capacity utilization			
				Skew Angle (deg.)				Skew Angle (deg.)			
				0	30	45	60	0	30	45	60
55 mph	30	18"	RPC	20	20	20	20	20	20	20	20
			HPC	20	20	20	20	20	20	20	20
	50	24"	RPC	20	20	20	20	20	20	20	20
			HPC	20	20	20	20	20	20	20	20
	76	30"	RPC	20	20	20	20	20	20	20	20
			HPC	20	20	20	20	20	20	20	20
	100	36"	RPC	20	20	20	20	20	20	20	20
			HPC	20	20	20	20	20	20	20	20
100 mph	30	18"	RPC	20	20	20	20	20	20	20	20
			HPC	20	20	20	20	20	20	20	20
	50	24"	RPC	20	20	20	20	20	20	20	20
			HPC	20	20	20	20	20	20	20	20
	76	30"	RPC	20	20	20	18.8	20	20	20	20
			HPC	16.4	16.0	15.2	14.4	20	19.2	18.4	17.6
	100	36"	RPC	20	20	20	15.0	20	20	20	19.3
			HPC	15.0	15.0	15.0	13.7	18.3	18.3	18.3	16.7
150 mph	30	18"	RPC	20	20	20	17.3	20	20	20	20
			HPC	20	17.3	16.0	0.0	20	20	20	15.3
	50	24"	RPC	20	20	20	16.5	20	20	20	20
			HPC	20	16.0	15.0	13.0	20	20	18.5	16
	76	30"	RPC	11.2	10.0	10.0	8.0	17.6	15.6	12.8	10.4
			HPC	8.4	7.6	x	x	10.4	10	9.6	9.2
	100	36"	RPC	14.0	x	x	x	18.7	12.7	12.7	x
			HPC	x	x	x	x	x	x	x	x

Table 6.7 Applicability of the allowable axial load table for pile bent provided in LA-DOTD BDM (2004) based on 75% pile capacity utilization

Limit State	Wind Velocity (mph)	Span (ft)	Rigid Pile Cap (RPC)Connection				Hinged Pile Cap (HPC)Connection			
			Skew Angle (deg.)				Skew Angle (deg.)			
			0	30	45	60	0	30	45	60
Str. V	55	30	√	√	√	√	√	√	√	√
		50	√	√	√	√	√	√	√	√
		76	√	√	√	√	√	√	√	√
		100	√	√	√	√	√	√	√	√
Str. III	100	30	√	√	√	√	√	√	√	√
		50	√	√	√	√	√	√	√	√
		76	√	√	√	×	×	×	×	×
		100	√	√	√	×	×	×	×	×
Str. III	150	30	√	√	√	×	√	×	×	×
		50	√	√	√	×	√	×	×	×
		76	×	×	×	×	×	×	×	×
		100	×	×	×	×	×	×	×	×

** √= applicable; ×= Not applicable.

Table 6.8 Applicability of the allowable axial load table for pile bent provided in LA-DOTD BDM (2004) based on 100% pile capacity utilization

Limit State	Wind Velocity (mph)	Span (ft)	Rigid Pile Cap (RPC)Connection				Hinged Pile Cap (HPC)Connection			
			Skew Angle (deg.)				Skew Angle (deg.)			
			0	30	45	60	0	30	45	60
Str. V	55	30	√	√	√	√	√	√	√	√
		50	√	√	√	√	√	√	√	√
		76	√	√	√	√	√	√	√	√
		100	√	√	√	√	√	√	√	√
Str. III	100	30	√	√	√	√	√	√	√	√
		50	√	√	√	√	√	√	√	√
		76	√	√	√	√	√	×	×	×
		100	√	√	√	×	×	×	×	×
Str. III	150	30	√	√	√	√	√	√	√	×
		50	√	√	√	√	√	√	×	×
		76	×	×	×	×	×	×	×	×
		100	×	×	×	×	×	×	×	×

** √= applicable; ×= Not applicable.

6.5.1 Piles with RPC Connections

Pile bents with Rigid Pile Cap (RPC) connection may be designed using the simplified approach for 55 mph wind velocity within the range of bridge parameters covered in this study. The only limitation on using the simplified method for 100 mph wind velocity is the higher skew angle (60^o) for the 76 ft and 100 ft span lengths. At 150 mph wind velocity most of the bridges fall outside the applicability of the simplified method except for bridges with 30 ft and 50 ft span lengths at skew angles less than or equal to 45^o.

6.5.2 Piles with HPC Connections

Tables 6.7 and 6.8 show that the piles with Hinged Pile Cap (HPC) connections are subjected to higher demands. At 55 mph wind velocity the LA-DOTD allowable axial load table (Table 2.4) is still applicable for all bridges covered in this study. However at 100 mph wind velocity only 30ft and 50 ft span bridges are acceptable. At 150 mph wind velocity 30ft and 50 ft span non-skew bridges are acceptable at 75% limit.

6.6 Conclusion

The following conclusions can be drawn from the above discussion. The pile design table provided in LA-DOTD BDM (2004) may not be applicable for all bridge configurations a designer may face. Therefore, it should be amended to reflect the limitations presented in this chapter. Other limitations may also be necessary and can be determined using studies similar to this research.

CHAPTER 7. CONCLUSIONS AND RECOMMENDATIONS

7.1 Summary

In this study, the feasibility of the simplified procedure provided in the current LA-DOTD BDM (2004) for the design of piles in bridge substructures was investigated. The procedure assists engineers as a quick design tool for determining pile sizes based on a maximum allowed factored axial load. Concerns about the limitations on the use of this procedure were raised since it requires axial load demands to be determined due to dead and live loads only. Furthermore, load demands have increased in recent years with the introduction of AASHTO-LRFD (2004) and the procedure needs to be evaluated in light of these changes as well.

The study first relies on a conventional method to analyze the bridges for all the static loads (dead load, live load, and wind load) in accordance with AASHTO-LRFD (2004). The method considers the analysis of a substructure (pile-cap) frame that is subjected to girder reactions obtained from the analysis of the superstructure.

More refined models based on the FE method were then developed to study the axial loads and bending moments applied on the piles in bridge bents considering the spatial behavior of the system under different limit states. The FE model was first verified by comparing its results to those obtained from conventional frame method. AASHTO load distribution factors were also used to verify the model. A parametric study was then conducted using three span bridge models. The piles in the bridge models were designed using the LA-DOTD simplified procedure. One hundred and twenty eight analytical bridge models were generated to study the effect of different parameters on pile capacity utilizations. The parameters considered in this study were span lengths, unsupported pile lengths, skew angles, pile-cap continuity, and wind velocities.

Axial loads and bending moments acting on the piles were obtained from FE analyses and used to investigate the pile capacity utilization which is defined as the ratio between factored

applied moment and factored capacity of the pile. The factored moment capacity for the applied axial load was determined using Prestressed Concrete Pile Interaction Diagram. Capacity utilizations of piles were used to investigate the applicability of simplified pile design procedure (LA-DOTD 2004) on different bridge parameters by determining whether it exceeds two identified threshold limits or not. The first threshold limit is 100% capacity utilization. Exceeding this limit indicates eminent failure for the slightest load increase. Because of the approximate nature of the simplified procedure, another more conservative limit was investigated that corresponds to 75% capacity utilization.

7.2 Conclusions

The following conclusion can be drawn from refined analysis conducted in this study:

(1) At low wind velocities (55mph), the simplified pile design procedure specified in LA-DOTD BDM (2004) is applicable for all the cases regardless of skew angles. The Strength V limit state controls the design and capacity utilizations of the piles were below 40% for all bridges considered in this study.

(2) At higher wind velocities (100 mph and 150 mph) the simplified procedure (LA-DOTD 2004) should be limited to certain bridge configurations. It was found that pile capacity utilizations increase with the increase in span lengths and skew angles. Capacity utilization also depends on the unsupported pile length.

(3) The pile-to-cap continuity assumption greatly affects the demands on the piles. Hinged pile-cap (HPC) connections cause higher capacity utilizations of the piles compared to rigid pile-cap (RPC) connection.

(4) Limitations on the use of LA-DOTD simplified design procedure for pile bents with RPC and HPC connections were identified based on the results obtained from this study for two thresholds of capacity utilization. It is recommended that the more conservative 75%

capacity utilization threshold be utilized to limit the applicability of the simplified procedure. The limitations are summarized in table form and are given in Chapter 6 (Tables 6.7 and 6.8). The limitations for piles with HPC connection should be used unless the rigid connection between pile and cap can be ensured in practice.

(5) A conventional frame analysis is an acceptable tool for the design of bent type bridge systems under extreme wind effects.

7.3 Recommendations for Future Research

1. In the present study, the pile capacity utilization is studied for bridges with different span lengths, skew angles and wind velocities. The identified limitations are based on the range of parameters covered in this study. Generalizing the simplified procedure requires further investigations to include span lengths and wind velocities beyond the ranges covered herein.
2. Bridge models covered in this study were of equal span lengths. A study of pile capacity utilization in bridge systems with different span lengths is needed.
3. Similarly, the effect of different bridge cross sections on the pile capacity utilization should also be investigated.
4. Four different sizes of square piles were selected to investigate the applicability of the simplified method. Future study should be conducted for other types and sizes of piles provided in the LA-DOTD simplified approach.
5. Similar study should be conducted for curved bridges where centrifugal forces might play important role in pile design.

REFERENCES

PCI Prestressed Concrete Pile Interaction Diagram Spreadsheet. [1]. 2004. Precast/Prestressed concrete Institute.
Ref Type: Computer Program

AASHTO (1994). "AASHTO LRFD Bridge design specifications." American Association of State Highway and Teansportation official, Washington DC.

AASHTO (2002). "AASHTO Standard Specification for Highway Bridges." American Association of State Highway and Teansportation official, Washington DC.

AASHTO (2004). "AASHTO LRFD Bridge design specifications." American Association of State Highway and Teansportation official, Washington D.C.

Anderson, A. R., and Moustafa, S. E. (1970). "Ultimate Strength Of Prestressed Concrete Piles And Columns." *J Amer Concrete Inst*, 67(8), 620-635.

Barr, P. J., Eberhard, M. O., and Stanton, J. F. (2001). "Live-load distribution factors in prestressed concrete girder bridges." *Journal of bridge engineering*, 6(5), 298-306.

Brockenbrough, R. L. (1986). "Distribution Factor for Curved I-Girder Bridges." *Journal of Structural Engineering*, 112(10), 2200-2215.

Chen, y., and Asward, A. (1996). "Stretching span capability of prestressed concrete bridges under AASHTO LRFD." *Journal of bridge engineering.*, 1(3), 112-120.

Chung, W. S., and Sotelino, E. D. (2006). "Three-dimensional finite element modeling of composite girder bridges." *Engineering Structures*, 28(1), 63-71.

Davisson, M. T., and Robinson, K. E. (1965). "Bending and Buckling of Partially Embedded Piles." *Proc. 6th International Conference on Soil Mechanics and Foundation Engineering*, 3, 243-246.

"Florida DOTD standards."(2004).
http://www.dot.state.fl.us/Structures/CADD/standards/CurrentStandards/standards.htm#Piling.

Gamble, W. L. (1979). "Capacity of reinforced and prestressed concrete pile sections." *ASTM special technical publication*,(670), 306-322.

Gaythwaite, J. W. (2004). "Design Of Marine Facilities For The Berthing, Mooring, And Repair Of Vessels." AASHTO Press.

Harries, K. A., and Petrou, M. F. (2001). "Behavior of Precast, Prestressed Concrete Pile to Cast-In-Place Pile Cap Connections." *PCI journal*, 46(4), 82.

Hays, C. O., Sessions, L. M., and Berry, A. J. (1986). "Further Studies on Lateral Load Distribution Using Finite Element Method." *Transportation Research Record*, 6-14.

Hognested, E. (1951). "A Study of Comobined Bending and Axial Load in Reinforced Concrete Members." *Bulletin 399, Engineering Experimental Station, University of Illinois, Urbana*, 128.

Hromadik, J. J. (1962). "Column Strength of Long Piles." *ACI Journal, Proceedings*, 59(6), 757-778.

Huang, H., Shenton, H. W., and Chajes, M. J. (2004). "Load Distribution for a Highly Skewed Bridge: Testing and analysis." *Journal of bridge engineering.*, 9(6), 558-562.

Imbsen, R. A., and Nutt, R. V. (1978). "Load Distribution Study on Highway Bridges Using STRUDL FEA Capabilities." ASCE, NewYork, NY, 639-654.

Kocsis, P. (2004). "Evaluation of AASHTO live load and line load distribution factors for I-girder bridge decks." *Practice periodical on structural design and construction*, 9(4), 211-215.

LA-DOTD (2004). "State of Louisiana Department of Transportation and Development Bridge Design Manual.".

Mays, T. W., Black, J. M., and Foltz, R. R. (2005). "A Simplified Design Procedure for Precast Prestressed Concrete Piling in Areas of High Seismicity to Include the Effects of Pile Buckling." 899-910.

Mish, K., Osterkamp, T., Zokaie, T., and Imbsen, R. (1995). "Interactive Finite-Element Generation of Bridge Load Distribution Factors." *Computing in civil engineering*, 1(1), 781-787.

Nathan, N. D. (1983). "Slenderness of Prestressed Concrete Columns." *Journal Prestressed Concrete Institute*, 28(2), 50-77.

NCHRP (1992). "Distribution of Wheel Loads on Highway Bridges." *NCHRP : leveraging resources for better transportation.*.

NCHRP (2001). "Static and Dynamic Lateral Loading of Pile Groups." *Rep. No. 461*, National Cooperative Highway research program, Washington, DC.

PCI (2002). "PCI Bridge Design Manual." Chicago, IL.

PCI (2004). "PCI Design Handbook, Precast and Prestressed Concrete.".

Powell, G. M., and Buckle, I. G. (1970). "Computer Programs for Bridge Deck Analysis." *Rep. No. UC SESM 70-6*, University of California, Barkley, Cliff..

Rodriguez-Gutierrez, J. A., and Aristizabal-Ochoa, J. D. (2001). "*M-P*- Diagrams for Reinforced, Partially, and Fully Prestressed Concrete Sections under Biaxial Bending and Axial Load." *J. Structural Engg.*, 127(7), 763-773.

SAP2000 (2002). "Analysis Reference Manual." Computers and Structures INC., Barkley, California.

Shuraim, A. B., and Naaman, A. E. (2003). "A New Design Methodology for the Ultimate Capacity of Slender Prestressed Concrete Columns." *PCI journal*, 48(1), 64.

Tarhini, K. M., and Frederick, G. R. (1992). "Wheel Load Distribution in I-Girder Highway Bridges." *Journal of Structural Engineering-Asce*, 118(5), 1285-1294.

Tarhini, K. M., Mabsout, M., Harajli, M., and Tayar, C. (1995). "Finite Element Modeling Techniques of Steel Girder Bridges." *Computing in civil engineering*, 1, 773-780.

Tarhini, K. M., Mabsout, M. E., and Naddaf, I. Y. (2000). "A Study of Multi-Design Trucks in Steel Bridges." *Computing in civil and building engineering : proceedings of the eighth international conference*, 2, 1248-1253.

Tonias, D. E. (1994). "Bridge Engineering: Design , Rehabilitation and Maintanace." Macgraw-Hill Professiona.

Young, W. C., and Budynas, R. G. (2002). "Roark's Formulas for Stress and Strain." McGraw-Hill, New York.

Zia, P., and Moreadith, F. L. (1966). "Ultimate Load Capacity of Prestressed Concrete Columns." *ACI Journal, Proceedings*, 63(7), 767-788.

Zokaie, T., Osterkamp, T., and Imbsen, R. (1991). "Distribution of wheel loads on highway bridges." *NCHRP 12-26/1 Final Rep. , National Cooperative Highway research program, Washington D. C.*.

Zokaie, T. (2000). "AASHTO-LRFD live load distribution specifications." *Journal of bridge engineering*, 5(2), 131-138.

APPENDIX A. COMPUTER PROGRAM TO CALCULATE BRIDGE LOADS

A.1 Program Source Code

```
C     COMPUTER PROGRAM TO CALCULATE BRIDGE LOADS THAT CAN BE APPLIED ON
C     A SIMPLE CAP-PILES FRAME BASED ON THE PROCEDURES DESCRIBED IN
C     CHAPTER 3.
      PROGRAM MAIN
      IMPLICIT DOUBLE PRECISION (A-H,O-Z)
      DIMENSION GL(9),GWSP(9),GWL(9),GB(9),RX(9),XWSP(9)
C     S1=SPAN1, S2=SPAN2
C     TW=TOTAL WIDTH, BW=BARRIER WIDTH, OH=OVERHANG
C     N =#OF GIRDER
C     SP= GIRDER SPACING, EXS= EXTERIOR GIRDER DIST FROM EXT FACE
C     WP1=1ST WHEEL POSITION
C     P=MAXM LL REACTION/LANE(i.e, wheel load)
C     LN # OF DESIGN LANE
C          GL(I)=GIRDER REAC DUE TO LL
C      PB=BREAKING FORCE PER VEHICLE
C          GB(I)=GIRDER REAC DUE TO BREAKING FORCE
      CALL READ_DATA (S1,S2,TW,BW,OH,N,SP,WP1,P,LN,PB,
      & BH,DH,HH,GH,GA,WT,WB,BA,HA,WS,CW,CH,CPL,DP,BWP,VDZ,SKW)
      CALL LL_GIRD_REAC (TW,BW,OH,N,SP,WP1,P,LN,GL)
      CALL BR_GIRD_REAC (TW,BW,OH,N,SP,WP1,PB,LN,GB)
      CALL WL_LL_GIRD_REAC (S1,S2,TW,BW,OH,N,SP,WP1,LN,RX,GWL)
      CALL WL_SUP_STR(S1,S2,GH,DH,HH,BH,SKW,VDZ,HF,FLP,FTP)
      CALL WL_SUPER_GIRD_REAC(BH,DH,HH,GH,N,SP,FTP,XWSP,GWSP)
      CALL WL_SUB(CW,CH,CPL,DP,BWP,VDZ,WTCAP,WLCAP,WTPILE)
      CALL DL_GIRD_REAC(S1,S2,SP,OH,BW,N,GH,GA,WT,WB,DH,
     &           HA,BA,WS,CW,CH,DP,DCI,DCE,DWI,DWE,WCAP,WPILE)
      OPEN (12,FILE='RESULT.OUT',status='OLD')
           WRITE(12,*)
      WRITE(12,*) 'GIRDER REACTION ON PILE CAP DUE TO LL(LL)'
      WRITE(12,*) 'GIRDER#       RY(K)'
810   FORMAT(I5,F15.4)
           DO I=1,N
           WRITE(12,810) I, -GL(I)
      ENDDO
      WRITE(12,*)'GIRDER REAC ON PILE CAP DUE TO BREAKING FORCE(BR)'
      WRITE(12,*) 'GIRDER#       RZ(K)'
      DO I=1,N
           WRITE(12,810) I, GB(I)
      ENDDO
      WRITE(12,*)'GIRDER REAC.ON PILE CAP DUE TO WL ON LL COMP.(WL)'
      WRITE(12,*) 'GIRDER#       RY(K)         RX(K)'
820   FORMAT(I5,F15.4,F15.4)
           DO I=1,N
           WRITE(12,820) I, -GWL(I),RX(I)
      ENDDO
      WRITE(12,*)'GIRD.REAC.ON PILE CAP DUE TO WL ON SUPER STR.(WS)'
      WRITE(12,*) 'GIRDER#       RY(K)         RX(K)'
```

```
      DO I=1,N
      WRITE(12,820) I, GWSP(I),XWSP(I)
      ENDDO
840         FORMAT(F15.4,F15.4,F15.4)
      WRITE(12,*)
      WRITE(12,*)'WL(K) ON SUP.  & CAP ALONG THEIR LONG DIR, LOAD HT'
      WRITE(12,840) FTP,FLP,HF
      WRITE(12,*)'CN.LD ON CAP & UDL ON PILE FOR TR.WL ON SUB STR(WS)'
      WRITE(12,*)'    CAP FACE(K)          PILE FACE(K/FT)'
           WRITE(12,830) WTCAP,WTPILE
      WRITE(12,*)'UDL ON CAP AND PILE DUE TO LONGI.W ON SUB STR(WS)'
      WRITE(12,*)'CAP_LONG.FACE(K/FT)     PILE FACE(K/FT)'
           WRITE(12,830) WLCAP,WTPILE
      WRITE(12,*)'GIRDER REAC. ON PILE CAP DUE TO SUPER STR. DL(DC)'
      WRITE(12,*)'       EXT GIRD.(K)    INT.GIRD.(K)'
830         FORMAT(F15.4,F15.4)
           WRITE(12,830) -DCE,-DCI
      WRITE(12,*)'GIRDER REACTION ON PILE CAP DUE TO FWS (DW)'
      WRITE(12,*)'       EXT GIRD.(K)    INT.GIRD.(K)'
           WRITE(12,830) -DWE,-DWI
      WRITE(12,*)'UDL ON CAP AND PILE DUE TO CAP SW AND PILE SW(DC)'
      WRITE(12,*)'    CAP WT(K/FT)      PILE WT.(K/FT)'
           WRITE(12,830) -WCAP,-WPILE
      CLOSE(12)
           STOP
      END

      SUBROUTINE READ_DATA (S1,S2,TW,BW,OH,N,SP,WP1,P,LN,PB,
     & BH,DH,HH,GH,GA,WT,WB,BA,HA,WS,CW,CH,CPL,DP,BWP,VDZ,SKW)
           IMPLICIT DOUBLE PRECISION (A-H,O-Z)
           OPEN (11,FILE='input.dat')
      READ (11,*)
      READ (11,*)
           READ (11,*) S1,S2
      READ (11,*)
      READ (11,*) TW, BW, OH
      READ (11,*)
      READ (11,*) N,SP
      READ (11,*)
      READ (11,*) WP1,P,LN
      READ (11,*)
      READ (11,*)
      READ (11,*) PB
      READ (11,*)
      READ (11,*) BH,DH,HH,GH
      READ (11,*)
      READ (11,*) GA,WT,WB
      READ (11,*)
      READ (11,*)      BA,HA
      READ (11,*)
      READ (11,*) WS
      READ (11,*)
```

```
      READ (11,*) CW,CH,CPL
      READ (11,*)
      READ (11,*) DP
      READ (11,*)
      READ (11,*) BWP, VDZ
      READ (11,*)
      READ (11,*)
      READ (11,*) SKW
      RETURN
      END

C GIRDER REACTION FOR LIVE LOAD
      SUBROUTINE LL_GIRD_REAC (TW,BW,OH,N,SP,WP1,P,LN,GL)
      IMPLICIT DOUBLE PRECISION (A-H,O-Z)
      DIMENSION GL(9),W(6),SPAN(12)
      W(1)=WP1+BW
      W(2)=W(1)+6
      W(3)=W(2)+4
      W(4)=W(3)+6
      IF (LN .EQ. 3) THEN
      W(5)=W(4)+4
      W(6)=W(5)+6
      ENDIF
      DO I=1,N
      GL(I)=0.0
      ENDDO
      ISP=0.
      SPAN(1)=BW
      SPAN(2)=SP+OH
      SPAN(N)=TW-BW
      DO I=3,N-1
      SPAN(I)=SPAN(I-1)+SP
      ENDDO
      DO I=2,N-1
            DO J=1,3
          IF((W(ISP+1).GE.SPAN(I-1)).AND.(W(ISP+1).LE.SPAN(I)))THEN
                D=SPAN(I)-W(ISP+1)
                GL(I-1)=GL(I-1)+P*D/SP
                GL(I)=GL(I)+P*(SP-D)/SP
                ISP=ISP+1
                IF(((LN .EQ. 2).AND.(ISP .GE. 4))
     & .OR.((LN .EQ. 3).AND.(ISP.GE. 6))) THEN
                  GOTO 10
                    ENDIF
            ENDIF
            ENDDO
      ENDDO
   10 DO J=1,3
            IF(((LN .EQ. 2).AND.(ISP .LT. 4))
     & .OR.((LN .EQ. 3).AND.(ISP.LT. 6))) THEN
         IF((W(ISP+1).GE.SPAN(N-1)).AND.(W(ISP+1).LE.SPAN(N)))THEN
             D=W(ISP+1)-SPAN(N-1)
```

```
            GL(N)=GL(N)+P*D/SP
            GL(N-1)=GL(N-1)+(P-GL(N))
            ISP=ISP+1
          ENDIF
        ENDIF
        ENDDO
        RETURN
        END

C GIRDER REACTION FOR BREAKING FORCE
        SUBROUTINE BR_GIRD_REAC (TW,BW,OH,N,SP,WP1,PB,LN,GB)
        IMPLICIT DOUBLE PRECISION (A-H,O-Z)
        DIMENSION GB(9),W(6),E(3),YG(9),Y(9)
        W(1)=WP1+BW
        W(2)=W(1)+6
        W(3)=W(2)+4
        W(4)=W(3)+6
        IF (LN .EQ. 3) THEN
        W(5)=W(4)+4
        W(6)=W(5)+6
        ENDIF
        DO I=1,N
        GB(I)=0.0
        ENDDO
        CL=TW/2.
        DO I=1,LN
            J=2*I-1
            E(I)=CL-(W(J)+W(J+1))/2
        ENDDO
        YG(1)=OH
         DO I=2,N
            YG(I)=YG(I-1)+SP
        ENDDO
        SUMY=0.
         DO I=1,N
            Y(I)=CL-YG(I)
           SUMY=SUMY+(Y(I))**2
        ENDDO
        DO I=1,N
            DO J=1,LN
           GB(I)=GB(I)+(PB/N+PB*E(J)*Y(I)/SUMY)
            ENDDO
        ENDDO
        RETURN
        END

C GIRDER REACTION FOR WL ON LL COMPONENT
        SUBROUTINE WL_LL_GIRD_REAC (S1,S2,TW,BW,OH,N,SP,WP1,LN,RX,GWL)
        IMPLICIT DOUBLE PRECISION (A-H,O-Z)
        DIMENSION GWL(9),SPAN(9),W(2),R(2),RX(9)
        W(1)=WP1+BW
        W(2)=W(1)+6
```

```
      R(1)=-0.1*(S1+S2)/2
      R(2)=0.1*(S1+S2)/2
      X=0.1*(S1+S2)/2
      DO I=1,N
      GWL(I)=0.0
      RX(I)=X/N
      ENDDO
      SPAN(1)=BW
      SPAN(2)=SP+OH
      SPAN(N)=TW-BW
      DO I=3,N-1
      SPAN(I)=SPAN(I-1)+SP
      ENDDO
      DO I=2,N-1
            DO J=1,2
            IF ((W(J).GE.SPAN(I-1)).AND. (W(J) .LE. SPAN(I)))THEN
                  D=SPAN(I)-W(J)
                  GWL(I-1)=GWL(I-1)+R(J)*D/SP
                  GWL(I)=GWL(I)+R(J)*(SP-D)/SP
            ENDIF
            ENDDO
      ENDDO
      RETURN
      END

C GIRDER REACTION FOR WL ON STRUCTURE
      SUBROUTINE WL_SUPER_GIRD_REAC(BH,DH,HH,GH,N,SP,FTP,XWSP,GWSP)
      IMPLICIT DOUBLE PRECISION (A-H,O-Z)
      DIMENSION GWSP(9),XWSP(9),GY(9)
      DO I=1,N
      XWSP(I)=FTP/N
      ENDDO
      FGLGDIST=(N-1)*SP
      GY(1)=FGLGDIST/2
      DO I=2,N
      GY(I)=GY(I-1)-SP
      ENDDO
      HT=(BH+DH+HH+GH)/2
      SUMGY=0.
      DO I=1,N
      SUMGY=SUMGY+GY(I)**2
      ENDDO
      DO I=1,N
      GWSP(I)=FTP*HT*GY(I)/SUMGY
      ENDDO
      RETURN
      END
      SUBROUTINE WL_SUB(CW,CH,CPL,DP,BWP,VDZ,WTCAP,WLCAP,WTPILE)
      IMPLICIT DOUBLE PRECISION (A-H,O-Z)
      PW=(VDZ/100)**2
            WTCAP=PW*BWP*CW*CH
      WLCAP=PW*BWP*CPL
```

```
            WTPILE=PW*BWP*DP
      RETURN
      END

C DEAD LOAD CALCULATION
C SUPER AND SUB STRUCTURE DL_ GIRDER REAC ON PILE CAP
      SUBROUTINE DL_GIRD_REAC(S1,S2,SP,OH,BW,N,GH,GA,WT,WB,DH,
     &           HA,BA,WS,CW,CH,DP,DCI,DCE,DWI,DWE,WCAP,WPILE)
      IMPLICIT DOUBLE PRECISION (A-H,O-Z)
      WG=.15*GA
      WSI=SP*DH*.15
      WSE=(.5*SP+OH)*DH*.15
      WH=HA*.15
      WDPI=.15*(GH-WB)*(SP-WT)*10/12
      WDPE=WDPI/2
      WBAR=BA*.15*2/N
      FWSI=WS*SP
      FWSE=WS*(.5*SP+OH-BW)
      DCI=(WG+WSI+WH+WBAR)*(S1+S2)/2+WDPI*2
      DCE=(WG+WSE+WH+WBAR)*(S1+S2)/2+WDPE*2
      DWI=FWSI*(S1+S2)/2
      DWE=FWSE*(S1+S2)/2
      WCAP=CW*CH*.15
      WPILE=DP*DP*.15
      RETURN
      END

C  GIRDER REAC DUE TO WIND LOAD ON SUPER STRUCTURE
      SUBROUTINE WL_SUP_STR(S1,S2,GH,DH,HH,BH,SKW,VDZ,HF,FLP,FTP)
      IMPLICIT DOUBLE PRECISION (A-H,O-Z)
      DIMENSION FTS(5),FLS(5),WLP(5),WTP(5)
      HW=GH+HH+DH+BH
      HF=HW/2
      PW=(VDZ/100)**2
      FTS(1)=PW*.05*HW*(S1+S2)/2
      FTS(2)=PW*.044*HW*(S1+S2)/2
      FTS(3)=PW*.041*HW*(S1+S2)/2
      FTS(4)=PW*.033*HW*(S1+S2)/2
      FTS(5)=PW*.017*HW*(S1+S2)/2
      FLS(1)=PW*0.
      FLS(2)=PW*.006*HW*(S1+S2)/1
      FLS(3)=PW*.012*HW*(S1+S2)/1
      FLS(4)=PW*.016*HW*(S1+S2)/1
      FLS(5)=PW*.019*HW*(S1+S2)/1
      DO I=1,5
            WLP(I)=FLS(I)*COS(SKW)+FTS(I)*SIN(SKW)
            WTP(I)=FTS(I)*COS(SKW)+FLS(I)*SIN(SKW)
      ENDDO
      FLP=0.
      FTP=0.
            DO I=1,5
      IF (FLP .LT.WLP(I)) THEN
```

```
      FLP=WLP(I)
ENDIF
IF (FTP .LT.WTP(I)) THEN
      FTP=WTP(I)
ENDIF
ENDDO
RETURN
END
```

A.2 Program Input File

Input.dat

```
*******************************************************************************************
INPUT FILE (UNIT: K,FT)
SPAN#1(S1), SPAN#2(S2)
70. 70.
TOTAL BRIDGE WIDTH(TW), BARRIER WIDTH(BW), OVERHANG(OH)
42.5 1.25 3.33
#OF GIRDER(N), GIRDER SPACING(SP)
6 7.167
1ST W POSI. FROM 1ST BAR.INT.FACE(WP1),WHLLOAD(WITH
MF)(P=Mf*((32+(32+8)*(sp-14)/sp)*.5+.5*.64*sp)),#OF DES LN(2/3)
2 46.24 3
BREAKING FORCE PER VEHICLE[(.25(32+32+8) 0R .05(72+SPAN*2*.64)]*M.F.(PB)
15.3
BARRIER HT(BH), DECK HT(DH),HAUNCH HT(HH),GIRDER HT(GH)
2.67 .67 .167 3.75
GIRDER AREA(GA),WEB THICKNESS(WT),HT OF THE WEB BOTTOM(WB)
3.89 .583 1.21
BARRIER AREA(BA), HAUNCH AREA(HA)
1.903 .222
WEARING SURFACE (KSF)(WS)
.03
CAP WIDTH(CW), HEIGHT(CH), LENGTH(CPL)
4 2.25 42.5
SQUARE PILE SIZE(DP)
2.5
BASE WIND PRESSURE(BWP, KSF), DESING WIND VELOCITY
[VDZ=2.5*Vo*(V30/VB)*LN(z/zo),MPH]
0.04 149.8
SKEW ANGLE(0/15/30/45/60 DEGREE)
0.
*******************************************************************************************
```

A.3 Program Output File

Result.out

```
*********************************************************************************************
 GIRDER REACTION ON PILE CAP DUE TO LL(LL)
 GIRDER#      RY(K)
  1      -54.8015
  2      -66.1567
  3      -63.9695
  4      -64.0018
  5      -28.5105
  6        .0000
GIRDER REAC ON PILE CAP DUE TO BREAKING FORCE(BR)
GIRDER#      RZ(K)
  1       15.1564
  2       12.5218
  3        9.8872
  4        7.2526
  5        4.6180
  6        1.9834
GIRDER REAC.ON PILE CAP DUE TO WL ON LL COMP.(WL)
GIRDER#      RY(K)       RX(K)
  1        5.8602       1.1667
  2       -5.8602       1.1667
  3         .0000       1.1667
  4         .0000       1.1667
  5         .0000       1.1667
  6         .0000       1.1667
GIRD.REAC.ON PILE CAP DUE TO WL ON SUPER STR.(WS)
GIRDER#      RY(K)       RX(K)
  1        4.1223       9.4994
  2        2.4734       9.4994
  3         .8245       9.4994
  4        -.8245       9.4994
  5       -2.4734       9.4994
  6       -4.1223       9.4994

WL(K) ON SUP. & CAP ALONG THEIR LONG DIR, LOAD HT
      56.9966       43.3174        3.6285
CN.LD ON CAP & UDL ON PILE FOR TR.WL ON SUB STR(WS)
    CAP FACE(K)        PILE FACE(K/FT)
        .8078         .2244
UDL ON CAP AND PILE DUE TO LONGI.W ON SUB STR(WS)
 CAP_LONG.FACE(K/FT)    PILE FACE(K/FT)
       3.8148         .2244
GIRDER REAC. ON PILE CAP DUE TO SUPER STR. DL(DC)
       EXT GIRD.(K)    INT.GIRD.(K)
     -100.5634     -104.4372
GIRDER REACTION ON PILE CAP DUE TO FWS (DW)
       EXT GIRD.(K)    INT.GIRD.(K)
      -11.8934      -15.0507
UDL ON CAP AND PILE DUE TO CAP SW AND PILE SW(DC)
    CAP WT(K/FT)     PILE WT.(K/FT)
       -1.3500        -.9375
```

APPENDIX B. SAMPLE DESIGN CALCULATION

B.1 Sample Bridge Layout

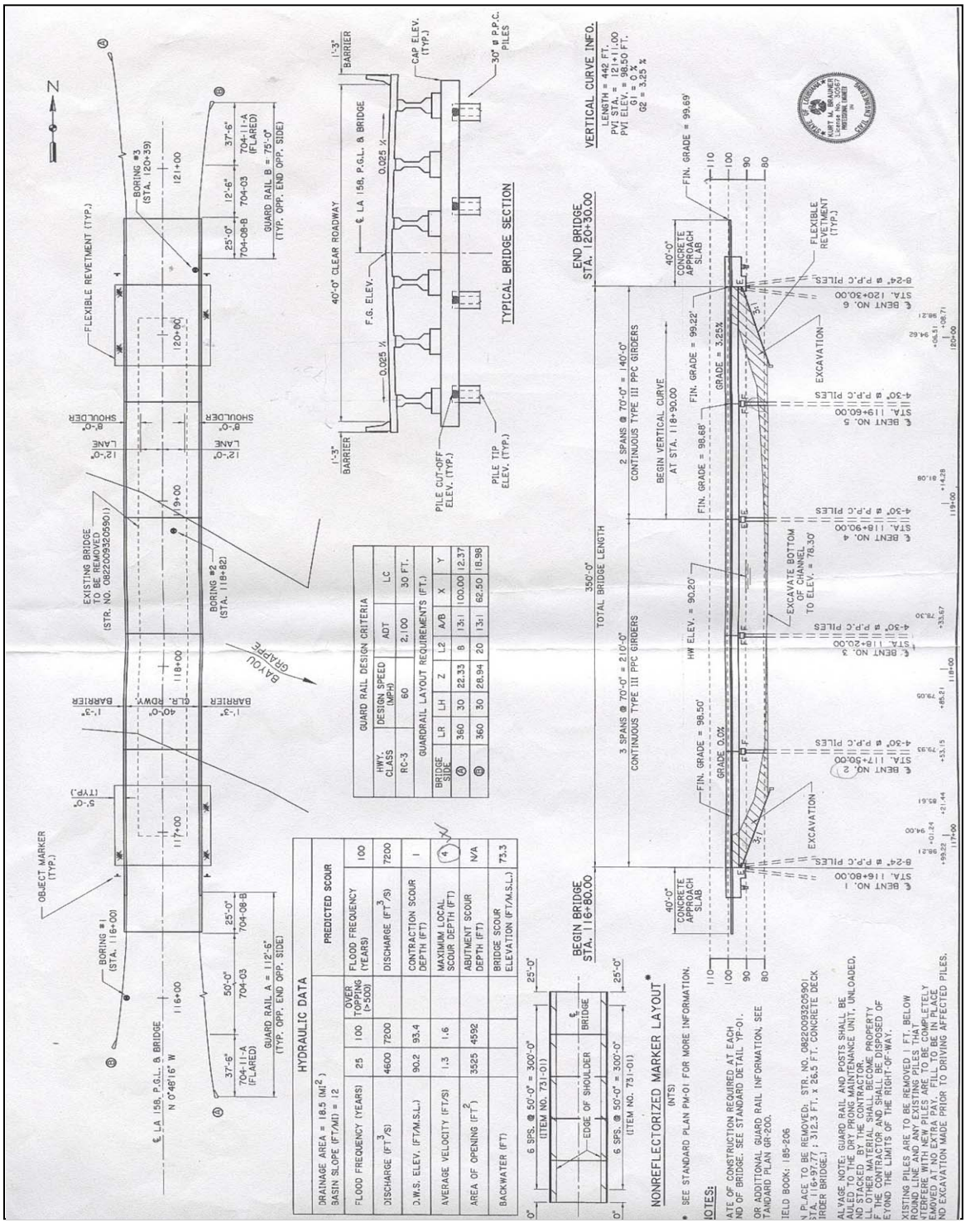

Figure B.1 General Plan for Bayou Grape Bridge (Source: LA-DOTD 2002)

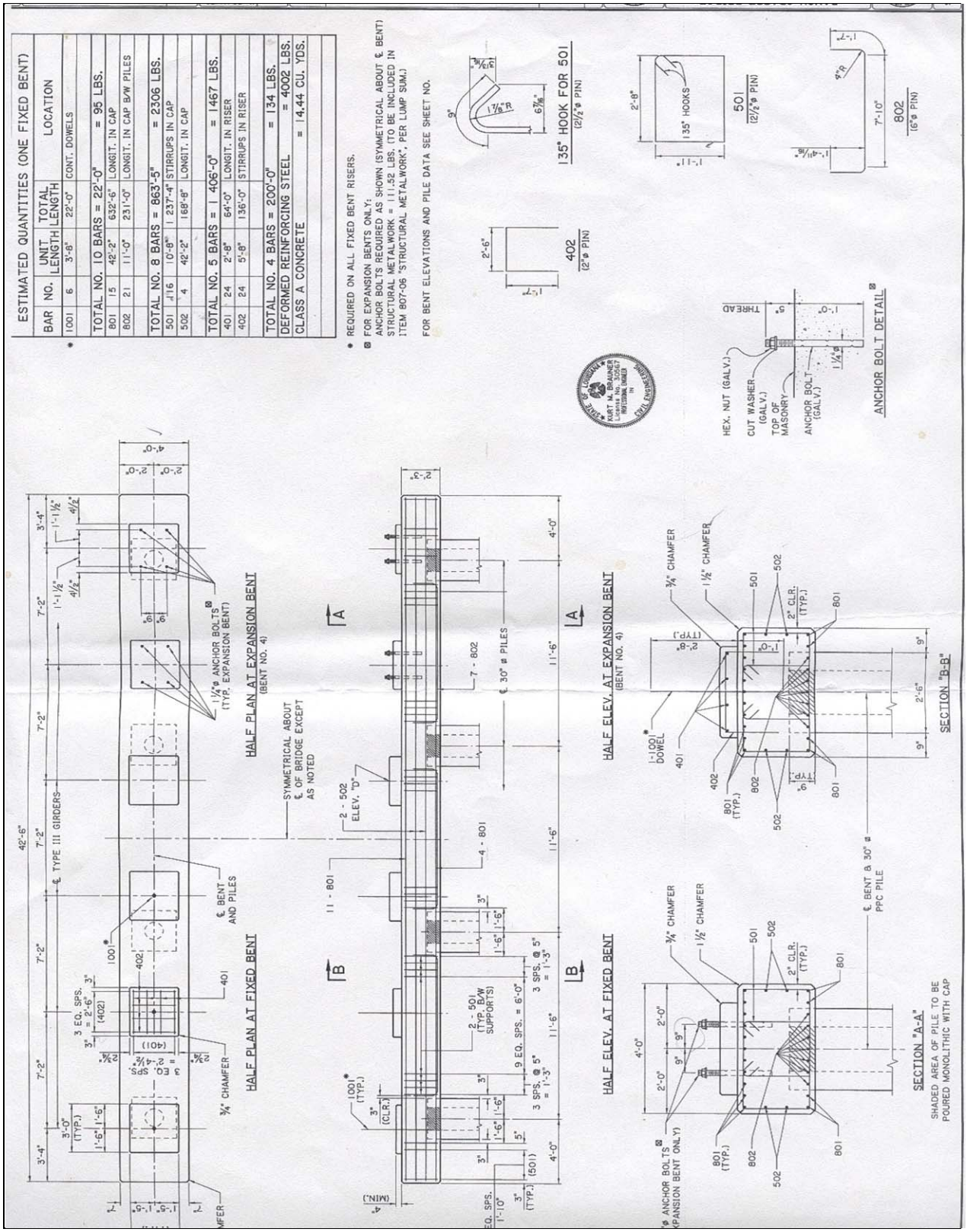

Figure B.2 Intermediate Bent details for Bayou Grape Bridge (Source: LA-DOTD 2002)

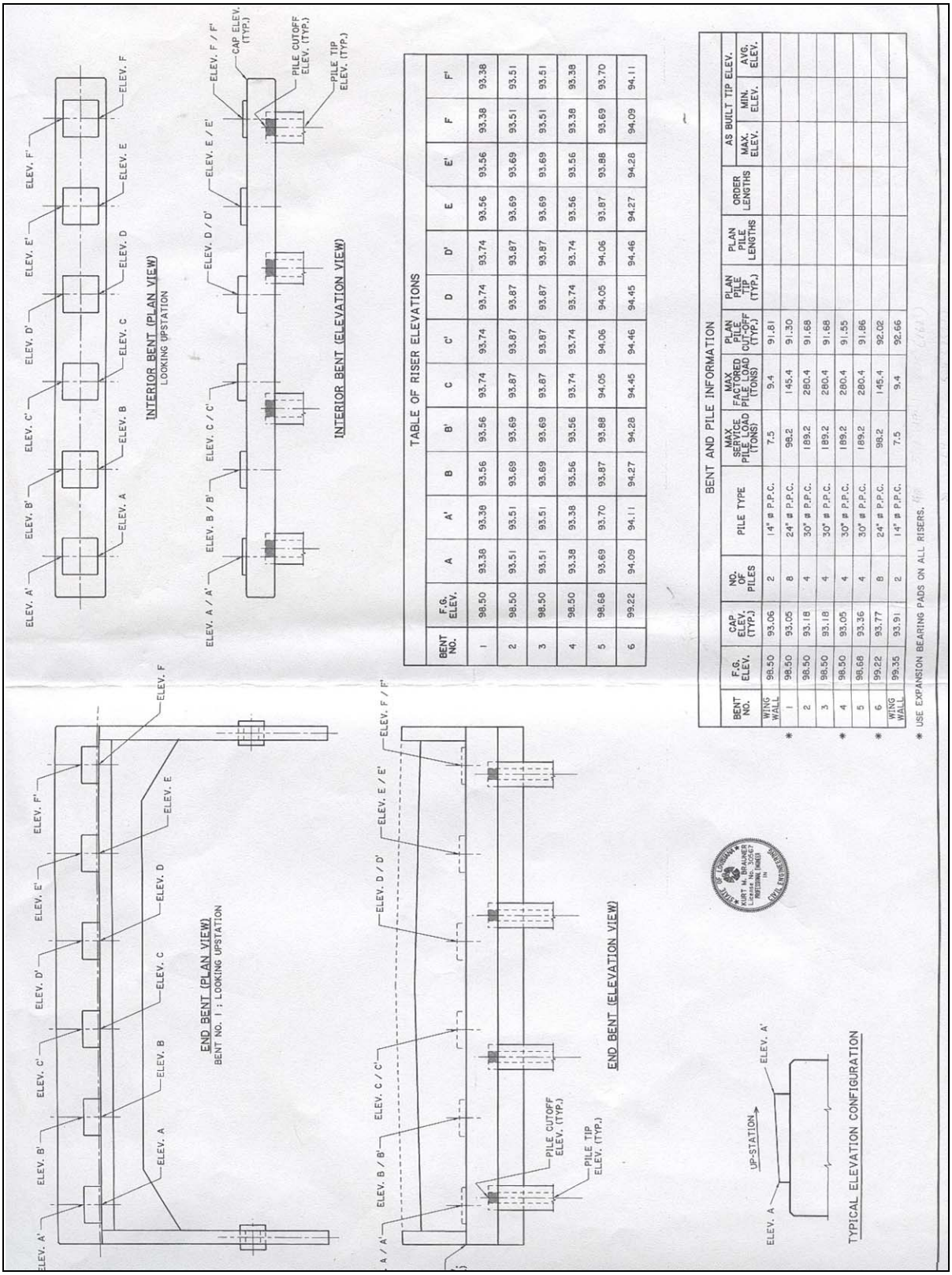

Figure B.3 Table of elevation for Bayou Grape Bridge (Source: LA-DOTD 2002)

B.2 Design Calculation

B.2.1 Dead Load (DC and DW)

Dead load from super structure(W_{DC}):

(a) $$W_{girder(I/E)} = 0.15 \times \frac{560}{144} = .583k / ft / girder$$

(b) $$W_{slab(I)} = 7.167 \times \frac{8}{12} \times 0.15 = .72k / ft / girder$$

$$W_{slab(E)} = \left(\frac{1}{2} \times 7.167 + 3.33 \right) \times \frac{8}{12} \times 0.15 = .69k / ft / girder$$

(c) $$W_{haunch} = \frac{2 \times 16}{144} \times 0.15 = .033k / ft / girder$$

(d) $$W_{diaphragm(I)} = \frac{8}{12} \times \frac{(45 - 14.5)}{12} \times \left(7.167 - \frac{7}{12} \right) \times 0.15 = 1.67k / girder$$

$$W_{diaphragm(E)} = \frac{1.67}{2} = 0.84k / girder$$

(e) $$W_{barrier} = \frac{275}{144} \times 0.15 \times \frac{2(barrier)}{6(girder)} = 0.095k / ft / girder$$

Girder reaction on pile cap due to DL (P_{DC})

$$P_{DC} = W_{girder} + W_{slab} + W_{haunch} + W_{barrier} + W_{diaphragm}$$

For Interior Girder, $$P_{DC_I} = (0.583 + .72 + .033 + .095) \times 70 + 1.67 \times 2 = 103k$$

For Exterior Girder, $$P_{DC_E} = (0.583 + .69 + .033 + .095) \times 70 + 0.84 \times 2 = 99.4k$$

Dead load from wearing surface and utilities (DW):

$$W_{FWS(I)} = 0.03 \times 7.167 = 0.215k / ft$$

$$W_{FWS(E)} = 0.03 \times \left(\frac{7.167}{2} + 3.33 - 1.25 \right) = 0.169k / ft$$

Girder reaction on pile cap due to Future Wearing Surface (DW)

For Interior Girder, $P_{DW_I} = 0.215 \times 70 = 15.05k$

For Exterior girder, $P_{DW_E} = 0.169 \times 70 = 11.89k$

B.2.2 Live Load (LL)

Live Load Case C (Figure 3.4c):

Using Equation 3.1, maximum LL reaction/span/wheel

$$P = \frac{1}{2} \times \left\{ 32 + 32 \times \frac{(70-14)}{70} + 8 \times \frac{(70-14)}{70} \right\} \times \frac{1}{2} + 0.64 \times \frac{70}{2} = 27.2k \text{ / span/wheel}$$

i.e. $P = 0.85 \times 27.2 = 23.12k$

Using Lever Rule (Figure B.4 and B.5)

$$R_1 = P \times \frac{(1.247 + 7.247)}{7.167} \qquad R_1 = 27.4k \ ; \qquad R_{2(1)} = 28.84k$$

$$R_{2(2)} = P \times \frac{4.417}{7.167} = 14.25k \quad R_2 = 33.1k \ ; \qquad R_{3(2)} = 8.85k$$

$$R_{3(3)} = 23k \ ; \qquad R_3 = 32k \ ; \qquad R_{4(3)} = 23.1k$$

$$R_{4(4)} = 8.89k \qquad R_4 = 32k \ ; \qquad R_5 = 28.47k$$

i.e. $2R_1 = 54.8k \ ; \ 2R_2 = 66.16k \ ; \ 2R_3 = 64k \ ; \ 2R_4 = 64k \ ; \ 2R_5 = 28.5k \ ; \ 2R_6 = 0k$

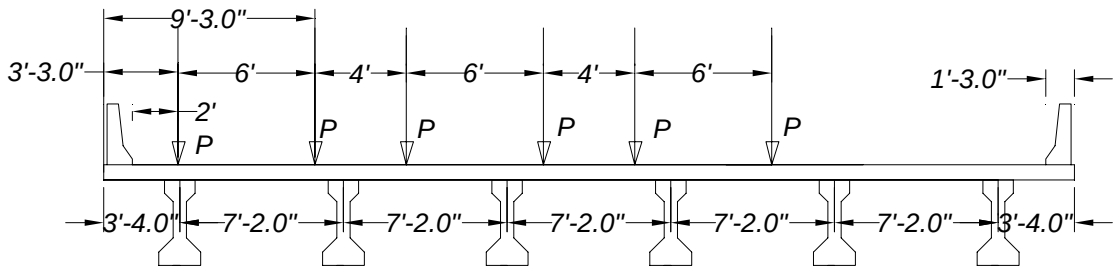

Figure B.4 Transverse LL wheel positions for Cases C (Figure 3.4c)

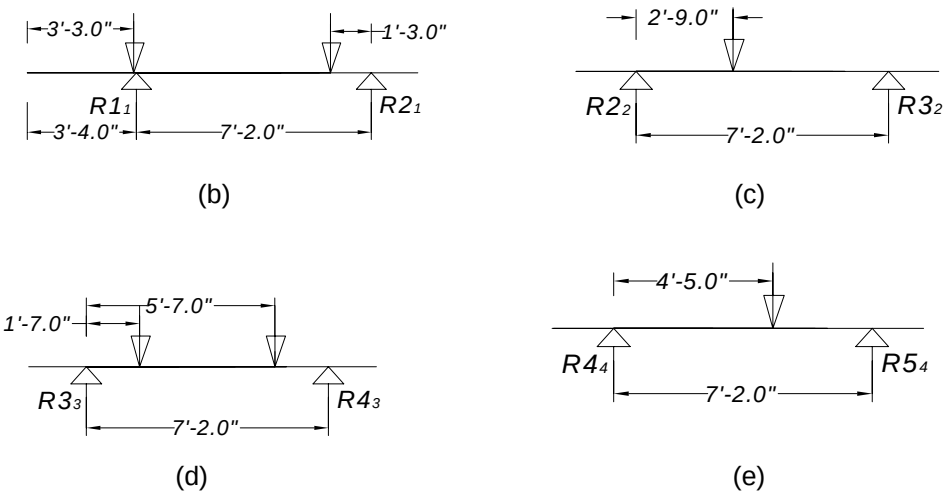

Figure B.5 Assumed Simply-supported deck segments for LL reaction calculations using lever rule

B.2.3 Breaking force (BR)

According to AASHTO (2004) article 3.6.4, breaking force,

$$\text{BR} = \text{greater of} \begin{cases} = 0.25 \times (DesignTruck) \times No.of\ lane \times m.f. \\ = 0.05 \times (DesignTruck + LaneLoad) \times No.of\ lane \times m.f \\ = 0.05 \times (DesignTendem + LaneLoad) \times No.of\ lane \times m.f \end{cases}$$

$$\text{BR} = \text{greater of} \begin{cases} = 0.25 \times (32 + 32 + 8) \times 3lane \times 0.85 = 45.9k \\ = 0.05 \times (72 + 70 \times 2 \times 0.64) \times 3lane \times 0.85 = 20.6k \\ = 0.05 \times (25 \times 2 + 70 \times 2 \times 0.64) \times 3lane \times 0.85 = 17.8k \end{cases}$$

i.e. Breaking force per vehicle , $P_B = \frac{45.9}{3} = 15.3k$ acting 6ft above the deck surface.

Using Equation 3.2 and Figure B.6

$$B_1 = \frac{15.3 \times 3}{6} + \frac{15.3 \times (15 + 5 - 5)}{2 \times \left(17.92^2 + 10.75^2 + 3.59^2\right)} \times 17.92 = 12.2k$$

$$B_2 = 10.4k \qquad B_3 = 8.6k \qquad B_4 = 6.7k$$

$$B_5 = 4.9k \qquad B_6 = 3.1k$$

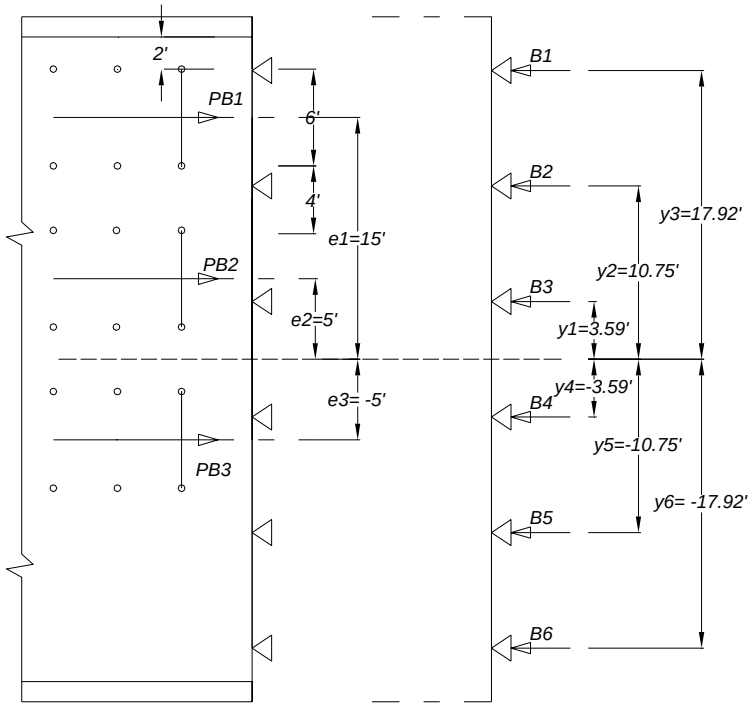

Figure B.6 Girder reactions on pile cap due to Breaking Force

B.2.4 Wind Load on Live Load (WL)

Transverse wind acting on vehicle $F_{TLL} = F_w \times \dfrac{\left(L_{back} + L_{ahead}\right)}{2}$

$$= 0.1 \times \frac{\left(70 + 70\right)}{2} = 7k \quad \text{(0deg skew)}$$

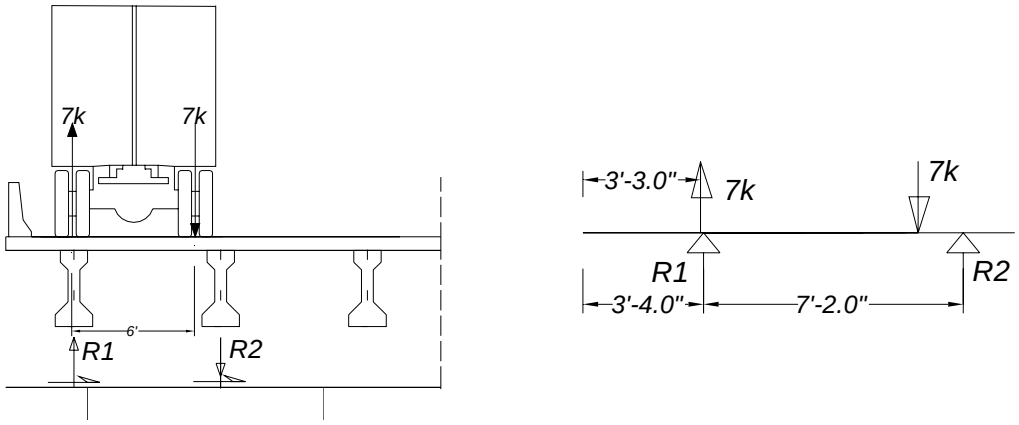

Figure B.7 Girder reactions on pile cap due to wind load on Live load

Girder reactions due to wind on live load:

1st wheel position 2 ft from barrier face:

Using Figure B.7 $R_1 = 7 \times \frac{(7.25 - 1.25)}{7.167} = 5.9k$; $R_2 = 5.9k$

$$R_{x1} = R_{x2} = R_{x3} = R_{x4} = R_{x5} = R_{x6} = \frac{7}{6} = 1.17k$$

B.2.5 Wind Load on Structure (WS)

Design wind pressure $P_w = P_B \times \left(\frac{V_{DZ}}{V_B}\right)^2 = P_B \times \left(\frac{V_{DZ}}{100}\right)^2 = 2.24\, P_B.$ (Article 3.8.1.2.1-1)

where, P_B= Base Wind Pressure

V_{DZ}=Design wind velocity $= 2.5 V_o \left(\frac{V_{30}}{V_B}\right) \ln\left(\frac{Z}{Z_0}\right)$=149.8 mph

V_{30}=150 mph (ASCE 7-02)

V_o = 8.2 mph; Z_o= 0.23 (Open Country)

B.2.5.1 Wind Load on Superstructure:

Wind load transverse to the superstructure

$$F_{T\,\mathrm{super}} = P_w \times H_{wind} \times \frac{(L_{back} + L_{ahead})}{2}$$

$$H_{wind} = H_{barrier} + H_{deck} + H_{haunch} + H_{girder} = 2.67 + \frac{(8 + 2 + 45)}{12} = 7.25\, ft$$

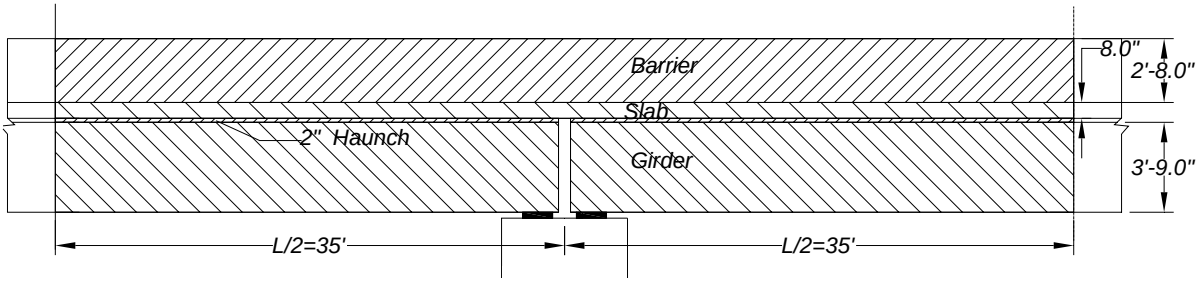

Figure B.8 Contributing area for transverse wind load for each pier line.

Using Table 3.6

For 0 degree wind angle $F_{T\,super} = 2.24 \times 0.05 \times 7.25 \times \frac{(70+70)}{2} = 56.8k$

For 60 degree wind angle $F_{T\,super} = 2.24 \times 0.017 \times 7.25 \times \frac{(70+70)}{2} = 19.3k$

Wind load along superstructure

$$F_{L\,super} = P_w \times H_{wind} \times \frac{(L_{back} + L_{ahead})}{N_{fixedpier}}$$

For 0 degree wind angle $F_{L\,super} = 0$

For 60 degree wind angle $F_{L\,super} = 2.24 \times 0.019 \times 7.25 \times \frac{(70+70)}{1} = 43.2k$

Resultant Wind load along pier axis

(a) WL perpendicular to plane of pier

$$F_{Lp} = F_{L\,super} \times \cos(\theta_{skew}) + F_{T\,super} \times \sin(\theta_{skew})$$

For 0 degree wind angle $F_{Lp} = 0 \times \cos(0) + 58.17 \times \sin(0) = 0$

For 60 degree wind angle $F_{Lp} = 43.2 \times \cos(0) + 19.3 \times \sin(0) = 43.2k$

(b) WL parallel to plane of pier

$$F_{Tp} = F_{L\,super} \times \sin(\theta_{skew}) + F_{T\,super} \times \cos(\theta_{skew})$$

For 0 degree wind angle $F_{Tp} = 0 \times \sin(0) + 56.8 \times cos(0) = 56.8k$

For 60 degree wind angle $F_{Tp} = 43.2 \times \sin(0) + 19.3 \times \cos(0) = 19.3k$

Wind load on superstructure act at 3.63 ft from top of pier cap.

Girder Reaction due to wind load on superstructure:

Using Equation 3.10 and Figure B.9,

$$R_1 = \frac{56.8 \times 3.63}{2 \times (17.92^2 + 10.75^2 + 3.59^2)} \times 17.92 = 4.1k$$

$R_2 = 2.5k$ $R_4 = 0.8k$ $R_5 = 2.5k$

$R_3 = 0.8k$ $R_6 = 4.1k$

$$R_x = \frac{56.8}{6} = 9.5k / girder$$

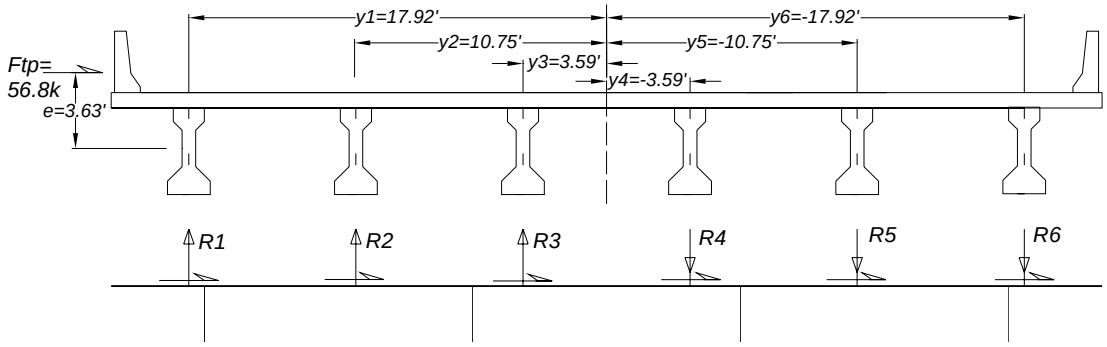

Figure B.9 Girder reactions on pile cap due to wind load on super structure

B.2.5.2 Wind Load on Substructures (WS)

(a) Wind load on cap

Transverse wind on cap face $= P_w \times$ *cap width* $= 2.24 \times 0.04 \times (4 \times 2.25) = 0.8k$

Longitudinal wind on cap $= P_w \times$ *cap length* $= 2.24 \times 0.04 \times (42.5) = 3.8k/ft$

(b) Wind load on pier

Transverse wind on end pile $= P_w \times$ *pile width* $= 2.24 \times 0.04 \times (2.5) = .2k/ft$

Longitudinal wind on cap $= P_w \times$ *cap length* $= 2.24 \times 0.04 \times (2.5) = 0.22k/ft$

APPENDIX C. IMPORTANT CHARTS AND FIGURES

Table C.1 Formulae for torsional constants (Young and Budynas 2002)

Forms and Dimensions of cross Sections	Formulae for Torsional Constant J
1. Solid Circular Section 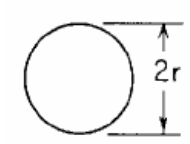	$J = \frac{1}{2}\pi r^4$
2. Solid Square section 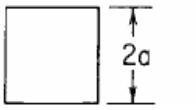	$J = 2.25a^4$
3. I section; Uniform flange thickness; R=fillet radius, D= diameter largest inscribed circle, t=b if b<d; t=d if d<b; t_1=b if b>d; t_1=d if d>b. 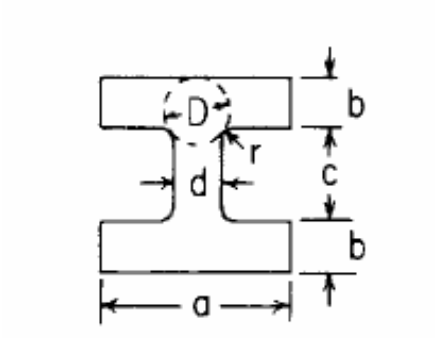	$J = 2J_1 + J_2 + 2\alpha D^4$ Where, $J_1 = ab^3\left[\frac{1}{3} - 0.21\frac{b}{a}\left(1 - \frac{b^4}{12a^4}\right)\right]$ $J_2 = \frac{1}{3}cd^3$ $\alpha = \frac{t}{t_1}\left(0.15 + 0.1\frac{r}{b}\right)$ $D = \frac{(b+r)^2 + rd + \frac{d^2}{4}}{2r+b}$ for $d < 2(b+r)$

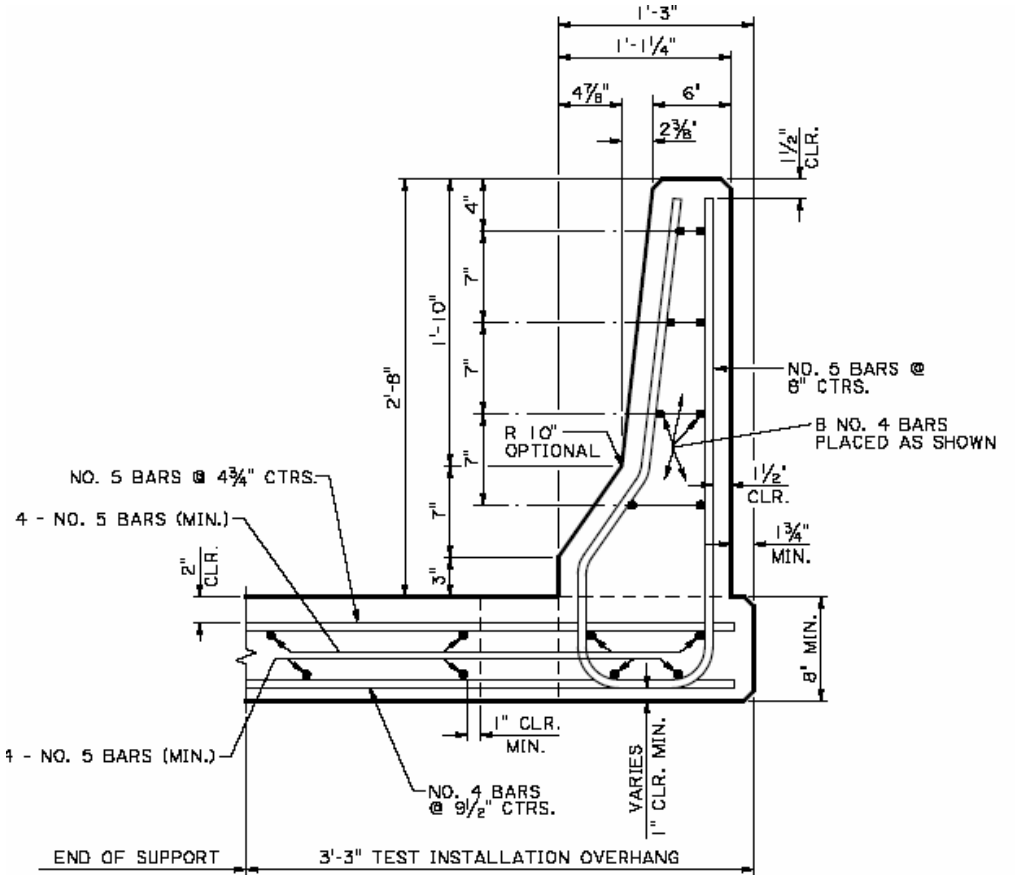

Figure C.1 F-Shape (PL-2) Barrier (LA-DOTD BDM 2004)

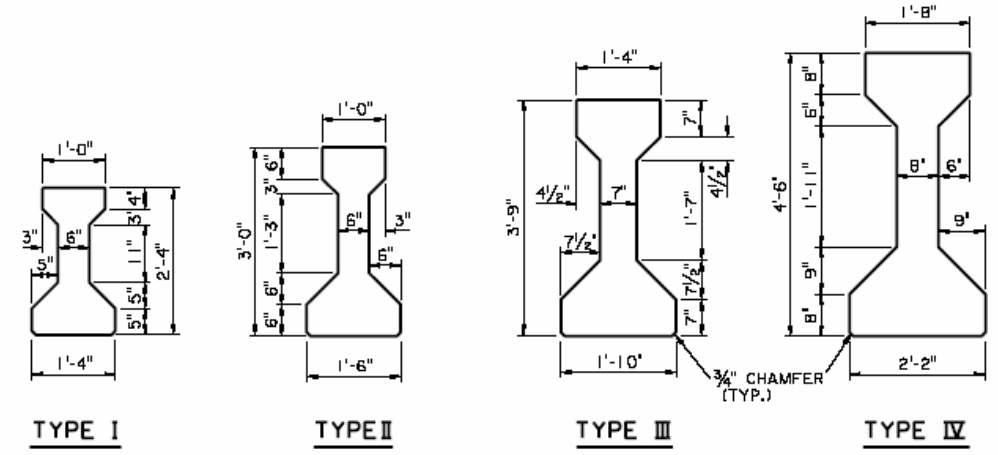

Figure C.2 Prestressed Girders Types (LA-DOTD BDM 2004)

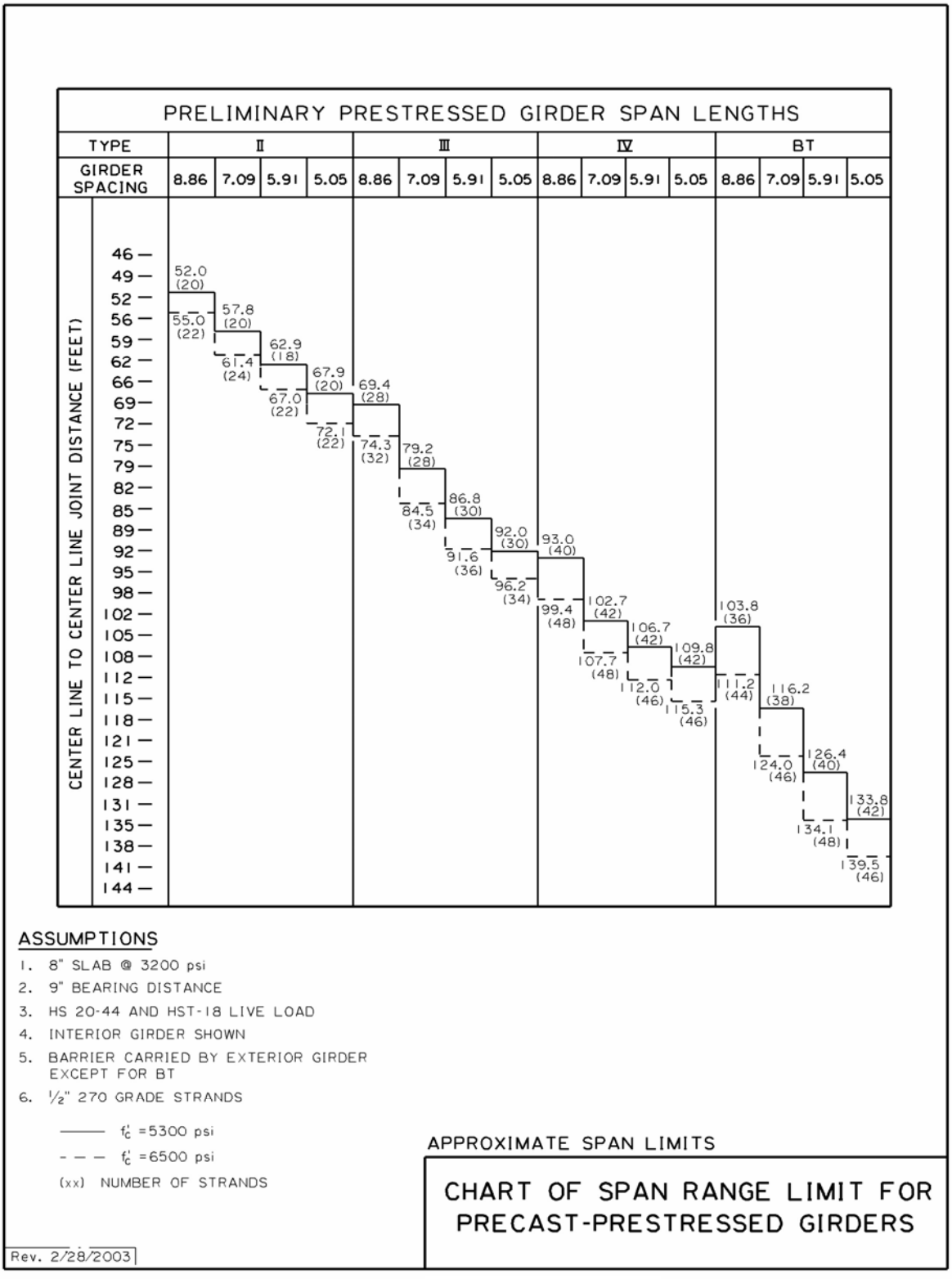

Figure C.3 Chart of Span Range Limit for Precast-Prestressed Girders (LA-DOTD BDM 2004)

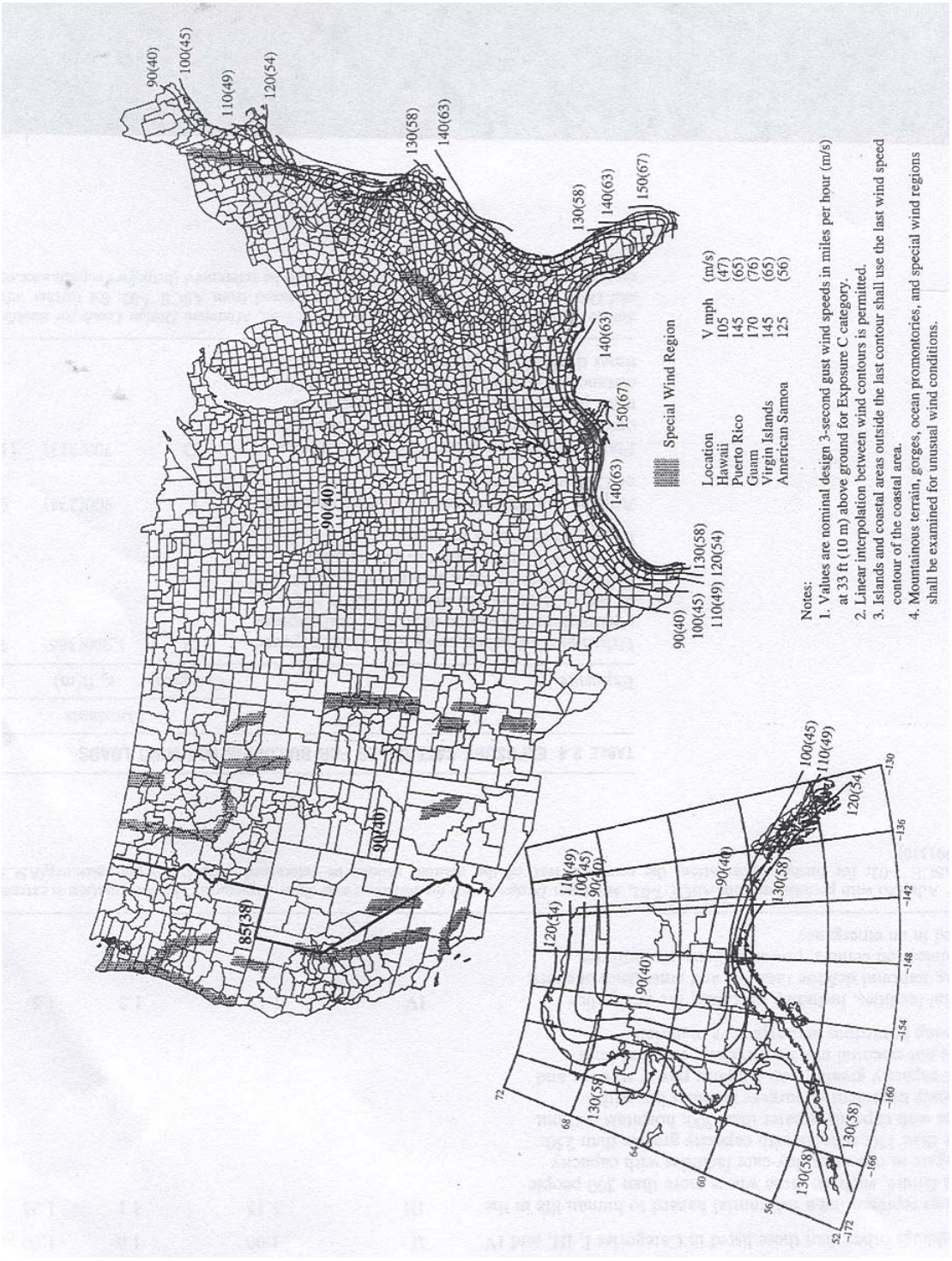

Figure C.4 Basic Wind Speed for the United States (ASCE 7-02)

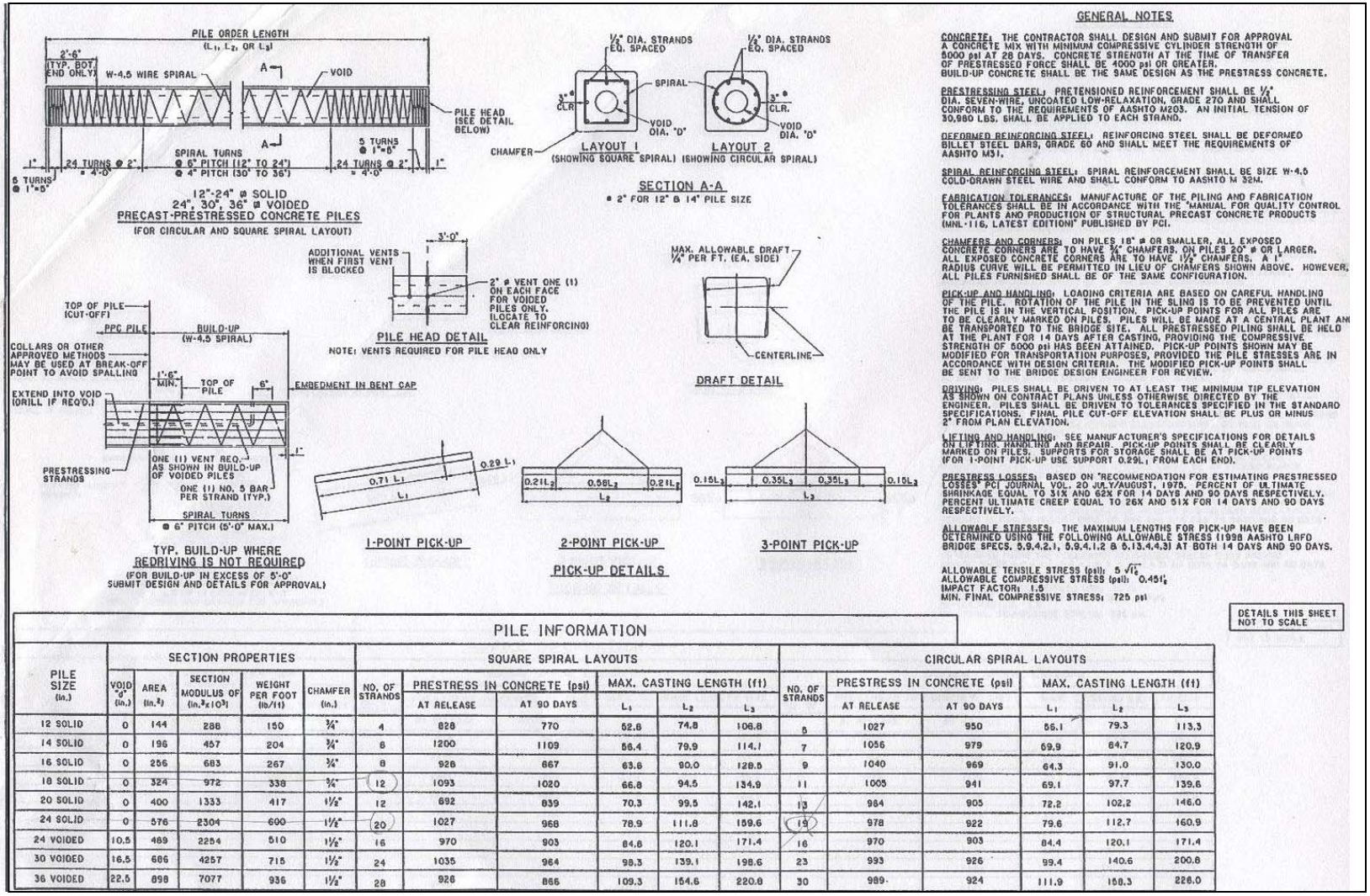

GENERAL NOTES

CONCRETE: THE CONTRACTOR SHALL DESIGN AND SUBMIT FOR APPROVAL A CONCRETE MIX WITH MINIMUM COMPRESSIVE CYLINDER STRENGTH OF 5000 psi AT 28 DAYS. CONCRETE STRENGTH AT THE TIME OF TRANSFER OF PRESTRESSED FORCE SHALL BE 4000 psi OR GREATER. BUILD-UP CONCRETE SHALL BE THE SAME DESIGN AS THE PRESTRESS CONCRETE.

PRESTRESSING STEEL: PRETENSIONED REINFORCEMENT SHALL BE 1/4" DIA. SEVEN-WIRE, UNCOATED LOW-RELAXATION, GRADE 270 AND SHALL CONFORM TO THE REQUIREMENTS OF AASHTO M203. AN INITIAL TENSION OF 30,980 LBS. SHALL BE APPLIED TO EACH STRAND.

DEFORMED REINFORCING STEEL: REINFORCING STEEL SHALL BE DEFORMED BILLET STEEL BARS, GRADE 60 AND SHALL MEET THE REQUIREMENTS OF AASHTO M31.

SPIRAL REINFORCING STEEL: SPIRAL REINFORCEMENT SHALL BE SIZE W-4.5 COLD-DRAWN STEEL WIRE AND SHALL CONFORM TO AASHTO M 32M.

FABRICATION TOLERANCES: MANUFACTURE OF THE PILING AND FABRICATION TOLERANCES SHALL BE IN ACCORDANCE WITH THE "MANUAL FOR QUALITY CONTROL FOR PLANTS AND PRODUCTION OF STRUCTURAL PRECAST CONCRETE PRODUCTS (MNL-116, LATEST EDITION)" PUBLISHED BY PCI.

CHAMFERS AND CORNERS: ON PILES 18" ø OR SMALLER, ALL EXPOSED CONCRETE CORNERS ARE TO HAVE 3/4" CHAMFERS. ON PILES 20" ø OR LARGER, ALL EXPOSED CONCRETE CORNERS ARE TO HAVE 1 1/2" CHAMFERS. A 1" RADIUS CURVE WILL BE PERMITTED IN LIEU OF CHAMFERS SHOWN ABOVE. HOWEVER, ALL PILES FURNISHED SHALL BE OF THE SAME CONFIGURATION.

PICK-UP AND HANDLING: LOADING CRITERIA ARE BASED ON CAREFUL HANDLING OF THE PILE. ROTATION OF THE PILE IN THE SLING IS TO BE PREVENTED UNTIL THE PILE IS IN THE VERTICAL POSITION. PICK-UP POINTS FOR ALL PILES ARE TO BE CLEARLY MARKED ON PILES. PILES WILL BE MADE AT A CENTRAL PLANT AND BE TRANSPORTED TO THE BRIDGE SITE. ALL PRESTRESSED PILING SHALL BE HELD AT THE PLANT FOR 14 DAYS AFTER CASTING, PROVIDING THE COMPRESSIVE STRENGTH OF 5000 psi HAS BEEN ATTAINED. PICK-UP POINTS SHOWN MAY BE MODIFIED FOR TRANSPORTATION PURPOSES, PROVIDED THE PILE STRESSES ARE IN ACCORDANCE WITH DESIGN CRITERIA. THE MODIFIED PICK-UP POINTS SHALL BE SENT TO THE BRIDGE DESIGN ENGINEER FOR REVIEW.

DRIVING: PILES SHALL BE DRIVEN TO AT LEAST THE MINIMUM TIP ELEVATION AS SHOWN ON CONTRACT PLANS UNLESS OTHERWISE DIRECTED BY THE ENGINEER. PILES SHALL BE DRIVEN TO TOLERANCES SPECIFIED IN THE STANDARD SPECIFICATIONS. FINAL PILE CUT-OFF ELEVATION SHALL BE PLUS OR MINUS 2" FROM PLAN ELEVATION.

LIFTING AND HANDLING: SEE MANUFACTURER'S SPECIFICATIONS FOR DETAILS ON LIFTING, HANDLING AND REPAIR. PICK-UP POINTS SHALL BE CLEARLY MARKED ON PILES. SUPPORTS FOR STORAGE SHALL BE AT PICK-UP POINTS (FOR 1-POINT PICK-UP USE SUPPORT 0.29L1 FROM EACH END).

PRESTRESS LOSSES: BASED ON "RECOMMENDATION FOR ESTIMATING PRESTRESSED LOSSES" PCI JOURNAL VOL. 20 JULY/AUGUST, 1975. PERCENT OF ULTIMATE SHRINKAGE EQUAL TO 31% AND 62% FOR 14 DAYS AND 90 DAYS RESPECTIVELY. PERCENT ULTIMATE CREEP EQUAL TO 26% AND 51% FOR 14 DAYS AND 90 DAYS RESPECTIVELY.

ALLOWABLE STRESSES: THE MAXIMUM LENGTHS FOR PICK-UP HAVE BEEN DETERMINED USING THE FOLLOWING ALLOWABLE STRESS (1998 AASHTO LRFD BRIDGE SPECS. 5.9.4.2.1, 5.9.4.1.2 & 5.13.4.4.3) AT BOTH 14 DAYS AND 90 DAYS.

ALLOWABLE TENSILE STRESS (psi): $5\sqrt{f'_c}$
ALLOWABLE COMPRESSIVE STRESS (psi): $0.45f'_c$
IMPACT FACTOR: 1.0
MIN. FINAL COMPRESSIVE STRESS: 725 psi

DETAILS THIS SHEET NOT TO SCALE

PILE INFORMATION

PILE SIZE (in.)	SECTION PROPERTIES					SQUARE SPIRAL LAYOUTS						CIRCULAR SPIRAL LAYOUTS					
	VOID "d" (in.)	AREA (in.²)	SECTION MODULUS OF (in.³x10³)	WEIGHT PER FOOT (lb/ft)	CHAMFER (in.)	NO. OF STRANDS	PRESTRESS IN CONCRETE (psi)		MAX. CASTING LENGTH (ft)			NO. OF STRANDS	PRESTRESS IN CONCRETE (psi)		MAX. CASTING LENGTH (ft)		
							AT RELEASE	AT 90 DAYS	L_1	L_2	L_3		AT RELEASE	AT 90 DAYS	L_1	L_2	L_3
12 SOLID	0	144	288	150	3/4"	4	828	770	52.8	74.8	106.8	5	1027	950	56.1	79.3	113.3
14 SOLID	0	196	457	204	3/4"	8	1200	1109	66.4	79.9	114.1	7	1056	979	69.9	84.7	120.9
16 SOLID	0	256	683	267	3/4"	8	928	867	63.8	90.0	128.5	9	1040	969	64.3	91.0	130.0
18 SOLID	0	324	972	338	3/4"	12	1093	1020	66.8	94.5	134.9	11	1005	941	69.1	97.7	139.6
20 SOLID	0	400	1333	417	1 1/2"	12	892	839	70.3	99.5	142.1	13	984	905	72.2	102.2	146.0
24 SOLID	0	576	2304	600	1 1/2"	20	1027	968	78.9	111.8	159.6	13	978	922	79.6	112.7	160.9
24 VOIDED	10.5	489	2254	510	1 1/2"	16	970	903	84.8	120.1	171.4	16	970	903	84.4	120.1	171.4
30 VOIDED	16.5	686	4257	715	1 1/2"	24	1035	964	98.3	139.1	198.6	23	993	926	99.4	140.6	200.8
36 VOIDED	22.5	898	7077	936	1 1/2"	28	926	866	109.3	154.6	220.8	30	989	924	111.9	158.3	226.0

Figure C.5 Details of Precast-Prestressed Concrete Piles, Standard Detail: CS-216 (LA-DOTD BDM 2004)

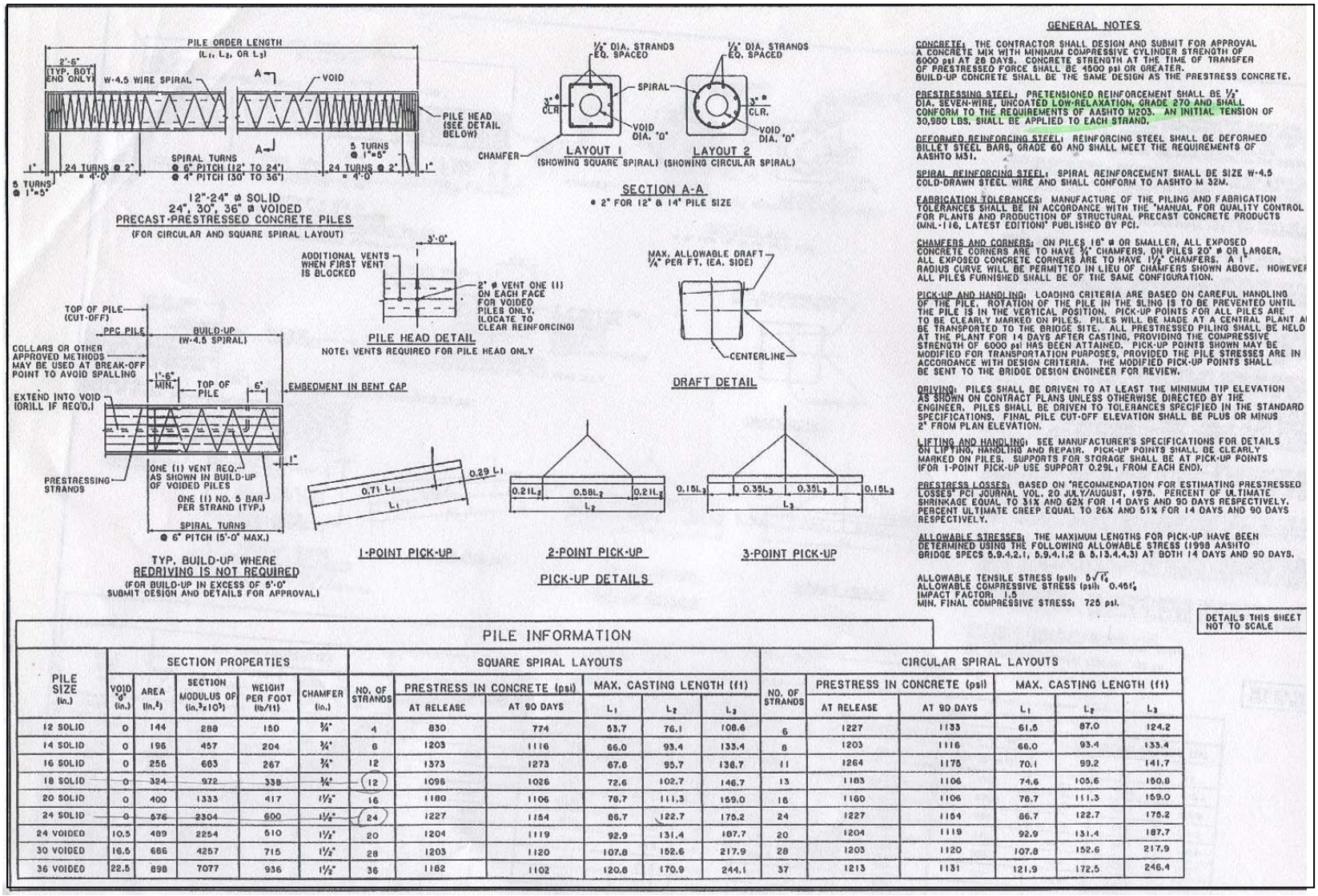

GENERAL NOTES

CONCRETE: THE CONTRACTOR SHALL DESIGN AND SUBMIT FOR APPROVAL A CONCRETE MIX WITH MINIMUM COMPRESSIVE CYLINDER STRENGTH OF 6000 psi AT 28 DAYS. CONCRETE STRENGTH AT THE TIME OF TRANSFER OF PRESTRESSED FORCE SHALL BE 4500 psi OR GREATER. BUILD-UP CONCRETE SHALL BE THE SAME DESIGN AS THE PRESTRESS CONCRETE.

PRESTRESSING STEEL: PRETENSIONED REINFORCEMENT SHALL BE 1/4" DIA. SEVEN-WIRE, UNCOATED LOW-RELAXATION, GRADE 270 AND SHALL CONFORM TO THE REQUIREMENTS OF AASHTO M203. AN INITIAL TENSION OF 30,980 LBS. SHALL BE APPLIED TO EACH STRAND.

DEFORMED REINFORCING STEEL: REINFORCING STEEL SHALL BE DEFORMED BILLET STEEL BARS, GRADE 60 AND SHALL MEET THE REQUIREMENTS OF AASHTO M31.

SPIRAL REINFORCING STEEL: SPIRAL REINFORCEMENT SHALL BE SIZE W-4.5 COLD-DRAWN STEEL WIRE AND SHALL CONFORM TO AASHTO M 32M.

FABRICATION TOLERANCES: MANUFACTURE OF THE PILING AND FABRICATION TOLERANCES SHALL BE IN ACCORDANCE WITH THE "MANUAL FOR QUALITY CONTROL FOR PLANTS AND PRODUCTION OF STRUCTURAL PRECAST CONCRETE PRODUCTS (MNL-116, LATEST EDITION)" PUBLISHED BY PCI.

CHAMFERS AND CORNERS: ON PILES 16" ø OR SMALLER, ALL EXPOSED CONCRETE CORNERS ARE TO HAVE 3/4" CHAMFERS. ON PILES 20" ø OR LARGER, ALL EXPOSED CONCRETE CORNERS ARE TO HAVE 1 1/2" CHAMFERS. A 1" RADIUS CURVE WILL BE PERMITTED IN LIEU OF CHAMFERS SHOWN ABOVE. HOWEVER ALL PILES FURNISHED SHALL BE OF THE SAME CONFIGURATION.

PICK-UP AND HANDLING: LOADING CRITERIA ARE BASED ON CAREFUL HANDLING OF THE PILE. ROTATION OF THE PILE IN THE SLING IS TO BE PREVENTED UNTIL THE PILE IS IN THE VERTICAL POSITION. PICK-UP POINTS FOR ALL PILES ARE TO BE CLEARLY MARKED ON PILES. PILES WILL BE MADE AT A CENTRAL PLANT AND BE TRANSPORTED TO THE BRIDGE SITE. ALL PRESTRESSED PILING SHALL BE HELD AT THE PLANT FOR 14 DAYS AFTER CASTING, PROVIDING THE COMPRESSIVE STRENGTH OF 6000 psi HAS BEEN ATTAINED. PICK-UP POINTS SHOWN MAY BE MODIFIED FOR TRANSPORTATION PURPOSES, PROVIDED THE PILE STRESSES ARE IN ACCORDANCE WITH DESIGN CRITERIA. THE MODIFIED PICK-UP POINTS SHALL BE SENT TO THE BRIDGE DESIGN ENGINEER FOR REVIEW.

DRIVING: PILES SHALL BE DRIVEN TO AT LEAST THE MINIMUM TIP ELEVATION AS SHOWN ON CONTRACT PLANS UNLESS OTHERWISE DIRECTED BY THE ENGINEER. PILES SHALL BE DRIVEN TO TOLERANCES SPECIFIED IN THE STANDARD SPECIFICATIONS. FINAL PILE CUT-OFF ELEVATION SHALL BE PLUS OR MINUS 2" FROM PLAN ELEVATION.

LIFTING AND HANDLING: SEE MANUFACTURER'S SPECIFICATIONS FOR DETAILS ON LIFTING, HANDLING AND REPAIR. PICK-UP POINTS SHALL BE CLEARLY MARKED ON PILES. SUPPORTS FOR STORAGE SHALL BE AT PICK-UP POINTS (FOR 1-POINT PICK-UP USE SUPPORT 0.29L1 FROM EACH END).

PRESTRESS LOSSES: BASED ON "RECOMMENDATION FOR ESTIMATING PRESTRESSED LOSSES" PCI JOURNAL VOL. 20 JULY/AUGUST, 1975. PERCENT OF ULTIMATE SHRINKAGE EQUAL TO 31% AND 62% FOR 14 DAYS AND 90 DAYS RESPECTIVELY. PERCENT ULTIMATE CREEP EQUAL TO 26% AND 51% FOR 14 DAYS AND 90 DAYS RESPECTIVELY.

ALLOWABLE STRESSES: THE MAXIMUM LENGTHS FOR PICK-UP HAVE BEEN DETERMINED USING THE FOLLOWING ALLOWABLE STRESS (1998 AASHTO BRIDGE SPECS 5.9.4.2.1, 5.9.4.1.2 & 5.13.4.4.3) AT BOTH 14 DAYS AND 90 DAYS.

ALLOWABLE TENSILE STRESS (psi): $5\sqrt{f'_c}$
ALLOWABLE COMPRESSIVE STRESS (psi): $0.45f'_c$
IMPACT FACTOR: 1.5
MIN. FINAL COMPRESSIVE STRESS: 725 psi.

DETAILS THIS SHEET NOT TO SCALE

PILE INFORMATION

PILE SIZE (in.)	SECTION PROPERTIES					SQUARE SPIRAL LAYOUTS					CIRCULAR SPIRAL LAYOUTS					
	VOID "d" (in.)	AREA (in.²)	SECTION MODULUS OF (in.³x10³)	WEIGHT PER FOOT (lb/ft)	CHAMFER (in.)	NO. OF STRANDS	PRESTRESS IN CONCRETE (psi)		MAX. CASTING LENGTH (ft)			NO. OF STRANDS	PRESTRESS IN CONCRETE (psi)		MAX. CASTING LENGTH (ft)		
							AT RELEASE	AT 90 DAYS	L_1	L_2	L_3		AT RELEASE	AT 90 DAYS	L_1	L_2	L_3
12 SOLID	0	144	288	150	3/4"	4	830	774	53.7	76.1	108.6	6	1227	1133	61.5	87.0	124.2
14 SOLID	0	196	457	204	3/4"	8	1203	1116	66.0	93.4	133.4	8	1203	1116	66.0	93.4	133.4
16 SOLID	0	256	683	267	3/4"	12	1373	1273	67.6	95.7	136.7	11	1264	1175	70.1	99.2	141.7
18 SOLID	0	324	972	338	3/4"	12	1096	1026	72.6	102.7	146.7	13	1183	1106	74.6	105.6	150.8
20 SOLID	0	400	1333	417	1 1/2"	16	1180	1106	76.7	111.3	159.0	16	1180	1106	78.7	111.3	159.0
24 SOLID	0	576	2304	600	1 1/2"	24	1227	1154	86.7	122.7	175.2	24	1227	1154	86.7	122.7	175.2
24 VOIDED	10.5	489	2254	510	1 1/2"	20	1204	1119	92.9	131.4	187.7	20	1204	1119	92.9	131.4	187.7
30 VOIDED	16.5	686	4257	715	1 1/2"	28	1203	1120	107.8	152.6	217.9	28	1203	1120	107.8	152.6	217.9
36 VOIDED	22.5	898	7077	936	1 1/2"	36	1182	1102	120.8	170.9	244.1	37	1213	1131	121.9	172.5	246.4

Figure C.6 Details of Precast-Prestressed Concrete Piles (Modified), Standard Detail: CS-216 MOD (LA-DOTD BDM 2004)

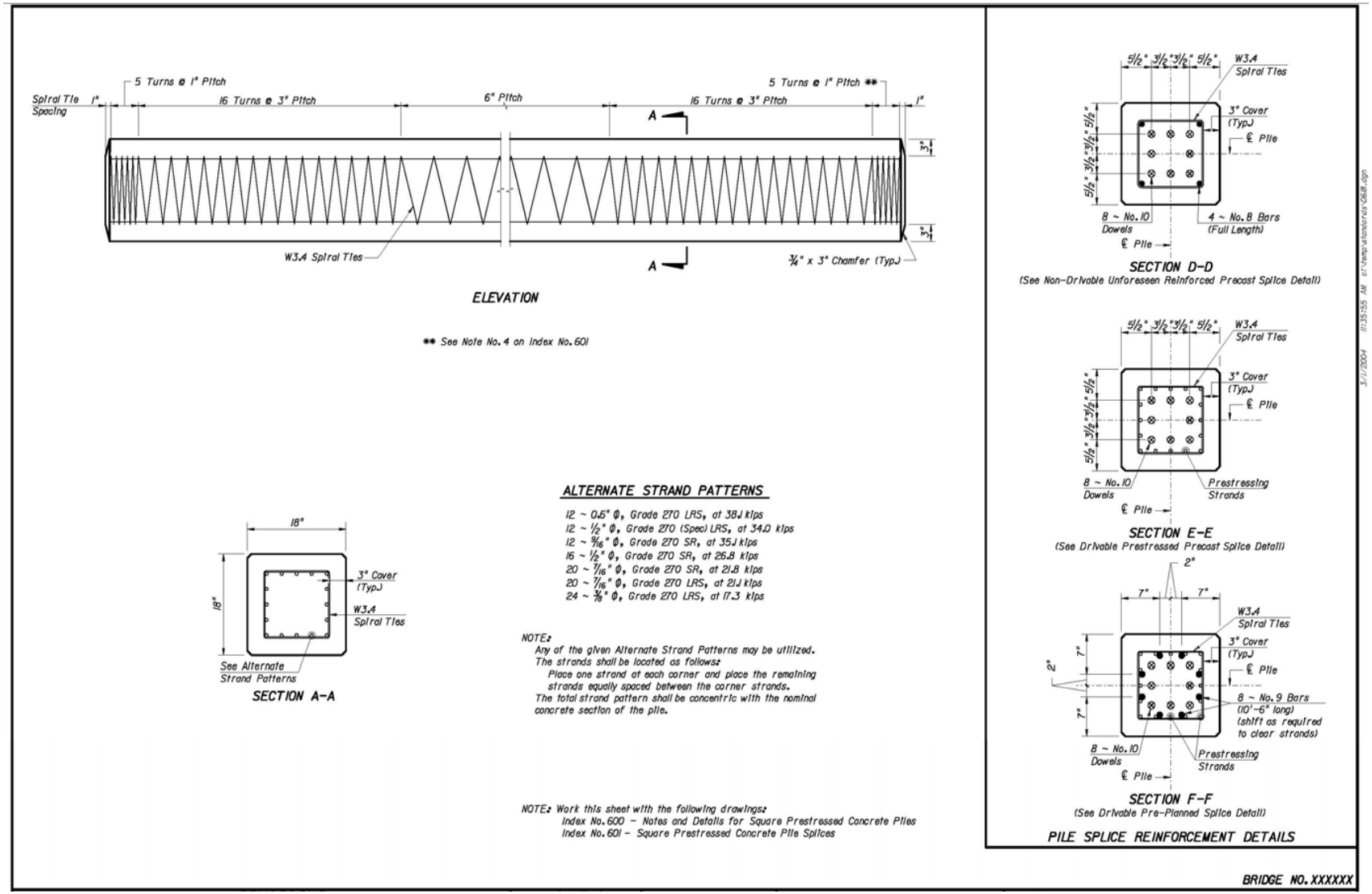

Figure C.7 Details of 18 inch Square Prestressed Concrete Piles (Florida-DOTD 2004)

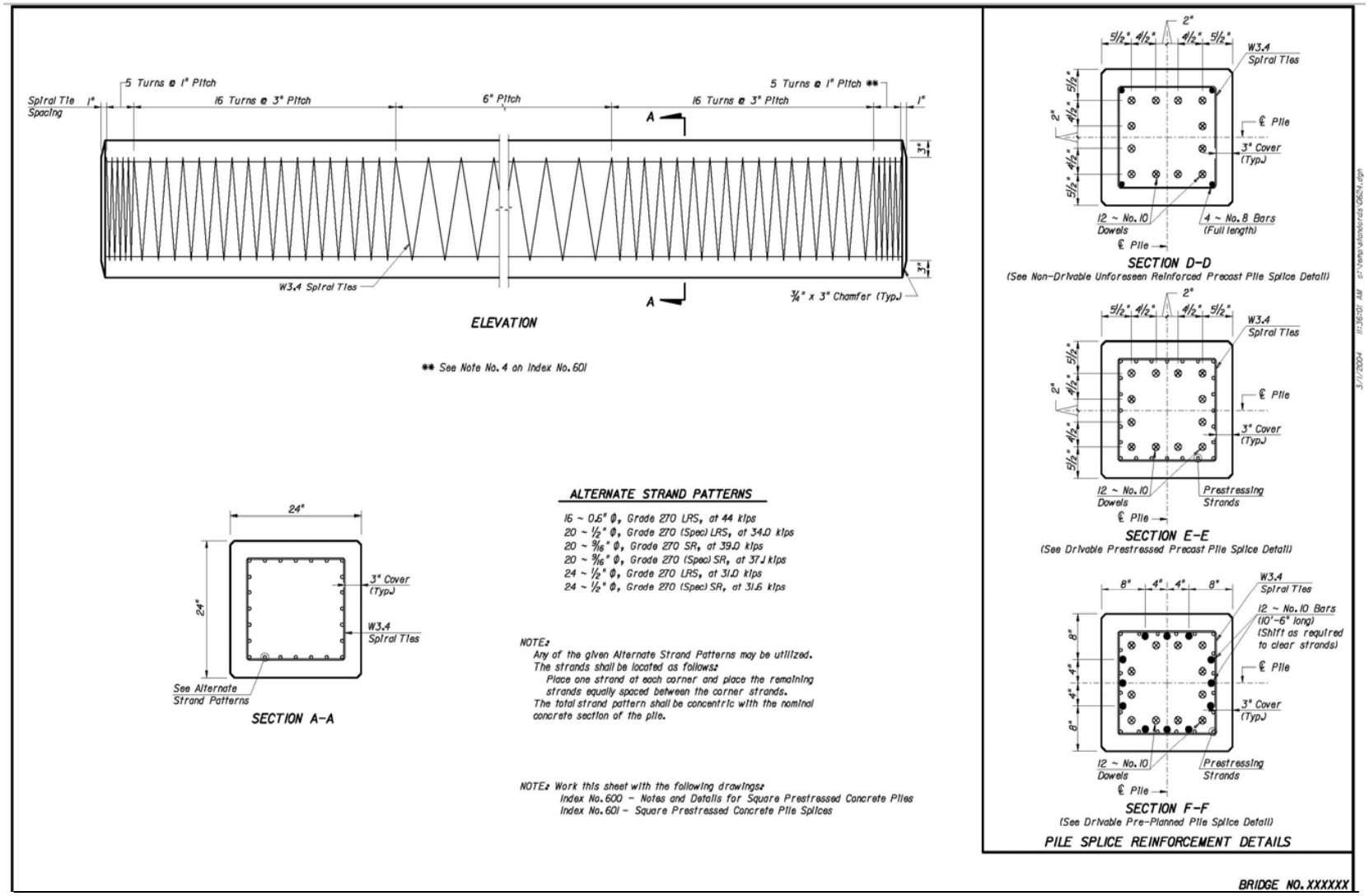

Figure C.8 Details of 24 inch Square Prestressed Concrete Piles (Florida-DOTD 2004)

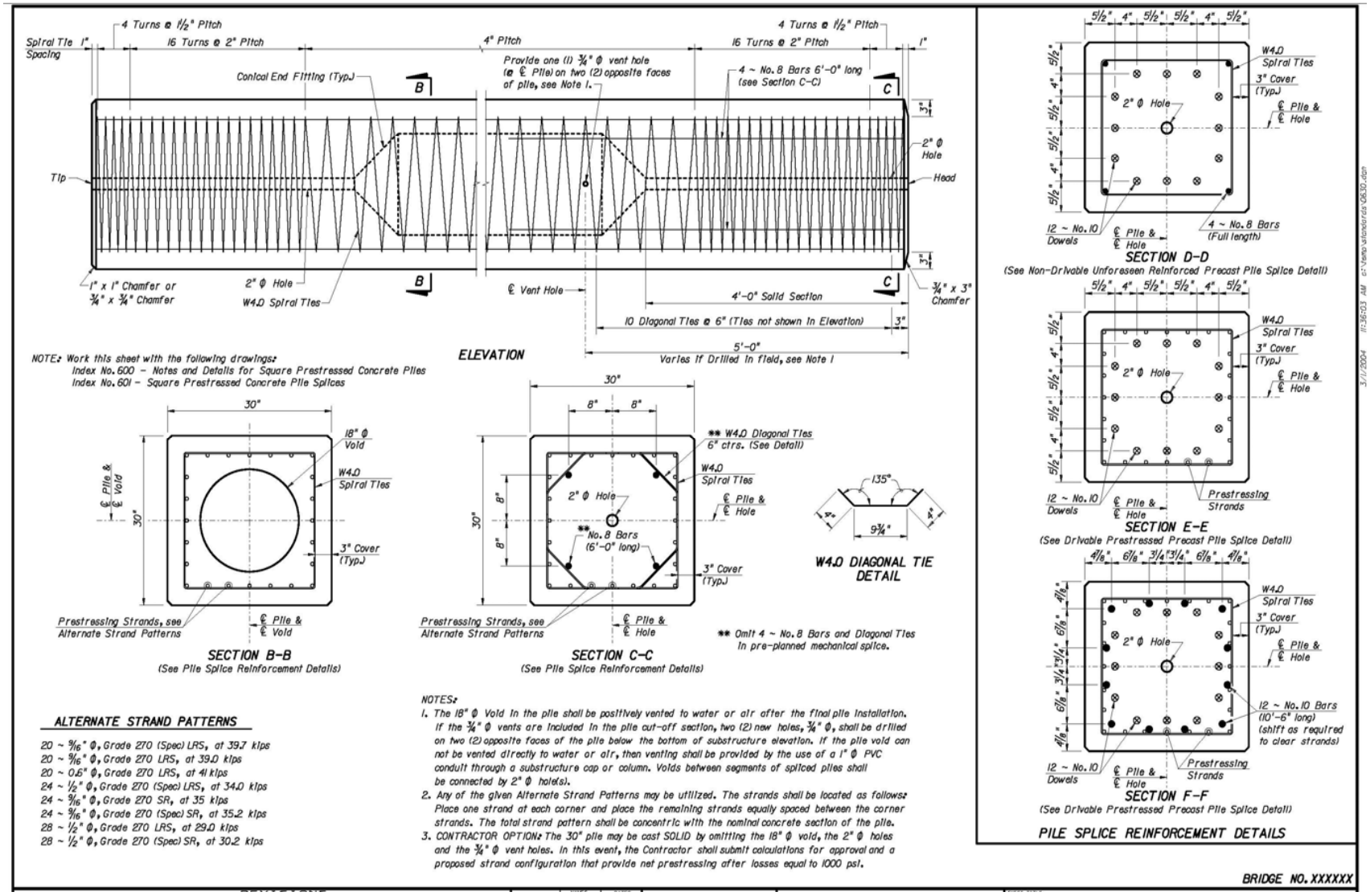

Figure C.9 Details of 30 inch Square Prestressed Concrete Piles (Florida-DOTD 2004)

APPENDIX D. EXTRACTED AND REDUCED RESULTS FROM SAP2000 FE ANALYSES

Moments and axial loads for the critical piles extracted from SAP 2000 FE analysis are presented in the following tables. The tables also contain the moment capacities of the critical piles determined using Prestressed Concrete Pile Interaction Diagram (PCI 2004) and the computed capacity utilization.

Table D.1 Data extracted and calculated for bridges with 0 deg. skew angle and piles with RPC connection at 55 mph wind velocity (Strength V Limit State)

Bridge Span (ft)	Un-supported Pile Length, $L_{P,}$ (ft)	Wind Direction	Live Load case and Vehicle position	Pile #	Location	Results from FE analysis (SAP2000)				From I.D.	Capacity Utilization (%)
						Axial Load P (k)	Moment $M_{u,33}$ (k-ft)	Moment $M_{u,22}$ (k-ft)	$M_{u,cr}$ (k-ft)	Factored Moment Capacity ϕM_n (k-ft)	
30 ft	18	→	2lane left	1	Top	-134	-2	25	25	211	12
	24	→	2lane left	1	Top	-134	31	2	31	205	15
	30	→	2lane left	1	Top	-133	28	2	28	198	14
50 ft	18	←	2lane left	5	Top	-133	4	-17	17	566	3
	24	←	2lane left	5	Top	-132	3	-17	17	560	3
	30	→	2lane left	1	Bottom	-252	-36	-4	37	485	8
	40	→	2lane left	1	Bottom	-253	-48	-3	48	464	10
76 ft	18	→	3lane left	3	Top	-394	3	71	71	891	8
	24	→	3lane left	3	Top	-395	3	75	76	881	9
	30	→	3lane left	3	Top	-386	-3	97	97	864	11
	40	→	3lane left	3	Top	-394	-104	-3	104	788	13
	50	→	3lane left	3	Top	-394	-121	-2	121	725	17
100 ft	30	→	3lane left	3	Top	-561	-4	112	112	1414	8
	40	→	3lane left	3	Top	-573	-132	-3	132	1380	10
	50	→	3lane left	3	Top	-577	-160	-2	160	1328	12
	60	→	3lane left	3	Top	-581	-191	-1	191	1265	15

Table D.2 Data extracted and calculated for bridges with 0 deg. skew angle and piles with HPC connection at 55 mph wind velocity (Strength V Limit State)

Bridge Span (ft)	Un-supported Pile Length, $L_{P,}$ (ft)	Wind Direction	Live Load case and Vehicle position	Pile #	Results from FE analysis (SAP2000)				From I.D.	Capacity Utilization (%)
					Axial Load P (k)	Moment $M_{u,33}$ (k-ft)	Moment $M_{u,22}$ (k-ft)	$M_{u,cr}$ (k-ft)	Factored Moment Capacity ϕM_n (k-ft)	
30 ft	18	→	2lane left	1	-146	-1	-10	10	205	5
	24	→	2lane left	1	-147	-23	0	23	195	12
	30	→	2lane left	1	-148	-26	0	26	182	14
50 ft	18	→	2lane left	1	-246	4	-18	18	494	4
	24	→	2lane left	1	-251	4	-23	24	482	5
	30	→	2lane left	1	-247	-53	-6	53	463	11
	40	→	2lane left	1	-243	-63	-6	63	425	15
76 ft	18	→	3lane left	3	-401	0	-49	49	883	6
	24	→	3lane left	3	-408	-2	-62	62	866	7
	30	→	3lane left	3	-399	-6	-81	81	840	10
	40	→	3lane left	1	-494	-175	2	175	808	22
	50	→	3lane left	1	-501	-203	-1	203	741	27
100 ft	30	→	3lane left	3	-590	-9	-107	107	1388	8
	40	→	3lane left	1	-697	-227	1	227	1369	17
	50	→	3lane left	1	-711	-287	-3	287	1273	23
	60	→	3lane left	1	-725	-349	-5	349	1156	30

Table D.3 Data extracted and calculated for bridges with 30 deg. skew angle and piles with RPC connection at 55 mph wind velocity (Strength V Limit State)

Bridge Span (ft)	Un-supported Pile Length, L_P, (ft)	Wind Direction	Live Load case and Vehicle position	Pile #	Location	Results from FE analysis (SAP2000)				From I.D.	Capacity Utilization (%)
						Axial Load P (k)	Moment $M_{u,33}$ (k-ft)	Moment $M_{u,22}$ (k-ft)	$M_{u,cr}$ (k-ft)	Factored Moment Capacity ϕM_n (k-ft)	
30 ft	18	→	2lane left	1	Top	-129	-13	26	29	214	13
	24	→	2lane left	1	Top	-129	36	0	36	208	18
	30	→	2lane left	1	Top	-129	33	0	33	201	17
50 ft	18	←	2lane left	5	Top	-150	27	-56	62	560	11
	24	←	2lane left	5	Top	-149	26	-59	64	553	12
	30	→	2lane left	1	Top	-218	69	-2	69	504	14
	40	→	2lane left	1	Bottom	-248	-71	5	71	463	15
76 ft	18	→	3lane left	3	Top	-382	-44	61	75	887	8
	24	←	3lane left	1	Bottom	-483	-19	77	79	905	9
	30	←	3lane left	1	Bottom	-489	-18	83	85	892	9
	40	→	3lane left	2	Top	-532	-55	88	104	868	12
	50	→	3lane left	2	Top	-532	-62	106	122	827	15
100 ft	30	←	3lane left	1	Bottom	-681	-81	118	143	1486	10
	40	→	3lane left	1	Bottom	-687	-122	91	153	1443	11
	50	→	3lane left	1	Bottom	-699	-155	89	179	1391	13
	60	→	3lane left	1	Bottom	-712	-187	96	211	1325	16

Table D.4 Data extracted and calculated for bridges with 30 deg. skew angle and piles with HPC connection at 55 mph wind velocity (Strength V Limit State)

Bridge Span (ft)	Un-supported Pile Length, $L_{P,}$ (ft))	Wind Direction	Live Load case and Vehicle position	Pile #	Results from FE analysis (SAP2000)				From I.D.	Capacity Utilization (%)
					Axial Load P (k)	Moment $M_{u,33}$ (k-ft)	Moment $M_{u,22}$ (k-ft)	$M_{u,cr}$ (k-ft)	Factored Moment Capacity ϕM_n (k-ft)	
30 ft	18	→	2lane left	1	-142	1	-10	10	204	5
	24	→	2lane left	1	-143	-25	-3	26	194	13
	30	→	2lane left	1	-144	-31	1	31	182	17
50 ft	18	→	2lane left	1	-239	1	-21	21	496	4
	24	→	2lane left	1	-244	1	-25	25	480	5
	30	→	2lane left	1	-249	-64	-5	64	463	14
	40	→	2lane left	1	-254	-83	-3	83	426	19
76 ft	18	←	3lane left	1	-472	-10	63	64	903	7
	24	←	3lane left	1	-477	-6	71	71	884	8
	30	←	3lane left	3	-395	6	84	84	839	10
	40	→	3lane left	1	-491	-183	2	183	808	23
	50	→	3lane left	1	-499	-230	6	230	741	31
100 ft	30	←	3lane left	3	-575	4	165	165	1382	12
	40	→	3lane left	1	-686	-223	7	223	1363	16
	50	→	3lane left	3	-699	-298	11	298	1268	24
	60	→	3lane left	1	-712	-370	24	370	1152	32

Table D.5 Data extracted and calculated for bridges with 45 deg. skew angle and piles with RPC connection at 55 mph wind velocity (Strength V Limit State)

Bridge Span (ft)	Un-supported Pile Length, L_P, (ft)	Wind Direction	Live Load case and Vehicle position	Pile #	Location	Results from FE analysis (SAP2000)				From I.D.	Capacity Utilization (%)
						Axial Load P (k)	Moment $M_{u,33}$ (k-ft)	Moment $M_{u,22}$ (k-ft)	$M_{u,cr}$ (k-ft)	Factored Moment Capacity ϕM_n (k-ft)	
30 ft	18	→	2lane left	1	Top	-126	-18	39	43	216	20
	24	→	2lane left	1	Top	-126	45	-13	47	210	22
	30	→	2lane left	1	Top	-127	42	-12	44	203	22
50 ft	18	←	2lane left	5	Top	-133	54	-63	83	566	15
	24	←	2lane left	5	Top	-134	49	-59	77	559	14
	30	→	2lane left	1	Top	-201	83	-6	83	516	16
	40	→	2lane left	1	Bottom	-230	-86	23	89	472	19
76 ft	18	→	3lane left	1	Top	-456	65	-49	82	910	9
	24	←	3lane left	1	Top	-462	68	-55	87	900	10
	30	←	3lane left	1	Top	-463	66	-57	87	886	10
	40	→	3lane left	2	Top	-531	-92	99	135	868	16
	50	→	3lane left	2	Top	-531	-118	125	172	827	21
100 ft	30	←	3lane left	1	Bottom	-660	-28	113	117	1474	8
	40	→	3lane left	2	Bottom	-753	55	-133	144	1476	10
	50	→	3lane left	1	Bottom	-667	-128	70	146	1375	11
	60	→	3lane left	2	Bottom	-768	65	-173	185	1349	14

Table D.6 Data extracted and calculated for bridges with 45 deg. skew angle and piles with HPC connection at 55 mph wind velocity (Strength V Limit State)

Bridge Span (ft)	Un-supported Pile Length, $L_{P,}$ (ft)	Wind Direction	Live Load case and Vehicle position	Pile #	Results from FE analysis (SAP2000)				From I.D.	Capacity Utilization (%)
					Axial Load P (k)	Moment $M_{u,33}$ (k-ft)	Moment $M_{u,22}$ (k-ft)	$M_{u,cr}$ (k-ft)	Factored Moment Capacity ϕM_n (k-ft)	
30 ft	18	→	2lane left	1	-140	1	-10	10	204	5
	24	→	2lane left	1	-143	-26	0	26	194	13
	30	→	2lane left	1	-144	-31	1	31	182	17
50 ft	18	→	2lane left	1	-223	4	-25	26	510	5
	24	→	2lane left	1	-228	3	-26	26	492	5
	30	→	2lane left	1	-233	-70	-1	70	470	15
	40	→	2lane left	1	-239	-95	11	96	428	22
76 ft	18	←	3lane left	3	-376	7	59	59	874	7
	24	←	3lane left	3	-381	5	68	68	858	8
	30	←	3lane left	3	-385	6	88	88	836	11
	40	→	3lane left	1	-480	-174	24	176	806	22
	50	→	3lane left	1	-484	-242	7	242	739	33
100 ft	30	→	3lane left	3	-590	-9	-108	108	1388	8
	40	→	3lane left	1	-697	-228	1	228	1369	17
	50	→	3lane left	1	-711	-288	-3	288	1273	23
	60	→	3lane left	1	-725	-351	-5	351	1156	30

Table D.7 Data extracted and calculated for bridges with 60 deg. skew angle and piles with RPC connection at 55 mph wind velocity (Strength V Limit State)

Bridge Span (ft)	Un-supported Pile Length, L_P, (ft)	Wind Direction	Live Load case and Vehicle position	Pile #	Location	Results from FE analysis (SAP2000)				From I.D.	Capacity Utilization (%)
						Axial Load P (k)	Moment $M_{u,33}$ (k-ft)	Moment $M_{u,22}$ (k-ft)	$M_{u,cr}$ (k-ft)	Factored Moment Capacity ϕM_n (k-ft)	
30 ft	18	←	2lane left	1	Top	-122	-60	46	76	219	35
	24	←	2lane left	1	Top	-123	75	-8	75	212	35
	30	←	2lane left	1	Top	-124	66	-8	67	204	33
50 ft	18	←	2lane left	5	Top	-135	95	-74	121	565	21
	24	←	2lane left	5	Top	-134	49	-59	77	559	14
	30	←	2lane left	1	Top	-202	120	-18	121	515	24
	40	←	2lane left	1	Top	-204	109	-17	110	493	22
76 ft	18	→	3lane left	1	Top	-456	151	-47	158	910	17
	24	→	3lane left	1	Top	-456	143	-42	149	898	17
	30	→	3lane left	1	Top	-461	134	-39	140	885	16
	40	→	3lane left	2	Top	-521	-134	79	155	866	18
	50	→	3lane left	2	Top	-521	-141	86	165	826	20
100 ft	30	←	3lane left	3	Bottom	-589	28	162	164	1433	11
	40	←	3lane left	3	Bottom	-608	-72	179	193	1400	14
	50	←	3lane left	3	Bottom	-622	-63	222	231	1352	17
	60	←	3lane left	3	Bottom	-554	8	257	257	1253	21

Table D.8 Data extracted and calculated for bridges with 60 deg. skew angle and piles with HPC connection at 55 mph wind velocity (Strength V Limit State)

Bridge Span (ft)	Un-supported Pile Length, $L_{P,}$ (ft)	Wind Direction	Live Load case and Vehicle position	Pile #	Results from FE analysis (SAP2000)				From I.D.	Capacity Utilization (%)
					Axial Load P (k)	Moment $M_{u,33}$ (k-ft)	Moment $M_{u,22}$ (k-ft)	$M_{u,cr}$ (k-ft)	Factored Moment Capacity ϕM_n (k-ft)	
30 ft	18	→	2lane left	1	-134	2	-11	11	205	6
	24	→	2lane left	1	-137	-26	6	27	195	14
	30	→	2lane left	1	-138	-31	7	32	182	18
50 ft	18	→	2lane left	1	-214	2	-27	27	517	5
	24	→	2lane left	1	-228	3	-26	26	492	5
	30	→	2lane left	1	-230	-71	11	71	473	15
	40	→	2lane left	1	-236	-89	15	91	430	21
76 ft	18	←	3lane left	3	-384	12	76	77	877	9
	24	←	3lane left	3	-387	11	91	92	860	11
	30	←	3lane left	3	-390	11	108	109	838	13
	40	→	3lane left	1	-480	-171	40	175	806	22
	50	→	3lane left	1	-485	-212	55	219	739	30
100 ft	30	←	3lane left	3	-585	20	166	167	1313	13
	40	→	3lane left	1	-688	-241	57	247	1364	18
	50	→	3lane left	1	-701	-297	90	310	1269	24
	60	→	3lane left	1	-633	-279	112	300	1124	27

Table D.9 Data extracted and calculated for bridges with 0 deg. skew angle and piles with RPC connection at 60 mph wind velocity (Strength III Limit State)

Bridge Span (ft)	Un-supported Pile Length, L_P, (ft)	Wind Direction From	Live Load case and Vehicle position	Pile #	Location	Results from FE analysis (SAP2000)				From I.D.	Capacity Utilization (%)
						Axial Load P (k)	Moment $M_{u,33}$ (k-ft)	Moment $M_{u,22}$ (k-ft)	$M_{u,cr}$ (k-ft)	Factored Moment Capacity ϕM_n (k-ft)	
30 ft	18	→	2lane left	1	Top	-83	-1	25	25	239	11
	24	→	2lane left	1	Top	-83	28	0	28	235	12
	30	←	2lane left	6	Bottom	-95	-28	0	28	225	12
50 ft	18	→	2lane left	1	Top	-137	4	24	24	567	4
	24	→	2lane left	1	Bottom	-154	3	-26	27	555	5
	30	→	2lane left	1	Bottom	-157	-38	-2	38	548	7
	40	→	2lane left	1	Bottom	-157	-51	-1	51	533	10
76 ft	18	→	3lane left	1	Top	-345	10	-55	56	868	6
	24	→	3lane left	1	Bottom	-349	8	-67	68	859	8
	30	→	3lane left	1	Bottom	-345	0	-112	112	845	13
	40	→	3lane left	1	Bottom	-354	-154	1	154	819	19
	50	→	3lane left	1	Bottom	-360	-178	1	178	786	23
100 ft	30	→	3lane left	1	Bottom	-513	3	-131	131	1369	10
	40	→	3lane left	1	Bottom	-528	-188	-1	188	1335	14
	50	→	3lane left	1	Bottom	-540	-227	-1	227	1289	18
	60	→	3lane left	1	Bottom	-552	-270	0	270	1231	22

Table D.10 Data extracted and calculated for bridges with 0 deg. skew angle and piles with HPC connection at 60 mph wind velocity (Strength III Limit State)

Bridge Span (ft)	Un-supported Pile Length, $L_{P,}$ (ft)	Wind Direction	Live Load case and Vehicle position	Pile #	Results from FE analysis (SAP2000)				From I.D.	Capacity Utilization (%)
					Axial Load P (k)	Moment $M_{u,33}$ (k-ft)	Moment $M_{u,22}$ (k-ft)	$M_{u,cr}$ (k-ft)	Factored Moment Capacity ϕM_n (k-ft)	
30 ft	18	→	2lane left	1	-96	0	-17	17	228	8
	24	→	2lane left	1	-96	-24	0	24	223	11
	30	←	2lane left	6	-95	-30	0	30	214	14
50 ft	18	→	2lane left	1	-154	4	-31	32	553	6
	24	→	2lane left	1	-159	3	-42	42	538	8
	30	→	2lane left	1	-153	-52	-2	52	537	10
	40	→	2lane left	1	-147	-65	-1	65	519	13
76 ft	18	→	3lane left	1	-350	10	-84	85	863	10
	24	→	3lane left	1	-355	9	-111	112	847	13
	30	→	3lane left	1	-354	0	-146	146	824	18
	40	→	3lane left	1	-366	-216	0	216	779	28
	50	→	3lane left	1	-372	-272	0	272	720	38
100 ft	30	→	3lane left	1	-524	3	-206	206	1348	15
	40	→	3lane left	1	-542	-309	-2	309	1286	24
	50	→	3lane left	1	-554	-398	-2	398	1201	33
	60	→	3lane left	1	-566	-492	-1	492	1096	45

Table D.11 Data extracted and calculated for bridges with 30 deg. skew angle and piles with RPC connection at 60 mph wind velocity (Strength III Limit State)

Bridge Span (ft)	Un-supported Pile Length, L_P, (ft)	Wind Direction	Live Load case and Vehicle position	Pile #	Location	Results from FE analysis (SAP2000)				From I.D.	Capacity Utilization (%)
						Axial Load P (k)	Moment $M_{u,33}$ (k-ft)	Moment $M_{u,22}$ (k-ft)	$M_{u,cr}$ (k-ft)	Factored Moment Capacity ϕM_n (k-ft)	
30 ft	18	←	2lane left	6	Top	-82	10	-25	27	239	11
	24	←	2lane left	6	Top	-82	28	-4	29	235	12
	30	←	2lane left	6	Bottom	-94	-26	11	28	225	13
50 ft	18	→	2lane left	1	Top	-147	-28	57	64	563	11
	24	←	2lane left	5	Top	-149	24	-57	62	557	11
	30	←	2lane left	5	Top	-149	67	-8	68	549	12
	40	←	2lane left	5	Bottom	-180	-69	31	76	516	15
76 ft	18	←	3lane left	3	Top	-339	5	116	116	868	13
	24	←	3lane left	3	Bottom	-341	7	114	115	858	13
	30	←	3lane left	3	Bottom	-346	11	130	130	846	15
	40	←	3lane left	3	Bottom	-355	-146	86	170	821	21
	50	←	3lane left	3	Bottom	-362	-167	107	199	788	25
100 ft	30	←	3lane left	3	Bottom	-509	-46	219	224	1373	16
	40	←	3lane left	3	Bottom	-523	-287	82	299	1339	22
	50	←	3lane left	3	Bottom	-535	-313	131	339	1294	26
	60	←	3lane left	3	Bottom	-548	-346	170	386	1237	31

Table D.12 Data extracted and calculated for bridges with 30 deg. skew angle and piles with HPC connection at 60 mph wind velocity (Strength III Limit State)

Bridge Span (ft)	Un-supported Pile Length, $L_{P,}$ (ft)	Wind Direction	Live Load case and Vehicle position	Pile #	Results from FE analysis (SAP2000)				From I.D.	Capacity Utilization (%)
					Axial Load P (k)	Moment $M_{u,33}$ (k-ft)	Moment $M_{u,22}$ (k-ft)	$M_{u,cr}$ (k-ft)	Factored Moment Capacity ϕM_n (k-ft)	
30 ft	18	→	2lane left	1	-93	-2	-19	19	229	8
	24	←	2lane left	6	-95	-22	12	25	222	11
	30	→	2lane left	1	-98	-26	25	36	207	17
50 ft	18	←	2lane left	5	-171	0	35	35	546	6
	24	←	2lane left	5	-176	1	45	46	531	9
	30	←	2lane left	5	-181	-58	27	64	514	13
	40	←	2lane left	5	-186	-79	40	88	478	18
76 ft	18	←	3lane left	3	-346	3	116	116	863	13
	24	←	3lane left	3	-348	2	126	126	845	15
	30	←	3lane left	3	-353	3	155	155	824	19
	40	←	3lane left	3	-365	-198	98	221	779	28
	50	←	3lane left	3	-372	-252	129	283	720	39
100 ft	30	←	3lane left	3	-524	-2	266	266	1347	20
	40	←	3lane left	3	-543	-325	131	350	1286	27
	50	←	3lane left	3	-553	-344	162	380	1201	32
	60	←	3lane left	3	-569	-465	222	515	1099	47

Table D.13 Data extracted and calculated for bridges with 45 deg. skew angle and piles with RPC connection at 60 mph wind velocity (Strength III Limit State)

Bridge Span (ft)	Un-supported Pile Length, L_P, (ft)	Wind Direction	Live Load case and Vehicle position	Pile #	Location	Results from FE analysis (SAP2000)				From I.D.	Capacity Utilization (%)
						Axial Load P (k)	Moment $M_{u,33}$ (k-ft)	Moment $M_{u,22}$ (k-ft)	$M_{u,cr}$ (k-ft)	Factored Moment Capacity ϕM_n (k-ft)	
30 ft	18	→	2lane left	1	Top	-79	-17	34	38	235	16
	24	→	2lane left	1	Top	-80	32	-13	35	228	15
	30	→	2lane left	1	Bottom	-94	-29	21	36	210	17
50 ft	18	→	2lane left	1	Top	-129	-51	58	77	568	14
	24	→	2lane left	1	Top	-130	-47	56	73	563	13
	30	←	2lane left	5	Top	-134	76	-10	77	554	14
	40	←	2lane left	5	Bottom	-164	-72	45	85	524	16
76 ft	18	←	3lane left	3	Top	-335	4	99	99	866	11
	24	←	3lane left	3	Bottom	-338	3	106	107	856	12
	30	←	3lane left	3	Bottom	-340	9	127	127	844	15
	40	←	3lane left	3	Bottom	-347	-115	120	167	818	20
	50	→	3lane left	3	Bottom	-348	-137	125	185	784	24
100 ft	30	←	3lane left	3	Bottom	-500	14	222	222	1394	16
	40	←	3lane left	3	Bottom	-509	-196	189	272	1382	20
	50	←	3lane left	3	Bottom	-516	-212	228	312	1347	23
	60	←	3lane left	3	Bottom	-524	-232	266	353	1300	27

Table D.14 Data extracted and calculated for bridges with 45 deg. skew angle and piles with HPC connection at 60 mph wind velocity (Strength III Limit State)

Bridge Span (ft)	Un-supported Pile Length, $L_{P,}$ (ft)	Wind Direction	Live Load case and Vehicle position	Pile #	Results from FE analysis (SAP2000)				From I.D.	Capacity Utilization (%)
					Axial Load P (k)	Moment $M_{u,33}$ (k-ft)	Moment $M_{u,22}$ (k-ft)	$M_{u,cr}$ (k-ft)	Factored Moment Capacity ϕM_n (k-ft)	
30 ft	18	→	2lane left	1	-93	0	-20	20	225	9
	24	→	2lane left	1	-95	-20	20	28	212	13
	30	→	2lane left	1	-98	-27	25	37	194	19
50 ft	18	→	2lane left	1	-152	2	-40	40	554	7
	24	←	2lane left	5	-161	0	46	46	538	9
	30	←	2lane left	5	-166	-53	43	68	521	13
	40	←	2lane left	5	-173	-73	58	94	484	19
76 ft	18	←	3lane left	3	-339	2	104	104	859	12
	24	←	3lane left	3	-344	3	128	128	843	15
	30	←	3lane left	3	-348	5	163	163	822	20
	40	←	3lane left	3	-356	-165	152	224	777	29
	50	←	3lane left	3	-361	-192	219	292	718	41
100 ft	30	→	3lane left	1	-524	3	-210	210	1348	16
	40	→	3lane left	1	-542	-315	-2	315	1286	24
	50	→	3lane left	1	-554	-405	-2	405	1201	34
	60	→	3lane left	1	-566	-500	-1	500	1096	46

Table D.15 Data extracted and calculated for bridges with 60 deg. skew angle and piles with RPC connection at 60 mph wind velocity (Strength III Limit State)

Bridge Span (ft)	Un-supported Pile Length, L_P, (ft)	Wind Direction	Live Load case and Vehicle position	Pile #	Location	Results from FE analysis (SAP2000)				From I.D.	Capacity Utilization (%)
						Axial Load P (k)	Moment $M_{u,33}$ (k-ft)	Moment $M_{u,22}$ (k-ft)	$M_{u,cr}$ (k-ft)	Factored Moment Capacity ϕM_n (k-ft)	
30 ft	18	→	2lane left	1	Top	-79	-52	36	64	239	27
	24	←	2lane left	6	Top	-85	57	-12	58	233	25
	30	←	2lane left	6	Top	-85	49	-13	51	227	22
50 ft	18	→	2lane left	1	Top	-130	-86	64	107	567	19
	24	→	2lane left	1	Top	-130	-47	56	73	562	13
	30	←	2lane left	5	Top	-138	120	-18	121	551	22
	40	←	2lane left	5	Bottom	-168	-89	65	110	518	21
76 ft	18	←	3lane left	3	Top	-343	-7	127	127	870	15
	24	←	3lane left	3	Bottom	-346	1	155	155	861	18
	30	←	3lane left	3	Bottom	-349	9	178	178	850	21
	40	←	3lane left	3	Bottom	-356	-117	186	219	824	27
	50	←	3lane left	3	Bottom	-360	-124	222	254	790	32
100 ft	30	←	3lane left	3	Bottom	-528	-14	300	300	1391	22
	40	←	3lane left	3	Bottom	-543	-270	287	394	1358	29
	50	←	3lane left	3	Bottom	-555	-295	368	472	1312	36
	60	←	3lane left	3	Bottom	-487	-249	433	500	1215	41

Table D.16 Data extracted and calculated for bridges with 60 deg. skew angle and piles with HPC connection at 60 mph wind velocity (Strength III Limit State)

Bridge Span (ft)	Un-supported Pile Length, $L_{P,}$ (ft)	Wind Direction	Live Load case and Vehicle position	Pile #	Results from FE analysis (SAP2000)				From I.D.	Capacity Utilization (%)
					Axial Load P (k)	Moment $M_{u,33}$ (k-ft)	Moment $M_{u,22}$ (k-ft)	$M_{u,cr}$ (k-ft)	Factored Moment Capacity ϕM_n (k-ft)	
30 ft	18	←	2lane left	6	-98	1	25	25	227	11
	24	←	2lane left	6	-101	-21	28	35	217	16
	30	←	2lane left	6	-103	-24	34	42	204	21
50 ft	18	←	2lane left	5	-159	-2	48	48	551	9
	24	←	2lane left	5	-161	0	45	45	537	8
	30	←	2lane left	5	-171	-53	58	79	516	15
	40	←	2lane left	5	-178	-68	80	105	478	22
76 ft	18	←	3lane left	3	-347	4	123	123	862	14
	24	←	3lane left	3	-350	8	154	154	846	18
	30	←	3lane left	3	-353	10	189	189	825	23
	40	←	3lane left	3	-361	-137	210	251	779	32
	50	←	3lane left	3	-366	-168	264	313	719	44
100 ft	30	←	3lane left	3	-535	6	287	287	1355	21
	40	←	3lane left	3	-552	-241	277	367	1293	28
	50	←	3lane left	3	-565	-293	364	467	1208	39
	60	←	3lane left	3	-497	-271	441	518	1077	48

Table D.17 Data extracted and calculated for bridges with 0 deg. skew angle and piles with RPC connection at 100 mph wind velocity (Strength III Limit State)

Bridge Span (ft)	Un-supported Pile Length, L_P, (ft)	Wind Direction	Live Load case and Vehicle position	Pile #	Location	Results from FE analysis (SAP2000)				From I.D.	Capacity Utilization (%)
						Axial Load P (k)	Moment $M_{u,33}$ (k-ft)	Moment $M_{u,22}$ (k-ft)	$M_{u,cr}$ (k-ft)	Factored Moment Capacity ϕM_n (k-ft)	
30 ft	18	→	2lane left	1	Top	-77	-1	35	35	239	15
	24	→	2lane left	1	Bottom	-83	-44	0	44	232	19
	30	←	2lane left	6	Bottom	-84	-53	-1	53	225	24
50 ft	18	→	2lane left	1	Bottom	-142	4	-52	52	563	9
	24	→	2lane left	1	Bottom	-145	3	-66	66	555	12
	30	→	2lane left	1	Bottom	-140	-82	-2	82	548	15
	40	→	2lane left	1	Bottom	-133	-109	-1	109	533	21
76 ft	18	→	3lane left	2	Bottom	-356	0	-149	149	877	17
	24	→	3lane left	2	Bottom	-360	9	-185	186	869	21
	30	→	3lane left	2	Bottom	-362	0	-302	302	856	35
	40	→	3lane left	1	Bottom	-335	-333	1	333	819	41
	50	→	3lane left	1	Bottom	-336	-405	2	405	786	52
100 ft	30	→	3lane left	2	Bottom	-534	3	-365	365	1398	26
	40	→	3lane left	1	Bottom	-498	-428	0	428	1335	32
	50	→	3lane left	1	Bottom	-504	-519	1	519	1289	40
	60	→	3lane left	1	Bottom	-510	-613	2	613	1231	50

Table D.18 Data extracted and calculated for bridges with 0 deg. skew angle and piles with HPC connection at 100 mph wind velocity (Strength III Limit State)

Bridge Span (ft)	Un-supported Pile Length, $L_{P,}$ (ft)	Wind Direction	Live Load case and Vehicle position	Pile #	Results from FE analysis (SAP2000)				From I.D.	Capacity Utilization (%)
					Axial Load P (k)	Moment $M_{u,33}$ (k-ft)	Moment $M_{u,22}$ (k-ft)	$M_{u,cr}$ (k-ft)	Factored Moment Capacity ϕM_n (k-ft)	
30 ft	18	→	2lane left	1	-92	0	-47	47	228	21
	24	→	2lane left	1	-85	-60	1	60	223	27
	30	←	2lane left	6	-80	-72	-1	72	214	34
50 ft	18	→	2lane left	1	-150	4	-88	88	553	16
	24	→	2lane left	1	-155	3	-118	118	538	22
	30	→	2lane left	1	-127	-125	-1	125	537	23
	40	→	2lane left	1	-107	-149	1	149	519	29
76 ft	18	→	3lane left	1	-345	10	-235	236	863	27
	24	→	3lane left	1	-350	9	-313	313	847	37
	30	→	3lane left	1	-348	-1	-408	408	824	49
	40	→	3lane left	1	-357	-558	0	558	779	72
	50	→	3lane left	1	-363	-712	-1	712	720	99
100 ft	30	→	3lane left	1	-517	2	-579	579	1348	43
	40	→	3lane left	1	-532	-798	-2	798	1286	62
	50	→	3lane left	1	-542	-1016	-1	1016	1201	85
	60	→	3lane left	1	-551	-1240	-1	1240	1096	113

Table D.19 Data extracted and calculated for bridges with 30 deg. skew angle and piles with RPC connection at 100mph wind velocity (Strength III Limit State)

Bridge Span (ft)	Un-supported Pile Length, L_P, (ft)	Wind Direction	Live Load case and Vehicle position	Pile #	Location	Results from FE analysis (SAP2000)				From I.D.	Capacity Utilization (%)
						Axial Load P (k)	Moment $M_{u,33}$ (k-ft)	Moment $M_{u,22}$ (k-ft)	$M_{u,cr}$ (k-ft)	Factored Moment Capacity ϕM_n (k-ft)	
30 ft	18	←	2lane left	6	Bottom	-83	4	37	37	237	16
	24	←	2lane left	6	Bottom	-84	-39	26	47	232	20
	30	←	2lane left	6	Bottom	-85	-45	32	55	225	25
50 ft	18	←	2lane left	5	Bottom	-154	7	78	79	558	14
	24	←	2lane left	5	Bottom	-158	11	94	95	549	17
	30	←	2lane left	5	Bottom	-160	-96	67	117	539	22
	40	←	2lane left	5	Bottom	-166	-117	89	147	516	29
76 ft	18	←	3lane left	3	Bottom	-333	37	268	270	868	31
	24	←	3lane left	2	Bottom	-359	22	277	278	868	32
	30	←	3lane left	2	Bottom	-364	29	324	325	857	38
	40	←	3lane left	3	Bottom	-339	-292	247	383	821	47
	50	←	3lane left	3	Bottom	-343	-343	305	459	788	58
100 ft	30	←	3lane left	2	Bottom	-539	-11	545	545	1401	39
	40	←	3lane left	3	Bottom	-504	-530	351	636	1339	48
	50	←	3lane left	3	Bottom	-512	-598	457	752	1294	58
	60	←	3lane left	3	Bottom	-521	-667	557	869	1237	70

Table D.20 Data extracted and calculated for bridges with 30 deg. skew angle and piles with HPC connection at 100mph wind velocity (Strength III Limit State)

Bridge Span (ft)	Un-supported Pile Length, $L_{P,}$ (ft)	Wind Direction	Live Load case and Vehicle position	Pile #	Results from FE analysis (SAP2000)				From I.D.	Capacity Utilization (%)
					Axial Load P (k)	Moment $M_{u,33}$ (k-ft)	Moment $M_{u,22}$ (k-ft)	$M_{u,cr}$ (k-ft)	Factored Moment Capacity ϕM_n (k-ft)	
30 ft	18	←	2lane left	6	-90	4	53	53	229	23
	24	←	2lane left	6	-87	-54	38	66	222	30
	30	→	2lane left	1	-93	-61	73	95	207	46
50 ft	18	←	2lane left	5	-166	4	95	95	546	17
	24	←	2lane left	5	-170	5	128	128	531	24
	30	←	2lane left	5	-171	-139	85	163	514	32
	40	←	2lane left	5	-172	-185	119	220	478	46
76 ft	18	←	3lane left	3	-345	16	309	309	863	36
	24	←	3lane left	3	-343	7	344	344	845	41
	30	←	3lane left	3	-348	10	428	428	824	52
	40	←	3lane left	3	-357	-505	294	584	779	75
	50	←	3lane left	3	-364	-641	378	745	720	103
100 ft	30	←	3lane left	3	-516	4	663	663	1347	49
	40	←	3lane left	3	-533	-763	411	867	1286	67
	50	←	3lane left	3	-542	-859	483	985	1201	82
	60	←	3lane left	3	-557	-1141	645	1311	1099	119

Table D.21 Data extracted and calculated for bridges with 45 deg. skew angle and piles with RPC connection at 100 mph wind velocity (Strength III Limit State)

Bridge Span (ft)	Un-supported Pile Length, L_P, (ft)	Wind Direction	Live Load case and Vehicle position	Pile #	Location	Results from FE analysis (SAP2000)				From I.D.	Capacity Utilization (%)
						Axial Load P (k)	Moment $M_{u,33}$ (k-ft)	Moment $M_{u,22}$ (k-ft)	$M_{u,cr}$ (k-ft)	Factored Moment Capacity ϕM_n (k-ft)	
30 ft	18	→	2lane left	1	Bottom	-81	-2	-46	46	233	20
	24	→	2lane left	1	Bottom	-83	-36	42	56	223	25
	30	→	2lane left	1	Bottom	-88	-47	59	76	210	36
50 ft	18	←	2lane left	5	Bottom	-140	2	92	92	564	16
	24	←	2lane left	5	Bottom	-143	10	115	116	556	21
	30	←	2lane left	5	Bottom	-147	-90	99	134	545	25
	40	←	2lane left	5	Bottom	-151	-116	149	189	524	36
76 ft	18	←	3lane left	3	Bottom	-328	35	223	226	866	26
	24	←	3lane left	3	Bottom	-328	52	276	281	856	33
	30	←	3lane left	3	Bottom	-328	67	336	343	844	41
	40	←	3lane left	3	Bottom	-330	-237	367	437	818	53
	50	←	3lane left	2	Bottom	-365	123	500	515	794	65
100 ft	30	←	3lane left	3	Bottom	-486	87	522	529	1367	39
	40	←	3lane left	3	Bottom	-491	-361	521	634	1332	48
	50	←	3lane left	3	Bottom	-495	-406	630	749	1284	58
	60	←	3lane left	3	Bottom	-499	-451	735	863	1226	70

Table D.22 Data extracted and calculated for bridges with 45 deg. skew angle and piles with HPC connection at 100 mph wind velocity (Strength III Limit State)

Bridge Span (ft)	Un-supported Pile Length, L_P, (ft)	Wind Direction	Live Load case and Vehicle position	Pile #	Results from FE analysis (SAP2000)				From I.D.	Capacity Utilization (%)
					Axial Load P (k)	Moment $M_{u,33}$ (k-ft)	Moment $M_{u,22}$ (k-ft)	$M_{u,cr}$ (k-ft)	Factored Moment Capacity ϕM_n (k-ft)	
30 ft	18	→	2lane left	1	-89	-4	-55	56	225	25
	24	→	2lane left	1	-88	-48	57	74	212	35
	30	→	2lane left	1	-93	-62	74	97	194	50
50 ft	18	←	2lane left	5	-151	1	104	104	552	19
	24	←	2lane left	5	-156	7	139	139	538	26
	30	←	2lane left	5	-158	-125	130	180	521	35
	40	←	2lane left	5	-162	-169	182	248	484	51
76 ft	18	←	3lane left	3	-334	9	276	277	859	32
	24	←	3lane left	3	-338	12	361	361	843	43
	30	←	3lane left	3	-342	16	456	456	822	55
	40	←	3lane left	3	-347	-425	447	617	777	79
	50	←	3lane left	3	-351	-541	578	791	718	110
100 ft	30	→	3lane left	1	-517	2	-591	591	1348	44
	40	→	3lane left	1	-531	-814	-2	814	1286	63
	50	→	3lane left	1	-541	-1035	-1	1035	1201	86
	60	→	3lane left	1	-550	-1263	-1	1263	1096	115

Table D.23 Data extracted and calculated for bridges with 60 deg. skew angle and piles with RPC connection at 100 mph wind velocity (Strength III Limit State)

Bridge Span (ft)	Un-supported Pile Length, $L_{P,}$ (ft)	Wind Direction	Live Load case and Vehicle position	Pile #	Location	Results from FE analysis (SAP2000)				From I.D.	Capacity Utilization (%)
						Axial Load P (k)	Moment $M_{u,33}$ (k-ft)	Moment $M_{u,22}$ (k-ft)	$M_{u,cr}$ (k-ft)	Factored Moment Capacity ϕM_n (k-ft)	
30 ft	18	←	2lane left	6	Bottom	-86	-8	62	62	235	27
	24	←	2lane left	6	Bottom	-88	-44	63	77	229	34
	30	←	2lane left	6	Bottom	-91	-45	77	89	221	40
50 ft	18	←	2lane left	5	Bottom	-142	-6	117	117	562	21
	24	←	2lane left	5	Bottom	-143	10	113	113	554	20
	30	←	2lane left	5	Bottom	-153	-102	149	181	541	33
	40	←	2lane left	5	Bottom	-160	-113	196	226	518	44
76 ft	18	←	3lane left	3	Bottom	-337	30	279	281	870	32
	24	←	3lane left	3	Bottom	-339	50	351	355	861	41
	30	←	3lane left	3	Bottom	-340	68	418	423	850	50
	40	←	3lane left	3	Bottom	-344	-187	487	522	824	63
	50	←	3lane left	3	Bottom	-347	-208	588	623	790	79
100 ft	30	←	3lane left	3	Bottom	-520	50	698	700	1391	50
	40	←	3lane left	3	Bottom	-532	-418	761	868	1358	64
	50	←	3lane left	3	Bottom	-542	-481	983	1095	1312	83
	60	←	3lane left	3	Bottom	-471	-459	1166	1253	1215	103

Table D.24 Data extracted and calculated for bridges with 60 deg. skew angle and piles with HPC connection at 100 mph wind velocity (Strength III Limit State)

Bridge Span (ft)	Un-supported Pile Length, $L_{P,}$ (ft)	Wind Direction	Live Load case and Vehicle position	Pile #	Results from FE analysis (SAP2000)				From I.D.	Capacity Utilization (%)
					Axial Load P (k)	Moment $M_{u,33}$ (k-ft)	Moment $M_{u,22}$ (k-ft)	$M_{u,cr}$ (k-ft)	Factored Moment Capacity ϕM_n (k-ft)	
30 ft	18	←	2lane left	6	-93	10	75	76	227	33
	24	←	2lane left	6	-95	-42	91	100	217	46
	30	←	2lane left	6	-96	-49	109	120	204	59
50 ft	18	←	2lane left	5	-153	7	126	127	551	23
	24	←	2lane left	5	-156	7	136	136	537	25
	30	←	2lane left	5	-164	-104	184	211	516	41
	40	←	2lane left	5	-170	-137	249	284	478	60
76 ft	18	←	3lane left	3	-341	15	305	305	862	35
	24	←	3lane left	3	-344	22	404	405	846	48
	30	←	3lane left	3	-347	27	506	507	825	61
	40	←	3lane left	3	-353	-320	596	676	779	87
	50	←	3lane left	3	-357	-396	751	849	719	118
100 ft	30	←	3lane left	3	-527	23	722	723	1355	53
	40	←	3lane left	3	-543	-488	781	921	1293	71
	50	←	3lane left	3	-555	-629	1035	1212	1208	100
	60	←	3lane left	3	-487	-679	1258	1430	1077	133

Table D.25 Data extracted and calculated for bridges with 0 deg. skew angle and piles with RPC connection at 150 mph wind velocity (Strength III Limit State)

Bridge Span (ft)	Un-supported Pile Length, L_P, (ft)	Wind Direction	Live Load case and Vehicle position	Pile #	Location	Results from FE analysis (SAP2000)				From I.D.	Capacity Utilization (%)
						Axial Load P (k)	Moment $M_{u,33}$ (k-ft)	Moment $M_{u,22}$ (k-ft)	$M_{u,cr}$ (k-ft)	Factored Moment Capacity ϕM_n (k-ft)	
30 ft	18	→	2lane left	1	Bottom	-72	0	-63	63	240	26
	24	→	2lane left	1	Bottom	-65	-82	1	82	238	34
	30	←	2lane left	6	Bottom	-62	-102	-1	102	234	44
50 ft	18	→	2lane left	1	Bottom	-126	3	-110	110	568	19
	24	→	2lane left	1	Bottom	-127	3	-144	144	562	26
	30	→	2lane left	1	Bottom	-107	-169	-1	169	561	30
	40	→	2lane left	5	Top	-213	-199	-1	199	486	41
76 ft	18	→	3lane left	2	Bottom	-364	0	-337	337	880	38
	24	→	3lane left	2	Bottom	-368	9	-418	418	871	48
	30	→	3lane left	2	Bottom	-368	0	-681	681	858	79
	40	→	3lane left	2	Bottom	-373	0	-743	743	832	89
	50	→	3lane left	2	Bottom	-380	0	-896	896	798	112
100 ft	30	→	3lane left	2	Bottom	-543	3	-825	825	1404	59
	40	→	3lane left	2	Top	-497	3	930	930	1335	70
	50	→	3lane left	1	Bottom	-433	-1088	6	1088	1254	87
	60	→	3lane left	2	Top	-488	2	1322	1322	1221	108

Table D.26 Data extracted and calculated for bridges with 0 deg. skew angle and piles with HPC connection at 150 mph wind velocity (Strength III Limit State)

Bridge Span (ft)	Un-supported Pile Length, $L_{P,}$ (ft)	Wind Direction	Live Load case and Vehicle position	Pile #	Results from FE analysis (SAP2000)				From I.D.	Capacity Utilization (%)
					Axial Load P (k)	Moment $M_{u,33}$ (k-ft)	Moment $M_{u,22}$ (k-ft)	$M_{u,cr}$ (k-ft)	Factored Moment Capacity ϕM_n (k-ft)	
30 ft	18	→	2lane left	1	-84	-1	-105	105	231	45
	24	→	2lane left	2	-115	-1	-117	117	207	56
	30	→	2lane left	2	-147	-1	-133	133	182	73
50 ft	18	→	2lane left	1	-142	3	-198	198	556	36
	24	→	2lane left	1	-147	3	-267	267	542	49
	30	→	2lane left	2	-303	1	-237	237	471	50
	40	→	2lane left	2	-391	-1	-252	252	431	58
76 ft	18	→	3lane left	1	-335	9	-531	531	859	62
	24	→	3lane left	1	-340	9	-705	705	844	84
	30	→	3lane left	1	-338	-1	-919	919	821	112
	40	→	3lane left	1	-342	-1226	-1	1226	775	158
	50	→	3lane left	1	-346	-1569	-2	1569	717	219
100 ft	30	→	3lane left	1	-504	0	-1306	1306	1340	97
	40	→	3lane left	1	-511	-1752	0	1752	1275	137
	50	→	3lane left	1	-517	-2221	0	2221	1191	187
	60	→	3lane left	1	-520	-2699	1	2699	1087	248

Table D.27 Data extracted and calculated for bridges with 30 deg. skew angle and piles with RPC connection at 150 mph wind velocity (Strength III Limit State)

Bridge Span (ft)	Un-supported Pile Length, L_P, (ft)	Wind Direction	Live Load case and Vehicle position	Pile #	Location	Results from FE analysis (SAP2000)				From I.D.	Capacity Utilization (%)
						Axial Load P (k)	Moment $M_{u,33}$ (k-ft)	Moment $M_{u,22}$ (k-ft)	$M_{u,cr}$ (k-ft)	Factored Moment Capacity ϕM_n (k-ft)	
30 ft	18	←	2lane left	6	Bottom	-71	16	71	72	241	30
	24	←	2lane left	6	Bottom	-68	-67	61	91	237	38
	30	←	2lane left	6	Bottom	-66	-82	74	111	232	48
50 ft	18	←	2lane left	5	Bottom	-139	32	144	148	564	26
	24	←	2lane left	5	Bottom	-140	42	183	187	557	34
	30	←	2lane left	5	Bottom	-138	-164	153	224	549	41
	40	←	2lane left	5	Bottom	-138	-211	202	293	531	55
76 ft	18	←	3lane left	3	Bottom	-323	98	563	572	864	66
	24	←	3lane left	2	Bottom	-365	48	624	626	870	72
	30	←	3lane left	2	Bottom	-370	63	729	732	859	85
	40	←	3lane left	2	Bottom	-376	158	828	843	833	101
	50	←	3lane left	3	Bottom	-306	-685	692	974	777	125
100 ft	30	←	3lane left	2	Bottom	-547	47	1215	1216	1406	86
	40	←	3lane left	2	Bottom	-559	199	1388	1402	1372	102
	50	←	3lane left	3	Bottom	-468	-1154	1092	1589	1269	125
	60	←	3lane left	3	Bottom	-469	-1294	1311	1842	1211	152

Table D.28 Data extracted and calculated for bridges with 30 deg. skew angle and piles with HPC connection at 150 mph wind velocity (for Strength III Limit State)

Bridge Span (ft)	Un-supported Pile Length, $L_{P,}$ (ft)	Wind Direction	Live Load case and Vehicle position	Pile #	Results from FE analysis (SAP2000)				From I.D.	Capacity Utilization (%)
					Axial Load P (k)	Moment $M_{u,33}$ (k-ft)	Moment $M_{u,22}$ (k-ft)	$M_{u,cr}$ (k-ft)	Factored Moment Capacity ϕM_n (k-ft)	
30 ft	18	←	2lane left	6	-82	10	119	120	232	52
	24	←	2lane left	6	-70	-116	89	146	229	64
	30	→	2lane left	1	-82	-129	166	210	213	99
50 ft	18	←	2lane left	5	-155	11	212	212	551	38
	24	←	2lane left	5	-160	14	288	289	536	54
	30	←	2lane left	5	-152	-297	198	357	524	68
	40	←	2lane left	5	-144	-391	275	478	496	96
76 ft	18	←	3lane left	3	-342	42	685	686	862	80
	24	←	3lane left	3	-332	18	769	769	841	91
	30	←	3lane left	3	-337	23	961	961	821	117
	40	←	3lane left	3	-342	-1104	674	1294	775	167
	50	←	3lane left	3	-347	-1402	864	1647	717	230
100 ft	30	←	3lane left	3	-501	14	1438	1438	1338	108
	40	←	3lane left	3	-513	-1619	957	1881	1276	147
	50	←	3lane left	2	-566	44	2217	2218	1212	183
	60	←	3lane left	3	-533	-2460	1469	2865	1091	263

Table D.29 Data extracted and calculated for bridges with 45 deg. skew angle and piles with RPC connection at 150 mph wind velocity (Strength III Limit State)

Bridge Span (ft)	Un-supported Pile Length, $L_{P,}$ (ft)	Wind Direction	Live Load case and Vehicle position	Pile #	Location	Results from FE analysis (SAP2000)				From I.D.	Capacity Utilization (%)
						Axial Load P (k)	Moment $M_{u,33}$ (k-ft)	Moment $M_{u,22}$ (k-ft)	$M_{u,cr}$ (k-ft)	Factored Moment Capacity ϕM_n (k-ft)	
30 ft	18	→	2lane left	1	Bottom	-70	-17	-85	87	241	36
	24	→	2lane left	1	Bottom	-68	-56	92	107	237	45
	30	→	2lane left	1	Bottom	-75	-81	133	155	229	68
50 ft	18	←	2lane left	5	Bottom	-126	40	184	188	568	33
	24	←	2lane left	5	Bottom	-127	58	239	246	562	44
	30	←	2lane left	5	Bottom	-129	-143	224	266	552	48
	40	←	2lane left	5	Bottom	-124	-201	350	404	537	75
76 ft	18	←	3lane left	2	Bottom	-357	0	495	495	878	56
	24	←	3lane left	2	Bottom	-360	60	643	646	869	74
	30	←	3lane left	3	Bottom	-304	177	740	761	835	91
	40	←	3lane left	3	Bottom	-296	-471	842	965	807	120
	50	←	3lane left	2	Bottom	-371	246	1136	1162	796	146
100 ft	30	←	3lane left	2	Bottom	-533	108	1158	1163	1397	83
	40	←	3lane left	3	Bottom	-457	-681	1161	1346	1311	103
	50	←	3lane left	3	Bottom	-454	-779	1403	1605	1262	127
	60	←	3lane left	3	Bottom	-450	-875	1641	1859	1204	154

Table D.30 Data extracted and calculated for bridges with 45 deg. skew angle and piles with HPC connection at 150 mph wind velocity (Strength III Limit State)

Bridge Span (ft)	Un-supported Pile Length, $L_{P,}$ (ft)	Wind Direction	Live Load case and Vehicle position	Pile #	Results from FE analysis (SAP2000)				From I.D.	Capacity Utilization (%)
					Axial Load P (k)	Moment $M_{u,33}$ (k-ft)	Moment $M_{u,22}$ (k-ft)	$M_{u,cr}$ (k-ft)	Factored Moment Capacity ϕM_n (k-ft)	
30 ft	18	→	2lane left	1	-80	-10	-124	124	233	53
	24	→	2lane left	1	-74	-100	129	164	227	72
	30	→	2lane left	1	-82	-131	168	213	213	100
50 ft	18	←	2lane left	5	-140	11	240	240	557	43
	24	←	2lane left	5	-145	21	318	318	543	59
	30	←	2lane left	5	-142	-263	300	399	529	75
	40	←	2lane left	5	-141	-352	422	549	497	111
76 ft	18	←	3lane left	3	-323	22	608	608	854	71
	24	←	3lane left	3	-327	29	808	808	839	96
	30	←	3lane left	3	-330	37	1021	1022	818	125
	40	←	3lane left	3	-331	-926	1015	1374	773	178
	50	←	3lane left	3	-332	-1211	1270	1755	714	246
100 ft	30	→	3lane left	1	-504	0	-1324	1324	1340	99
	40	→	3lane left	1	-510	-1775	0	1775	1275	139
	50	→	3lane left	1	-517	-2250	0	2250	1191	189
	60	→	3lane left	1	-520	-2733	1	2733	1087	251

Table D.31 Data extracted and calculated for bridges with 60 deg. skew angle and piles with RPC connection at 150 mph wind velocity (Strength III Limit State)

Bridge Span (ft)	Un-supported Pile Length, $L_{P,}$ (ft)	Wind Direction	Live Load case and Vehicle position	Pile #	Location	Results from FE analysis (SAP2000)				From I.D.	Capacity Utilization (%)
						Axial Load P (k)	Moment $M_{u,33}$ (k-ft)	Moment $M_{u,22}$ (k-ft)	$M_{u,cr}$ (k-ft)	Factored Moment Capacity ϕM_n (k-ft)	
30 ft	18	←	2lane left	6	Bottom	-75	18	128	129	239	54
	24	←	2lane left	6	Bottom	-76	-55	150	160	235	68
	30	←	2lane left	6	Bottom	-77	-60	180	189	228	83
50 ft	18	←	2lane left	5	Bottom	-130	38	236	239	567	42
	24	←	2lane left	5	Bottom	-127	57	236	242	562	43
	30	←	2lane left	5	Bottom	-138	-135	347	372	549	68
	40	←	2lane left	5	Bottom	-142	-159	452	479	529	91
76 ft	18	←	3lane left	3	Bottom	-325	104	576	585	865	68
	24	←	3lane left	3	Bottom	-325	147	734	749	855	88
	30	←	3lane left	3	Bottom	-323	185	885	904	842	107
	40	←	3lane left	3	Bottom	-323	-325	1075	1123	815	138
	50	←	3lane left	3	Bottom	-321	-372	1302	1354	781	173
100 ft	30	←	3lane left	3	Bottom	-504	174	1476	1486	1378	108
	40	←	3lane left	3	Bottom	-511	-707	1684	1827	1343	136
	50	←	3lane left	3	Bottom	-516	-844	2184	2341	1296	181
	60	←	3lane left	3	Bottom	-441	-871	2595	2737	1198	228

Table D.32 Data extracted and calculated for bridges with 60 deg. skew angle and piles with HPC connection at 150 mph wind velocity (Strength III Limit State)

Bridge Span (ft)	Un-supported Pile Length, $L_{P,}$ (ft)	Wind Direction	Live Load case and Vehicle position	Pile #	Results from FE analysis (SAP2000)				From I.D.	Capacity Utilization (%)
					Axial Load P (k)	Moment $M_{u,33}$ (k-ft)	Moment $M_{u,22}$ (k-ft)	$M_{u,cr}$ (k-ft)	Factored Moment Capacity ϕM_n (k-ft)	
30 ft	18	←	2lane left	6	-84	27	173	175	232	76
	24	←	2lane left	6	-83	-82	213	228	223	102
	30	←	2lane left	6	-82	-98	255	273	213	128
50 ft	18	←	2lane left	5	-141	25	279	280	556	50
	24	←	2lane left	5	-145	21	313	314	543	58
	30	←	2lane left	5	-151	-203	429	474	525	90
	40	←	2lane left	5	-154	-272	579	639	489	131
76 ft	18	←	3lane left	3	-329	37	659	660	857	77
	24	←	3lane left	3	-333	49	891	892	841	106
	30	←	3lane left	3	-335	61	1125	1127	820	137
	40	←	3lane left	3	-338	-677	1349	1509	774	195
	50	←	3lane left	3	-340	-843	1700	1898	715	265
100 ft	30	←	3lane left	3	-511	55	1571	1571	1344	117
	40	←	3lane left	3	-525	-970	1763	2012	1282	157
	50	←	3lane left	3	-536	-1284	2345	2674	1199	223
	60	←	3lane left	3	-467	-1474	2853	3211	1077	298

VITA

Md Rubiat Ferdous was born in the city of Dhaka, Bangladesh. He earned the degree of Bachelor of Science in Civil Engineering from Bangladesh University of Engineering and Technology, Dhaka. He came to Louisiana State University in August 2005 and will graduate in August 2007 with a Master of Science in Civil Engineering (MSCE).